8-2019

Understanding the Warburg Phenotype and the Metabolic Plasticity of Proliferative Mammalian Cells Using ^{13}C Metabolic Flux Analysis

Daniel Odenwelder
Clemson University, dan.odenwelder@gmail.com

UNDERSTANDING THE WARBURG PHENOTYPE AND THE METABOLIC PLASTICITY OF PROLIFERATIVE MAMMALIAN CELLS USING ^{13}C METABOLIC FLUX ANALYSIS

A Dissertation
Presented to
the Graduate School of
Clemson University

In Partial Fulfillment
of the Requirements for the Degree
Doctor of Philosophy
Bioengineering

---

by
Daniel C. Odenwelder
August 2019

Accepted by:
Dr. Sarah W. Harcum, Committee Chair
Dr. Kim Paul
Dr. Ying Mei
Dr. Agneta Simionescu

ABSTRACT

Proliferative cells, including many types of cancer and pluripotent stem cells, rely primarily on glycolysis and lactate metabolism for energy, regardless of oxygen availability. This metabolic phenotype – referred to as the Warburg effect – results in wasteful lactate accumulation. Although cancer cells and pluripotent stem cells share this central metabolic characteristic, the sensitivities of each of these cell types to lactate stress appear contradictory. While lactate accumulation is thought to adversely impact pluripotent stem cell proliferation and differentiation capacities, cancer cells have been shown to possess bioenergetic plasticity to utilize lactate catabolism for fuel. As a result, lactate buildup within the hypoxic tumor microenvironment has been hypothesized to promote cancer progression and malignancy, in part by selecting for cancer populations capable of catabolizing lactate. Moreover, lactate has been shown to promote "stemness" gene expression in cancer, suggesting that lactate plays a functional role in regulating pluripotency gene expression. However, an incomplete understanding of the impact of lactate on intracellular metabolism for proliferative cells remains. In this work, ^{13}C-metabolic flux analysis was used to quantify the intracellular metabolic responses of breast cancer cells and induced pluripotent stem cells (iPSCs) to high extracellular lactate; in particular, to determine the role of lactate as a metabolic substrate. In this research, it was demonstrated that both iPSCs and breast cancer cells employ dual consumption of glucose and lactate to support growth. In addition, this is the first study to determine and quantify intracellular contribution of lactate in proliferative iPSC metabolism. These results provide insight into the metabolic flexibility of highly proliferative cells with respect to lactate

metabolism and suggest that, much like many types of cancer cells, iPSCs possess the capacity to metabolize lactate to promote exponential growth and maintain pluripotency.

DEDICATION

I would like to dedicate this dissertation to my parents – Kathleen and Charles Odenwelder Jr. The success of my work is in large part due to their tremendous sacrifices and unwavering support throughout my life. I will be forever grateful for the work ethic they have instilled in me and for always prioritizing my education above everything else. This dissertation would not be possible without their sacrifice and encouragement.

ACKNOWLEDGMENTS

Throughout my time as a graduate student, I have received a tremendous amount of support. First, I am extremely grateful to my advisor, Dr. Sarah Harcum, for providing me with the incredible opportunity to pursue this degree under her supervision and for her profound belief in my ability. It has been a pleasure to learn from her over the years during my development as a researcher. I would also like to thank my thesis committee for providing valuable feedback and guidance to me throughout this project.

I would like to thank all of my current labmates for their friendship and support throughout this long journey. Tom Caldwell and Dr. Xiaoming Lu deserve special thanks for their assistance with the induced pluripotent stem cell (iPSC) project. I would also like to acknowledge my former labmates – Dr. Yogender Gowtham and Dr. Arthur Nathan Brodsky – who helped me acclimate to the lab and served as my mentors early on. Arthur deserves special thanks for including me in his cancer research project and for introducing me to metabolic flux analysis. It was a pleasure to work alongside all of you. Also, many thanks to the Clemson University Bioengineering department for the opportunity to pursue my doctoral degree.

Special thanks go to Paul Gulde and Serena Smith from Thermo Fisher for donating custom media for the iPSC project. Without their generous donation, much of this work would not have been possible. Also, thank you to Dr. Stephen A. Duncan at the Medical

University of South Carolina for donating the K3 iPSCs. Additionally, I'd like to recognize the Advanced Mammalian Biomanufacturing Innovation Center and my funding sources – NSF IPP-1624641 and NSF CBET-1218345 – for financially supporting me and my graduate research projects.

Finally, I would like to thank all my friends and family for the immense support, and for contributing to my personal growth these past few years. I could not have accomplished any of this without their laughter, guidance, and encouragement.

ABBREVIATIONS

Abbreviations	Full Form
2D	Two-dimensional
3D	Three-dimensional
3PG	3-phosphoglycerate
AcCoA	Acetyl coenzyme A
ACL	ATP citrate lyase
ACON	Aconitase
AKG	α-ketoglutarate
AKGD	α-ketoglutarate dehydrogenase
Ala	Alanine
ANCOVA	Analysis of covariance
Asp	Aspartate
AT	Aminotransferase
ATP	Adenosine triphosphate
CHO	Chinese hamster ovary
Cit	Citrate
CM	Cardiomyocyte
CO_2	Carbon dioxide
CoA	Coenzyme A
CS	Citrate synthase
CSC	Cancer stem cell
DHAP	Dihydroxyacetone phosphate
DMEM	Dulbecco's modified Eagle medium
DMFA	Dynamic metabolic flux analysis
DNA	Deoxyribonucleic acid
EMU	Elementary metabolite unit
ESC	Embryonic stem cell
ETA	Extracellular Time-Course Analysis

Abbreviations	Full Form
FA	Fatty acid
FAME	Fatty acid methyl ester
FBS	Fetal bovine serum
Fum	Fumarate
FUM	Fumarase
GC-FID	Gas chromatography-flame ionization detector
GC-MS	Gas chromatography-mass spectrometry
GDH	Glutamate dehydrogenase
GLM	Generalized linear model
Gln	Glutamine
Glu	Glutamate
GMP	Good manufacturing practices
H3K4me3	Histone H3 lysine 4
hESC	Human embryonic stem cell
HIF	Hypoxia inducible factor
HK	Hexokinase
hPSC	Human pluripotent stem cell
HRP	Horseradish peroxidase
HSD	Honestly significant difference
ICM	Inner cell mass
IDH	Isocitrate dehydrogenase
INCA	Isotopomer Network Compartmental Analysis
iPSC	Induced pluripotent stem cell
Lac	Lactate
LC	Liquid chromatography
LDH	Lactate dehydrogenase
Mal	Malate
MCT	Monocarboxylate transporter

Abbreviations	Full Form
MDH	Malate dehydrogenase
ME	Malic enzyme
MEF	Mouse embryonic fibroblast
mESC	Murine embryonic stem cell
MFA	Metabolic flux analysis
MID	Mass isotopomer distribution
miPSC	Murine induced pluripotent stem cell
MS	Mass spectrometry
MTBSTFA	N-methyl-N-(tert-butyldimethylsilyl)-trifluoroacetamide
NAD+	Nicotinamide adenine dinucleotide (oxidized)
NADH	Nicotinamide adenine dinucleotide (reduced)
NADPH	Nicotinamide adenine dinucleotide phosphate
Oct4	Octamer-binding transcription factor 4
OXPHOS	Oxidative phosphorylation
PBS	Phosphate buffered saline
PC	Pyruvate carboxylase
PDH	Pyruvate dehydrogenase
PDK	Pyruvate dehydrogenase kinase
PFK	Phosphofructokinase
PGK	Phosphoglycerate kinase
PK	Pyruvate kinase
PPP	Pentose phosphate pathway
PSC	Pluripotent stem cell
PVDF	Polyvinylidene difluoride
Pyr	Pyruvate
qRT-PCR	Quantitative reverse transcriptase polymerase chain reaction
RNA	Ribonucleic acid

Abbreviations	Full Form
ROCKi	Rho-associated, coiled-coil containing protein kinase inhibitor
ROS	Reactive oxygen species
SAM	S-adenosylmethionine
SCID	Severe combined immunodeficient
SCS	Succinyl coenzyme A synthetase
SDH	Succinate dehydrogenase
SE	Standard error
SEM	Standard error of mean
SIM	Single ion mode
Sox2	Sex determining region Y-box 2
SSR	Sum of squared residuals
Suc	Succinate
TBS	Tris buffered saline
TBST	Tris buffered saline with Tween
TCA	Tricarboxylic acid cycle
TDH	Threonine dehydrogenase
TOF	Time-of-flight
UCP2	Uncoupling protein 2

TABLE OF CONTENTS

Page

Table of Contents (Continued)

Page

Table of Contents (Continued)

Page

Table of Contents (Continued)

Page

Table of Contents (Continued)

Page

Table of Contents (Continued)

Page

LIST OF TABLES

LIST OF FIGURES

List of Figures (Continued)

Page

List of Figures (Continued)

Page

CHAPTER ONE

INTRODUCTION

1.1. Motivation

Induced pluripotent stem cells (iPSCs) have the potential to drastically improve cell-based therapies and diagnostics in the near future; however, stem cell applications are currently limited by our capability to generate sufficient quantities of undifferentiated stem cells that meet Good Manufacturing Practices (GMP). Current technologies are capable of generating 10^6 cells/mL; however current estimates indicate that between 10^9 and 10^{10} cells will be required per patient (Abecasis et al., 2017; Kehoe et al., 2010; Kropp et al., 2016; Kumar et al., 2017). An incomplete understanding of the conditions that cause iPSC differentiation is one obstacle preventing further scale-up capabilities. However, since culture variability is known to cause differentiation, providing a constant environment is favorable for expansion, also called proliferation. To bridge the gap between small-scale iPSC culture and controlled bioreactors, it is essential to develop a comprehensive understanding of the metabolic responses of iPSCs to environmental factors such as glucose, glutamine, and lactate concentrations. This will aid in the development of control parameters, thresholds, and set points for future bioreactor processes.

Highly proliferative cells, including cancer and pluripotent stem cells, rely primarily on aerobic glycolysis and lactate fermentation for energy, a process known as the Warburg effect (Gaspar et al., 2014; Vander Heiden et al., 2009; Varum et al., 2011; Warburg, 1956). While this distinct metabolic trait appears wasteful and energy inefficient, in cancer cells, it promotes tumor malignancy and induces a stem cell-like phenotype in certain cancer

populations (Bonuccelli et al., 2010; Kennedy and Dewhirst, 2010; Martinez-Outschoorn et al., 2011). Additionally, some cancer cell populations catabolize lactate as a carbon source, conceivably providing these adaptive cells with a competitive advantage over normal cell populations in highly acidic and lactic acid filled tumors (Kennedy and Dewhirst, 2010; Kennedy et al., 2013; Martinez-Outschoorn et al., 2011; Pavlides et al., 2010; Sonveaux et al., 2008). Therefore, this Warburg phenotype has been widely investigated as a target for cancer therapies (Doherty and Cleveland, 2013; Sonveaux et al., 2008). On the other hand, lactate accumulation in *in vitro* iPSC culture is viewed primarily as a wasteful metabolic byproduct that adversely impacts cell proliferation capacity and pluripotency (Chen et al., 2010; Olmer et al., 2012; Wang et al., 2013). Yet, an incomplete understanding of the impact of lactate on intracellular metabolism of iPSCs remains. In order develop cell culture techniques to improve iPSC quality and proliferation capacity, a more comprehensive understanding of the impact of lactate accumulation on iPSC metabolism and strategies to reduce this lactate accumulation are required.

Recent computational techniques have made it possible to quantify intracellular metabolic fluxes through complex metabolic pathways (Sa et al., 2015; Stephanopoulos et al., 1998). In this dissertation, ^{13}C metabolic flux analysis (^{13}C-MFA) was used to quantify intracellular metabolic fluxes through central metabolic pathways for breast cancer cells and iPSCs to understand the Warburg phenotype and uncover the roles of glucose and lactate in intracellular metabolism for highly proliferative cells. Using ^{13}C-MFA for this research provided a temporal representation of intracellular metabolic shifts in breast cancer and iPSC metabolism due to glucose and lactate perturbations. The

findings from this work can improve the understanding of iPSC metabolism and could be useful to design/optimize improved iPSC culture processes. The data in this work will also add to the current body of work related to cancer and iPS cell metabolism and provide further evidence of the metabolic plasticity of highly proliferative cells.

1.2. Organization

This dissertation is divided into five chapters. Chapter One outlines the motivation for this research. Chapter Two contains a literature review of key topics related to breast cancer and iPSC metabolism research. This includes a brief history of pluripotent stem cells (PSCs), the development of iPSCs, and the similarities between cancer and PSCs. A detailed description of the metabolic characteristics of PSCs and cancer, including the roles of glycolysis and lactate fermentation, are also included in the literature review. Finally, a brief introduction to metabolic flux analysis (MFA), the applications of MFA as a computational tool, and a review of previous studies that used MFA to study Chinese hamster ovary (CHO), cancer, and PSC metabolism is also provided. Chapter Three contains the recently published research paper, titled *High extracellular lactate causes reductive carboxylation in breast tissue cell lines grown under normoxic conditions*. This paper examined the effects of elevated extracellular lactate levels on intracellular metabolism for three different breast cancer cell lines using ^{13}C-MFA. The authors on this paper are Dr. Arthur Nathan Brodsky and Dr. Sarah W. Harcum. Arthur and I shared co-first authorship (Brodsky et al., 2019). Arthur was responsible for conceptualization of the project, methodology, data curation, investigation, formal analysis, and writing the original

draft, while I was responsible for methodology, data curation, investigation, formal analysis, writing the original draft, responding to reviewer comments and edits, and writing the final draft of the publication. Chapter Four describes the effects of glucose and lactate concentrations on iPSC metabolism and pluripotency, which was the majority of my dissertation research project. It is intended that this chapter will be submitted as a manuscript to a peer reviewed journal in the near future, where I am the first author, and Dr. Xiaoming Lu and my advisor, Dr. Sarah W Harcum, are co-authors. Dr. Xiaoming Lu assisted with gene expression analysis for the iPSC project. Finally, Chapter Five discusses conclusions and the future direction of the iPSC work.

CHAPTER TWO

LITERATURE REVIEW

2.1. Pluripotent stem cells

Since James Thompson first isolated human embryonic stem cells from surplus *in vitro* fertilized embryos in 1998, pluripotent stem cells (PSCs) have served as an exciting potential resource for cell-based therapies and regenerative medicine (Kimbrel and Lanza, 2015; Mitalipov and Wolf, 2009; Thomson et al., 1998). Stem cells are considered to be pluripotent if capable of 1) indefinite self-renewal and 2) differentiation to cell types from each of the three germ layers – the endoderm, ectoderm, and mesoderm (Melton, 2014). These two characteristics make pluripotent stem cells ideal tools for regenerative medical applications (Avior et al., 2016; Trounson and DeWitt, 2016).

2.1.1. Embryonic stem cells

Embryonic stem cells (ESCs) are isolated from the inner cell mass (ICM) of embryos in the blastocyst stage of development (Mitalipov and Wolf, 2009). ESCs cultured *in vitro* express the same stage specific transcription factors associated with "stemness", including octamer-binding transcription factor 4 (Oct4), SRY (sex determining region Y)-box 2 (Sox2), and Nanog (Yu and Thomson, 2014). While pluripotent cells found in the ICM only transiently express these transcription factors prior to differentiation during development, ESCs grown *in vitro* may be cultured indefinitely while maintaining expression of these "stemness" genes and a pluripotent phenotype; because of this, ESCs are considered to be immortalized cell lines (Luong and Gerecht, 2008). Given this

seemingly limitless *in vitro* expansion capacity, it is understandable that ESCs have long been thought of as the optimal tool for regenerative medicine. However, due to the ethical concerns surrounding harvesting cells from the ICM of human embryos, the use of ESCs in regenerative therapies has been heavily restricted by US government regulations. Since it is currently illegal to destroy an embryo to create any hESC line, researchers in the United States are restricted to using hESC lines generated prior to August 9, 2001 (Volarevic et al., 2018). Along with these government restrictions, there is also a divide in popular opinion over the use of hESCs (Green, 2007). Despite these limitations, a number of ESC treatments are undergoing clinical trials for severe heart failure, macular degenerative disease, retinitis pigmentosa, and amyotrophic lateral sclerosis (clinicaltrials.gov).

2.1.2. Induced pluripotent stem cells

The ethical concerns associated with using ESCs as a therapeutic was alleviated with the discovery that pluripotency could be "induced" in somatic cells. Induced pluripotent stem cells (iPSCs) are pluripotent stem cells derived by nuclear reprogramming of adult somatic cells. IPSCs are reprogrammed to a pluripotent state by overexpression of transcription factors associated with pluripotency; this was first discovered by Takahashi et al. in 2006 through ectopic expression of four transcription factors – Oct4, Sox2, c-Myc, and Klf4 – in adult murine fibroblasts (Takahashi and Yamanaka, 2006). This approach has since been used to develop both normal and diseased human iPSC lines (Cayo et al., 2012; Si-Tayeb et al., 2010; Takahashi et al., 2007; Yu et al., 2007). iPSCs share the same self-renewal and differentiation capacity as ESCs. In addition, iPSCs exhibit similar colony

morphology to ESCs and have been shown to acquire a more ESC-like phenotype with prolonged culture *in vitro* (Panopoulos et al., 2012). Originally, reprogramming of somatic cells to iPSCs was performed using retroviruses or lentiviruses; however, these methods can result in integration of viral DNA into the host cell genome (Si-Tayeb et al., 2010; Takahashi and Yamanaka, 2006). More recently, integration-free approaches, such as infection of cells with adenoviruses, synthetic modified mRNAs, and transient transfection of plasmid DNA, have been implemented to improve iPSC safety (Si-Tayeb et al., 2010; Stadtfeld et al., 2008; Warren et al., 2010). Overall, the end result of nuclear reprogramming is a rewiring of iPSC epigenetics towards an embryonic stem cell-like state (Mitalipov and Wolf, 2009).

Since patient-specific human iPSC (hiPSC) lines can be derived for cell therapy applications, this reduces the concerns over immune rejection (Shi et al., 2017). With proper differentiation, hiPSCs can be used to perform personalized patient cell replacement therapies tissue regeneration, and *in vitro* drug screening studies (Avior et al., 2016; Kimbrel and Lanza, 2015; Trounson and DeWitt, 2016; Wu and Hothedlinger, 2011). Furthermore, hiPSCs may be used to investigate disease progression of normal and pathological human cell development *in vitro* (Figure 2.1) (Avior et al., 2016; Kimbrel and Lanza, 2015; Paes et al., 2017). Currently, a number of iPSC-derived therapies are undergoing clinical trials to treat various types of cancers, heart failure, thalassemia, and age-related macular degeneration using hiPSC-derived cell therapies (clinicaltrials.gov).

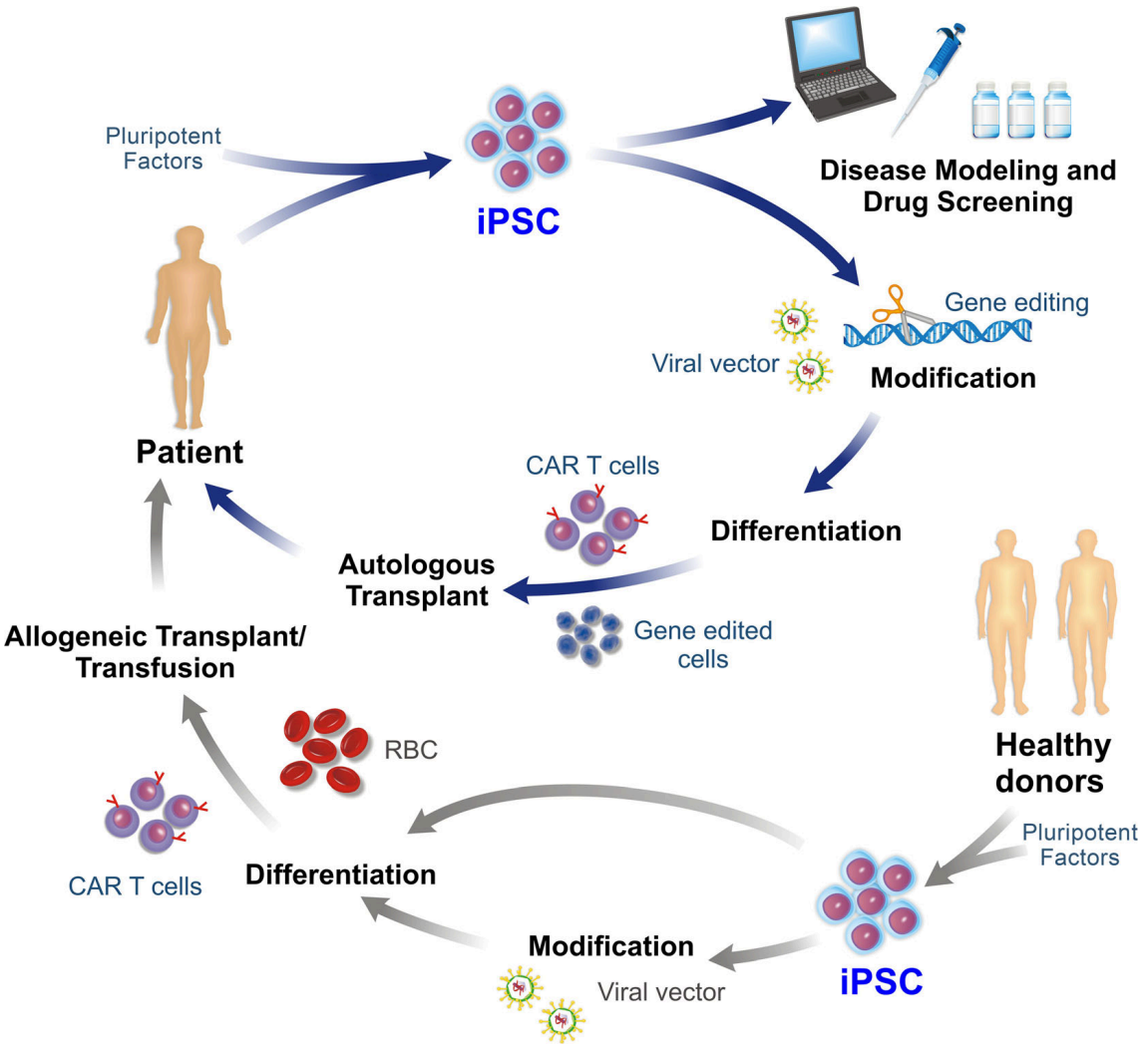

Figure 2.1. Applications of iPSCs for disease modeling, drug screening, and cell replacement therapy approaches. Patient-derived iPSCs can be used to study disease progression *in vitro* and perform drug screening studies on diseased cells. Patient-specific iPSCs may also be genetically modified to correct a mutation, differentiated into the desired cell type, and transplanted back into the donor patient (autologous transplant). Alternatively, iPSCs can be derived from a healthy donor and differentiated to a desired cell type to be used for allogeneic transplantation. Translated with permission from [Springer Nature]: [Springer Nature] [Cell Biology and Toxicology] (Bárbara Cristina Martins Fernandes Paes, Pablo Diego Moço, Cristiano Gonçalves Pereira et al), [COPYRIGHT] (2016).

2.1.3. Pluripotent stem cells and cancer

The extraordinary ability of PSCs to self-renew and differentiate towards each germ layer provides therapeutic potential and challenges. While these characteristics make PSCs ideal candidates for cell-based therapies, the plasticity of PSCs makes it difficult to control differentiation, eliminate undifferentiated cells, and control cellular expansion (Volarevic et al., 2018). In addition, both iPSCs and ESCs form teratomas—a benign germ-line tumor containing cells from each of the three germ layers—in severe combined immunodeficient (SCID) mice (Ben-David and Benvenisty, 2011). Moreover, iPSCs have also been shown to form teratocarcinomas—a malignant germ-layer tumor—and be more tumorigenic than ESCs (Mayshar et al., 2010; Miura et al., 2009). Given the tumorigenic nature of PSCs and the ability of many cancers to repopulate a tumor following treatment, some researchers have hypothesized that malignant tumors propagate from a small subset of stem cell-like cells, which are commonly referred to as cancer stem cells (CSC) (Hope et al., 2004). To this point, some carcinoma cells undergoing epithelial-to-mesenchymal transition—a process associated with cancer migration and malignancy—were shown to possess stem cell-like characteristics (Chen et al., 2012; Rhim et al., 2012; Yu et al., 2013). Furthermore, under elevated lactate exposures similar to that found in metastatic tumors, human tumorigenic, luminal breast cells exhibited elevated expression of genes which are upregulated in ESCs and are associated with "stemness" (Martinez-Outschoorn et al., 2011). As a result, there appear to be numerous similarities between cancer and PSCs. In order for PSCs to become routinely used cell-based therapy tools, it is paramount to determine what makes PSCs and CSCs different from each other.

2.2. Metabolic requirements of pluripotent stem cells

2.2.1. Glucose – an essential sugar

Glucose is rich in potential energy and serves as the primary metabolic substrate for most mammalian cells. In fact, the complete oxidation of glucose to carbon dioxide and water generates large amounts of energy in the form of 36 molecules of adenosine triphosphate (ATP) (Nelson et al., 2008). Furthermore, proliferating cells must also synthesize sufficient macromolecules to support rapid cell growth (Lunt et al., 2011). Glucose supports all of these metabolic needs, with glucose-derived carbon contributing to the synthesis of nucleotides, lipids, glycogen, and energy production through glycolysis (in the cytosol) and the tricarboxylic acid (TCA) cycle and oxidative phosphorylation (in the mitochondria) (Lunt et al., 2011).

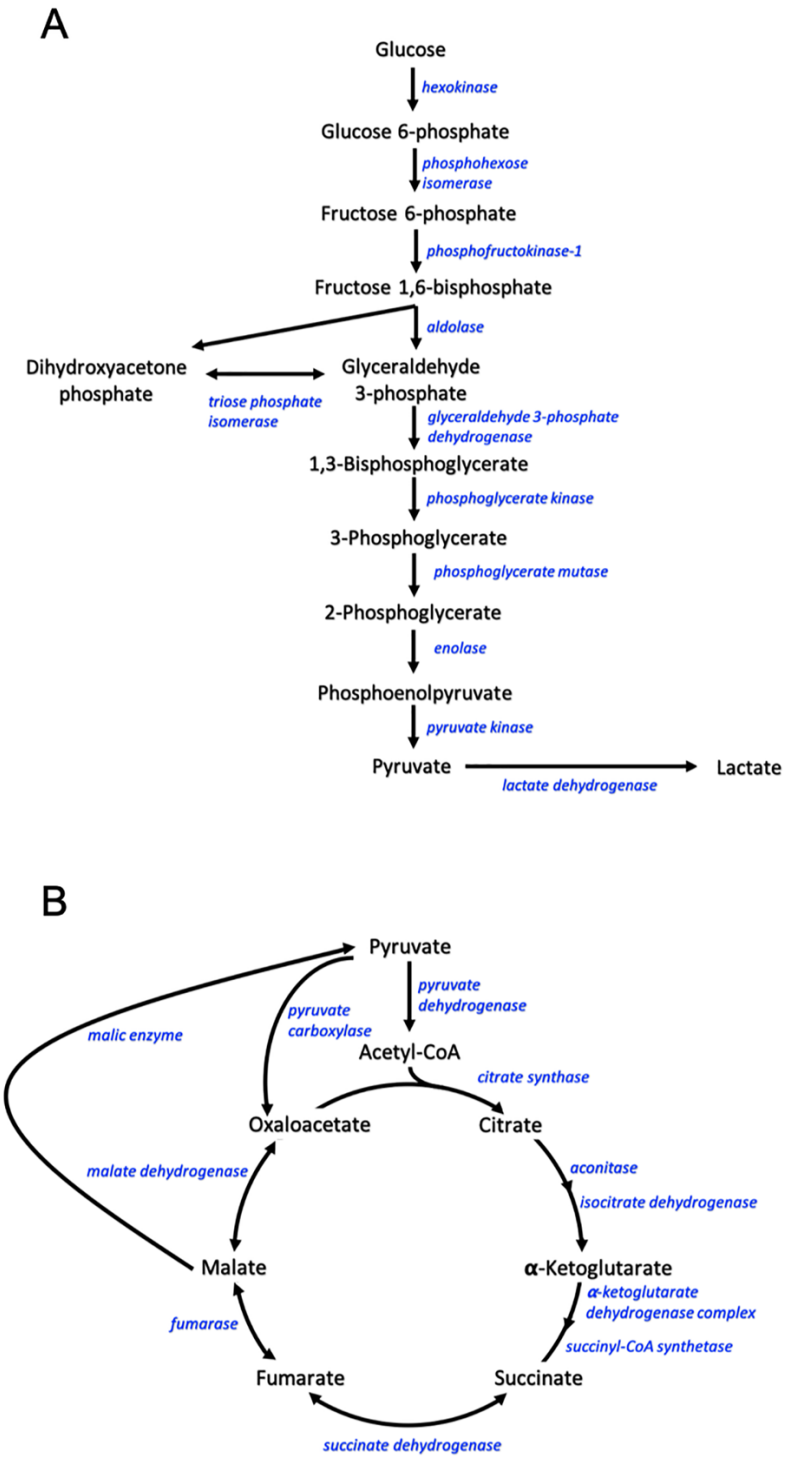

Figure 2.2. Simplified mammalian metabolic pathways through A) glycolysis and B) tricarboxylic acid (TCA) cycle. Metabolites are shown in black and enzymes responsible for each reaction are shown in blue italics.

2.2.1.1. Glycolysis and the Warburg effect

Glycolysis is the central pathway responsible for glucose catabolism in the cytosol, in which one six-carbon molecule of glucose is converted into two three-carbon molecules of pyruvate. Glycolysis is broken down into two parts: a preparatory phase and an energy pay-off phase. In the preparatory phase, two ATP are consumed to phosphorylate glucose to glucose 6-phosphate (by hexokinase (HK)) and fructose 6-phosphate to fructose 1,6-bisphosphate (by phosphofructokinase-1 (PFK-1)) (Nelson et al., 2008). Four ATP molecules are generated in the pay-off phase of glycolysis from the conversions of 1,3-biphosphoglycerate to 3-phosphoglycerate (by phosphoglycerate kinase (PGK)) and phosphoenolpyruvate to pyruvate (by pyruvate kinase (PK)) (Nelson et al., 2008). Overall, metabolism of glucose to pyruvate results in a net gain of energy in the form of two ATP molecules and two nicotinamide adenine dinucleotide (NADH) reducing molecules; moreover, key intermediate biomass building blocks such as lipids, proteins, and nucleic acids are also generated through glycolysis (Hume and Weidemann, 1979; Vander Heiden et al., 2009).

Glucose catabolism for energy production is regulated in normal mammalian cells in part by oxygen availability (Semenza et al., 1994). In oxygen rich environments, cells can further oxidize pyruvate to CO_2 in the TCA cycle and produce large quantities of ATP through oxidative phosphorylation (OXPHOS) (Lunt et al., 2011). On the other hand in the absence of oxygen, pyruvate is reductively metabolized to lactate through fermentation (Vander Heiden et al., 2009). Anaerobic fermentation of pyruvate to lactate by lactate dehydrogenase (LDH) generates reducing cofactors required to sustain continuous flux

through glycolysis, as described further below (Vander Heiden et al., 2009). However, in the 1920's, Otto Warburg discovered that proliferating cells—including cancer and stem cells—primarily rely on glycolysis and lactate fermentation for energy production irrespective of oxygen availability; this is commonly referred to as the Warburg Effect (Warburg, 1956). This reliance on aerobic glycolysis is now widely accepted as a metabolic feature of both cancer and stem cells (Folmes et al., 2012; Folmes et al., 2011; Gaspar et al., 2014; Vander Heiden et al., 2009; Varum et al., 2011; Zhang et al., 2011).

In order for complete oxidation of glucose, pyruvate generated from glycolysis is transported into the mitochondria and converted to acetyl-CoA and CO_2 by the pyruvate dehydrogenase (PDH) enzyme complex. The rate of pyruvate entry into the mitochondria is partially dependent on reducing equivalent shuttles, specifically reduced NADH transport from the cytosol to mitochondria via either the malate-aspartate shuttle or the glycerol 3-phosphate shuttle (Mulukutla et al., 2010). It was previously proposed that the high glycolytic flux state of proliferating cells might outpace the maximum PDH activity (Curi et al., 1988). Also, pluripotent stem cells exhibited decreased activity of PDH compared to somatic cells (Chandel et al., 2016; Teslaa and Teitell, 2015). Furthermore, uncoupling protein 2 (UCP2) was shown to regulate hPSC metabolism by blocking glucose oxidation in the mitochondria and promoting aerobic glycolysis (Zhang et al., 2011). As a result of the factors listed above, the conversion of pyruvate to acetyl-CoA within the mitochondria is slow, and PSCs quickly reduce excess cytosolic pyruvate to lactate instead (DeBerardinis et al., 2007).

As mentioned previously, the incomplete oxidation of glucose to lactate by LDH generates oxidized nicotinamide adenine dinucleotide (NAD^+) and maintains a cytosolic NAD^+/NADH ratio necessary to sustain glycolytic activity and promote cell proliferation (DeBerardinis et al., 2008). Moreover, NAD^+ is required for nucleotide and amino acid biosynthesis, which might also contribute to rapid biomass accumulation and proliferation (Lunt et al., 2011). Although incomplete oxidation of glucose to lactate is an energy inefficient process, with 2 ATP produced as compared to the 36 ATP produced from the complete oxidation of glucose through the TCA cycle and OXPHOS, rapidly proliferating cells consume glucose at an elevated rate in order to compensate for this inefficient energy output (Guppy et al., 1993; Pfeiffer et al., 2001). It also has been suggested that proliferating cells rely primarily on glycolysis because of the significant biomass building blocks – proteins, lipids, and nucleic acids – required to support cell division (DeBerardinis et al., 2008; Vander Heiden et al., 2009; Zhang et al., 2012).

2.2.1.2. Glucose concentration and stem cell metabolism

Since PSCs rely on glycolysis for growth, commercially available PSC cell culture media consists of high glucose concentrations – mTeSR (2.5 g/L) and Essential 8 Flex (3.15 g/L) – relative to physiological blood glucose concentrations, which range from 0.6 to 1.0 g/L (Güemes et al., 2016; Rathjen et al., 2014; Varum et al., 2011; Zhang et al., 2011). As a result, PSCs grown *in vitro* have been observed to consume copious amounts of glucose and secrete a significant proportion of glucose-derived carbon as lactate (Cliff et al., 2017; Folmes et al., 2011; Gaspar et al., 2014; Gu et al., 2016; Moussaieff et al.,

2015). Although this Warburg phenotype results in wasteful lactate accumulation as well as an undesirable drop in pH, few studies have evaluated the effects of glucose concentration on PSC growth, extracellular metabolism, and pluripotency (Chen et al., 2010; Horiguchi et al., 2018; Kim et al., 2009; Mochizuki et al., 2011; Tohyama et al., 2016; Wang et al., 2006).

Interestingly, the effect of glucose concentration on establishing ESC lines from mouse blastocysts has previously been disputed. Wang et al. 2006 illustrated that culturing mESCs in physiological glucose (1 g/L) improved cell proliferation, reduced oxidative stress, and overall was more effective for establishing a stable ES cell line when compared to high glucose (4.5 g/L) media (Wang et al., 2006). In contrast, Kim et al. 2009 showed that culture of mESCs in high glucose containing media resulted in increased expression of Oct4, Sox2, and Nanog during early cell line generation from blastocysts. This was suggested to be a result of glucose concentration regulating pluripotency gene expression, as well as due to DNA methylation and histone acetylation (Kim et al., 2009). The discrepancies between these studies partially arose because different basal medias were used. As a result, the effect of glucose concentration on mESC proliferation and pluripotency could not be deconvoluted from the effects of each unique basal media used. In addition, low glucose (1 g/L) did not impact embryoid body formation for mESCs; however, glucose concentration influenced differentiation potential; high glucose (4.5 g/L) resulted in more efficient cardiomyocyte production, while low glucose caused more efficient differentiation towards neural cells (Mochizuki et al., 2011).

Similar to mESCs, glucose concentration has been shown to have variable effects on

hPSC metabolism and pluripotency. For instance, growth of hESCs in low glucose media (1.5 g/L) with daily media replacement resulted in a 10% reduction in lactate production and a 40% increase in final cell yields when compared with the control glucose (3 g/L) feed strategy (Chen et al., 2010). Alternatively, when implementing less frequent media changes, high glucose concentrations improved maintenance of PSCs and reduced differentiation gene expression (Horiguchi et al., 2018). Interestingly, hESCs also previously were shown to survive for up to 24-h in glucose deficient media (Tohyama et al., 2016). However, glucose depleted media supplemented with lactate was shown to support only cardiomyocyte survival and loss of residual pluripotent stem cell population during differentiation and selection process (Tohyama et al., 2013). Similarly, growth of PSC-derived cardiomyocytes in glucose-depleted medium supplemented with fatty acid and 3,3',5-Triiodo-L-Thyronine facilitated cardiomyocyte selection and maturation in a similar manner to lactate supplemented medium, and also improved mature cell functionality (Lin et al., 2017). As a whole, these results suggest that the effect of glucose concentration on PSC metabolism and pluripotency is highly dependent on the cell lines and media used.

2.2.2. Anaplerosis and amino acid metabolism

Pluripotent stem cells primarily oxidize pyruvate to acetyl-CoA and depend on amino acid anaplerosis to maintain TCA cycle function (Gaspar et al., 2014; Wellen and Thompson, 2012). In addition, mammalian cells are composed of ~ 70% protein by dry cell weight; this causes a significant amino acid demand on proliferating cells (Bonarius et

al., 1996). In particular, since glutamine is the most abundant free amino acid in circulating blood, glutamine catabolism is crucial for mammalian cell metabolism (Bergström et al., 1974; Folmes and Terzic, 2016). Glutamine serves as an important substrate for bioenergetics and macromolecule synthesis (Eagle, 1955; Kovacevic and McGivan, 1983). For example, glutamine carbons are metabolized to TCA cycle intermediates and used to synthesize four nonessential amino acids (aspartate, asparagine, glutamate, and proline) (Lunt et al., 2011). Also, glutaminolysis through malic enzyme generates lactate and NADPH (DeBerardinis et al., 2007). Proliferating cells require significant amounts of reducing cofactors, including NADPH, to fulfill biosynthesis requirements for cell replication, including lipid synthesis, and to limit damage related to reactive oxygen species (ROS) (DeBerardinis et al., 2008; Folmes et al., 2012; Vander Heiden et al., 2009). Furthermore, glutamine has been shown to be reductively metabolized to citrate by cytosolic isocitrate dehydrogenase (IDH1) and used for lipid biosynthesis (Metallo et al., 2012; Yoo et al., 2008). In fact, proliferative cells have been observed to favor reductive glutamine metabolism for lipid biosynthesis in hypoxic (1-5% O_2) environments (Fan et al., 2013; Fendt et al., 2013; Grassian et al., 2014; Jiang et al., 2016; Metallo et al., 2012; Metallo et al., 2009; Wise et al., 2011). Thus, glutamine catabolism is integral to cell metabolism and proliferation. Furthermore, Tohyama et al. 2016 showed that glutamine oxidation was required for hPSC survival, with glutamine depletion resulting in rapid cell death within 24-h (Tohyama et al., 2016). This is in part because hPSCs oxidize pyruvate poorly (Tohyama et al., 2016; Varum et al., 2011; Zhang et al., 2011). Moreover, glutamine consumption and its contribution to succinate, fumarate and malate metabolite pools was

observed to increase in glucose-deficient media (Tohyama et al., 2016). In fact, glutamine consumption also was observed to modulate hematopoietic cell differentiation; glutamine uptake and metabolism drove erythroid development, while glutamine deprivation preferentially favored myeloid lineage development instead (Oburoglu 2014).

Since the essential amino acids—histidine, isoleucine, lysine, leucine, methionine, phenylalanine, threonine, tryptophan, and valine—cannot be de novo synthesized by mammalian cells, these amino acids must be supplemented to support cell metabolism and growth (Figure 2.3). A number of essential amino acids have previously been shown to influence pluripotent stem cell metabolism and maintenance of pluripotency (Edgar, 2002; Shiraki et al., 2014; Shyh-Chang et al., 2013; Wang et al., 2009). Wang et al. (2009) showed that murine ESCs were sensitive to threonine availability and could not proliferate in threonine depleted medium (Wang et al., 2009). Murine ESCs were shown to convert threonine to acetyl coenzyme A (acetyl-CoA) and glycine via threonine dehydrogenase (TDH), which was expressed at high levels in pluripotent mESCs and rapidly decreased in expression levels early in differentiation (Wang et al., 2009). Whereas, supplementing media with pyruvate and glycine mitigated the effects of threonine depletion on mESCs (Shyh-Chang et al., 2013). On the other hand, human PSCs were shown to have an inactive TDH enzyme, and therefore were not sensitive to threonine depletion (Edgar, 2002; Shiraki et al., 2014). Yet, deprivation of leucine, lysine, methionine, or tryptophan resulted in reduced cell growth for human ESCs and iPSCs (Shiraki et al., 2014). Moreover, leucine, lysine, and methionine induced apoptosis during prolonged deprivation (Shiraki et al., 2014). Therefore, while murine and human PSCs possess unique essential amino acid

metabolic requirements, amino acid metabolism is crucial for sustaining proliferation and preventing differentiation.

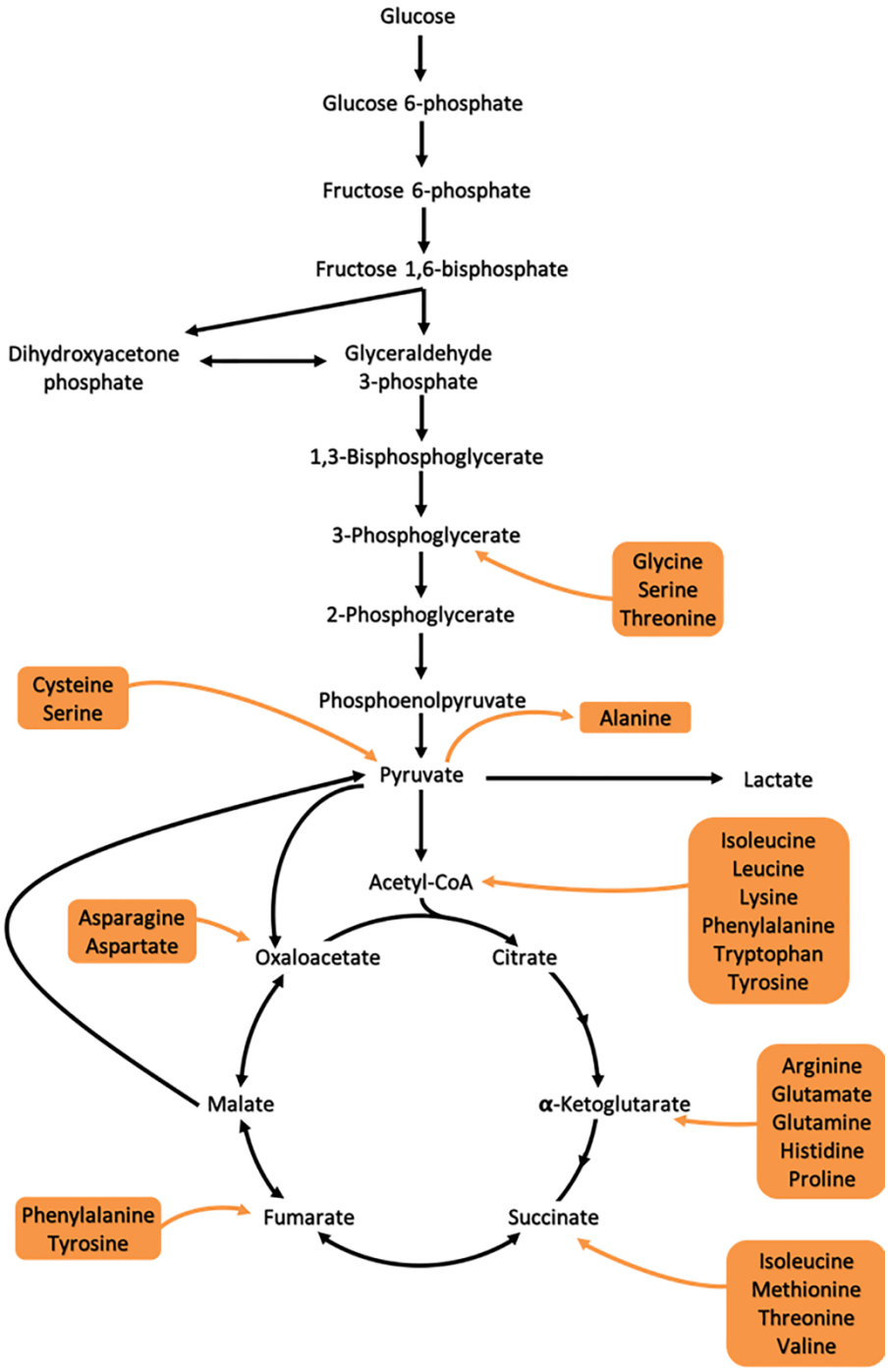

Figure 2.3. Simplified schematic of amino acid metabolism for mammalian cells.

Gene expression and chromatin structure are regulated by histone and DNA methylation (Cedar and Bergman, 2009). Central to this, methyltransferases utilize S-adenosylmethionine (SAM) as a methyl donor (Goll and Bestor, 2005; Lu et al., 2008). SAM production depends on one-carbon metabolism and is influenced by specific amino acid availability (Shiraki et al., 2014; Shyh-Chang et al., 2013). Strikingly, intracellular SAM levels were higher in mouse and human PSCs compared to fibroblasts (Deng et al., 2009; Panopoulos et al., 2012; Shyh-Chang et al., 2013). Furthermore, SAM levels increased during the later stages of reprogramming and were elevated in iPSCs compared to hESCs; this suggests a causative role in reprogramming and regulation of pluripotency (Deng et al., 2009; Panopoulos et al., 2012; Shyh-Chang et al., 2013). In particular, PSCs were shown to be sensitive to SAM histone methylation of histone H3 lysine 4 (H3K4me3) (Shiraki et al., 2014; Shyh-Chang et al., 2013). In murine ESCs, threonine deprivation or knockout of TDH negatively affected SAM production and gene expression (Shyh-Chang et al., 2013). In human ESCs and iPSCs, reduction of intracellular SAM led to a decline in H3K4me3 methylation and global DNA methylation (Shiraki et al., 2014). Consequently, reduction of intracellular SAM resulted in decreased Nanog expression and enhanced differentiation towards all 3 germ layers (Shiraki et al., 2014). In this way, threonine and methionine seem to affect metabolism and cell fate of murine and human PSCs respectively through the same SAM-related mechanism.

2.2.3. Lactate fermentation and accumulation

2.2.3.1. Lactate metabolism as a result of oxygen tension

Lactate production and accumulation in mammalian cell metabolism was originally viewed as an oxygen dependent characteristic, with only oxygen deprived cells participating in lactate fermentation (Warburg et al., 1927). Notwithstanding, lactate fermentation has also been shown to be a byproduct of aerobic metabolism, and accumulates significantly in mammalian cell culture (Eagle et al., 1958). As mentioned above, the reliance on glycolysis and lactate fermentation by proliferating cells for macromolecule synthesis and energy production irrespective of oxygen level is referred to as the Warburg Effect (Warburg, 1956). The rate of lactate accumulation is based on the carbohydrate conversion rates to either glucose- or fructose-phosphate (Eagle et al., 1958). Until recently, the general consensus has been that pyruvate is the end product of glycolysis for well oxygenated systems, and lactate is the glycolytic end product for poorly oxygenated systems (Mulukutla et al., 2010; Vander Heiden et al., 2009). However, since the LDH reaction is nearly at equilibrium, and because LDH activity has been shown to be much higher than important regulatory enzymes for glycolysis and oxidative metabolism, lactate has recently been hypothesized to be the true end product of glycolysis, irrespective of oxygen availability (Kane, 2014; Rogatzki et al., 2015; Schurr, 2017).

Hypoxia-inducible factors (HIFs) are transcription factors that regulate oxygen homeostasis in response to cellular environment conditions (Semenza, 2012). HIF-1 is a heterodimer composed of 2 subunits (HIF-1α and HIF-1β). HIF activity is regulated by O_2 concentrations and is dependent on the stability of the α-subunit (Manalo et al., 2005; Wang

and Semenza, 1995); under normoxic conditions HIF-1α is inactivated and degraded, while in hypoxic conditions it is stabilized and activated (Berra et al., 2001; Jaakkola et al., 2001). Under hypoxic conditions, HIF-1 was shown to activate the transcription of genes encoding glucose transporters and glycolytic enzymes (Semenza et al., 1994). In addition, HIF-1 activation resulted in increased expression of pyruvate dehydrogenase kinase (PDK1), which phosphorylated and inactivated the PDH complex and prevented pyruvate from entering into the TCA cycle (Papandreou et al., 2006; Semenza, 2012). Therefore, in hypoxic conditions, pyruvate is converted to lactate in order to maintain a high carbon flux through glycolysis. Interestingly, lactate and pyruvate have also recently been shown to cause HIF-1α accumulation and stabilization independent of hypoxia (De Saedeleer et al., 2012; Lu et al., 2002; Sonveaux et al., 2012). This suggests that lactate also reciprocally activates HIF-1 and contributes to the Warburg phenotype (Ferguson et al., 2018).

2.2.3.2. Lactate transport across the cell membrane

Intracellular lactate homeostasis and transport across the plasma membrane is facilitated by monocarboxylate transporters (MCT) (Halestrap, 2012). MCTs are proton-linked plasma membrane transporters responsible for shuttling lactate, pyruvate, and ketone bodies across the cell membrane (Halestrap, 2012). MCT transport is based on the presence of H^+ and the direction of the metabolite concentration gradient (Halestrap, 2012). By coupling transport of protons with lactate, MCTs control intracellular pH and prevent toxic levels of intracellular lactate buildup (Doherty and Cleveland, 2013). There are four MCTs responsible for lactate transport (MCT 1-4), with MCT1 exhibiting the highest

affinity for lactate uptake and MCT4 primarily responsible for lactate secretion (Dubouchaud et al., 2000; Halestrap, 2012). For example, within the tumor microenvironment, cancer cells which exhibit high MCT1/MCT4 ratios have been shown to consume and utilize lactate for energy (Corbet et al., 2014; Kennedy et al., 2013; Perez-Escuredo et al., 2016; Sonveaux et al., 2012). As a result, MCT1 inhibitors are one of many potential anti-cancer treatments. Interestingly, high MCT1 expression levels were also associated with a naïve pluripotent cell state for both hESCs and hiPSCs (Gu et al., 2016). As MCT1 is associated with lactate uptake, this may suggest that PSCs are capable of consuming lactate as a metabolic substrate, while maintaining pluripotency.

2.2.3.3. Lactate as a metabolic substrate (in tissues)

In anaerobic exercise, contracting skeletal muscle cells secrete lactate. Normal blood lactate levels are maintained below 1.0 mM, while during intense exercise, blood lactate levels can rise to as high as 11 mM (Ferguson et al., 2018). Originally, circulating lactate secreted from muscles was thought to accumulate and act as a dead-end waste product (Hill et al., 1924). More recently, however, a cell-to-cell lactate shuttle was proposed, which postulates that lactate secreted by contracting muscle cells acts as an energy intermediate and can be oxidized, or undergo gluconeogenesis or glycogenesis in neighboring tissues (Brooks, 1985). In support of this hypothesized lactate shuttle, during exercise, normal human myocardium exhibited elevated exogenous lactate oxidation (Gertz et al., 1988). Also, cardiomyocytes preferentially metabolized lactate over glucose during fetal heart development (Werner and Sicard, 1987). Notably, neural tissue were also

shown to be capable of metabolizing plasma lactate; circulating lactate supported up to 10% of oxidative requirements under physiological conditions and was capable of supporting a larger fraction of energy requirements as circulating lactate levels rose during exercise (Boumezbeur et al., 2010). Moreover, in mice, lactate was shown to feed TCA metabolism for all tissues via circulating blood during both fed and starved metabolic states (Hui et al., 2017). This suggests that lactate is an energy intermediate during resting and active metabolic states.

2.2.3.4. Lactate as a metabolic substrate (cell culture)

Lactate has also been shown to serve as a substrate to numerous types of mammalian cells *in vitro*. In the field of recombinant protein production, mammalian cells— including Chinese hamster ovary (CHO), hybridoma, and NS0 cells—have been observed to shift from relying on glycolysis and lactate fermentation for rapid growth, towards a lactate consumption state during the stationary growth phase of fed-batch processes (Altamirano et al., 2006; Mulukutla et al., 2012; Zhou et al., 1997). Lactate consumption metabolism was also found to correlate with increased cellular productivity for CHO cells, while lactate production and accumulation corresponded to poor processes and product qualities (Charaniya et al., 2010; Mulukutla et al., 2012; Mulukutla et al., 2015). Therefore, the metabolic shift from lactate production to consumption is often encouraged in mammalian bioprocessing. In order to reduce lactate accumulation and promote lactate oxidation, a number of media formulations and feeding strategies have been adopted, including: low initial glucose concentrations, supplementation with

galactose, and glutamine limiting feed rates (Altamirano et al., 2006; Chee Furng Wong et al., 2005; Lee et al., 2015). Interestingly, lactate has also previously been fed to CHO cells to promote lactate consumption, control pH, and reduce ammonia buildup (Li et al., 2012). Moreover, cells undergoing lactate oxidation produced up to six times more ATP per mole of carbon consumed than cells using glycolysis and lactate production for energy (Martínez et al., 2013).

2.2.3.5. Lactate in cancer cell metabolism

Since the seminal work of Otto Warburg in the 1920s, numerous types of cancer have been shown to rely heavily on glycolysis and lactate fermentation to support proliferation irrespective of oxygen availability (Cairns et al., 2011; DeBerardinis et al., 2008; Vander Heiden et al., 2009; Warburg, 1956). Moreover, within the tumor microenvironment, select populations of cancer cells can also catabolize lactate, a process referred to as the Reverse Warburg Effect (Kennedy and Dewhirst, 2010; Kennedy et al., 2013; Martinez-Outschoorn et al., 2011; Pavlides et al., 2010; Sonveaux et al., 2008). Consequently, the cell-to-cell lactate shuttle has been extended to describe the tumor microenvironment, where cancer-associated fibroblasts generated lactate from aerobic glycolysis and epithelial cancer cells oxidized lactate for fuel (Kennedy et al., 2013; Martinez-Outschoorn et al., 2011; Pavlides et al., 2010; Sonveaux et al., 2008). This symbiotic relationship between hypoxic tumor populations generating lactate and oxidative tumor cells consuming lactate has been linked to varying expression levels of lactate transporters (MCT1 and MCT4); cancer cell lines that preferentially oxidize lactate for

energy exhibited elevated expression levels of MCT1, while tumor cells exhibiting the Warburg phenotype had elevated expression of MCT4 (Kennedy et al., 2013; Sonveaux et al., 2008).

Lactate oxidation also appears to promote cancer progression. Intratumoral lactate injections have been shown to result in increased cancer metastasis *in vivo* (Bonuccelli et al., 2010). Lactic acidosis is also used as a diagnostic indicator in some types of cancer, with high intratumoral lactate levels correlating with treatment resistance as well as poor patient prognosis (Kennedy and Dewhirst, 2010). One hypothesis is that the Warburg phenotype provides cancer cells with a competitive advantage. In this way, lactate secretion and tumor acidification have been shown to promote cell invasion and metastasis (Gatenby and Gillies, 2004). Furthermore, exposure to lactate *in vitro* caused an upregulation of genes associated with stemness and resulted in a shift towards the "cancer stem cell" phenotype (Martinez-Outschoorn et al., 2011). When catabolized, lactate-derived acetyl-CoA was either used for mitochondrial metabolism or for histone acetylation (Martinez-Outschoorn et al., 2011). Besides, exposure to extracellular lactate (10 mM) resulted in increased histone acetylation for breast cancer cells and promoted increased malignancy and stemness gene expression (Martinez-Outschoorn et al., 2011). In addition, HeLa and H460 cells metabolized exogenous lactate for lipid synthesis, with lactate derived carbon playing a more significant role in lipid synthesis than glucose (Chen et al., 2016). Moreover, in an *in vivo* human lung tumor model, lactate was metabolized and contributed more to TCA cycle metabolism than glucose (Faubert et al., 2017). These results suggest that

lactate-derived acetyl-CoA serves both a metabolic and regulatory role in cancer progression.

2.2.3.6. Lactate in iPSC metabolism

Lactate accumulates rapidly in iPSC culture as well, and as a result, daily media exchanges are routinely performed, in part to prevent lactate stresses (Olmer et al., 2012; Wang et al., 2013). Unlike other mammalian cells, PSCs have been shown to be dependent on glycolysis and lactate fermentation for growth, with decreased rates of glycolysis and lactate productions previously corresponding to increased rates of PSC differentiation; therefore, lactate accumulation appears to be a byproduct of healthy PSCs (Folmes et al., 2011; Gaspar et al., 2014; Gu et al., 2016; Moussaieff et al., 2015; Panopoulos et al., 2012; Varum et al., 2011). A number of studies have investigated the effects of lactate accumulation on murine and human PSCs and shown variable sensitivities between species. For example, murine embryonic stem cells (mESC) efficiently proliferated in 10 mM lactate, with lactate concentrations as high as 40 mM not affecting mESC pluripotency (Chaudhry et al., 2009; Martinez-Outschoorn et al., 2011). Also, miPSCs cultured in high lactate containing media exhibited no changes to cellular proliferation or pluripotency for lactate concentrations below 39 mM; although, supplementation of 22 mM lactate or higher resulted in a decreased lactate production flux (Gupta et al., 2017). However, these studies did not determine whether extracellular lactate was metabolized as a carbon source or if lactate production was inhibited.

Conversely, hESCs grown in media containing lactate above 11 mM exhibited

decreased cell growth (Chen et al., 2010). Likewise, lactate accumulation has been suggested to be the limiting factor in prolonged hiPSC expansion, with lactate accumulation adversely impacting growth rates (Horiguchi et al., 2018). Similar to mESCs, lactate production rates decreased for hESCs grown in media with lactate between 22-55 mM. Additionally, continuous passaging of hESCs in high extracellular lactate (11-22 mM) resulted in decreased pluripotency (Chen et al., 2010). Furthermore, elevated lactate conditions preferentially induced cardiomyocyte differentiation for iPSCs in glucose deficient differentiation media (Tohyama et al., 2013). On the other hand, Wilmes et al. 2017 showed that iPSCs were extremely sensitive to extracellular acidification, and that media acidification contributed to reduced glucose consumption, proliferation, and pluripotency (Wilmes et al., 2017). In addition, glycolysis, lactate production, and cell growth rates were modulated by media pH (Gupta et al., 2017; Liu et al., 2018; Wilmes et al., 2017). This suggests that daily media replacement partially is used for pH control and that improved media buffering capacity could alleviate some of these issues. Nonetheless, no previous hPSC study has fully characterized the effects of high extracellular lactate on intracellular metabolism.

2.2.4. Metabolic remodeling during the acquisition and loss of pluripotency

Metabolic remodeling appears to directly contribute to cell fate, with glycolysis playing a critical functional role in the acquisition and maintenance of pluripotent stem cells (DeBerardinis et al., 2008; Folmes et al., 2012; Folmes et al., 2011; Ryall et al., 2015). For example, PSCs have been shown to exhibit an increased dependence on glycolysis and

lactate production compared to primed and fully differentiated cells; this coincided with an elevated glucose contribution to nucleotide production (Folmes et al., 2011; Gaspar et al., 2014; Gu et al., 2016; Moussaieff et al., 2015; Panopoulos et al., 2012; Varum et al., 2011). This dependence on glycolysis was also coupled with an increased uncoupling of respiration and energy metabolism (Folmes et al., 2011; Zhang et al., 2011). Stimulation of glycolysis also was observed to promote maintenance of stemness for PSCs and augmented somatic reprogramming to iPSCs, while inhibition of specific glycolytic reactions in turn inhibited reprogramming (Ezashi et al., 2005; Folmes et al., 2011; Mohyeldin et al., 2010). Furthermore, somatic cells with elevated glycolytic metabolism reprogrammed more efficiently to iPSCs; this suggests a degree of metabolic memory of the somatic cells from which iPSCs are derived (Panopoulos et al., 2012). Interestingly, the shift towards aerobic glycolysis during somatic cell reprogramming preceded pluripotency gene expression (Folmes et al., 2011). Also, acetyl-CoA generated from glycolysis contributed to the epigenetic regulation of PSCs through histone acetylation and maintenance of an open chromatin structure (Moussaieff et al., 2015). These results demonstrate that maintaining a high glycolytic flux is a defining metabolic characteristic of PSCs and critical for maintaining stemness.

In addition to the metabolic shifts which have been observed during reprogramming of somatic cells to iPSCs, regulation of glucose metabolism guides cell differentiation towards each of the three germ layers—ectoderm, endoderm, and mesoderm (Folmes et al., 2013; Folmes and Terzic, 2016; Gaspar et al., 2014; Mathieu and Ruohola-Baker, 2017; Wanet et al., 2015). Spontaneous differentiation of PSCs is accompanied by a decrease in

glycolytic fluxes and increased OXPHOS; this metabolic shift also occurs prior to a loss of pluripotency. Furthermore, inhibition of glycolysis has been shown to promote spontaneous differentiation, suggesting that metabolism plays a functional role in regulating cell self-renewal and differentiation (Gu et al., 2016; Moussaieff et al., 2015; Zhang et al., 2011). With the increased OXPHOS and mitochondrial activity associated with spontaneous differentiation, mitochondrial structures also shift from the small, circular mitochondria found in PSCs to the elongated tubular structures found within somatic cells (Varum et al., 2011). And, differentiated cells have more mitochondrial mass and mitochondrial DNA (Cho et al., 2006; Prigione et al., 2010; Varum et al., 2011). With this, PSCs undergoing differentiation exhibits elevated levels of intracellular ATP and decreased lactate production (Cho et al., 2006; Folmes et al., 2011; Prigione et al., 2010; Varum et al., 2011). These alterations to the mitochondria support the shift from glycolysis to oxidative metabolism for differentiating cells and increases cellular energy production required to perform specific cell functions (Gaspar et al., 2014).

Understanding the dynamics of PSC metabolism is critical to initiate differentiation towards specific somatic cell types. As mentioned above, the general assumption has been that PSC metabolism shifts away from relying on glycolysis and towards a dependence on OXPHOS upon differentiation (Gu et al., 2016; Moussaieff et al., 2015; Varum et al., 2011; Zhang et al., 2011). These, previous studies have primarily compared PSC metabolism with either fully developed somatic cells or spontaneously differentiated cell populations (embryoid bodies), thus were not able to provide sufficient information about the unique metabolic remodeling associated with the development of germ layer-specific cells (Gu et

al., 2016; Moussaieff et al., 2015; Varum et al., 2011; Yanes et al., 2010; Zhang et al., 2011). In contrast, it was recently shown that metabolic remodeling during differentiation was germ layer-specific, with endodermal and mesodermal differentiation coupled with shifts from elevated glycolysis to oxidative phosphorylation, while PSCs undergoing ectodermal differentiation maintain elevated glycolytic fluxes (Cliff et al., 2017). Therefore, it is important to understand the unique metabolic requirements of each germ layer in order to generate fully developed, functional somatic cells, since metabolism contributes to the acquisition and loss of pluripotency.

2.2.5. Metabolic effects from xeno-free conditions

Given that the iPSC phenotype must be tightly controlled in order to develop high quality cell sources for cell therapies, the use of chemically defined xeno-free surface matrices and medias have become increasingly important to meet regulatory safety concerns. In contrast, pluripotent stem cells were first cultured directly on mouse embryonic fibroblast feeder cells (MEFs) or on animal-derived matrices (i.e. Matrigel); the first PSC media also contained fetal bovine serum (FBS) (Desai et al., 2015). There are several issues with using animal-derived components in cell therapies, including: the risk of animal pathogens exposure, broad lot-to-lot variability, and ill-defined components (Desai et al., 2015; Hughes et al., 2010; Nagaoka et al., 2010).

In addition to regulatory concerns, surface substrates and media components have both previously been shown to affect PSC metabolism in variable manners. HESCs grown on Matrigel-coated exhibited higher growth rates and metabolic activity than a number of

chemically defined surface matrices (Silva et al., 2015). In addition, PSCs shifted from glycolysis to oxidative phosphorylation when grown in 3D aggregates compared to 2D monolayers (Kropp et al., 2016; Silva et al., 2015). Interestingly, xeno-free cell culture media (Essential 8™ (E8) and mTeSR™) have been shown to alter lipid metabolism and increase ROS generation for iPSCs when compared to knockout serum replacement media (Bangalore et al., 2017; Zhang et al., 2016). Moreover, glutamine anaplerosis for both iPSCs and hESCs, increases 4-fold in chemically defined E8™ medium compared to conditioned medium (Zhang et al., 2016). Besides, the addition of 20% FBS to chemically defined mTeSR1™ medium resulted in increased reliance of hESCs on glutamine anaplerosis and decreased pluripotency (Rathjen et al., 2014). Transcriptomics and metabolomics analysis have shown that stem cell phenotypes converge with tightly controlled and reproducible conditions (Silva et al., 2015). Therefore, it is important to characterize PSCs in each media to understand the media-dependent growth and metabolic characteristics.

2.3. Metabolic flux analysis (MFA)

Metabolic flux analysis (MFA) is a powerful technique used to determine intracellular metabolic pathway fluxes and resolve the contribution of individual metabolic pathways to overall cell metabolism (Sa et al., 2015; Stephanopoulos et al., 1998). In MFA, intracellular fluxes are determined by coupling extracellular uptake and secretion rates of nutrients and waste products with a discrete stoichiometric metabolic network model (Stephanopoulos et al., 1998). While metabolomics approaches alone provide a view of the

cell potential, coupling concentration changes with a functional network through MFA offers a representation of cellular phenotype and pathway interactions (Niklas and Heinzle, 2011; Sauer, 2006; Stephanopoulos et al., 1998). The fluxome (compilation of intracellular metabolic fluxes) represents the interplay between the genome, transcriptome, proteome, and metabolome of a cell (Figure 2.4) (Sauer, 2006). As a result, MFA is frequently used to examine cell lines and cell culture conditions to compare the degree of engagement of individual metabolic pathways under each condition (Niklas and Heinzle, 2011). In addition, MFA can be used to determine targets for metabolic engineering and to optimize cell culture media and feed strategies based on cellular metabolic capacities (Bonarius et al., 1997; Wiechert, 2001).

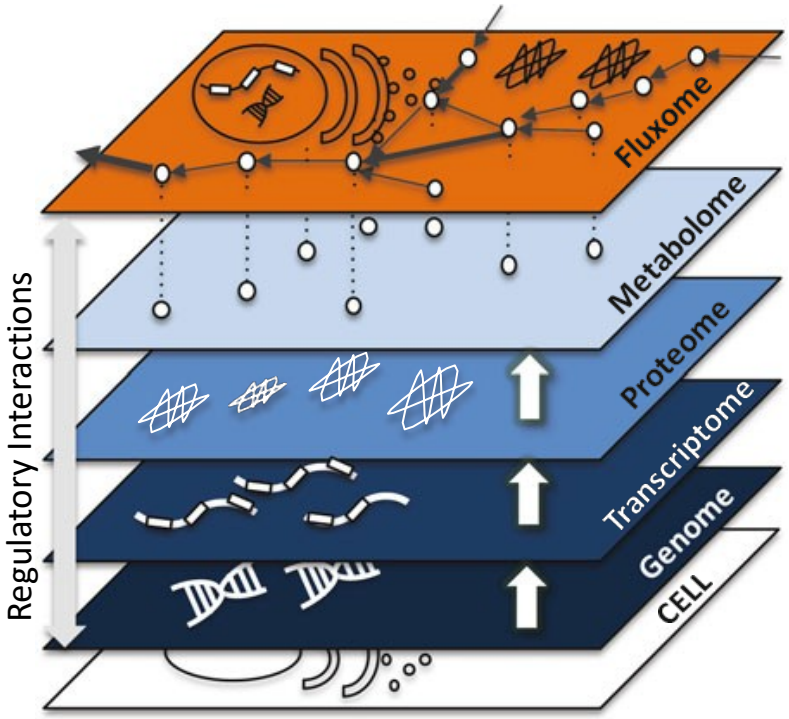

Figure 2.4. Schematic of the fluxome showing the cooperative regulation between the genome, transcriptome, proteome, and metabolome. Image from (Sa et al., 2015). Translated with permission from [Springer Nature]: [Springer Nature] [Springer eBook] (João V. Sá, Tiago M. Duarte, Manuel J. T. Carrondo et al.), [COPYRIGHT] (2015).

2.3.1. History of MFA

In classic MFA, extracellular consumption and production fluxes are coupled with a metabolic network model and a mass balance is performed to determine intracellular metabolic fluxes (Sa et al., 2015; Stephanopoulos et al., 1998). Also, in classic MFA, a pseudo steady-state hypothesis is assumed while cells are in exponential growth. The pseudo steady-state hypothesis implies that changes to metabolite pools due to small perturbations are rapid in comparison to cell growth and the intracellular pool sizes remain constant during an experiment (Stephanopoulos et al., 1998; Wiechert, 2001). One limitation to classical MFA is that complex intracellular pathways—bidirectional reactions, parallel pathways (glycolysis vs. pentose phosphate pathway), and cyclic fluxes (TCA cycle)—cannot be resolved well if only extracellular data is used (Sa et al., 2015; Stephanopoulos et al., 1998). In addition, classic MFA is limited by the number of accurate metabolite measurements used to constrain the metabolic model to physiologically feasible solutions (Sa et al., 2015).

More recently, MFA using stable isotopes has been used to uniquely determine complex intracellular fluxes, including cyclic pathways and bidirectional fluxes; these fluxes cannot be quantified reliably using unlabeled MFA approaches (Hiller and Metallo, 2013; Metallo et al., 2009; Nicolae et al., 2014; Sauer, 2006). Asymmetries of metabolite labeling which arise from branchpoint reactions allow for intermediate reaction fluxes to be determined (Figure 2.5A and B) (Stephanopoulos and Stafford, 2002). While the classic MFA approach is a relatively straightforward metabolite balance, with measured extracellular fluxes serving as the model constraints, ^{13}C-MFA is more computationally

challenging; the use of intracellular isotopomer measurements results in a nonlinear least squares problem (Niklas and Heinzle, 2011). Similar to classic MFA, ^{13}C-MFA also relies on the pseudo steady-state assumption of cell metabolism (Sa et al., 2015). Further, in ^{13}C-MFA, isotopically labeled intracellular metabolite pools are assumed to be at an isotopic steady-state (Kelleher, 2001). This means that the fractional isotope labeling of any given metabolite remains constant for the simulation timepoint; the distribution of labeling for a metabolite may fluctuate but the ratio of labeled-to-unlabeled metabolite does not change (Sa et al., 2015). Since current isotope measurement techniques cannot detect individual compartmental metabolite labeling (mitochondrial vs. cytosolic), a single pooled labeling approach is most often used for ^{13}C-MFA (Metallo et al., 2012; Zamboni, 2011).

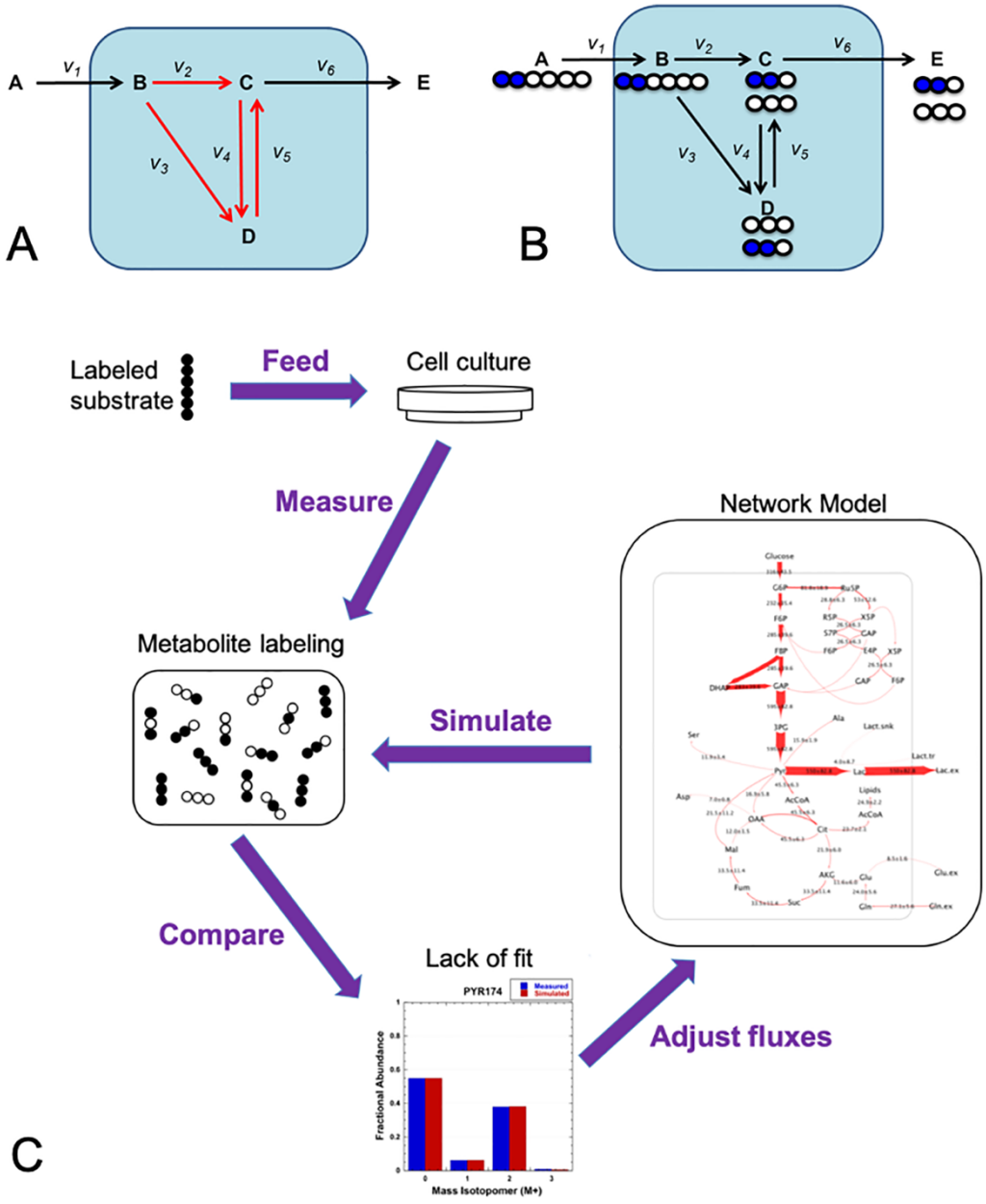

Figure 2.5. Metabolic network using classic MFA and ^{13}C-MFA. A) Bidirectional pathway using classic MFA. The substrate A and metabolite E can be measured extracellularly, but metabolites B, C, and D cannot be measured. It is impossible to calculate the intracellular fluxes v_2, v_3, v_4, and v_5, because the system is underdetermined (i.e. multiple solutions satisfy the observed measurements); B) Bidirectional pathway using ^{13}C-MFA. Measuring the isotope profile of metabolites C and D provide a unique solution to the intracellular fluxes. In addition, the ratio of labeled vs. unlabeled metabolites provides the degree of exchange occurring. C) Flow chart of ^{13}C-MFA proce**ss.** Image adapted from (Duckwall et al., 2013).

Given the relatively slow growth rates of mammalian cells and the long-time frame to reach isotopic steady-state, new MFA methods have shifted towards isotopically nonstationary MFA – INST-MFA (Jazmin and Young, 2013) or dynamic MFA (DMFA) (Leighty and Antoniewicz, 2011). Isotopic nonstationary MFA is ideal for systems where isotope labeling is slowly incorporated. Nonstationary MFA can be used to identify bottlenecks in cell metabolism for extended processes or due to environmental perturbations, and allow for modeling more dynamic bioprocessing systems, such as fed-batch cultures (Ahn and Antoniewicz, 2012; Leighty and Antoniewicz, 2011). In isotopic nonstationary MFA, a complete set of extracellular metabolite and intracellular mass isotopomer distribution (MID) time-series measurements are fit simultaneously to a metabolic model; this provides the metabolic transients throughout an entire cell culture process (Leighty and Antoniewicz, 2011).

2.3.2. ^{13}C-MFA in Chinese hamster cell culture

^{13}C-MFA has previously been used to characterize various mammalian cell systems for bioprocess development and metabolic engineering approaches (Altamirano et al., 2006; Ivarsson et al., 2015; Templeton et al., 2017b). As CHO cells serve as the primary mammalian host used for industrial manufacturing of therapeutic proteins, these cells were the focus of most mammalian cell bioprocess MFA studies (Wurm, 2004). Previously, ^{13}C-MFA has been used to evaluate the effects of growth phases (exponential vs. stationary), carbon sources, and pH on metabolism and protein production (Ahn and Antoniewicz, 2011; Ahn and Antoniewicz, 2013; Altamirano et al., 2006; Bonarius et al., 2001; Duarte

et al., 2014; Ivarsson et al., 2015; Lee et al., 2015; Sengupta et al., 2011; Templeton et al., 2013; Templeton et al., 2017b). In addition, ^{13}C-MFA has been used to determine the metabolic phenotypes of high productivity CHO cell lines to improve cell line engineering and clonal selection (Templeton et al., 2017a). Overall, the use of ^{13}C-MFA to understand CHO cell metabolism has resulted in improved bioprocessing conditions, higher peak cell densities, and higher product yields.

2.3.3. ^{13}C-MFA and cancer metabolism

Metabolic alterations have been suggested to play a functional role in cancer progression (Cairns et al., 2011). Therefore, MFA approaches have been used to establish the baseline metabolic states of various types of cancer. In addition, ^{13}C-MFA has been used to determine the response of cancer cells to different cell culture conditions, such as glucose and O_2 concentrations (Gaglio et al., 2011; Jiang et al., 2016; Metallo et al., 2012), and to investigate the effects of genetic mutations on cancer cell metabolism and invasiveness (Grassian et al., 2014; Jiang et al., 2017; Parker et al., 2017). In particular, hypoxia was shown to rewire TCA metabolism in cancer cells, which resulted in reductive carboxylation of glutamine to citrate via isocitrate dehydrogenase (IDH) for lipogenesis (Metallo et al., 2012; Wise et al., 2011). This metabolic flexibility was hypothesized to provide an adaptive advantage for cancer cells within the hypoxic tumor microenvironment (Mullen et al., 2012). Recently, reductive carboxylation has also been suggested to be a metabolic response to stress, including reactive oxygen species generation and lactate accumulation (Brodsky et al., 2019; Fendt et al., 2013; Jiang et al., 2016). Furthermore,

Pancreatic ductal adenocarcinoma was shown to consume more glucose and secrete more lactate when undergoing epithelial-mesenchymal transition (Liu et al., 2016). Recently, ^{13}C-MFA was used to elucidate the *in vivo* metabolism of non-small cell lung cancer (NSCLC), where Faubert et al. 2017 found that lactate was metabolized and contributed a greater fraction of carbon to the TCA cycle than glucose (Faubert et al., 2017; Hensley et al., 2016). In this way, MFA has been used to investigate the metabolic wiring of various types of cancer and uncover pathways for therapeutic targeting.

2.3.4. ^{13}C-MFA and stem cell metabolism

As mentioned previously, PSCs exhibit unique metabolic phenotypes during different stages of growth and differentiation (Gu et al., 2016; Moussaieff et al., 2015; Varum et al., 2011; Zhang et al., 2011). However, unlike with CHO and cancer cells, only a few studies have used MFA approaches to determine the fluxome of pluripotent stem cell metabolism. Instead, most studies to date have performed isotope tracer experiments and measured extracellular metabolite profiles, but have not perform ^{13}C-MFA or constructed a metabolic flux model (Carey et al., 2015; Gaspar et al., 2014; Gu et al., 2016; Moussaieff et al., 2015; Varum et al., 2011). Extracellular metabolism and intracellular pathway activity could be assessed, but the relative rates of intracellular reactions could not be determined. For MFA studies that have been performed in PSCs, these studies have focused primarily on the effects of cell culture conditions (oxygen and media), and metabolic shifts associated with differentiation (Table 2.1) (Badur et al., 2015; Correia et al., 2018; Sa et al., 2017; Sepúlveda et al., 2010; Turner et al., 2014; Zhang et al., 2016). In Turner et al.

(2014), a Warburg phenotype was observed for hESCs grown either in 20% or in 2% oxygen, with a stoichiometric conversion of glucose to lactate (Turner et al., 2014). MFA was performed using only extracellular metabolite measurements to constrain the metabolic model, which resulted in overlapping and broad flux determination between conditions and limited intracellular flux resolution (Turner et al., 2014). In Zhang et al. (2016) and Badur et al. (2015), a metabolic model of fatty acid metabolism was constructed for hESC and iPSC using ^{13}C-MFA to determine the effects of chemically defined media and enzymatic passaging, respectively; however, a general metabolic flux model for central carbon metabolism was not reported (Badur et al., 2015; Zhang et al., 2016). On the other hand, Sà et al. 2017 and Correia et al 2018 each used ^{13}C-MFA to construct detailed metabolic flux models for central carbon metabolism to describe the metabolic shifts associated with targeted differentiation of ESC and iPSC (Correia et al., 2018; Sa et al., 2017). A detailed metabolic flux model of central carbon metabolism has not been constructed using ^{13}C-MFA to elucidate the metabolic plasticity of PSCs during self-renewal. Hopefully in the future, understanding the metabolic regulations for iPSCs under cell culture relevant conditions will help to understand the metabolic features of stem cells and aid in the development of robust cell culture processes. Utilizing MFA to predict the phenotype of a cell population will be integral to understand the cellular response to cell culture processes and to generate high quality cell-based therapies.

Table 2.1 List of metabolic flux analysis studies for pluripotent stem cells.

Cell Types	Flux Analysis Method	Isotopes Used	Major Observations	Reference
mESC	MFA	None	- Analyzed the metabolic shifts between three different differentiation protocols: embryoid body formation, matrigel surface coating, and gelatin surface coating. - Observed differences in lactate metabolism between the embryoid body samples compared to the matrigel and gelatin samples. This difference was attributed to differences in oxygen availability between conditions.	(Sepúlveda et al., 2010)
hESC	MFA	None	- Compared metabolism in 20% and 2% oxygen. - Observed the Warburg phenotype in both conditions, with a stoichiometric conversion of glucose to lactate. - No changes to fluxome due to oxygen concentration.	(Turner et al., 2014)
hESC	^{13}C-MFA	[U-^{13}C] glucose	- Enzymatic passaging of hESCs caused reduction in glucose consumption, TCA metabolism, and de novo lipogenesis. Enzymatic passaging may have a lasting metabolic effect on hESCs.	(Badur et al., 2015)
hESC & hiPSC	^{13}C-MFA	[1,2-^{13}C] glucose, [U-^{13}C] glucose [U-^{13}C] glutamine [1-^{13}C] glutamine	- hPSCs were capable of utilizing either glycolysis or oxidative phosphorylation for growth. - Metabolic phenotype of hPSCs was dependent on nutrient availability.	(Zhang et al., 2016)
mESCs & astrocytes	^{13}C-MFA (INST-MFA)	[1-^{13}C] glucose [U-^{13}C] glutamine	- Observed a reduction in central carbon metabolism in the astrocytes and a slower incorporation of isotope labeling. - mESC consumed glutamine and utilized reductive carboxylation for lipogenesis, while astrocytes produced glutamine.	(Sa et al., 2017)
hESC and hiPSC	^{13}C-MFA	[1,2-^{13}C] glucose	- Compared hPSC metabolism to hPSC- derived cardiomyocytes (ESC and iPSC-CM). - Observed a shift from glycolysis to oxidative phosphorylation in hPSC-CMs cultured as 3D aggregates	(Correia et al., 2018)

CHAPTER THREE

HIGH EXTRACELLULAR LACTATE CAUSES REDUCTIVE CARBOXYLATION IN BREAST TISSUE CELL LINES GROWN UNDER NORMOXIC CONDITIONS

3.1. Abstract

In cancer tumors, lactate accumulation was initially attributed to high glucose consumption associated with the Warburg Effect. Now it is evident that lactate can also serve as an energy source in cancer cell metabolism. Additionally, lactate has been shown to promote metastasis, generate gene expression patterns in cancer cells consistent with "cancer stem cell" phenotypes, and result in treatment resistant tumors. Therefore, the goal of this work was to quantify the impact of lactate on metabolism in three breast cell lines (one normal and two breast cancer cell lines – MCF 10A, MCF7, and MDA-MB-231), in order to better understand the role lactate may have in different disease cell types. Parallel labeling metabolic flux analysis (^{13}C-MFA) was used to quantify the intracellular fluxes under normal and high extracellular lactate culture conditions. Additionally, high extracellular lactate cultures were labelled in parallel with [U-^{13}C] lactate, which provided qualitative information regarding the lactate uptake and metabolism. The ^{13}C-MFA model, which incorporated the measured extracellular fluxes and the parallel labeling mass isotopomer distributions (MIDs) for five glycolysis, four tricarboxylic acid cycle (TCA), and three intracellular amino acid metabolites, predicted lower glycolysis fluxes in the high lactate cultures. All three cell lines experienced reductive carboxylation of glutamine to

citrate in the TCA cycle as a result of high extracellular lactate. Reductive carboxylation previously has been observed under hypoxia and other mitochondrial stresses, whereas these cultures were grown aerobically. In addition, this is the first study to investigate the intracellular metabolic responses of different stages of breast cancer progression to high lactate exposure. These results provide insight into the role lactate accumulation has on metabolic reaction distributions in the different disease cell types while the cells are still proliferating in lactate concentrations that do not significantly decrease exponential growth rates.

3.2. Introduction

Since the 1920s, many types of cancers have been shown to rely heavily on glycolysis and lactate fermentation to produce energy rather than the more energy efficient complete oxidation of glucose in the mitochondria, even in the presence of sufficient oxygen. This metabolic state is called the Warburg Effect (Cairns et al., 2011; DeBerardinis et al., 2008; Heiden et al., 2009; Warburg, 1956). In addition, lactate can be utilized by cancer cells in the presence of glucose, a process known as the Reverse Warburg Effect (Kennedy and Dewhirst, 2010; Kennedy et al., 2013; Martinez-Outschoorn et al., 2011; Pavlides et al., 2010; Sonveaux et al., 2008). Not only does this capability to use lactate provide cancer cells a metabolic advantage *in vivo*, it seems to favor cancer progression. For example, when lactate was injected into mice with xenografts of the human breast cancer cell line MDA-MB-231, metastasis increased ten-fold (Bonuccelli et al., 2010). When the human breast cancer cell line MCF7 was exposed to lactate *in vitro*, genes associated with

"stemness" were upregulated and gene expression patterns consistent with the "cancer stem cell" phenotype were observed (Martinez-Outschoorn et al., 2011). In several other types of cancers, intratumoral lactate levels – which can rise to as high as 40 mM – correlated with treatment resistance as well as poor patient prognosis (Kennedy and Dewhirst, 2010). Further, it has been shown in xenotransplants and mouse cancer models that inhibiting the ability of cancer cells to utilize lactate can force the cells to become glycolytic and retard tumor growth through glucose starvation, while rendering the remaining cells more susceptible to radiation treatments (Sonveaux et al., 2008). Since lactate accumulation and its subsequent utilization by surrounding cancer cells appears to negatively affect cancer patient outcomes, deciphering the role of lactate at the metabolic level within central carbon metabolism is crucial.

Metabolic flux analysis (MFA) is a computational tool that is used to quantify the intracellular metabolic fluxes of individual metabolic pathways (Bonarius et al., 1997; Stephanopoulos, 1999). MFA can be used to compare changes in metabolic activity due to particular factors (Bonarius et al., 2001; Munger et al., 2008). Classical MFA uses extracellular uptake and secretion rates of nutrients and waste products, and a discrete metabolic network model of the relevant metabolic reactions (Hiller and Metallo, 2013; Nicolae et al., 2014). The use of stable isotopic tracers, typically ^{13}C-labeled nutrients, and the resulting mass isotopomer distribution (MID) data increases the resolution of individual fluxes within the defined metabolic reaction network (Metallo et al., 2009; Sauer, 2006; Tang et al., 2009). Several mammalian systems have been characterized including Chinese hamster ovary (CHO) cells at both stationary and exponential growth phases (Ahn and

Antoniewicz, 2011; Ahn and Antoniewicz, 2013; Templeton et al., 2013), MDA-MB-231 cells under various nutrient conditions (Gaglio et al., 2011), and several other cancer cell lines under hypoxia (Jiang et al., 2016; Metallo et al., 2012). There are several software tools available to assist researchers with resolving the intracellular fluxes including Metran, OpenFLUX, 13CFlux2, INCA and FiatFlux (Ahn and Antoniewicz, 2011; Quek et al., 2009; Weitzel et al., 2013; Young, 2014; Zamboni et al., 2009). All of these software tools rely upon regression analysis to solve the system of linear equations specified by the metabolic network.

The aim of this study was to determine the role of extracellular lactate on the metabolism of three different proliferating breast cell lines (one non-tumorigenic epithelial breast cell line and two breast cancer cell lines). Each cell line was grown in a low glucose control (e.g., normal or typical laboratory) media or in a high-lactate media, where sodium lactate was added to the control medium to make the high-lactate medium. The high-lactate concentration was selected for each cell line such that equivalent exponential growth rates for the control and high-lactate cultures were maintained. These equivalent exponential growth rates were important for the modeling assumptions for two reasons: 1) the quasi-steady state assumption was met equally well by both conditions, and 2) it allowed for normalizations of fluxes between the conditions for the same cell line based on biomass generation. Parallel labeling experiments were conducted with [1,2-^{13}C] glucose, [U-^{13}C] L-glutamine, and [U-^{13}C] sodium lactate, where the control cultures were only labeled with [1,2-^{13}C] glucose and [U-^{13}C] L-glutamine. The lactate labeling data for the high-lactate cultures provided uptake and direct intermediate tricarboxylic acid (TCA) cycle labeling

information. The intracellular metabolic fluxes were predicted for each cell line and each condition from the glucose and glutamine labeling data.

3.3. Materials and Methods

3.3.1. Cell lines and media formulations

MCF 10A (ATCC® CRL-10317™), MCF7 (ATCC® HTB-22™) and MDA-MB-231 (ATCC® HTB-26™) cells were from the American Tissue Culture Collection (ATCC). MCF 10A cells are a non-tumorigenic breast cell line, MCF7 cells are a tumorigenic, luminal breast cancer cell line, and MDA-MB-231 cells are a metastatic, basal breast cancer cell line (Zancan et al., 2010). Dulbecco's modified Eagle medium (DMEM) without glucose, glutamine, sodium pyruvate, and phenol red (Life Technologies) was used as the growth media. The growth media was supplemented to contain 5 mM glucose (Thermo Fisher), 3 mM glutamine (Life Technologies), 10% dialyzed fetal bovine serum (dFBS, Life Technologies), 100 U/mL penicillin, and 100 □g/mL streptomycin (100X Penicillin-Streptomycin solution, Life Technologies). High-lactate cultures were supplemented with 10 mM sodium L-lactate (Sigma) for the MCF 10A cultures and 20 mM for the MCF7 and MDA-MB-231 cultures. The isotopic tracers were [1,2-^{13}C] glucose, [U-^{13}C] L-glutamine, and [U-^{13}C] sodium lactate, all purchased from Sigma-Aldrich.

3.3.2. Cell growth and parallel labeling experiments

All cell lines were seeded at 2 x 10^4 cells/cm^2 into either 6-well plates or T-25 flasks in the control growth media. Cells were cultured at 37°C in a 5% CO_2 humidified incubator.

After 24-h, the media for the MDA-MB-231 cultures was exchanged and the experimental conditions were introduced. The media exchange time is used to set time 0 for all cell lines. For MCF 10A and MCF7 cell lines the lag phase was longer, so the media was replenished at 24-h post seeding. The media was exchanged 48-h post seeding for MCF10A and MCF 7 to introduce the experimental conditions. For clarity, the full experimental setup is shown in Figure 3.1. Cell numbers and extracellular metabolite concentrations were measured as shown in Figure 3.1, where all times are relative to the isotope media exchange. Cell numbers and glucose and lactate concentrations were obtained from the six-well plates, while the amino acid concentrations were obtained from the T-25 flasks. Cells for intracellular metabolite analysis were obtained from the T-25 flasks 24-h after the media exchange, since 24-h has previously been shown to provide sufficient amount of time for isotopic steady state to be achieved for intracellular glycolytic metabolites in CHO cells (Ahn and Antoniewicz, 2013). Parallel cultures of glucose (95% molar enriched [1,2-^{13}C] glucose) and glutamine tracers (95% molar enriched [U-^{13}C] L-glutamine) were performed for the control cultures, whereas the high-lactate cultures also had parallel replicates for the lactate tracer (50% molar enriched [U-^{13}C] sodium L-lactate). Six-well plates (Nunc) were used to obtain cell numbers and glucose and lactate concentrations with six replicates for each time point. T-25 flasks were used to obtain extracellular amino acid concentrations and intracellular MID measurements in triplicate.

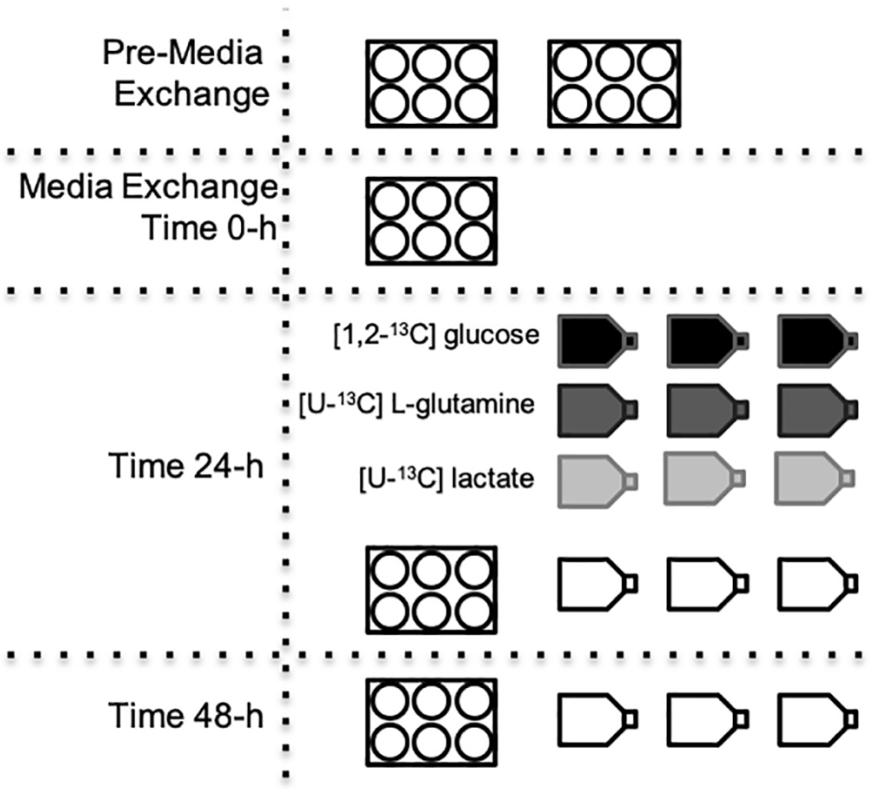

Figure 3.1. Experimental setup for the parallel labeling experiments for each of the three breast cell lines. The four or five six-well plates and 15 T-25 flasks were seeded simultaneously for each cell line examined. The times shown indicate when the plates or flasks were harvested for analysis relative to the isotope media exchange. Isotopic labeling is graphically shown by shading (white – no isotope, black – glucose, dark grey – glutamine, and light grey – lactate). The six-well plates did not contain isotopically-labeled media.

3.3.3. Cell numbers, and glucose and lactate concentrations

Cell numbers were obtained using the Scepter 2.0 Handheld Automated Cell Counter (Millipore). Glucose and lactate concentrations were measured using a YSI 2700 Bioanalyzer.

3.3.4. Preparation of samples for gas chromatography-mass spectrometry analysis

Intracellular and extracellular metabolites and specific metabolite fragments used for identification were extracted and derivatized according to the protocol outlined by Ahn and Antoniewicz (Ahn and Antoniewicz, 2011), with a few minor changes. Samples were incubated and derivatized for 60 min, and the final sample volumes were increased to 1 mL after derivatization by adding additional pyridine. The injection volumes were 3 μL and samples were injected in splitless mode. Amino acid standards were used to calculate amino acid concentrations in the [U–^{13}C] algal amino acid solution, which were then used to quantify the amino acid concentrations in the extracellular medium.

3.3.5. Extracellular amino acid concentration and intracellular MID measurements

GC-MS analysis was performed using a Hewlett Packard 7683 GC equipped with an HP-5 (30 m x 0.32 mm i.d. x 0.25 μm; J&W Scientific) capillary column, interfaced with a Hewlett Packard 5973 MS operating under ionization by electron impact as 70 eV and 200°C ion source temperature. The injection port and interface temperatures were both 250°C while helium flow was maintained at 1 mL/min. Mass spectra were recorded in full

scan mode for amino acid quantification and in single ion mode (SIM) for MIDs as well as internal standards and standardization curves. MIDs were obtained by integration of single ion chromatograms and corrected for natural isotope abundances using the Metran software (Fernandez et al., 1996; Yoo et al., 2008).

3.3.6. Determination of biomass specific consumption and production rates

Specific consumption and production rates for nutrients and waste metabolites in the extracellular medium were determined based on cell growth rate and nutrient time profiles, where the times are relative to media exchange and not to seeding (Meadows et al., 2008). For each sample calculation, statistical analysis of the amino acid concentration data was conducted using JMP 10.0.0 (SAS Institute, Inc.). The generalized linear model was used where cell line, condition, and time were examined as effectors of the amino acid concentration ($p \leq 0.05$). All amino acid concentrations were determined to be significantly affected by time ($p \leq 0.05$). Several amino acid concentrations were not significantly affected by cell line, condition, or both ($p > 0.05$). The spontaneous glutamine degradation rate was accounted for in the glutamine flux calculation, with a degradation rate of 0.0019 h^{-1} (Meadows et al., 2008).

3.3.7. Metabolic network model

To model central carbon metabolism for the three breast cell lines, a general mammalian cell model was used. This generalized mammalian cell model was adapted from the previously developed framework by Ahn and Antoniewicz (2013). Major

reactions for glycolysis, the pentose phosphate pathway (PPP), the TCA cycle, amino acid metabolism, lactate metabolism, and fatty acid metabolism were included in the mammalian cell model. Carbon flux to cellular biomass was broken down into two separate compartments – the Biomass pool, which included proteins, nucleotides, and carbohydrates, and the Lipid Biomass pool, which included lipids and phospholipid (Ahn and Antoniewicz, 2013; Bonarius et al., 1996; Metallo et al., 2012). The Biomass and Lipid Biomass fractions were based on cell mass compositions from literature for hybridoma and MCF7 cells (Bonarius et al., 1996; Meadows et al., 2008; Sheikh et al., 2005), and the reported dry cell weight for hybridoma (470 pg per cell) (Bonarius et al., 1996). These values were used for all three cell lines. The dry cell weights were used to convert the measured growth rates to biomass-specific fluxes (Bonarius et al., 1996). In order to reduce the complexity of the model to align with the number and detail of measurements taken, only citrate and acetyl-CoA were modeled with both cytosolic and mitochondrial compartments (Ahn and Antoniewicz, 2013; Metallo et al., 2012; Metallo et al., 2009). A lactate exchange reaction was included to account for dilution of the intracellular labeled lactate pool by uptake of exogenous lactate (v38 in Table B1 in Appendix B). This type of exchange reaction has previously been used to account for the dilution of carbon dioxide labeling and does not influence the intracellular carbon balance (Leighty and Antoniewicz, 2012). Carbon dioxide was treated as an unbalanced metabolite and was not measured. Oxygen uptake was excluded from the model and was also not measured. Cofactor balances, such as NADH and NADPH were not included in the model, as different isozymes have varying cofactor requirements and the inclusion of these assumptions can skew subsequent analysis

(Ahn and Antoniewicz, 2011). The breast cell metabolic flux model has 38 reactions. The full breast cell metabolic flux model with atom transitions is included in Table B1 in Appendix B.

3.3.8. Metabolic flux analysis

^{13}C-Metabolic flux analysis was performed using the software package Metran (Yoo et al., 2008), which utilizes the elementary metabolite unit (EMU) framework (Antoniewicz et al., 2007b). Metabolic fluxes were estimated using experimentally measured-values for extracellular consumption and production rates and from MIDs obtained for intracellular metabolites. In Metran, the intracellular and extracellular metabolic flux predictions were based on quantities that minimized the variance-weighted sum of squared residuals (SSRes) between the measured values input into the model and the simulated values. Metran can process MID data from parallel labeling experiments to predict the metabolic fluxes, a capability that has been validated using both *E. coli* and CHO cells experimental data (Ahn and Antoniewicz, 2013; Leighty and Antoniewicz, 2012). In this study, random initial fluxes were used, and the MID error was calculated from the biological replicates. Additionally, a minimum MID error threshold of 0.6 mol% was applied if the biological error was less than 0.6 mol%; this falls within the standard error range that has been used in previous MFA studies (Ahn and Antoniewicz, 2013; Metallo et al., 2009). Most of the standard errors observed in this study for the biological replicates were higher than the 0.6 mol% machine error used previously when replicates were not available (Ahn and Antoniewicz, 2013). The MIDs metabolites labeled by [1,2-^{13}C] glucose included in the

MFA simulations were 3-phosphoglycerate (3PG), dihydroxyacetone phosphate (DHAP), pyruvate, lactate, and alanine. The MIDs metabolites labeled by [U-^{13}C] glutamine included in the MFA simulations were succinate, malate, α-ketoglutarate (AKG), glutamate, citrate, glutamine, and pyruvate. The MIDs of metabolites labeled by [U-^{13}C] lactate were not included in the MFA simulations.

The extracellular flux for each metabolite was calculated as described in Meadows et al. (2008) (Meadows et al., 2008), and adapted to the media exchange time as:

$$Flux\left(\frac{nmol}{10^6\ cells \cdot h}\right) = \frac{10^9 \mu (C_{48} - C_{24})}{X_{24}(e^{\mu t} - 1)} \qquad \text{(Eq. 1)}$$

where, μ is the growth rate (h^{-1}). C_{48} and C_{24} are the individual metabolite concentrations (mM) at 48 and 24 hours after the media exchange, respectively. X_{24} is the cell concentration (cells/mL) at 24 hours after the media exchange. In Meadows et al. (2008) (Meadows et al., 2008), only the term X_0 was used in the flux equation instead of X_{24}, as their flux calculation included the initial time, time 0. In the current study, the flux calculation only includes the time points 24-h and 48-h, thus the cell concentration uses the 24-h time point as the reference point for the cell concentration. The value for the term *t* is 24 hours for all of the current flux calculations.

3.3.9. Statistical Analysis

Statistical analysis was performed using the software JMP pro 10 (SAS Institute, Cary, NC). The generalized linear model (GLM) procedure ($p \leq 0.05$) and least squares method (LS mean) with Tukey HSD (honestly significant difference) were used to

determine if growth rates, cell numbers 24-h after the medium exchange, glucose, lactate, and amino acid concentrations were affected by the cell line and/or condition. To estimate the standard deviation for each metabolite flux, Monte Carlo simulations were conducted using 1,000,000 iterations of the flux equation, where the standard deviation for each input μ, $(C_{48} - C_{24})$, and X_{24} was applied. For Metran, metabolic flux simulations were determined to have converged when a global solution was achieved that satisfied the accepted SSRes criteria, unless otherwise specified. This was determined from analyzing the simulated fit results via a chi-square statistical test to measure goodness-of-fit (Antoniewicz et al., 2006; Antoniewicz et al., 2007a). After convergence, 95% confidence intervals were generated for all parameters based on the SSRes parameter (Antoniewicz et al., 2006).

3.4. Results

3.4.1. Cell growth

To determine the effects of high extracellular lactate on breast cancer metabolism, three human breast cell lines, MCF 10A, MCF7, and MDA-MB-231, were grown under both control and high-lactate conditions. MCF 10A is a non-tumorigenic epithelial cell line, and MCF7 and MDA-MB-231 are two different stages of breast cancer (tumorigenic, luminal and metastatic, basal respectively). Sodium lactate was used for the high-lactate conditions to reduce the initial media pH shift and prevent shocking the cells due to the lactate addition. For MCF7 and MDA-MB-231, the high-lactate culture media consisted of the control media supplemented with 20 mM sodium lactate. For MCF 10A, the high-lactate culture

media consisted of the control media supplemented with 10 mM sodium lactate. MCF 10A cells were unable to grow under the 20 mM lactate stress; however, MCF 10A could grow at equal growth rates to the control culture in 10 mM lactate-supplemented media. Both 10 mM and 20 mM lactate represent normal physiological concentration ranges (Kennedy and Dewhirst, 2010; Kennedy et al., 2013; Martinez-Outschoorn et al., 2011). Regrettably, the MCF 10A high-lactate cultures had to be cultured at a lower lactate concentration than the MCF7 and MDA-MB-231 high-lactate cultures, which prevented direct comparisons across all three cell lines. Yet, maintaining equal growth rates between the control and high-lactate conditions within each cell line was central to the experimental design. This allowed for any observed metabolic changes to be attributed to media condition alone and not to a shift in growth rate.

The control media was composed of Dulbecco's modified Eagle medium (DMEM) with a lower initial glucose concentration (5 mM) than standard DMEM (25 mM), in order to be more representative of physiological glucose concentrations, where 5 mM is equal to 0.90 g/L or 90 mg/dL. To minimize the interference of other carbon sources on the labeling of the intracellular metabolites, other potential carbon sources in the media were reduced or eliminated. For example, sodium pyruvate was eliminated from the standard DMEM formulation, and dialyzed fetal bovine serum (FBS) was used to eliminate glucose and glutamine carryover and reduce the unquantified amino acids from FBS. These modifications to the media allowed for the labeling studies to be conducted with 95% labeled glucose and glutamine.

To characterize cell growth, cell counts were taken every 24-h; growth profiles for the three cell lines are shown in Figure 3.2. All three cell lines exhibited significant reproducible lag phases when passaged in the control media, likely due to either the lower than normal glucose concentration and/or the lack of pyruvate in the media, despite previously being adapted to this media formulation for over three passages. The lag phases were 48-h for MCF 10A and MCF7 and 24-h for MDA-MB-231. After the lag phases, the culture media was exchanged to either fresh control media or the high-lactate media, as indicated at time 0 in Figure 3.2. For the labeling studies, ^{13}C isotopes replaced the unlabeled glucose, glutamine, or lactate in the parallel cultures, at the same concentrations. After the lag phase and media exchange, cells from all culture conditions maintained exponential growth for 48-h, confirming that the high-lactate media did not significantly affect the growth rates of any cell line ($p > 0.05$). The exponential growth rates were 0.017 h^{-1}, 0.018 h^{-1}, and 0.021 h^{-1} for the MCF 10A, MCF7, and MDA-MB-231 cell lines, respectively. Previously, 24-h was shown to be sufficient amount of time for isotopic steady-state to be reached for glycolysis and PPP metabolites from glucose labeling, while TCA metabolites also approach isotopic steady state from glutamine labeling within 24-h for mammalian cells (Ahn and Antoniewicz, 2013; Metallo et al., 2009). Therefore, in these studies, samples for intracellular MID analysis were taken 24-h after ^{13}C-labeled media addition, indicated by the black boxes. The experiments were designed such that all cultures were in the mid-exponential phase at the time of harvest for intracellular MID analysis (Figure 3.2); this represents a pseudo-steady state, a condition consistent with the MFA assumptions (Stephanopoulos, 1999).

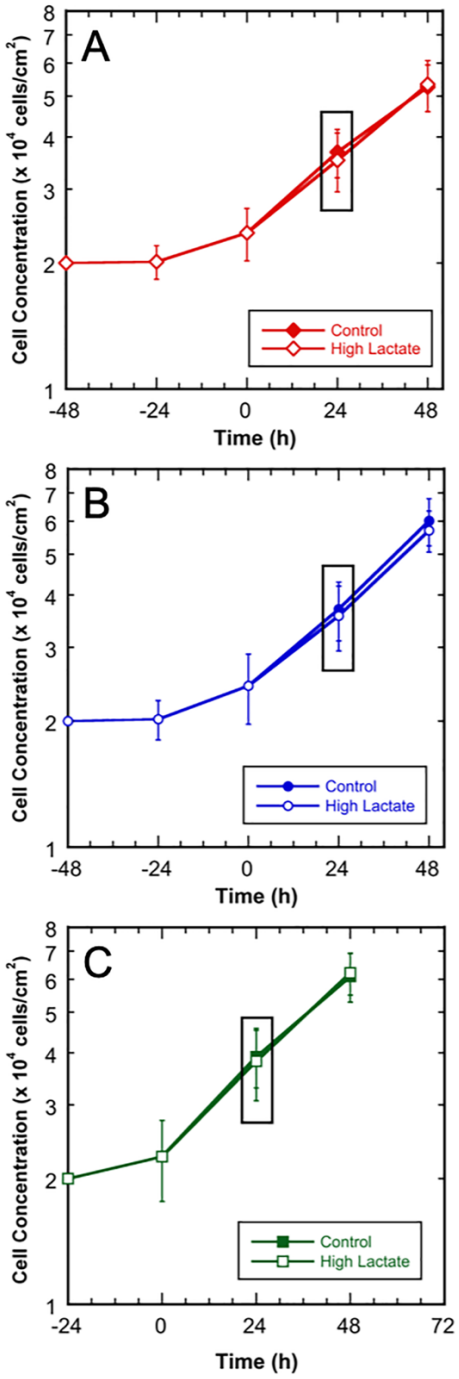

Figure 3.2. Growth profiles for MCF 10A, MCF7, and MDA-MB-231 cultures in control and high-lactate media. The isotope media exchange occurred at 0-h and samples for MID analysis were taken at 24-h. Control media – ◆●■; high-lactate media – ◇○□. A) MCF 10A – ◆◇; B) MCF7 – ●○; and C) MDA-MB-231 – ■□. Error bars represent standard deviations.

3.4.2. Glucose, lactate, and amino acid metabolism

The control and high-lactate conditions exhibited equal growth rates within each cell line; however, high extracellular lactate resulted in reduced glucose utilization and reduced lactate accumulation for each cell line ($p \leq 0.05$). Figure 3.3 shows the glucose and lactate concentration time profiles for each cell line and condition. The average glucose and lactate concentrations for all the 24-h and 48-h samples are listed with the standard deviations in Tables A1-A3 in Appendix A. Glucose and lactate fluxes were calculated using concentrations measured at 24-h and 48-h with the cell number at 24-h and the growth rates as per Eq.1 and are listed with standard deviations in Table 3.1. The standard deviations for the glucose and lactate fluxes were determine using Monte Carlo simulations due to sample independence (Forbes et al., 2006). The three control cultures exhibited higher glycolytic efficiencies compared to the high lactate cultures. Specifically, the glycolytic efficiencies for the control conditions were 1.7, 1.5, and 1.8 moles lactate produced per mole glucose consumed, respectively, for the MCF 10A, MCF7, and MDA-MB-231 cell lines. The glycolytic efficiencies for the high-lactate conditions were 1.4, 0.8 and 1.3 moles lactate produced per mole glucose consumed, respectively, for MCF 10A, MCF7, and MDA-MB-231 cell lines. In comparison, the theoretical maximum glycolytic efficiency is 2.0 moles lactate produced per mole glucose consumed (Zancan et al., 2010).

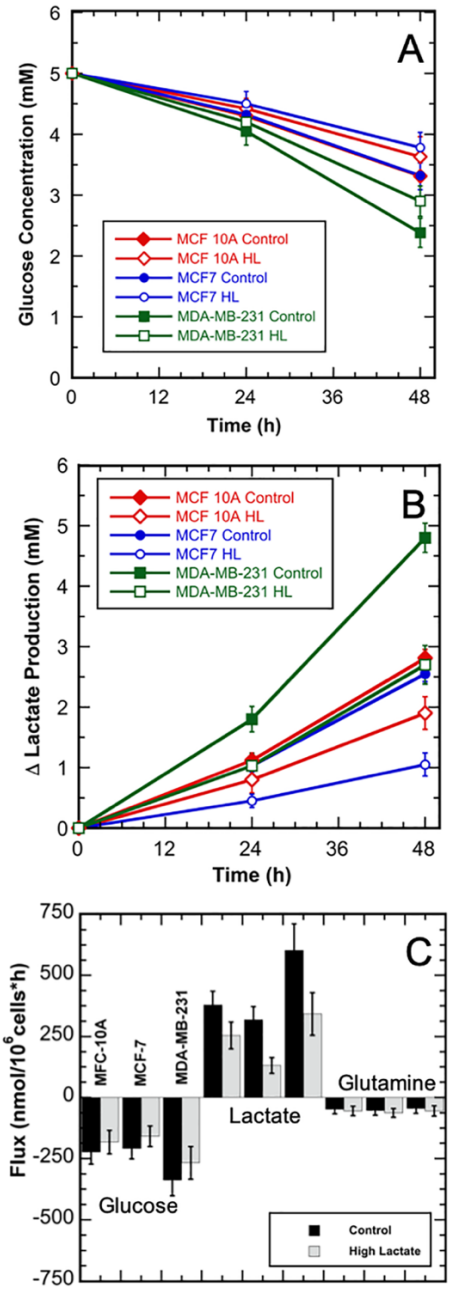

Figure 3.3. Glucose and lactate concentration and glucose, lactate, and glutamine flux profiles for the three breast cell line cultures in the control and high-lactate media shown relative to the time of the media exchange. A) Glucose concentrations; B) Change in lactate concentrations. Control media – ◆●■; high-lactate (HL) media – ◇○□. MCF 10A – ◆◇, MCF7 – ●○, and MDA-MB-231 – ■□. C) Glucose, lactate, and glutamine fluxes. Control media – ■; high-lactate media – ■. All error bars represent standard deviations

Table 3.1. Measured extracellular fluxes for glucose, lactate, and amino acids for the MCF 10A MCF7, and MDA-MB-23 cell lines in the control and high-lactate media. Standard deviations were determined using Monte Carlo simulations of the flux equation due to sample independence (Zancan et al., 2010). Negative values represent consumption rates and positive values represent production rates.

Flux (nmol/10^6 cells·h)												
Cell line	**MCF 10A**				**MCF7**				**MDA-MB-231**			
Condition	**Control**		**High-Lactate**		**Control**		**High-Lactate**		**Control**		**High-Lactate**	
Metabolite	**Flux**	**SD**	**Flux**	**SD**	**Flux**	**SD**	**Flux**	**SD**	**Flux**	**SD**	**Flux**	**SD**
Glucose (N=6)	-222	51	-182	48	-208	44	-158	42	-337	65	-267	67
Lactate (N=6)	379	56	254	55	318	54	131	32	603	108	342	87
Glutamine (N=3)	-48	18	-55	19	-53	19	-63	18	-44	21	-55	21
Amino Acid (N=3)												
Alanine	11	1.5	11	1.9	14	2.3	12	2.3	10	1.8	8.2	2.0
Aspartate	4.9	0.8	3.7	0.7	6.5	1.3	5.4	1.1	3.5	0.7	4.5	1.1
Glutamate	12	1.9	10	1.8	11	2.0	12	2.3	8.5	1.6	10	2.5
Glycine	6.2	1.6	5.7	3.1	9.6	3.0	9.4	3.2	7.8	2.1	7.0	2.6
Isoleucine	-8.3	2.3	-8.4	2.0	-9.5	2.0	-9.2	2.3	-4.7	1.6	-8.4	2.4
Leucine	-6.6	2.1	-7.5	2.7	-8.3	2.7	-7.5	2.2	-4.7	2.1	-8.8	2.4
Methionine	-2.6	1.0	-1.5	0.8	-3.1	1.1	-2.2	0.8	-1.4	0.5	-2.2	1.0
Phenylalanine	-4.7	1.9	-4.4	1.5	-3.8	1.3	-3.8	1.5	-3.4	0.9	-4.0	2.0
Proline	1.5	0.3	1.3	0.3	2.8	0.5	2.3	0.5	0.8	0.2	1.3	0.3
Serine	-19	2.9	-20	4.0	-20	4.0	-23	5.2	-16	3.4	-20	5.0
Threonine	-1.9	1.1	-1.9	0.9	-1.2	0.5	-1.2	0.6	-1.2	0.6	-1.6	0.9
Tyrosine	-3.6	1.5	-3.7	1.9	-4.0	1.2	-3.8	1.5	-3.5	1.6	-3.8	1.8
Valine	-5.8	1.7	-6.2	1.6	-9.4	2.0	-10	3.3	-6.3	1.7	-9.1	2.3

Amino acid metabolism plays an important role in protein and nucleotide synthesis, and anaplerosis for mammalian cells. Extracellular amino acid concentrations were measured at 24-h and 48-h after the media exchange to quantify amino acid fluxes. Prior to calculating the amino acid fluxes, statistical analysis was conducted for the amino acid concentrations with respect to culture condition, cell line, and time. All the amino acid concentrations were statistical different with respect to time ($p \leq 0.05$), such that fluxes could be calculated; however, many of the amino acid concentrations were not statistically different between the cell lines or culture condition ($p > 0.05$). For example, glutamine (Figure 3.3C), methionine, phenylalanine, and tyrosine concentrations were not significantly different between cell lines or between the culture conditions ($p > 0.05$). Whereas, aspartate, glutamate, glycine, and threonine concentrations were significantly different between cell lines ($p \leq 0.05$), but were not significantly different within the same cell line between the control and high-lactate conditions ($p > 0.05$). In addition, leucine concentrations were not significantly different between cell lines ($p > 0.05$), but were significantly different between the control and high-lactate conditions ($p \leq 0.05$). Table 3.1 lists the calculated amino acid fluxes with the standard deviations determined using Monte Carlo simulations due to sample independence (Forbes et al., 2006). The average amino acid concentrations for all the 24-h and 48-h samples with the standard deviations are shown in Tables A1-A3 in Appendix A.

3.4.3. Lactate tracer update

To further understand the role of lactate as a metabolic substrate, cells were grown with

^{13}C-labeled lactate for the high extracellular lactate conditions. This allowed for intracellular metabolite labeling due to lactate uptake and metabolism. Labeled intracellular metabolites measured included: lactate, pyruvate, alanine, citrate, AKG, glutamate, succinate, fumarate, malate, and aspartate (Figure 3.4A). The intracellular lactate MIDs from [U-^{13}C] lactate labeling of the MCF 10A, MCF7, and MDA-MB-231 cultures exposed to 10 mM, 20 mM, and 20 mM extracellular lactate, respectively, are shown in Figure 3.4B. MCF7 cells had the highest intracellular lactate isotopomer labeling. The TCA metabolites had low levels of labeling, which was primarily M1, for all cell lines. These results indicate that extracellular lactate was consumed by the cells even in the presence of glucose. For completeness, Figure C1 in Appendix C illustrates the intermediate TCA metabolite labeling from [U-^{13}C] lactate, as the primary carbon source, as well as the TCA carbon labeling from unlabeled pyruvate and dilution of the labeled metabolite pools. All raw uncorrected lactate-derived MIDs for the three cell lines and for both conditions are provided in Tables D1-D3 in Appendix D.

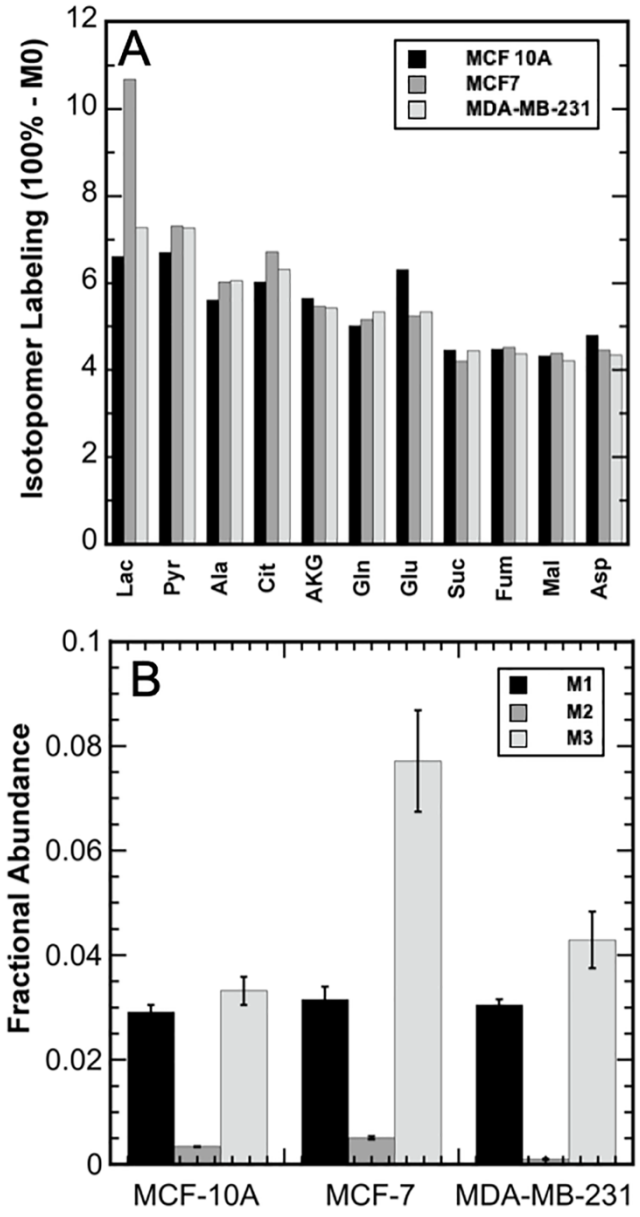

Figure 3.4. Uptake of [U-^{13}C] lactate by the three breast cell lines. A) Percent carbon labeling for intracellular metabolites due to extracellular [U-^{13}C] lactate in the media. MCF 10A – ■; MCF7 – ■; and MDA-MB-231 – ■. B) Lactate intracellular mass isotopomer distributions (MIDs) due to extracellular [U-^{13}C] lactate. Control media – ■; high-lactate media – ■. Error bars represent standard deviations.

3.4.4. Intracellular labeling from [1,2-^{13}C] glucose and [U-^{13}C] glutamine

[1,2-^{13}C] glucose and [U-^{13}C] glutamine isotopes were used for the parallel labeling studies to characterize the relative metabolic contribution of each substrate and estimate intracellular metabolic fluxes for glycolysis, the PPP, and the TCA cycle. These isotopes have previously been shown to be suitable tracers for characterizing fluxes for mammalian cells through glycolysis and the PPP ([1,2-^{13}C] glucose) and the TCA cycle ([U-^{13}C] glutamine) pathways (Metallo et al., 2009). The percent isotopomer labeling (100% - M0) was calculated for each metabolite using MIDs corrected for natural abundance (Ahn and Antoniewicz, 2013; Fernandez et al., 1996). Using [1,2-^{13}C] glucose, the percent isotope labeling for DHAP, 3PG, pyruvate, alanine, and lactate were 40% or higher for all three cell lines. No significant differences were observed for MIDs from glycolytic metabolites (DHAP, 3PG, pyruvate, alanine, and lactate) between the three cell lines and between the control and high-lactate conditions. These results reflect the consistently high flux through glycolysis for each of the three cell lines and the equivalent growth rates between conditions within a given cell line. These results also confirm that the 24-h labeling time was sufficient to reach isotopic steady state for [1,2-^{13}C] glucose. The intracellular MID profiles for all three cell lines are included in Figure E1 in Appendix E. All raw uncorrected MIDs for each cell line and condition are provided in Tables D1-D3 in Appendix D. Additionally, all the measured MIDs, corrected for natural isotope abundance, are shown in Figures E1 and E2 in Appendix E.

For the three cell lines and both conditions, glutamine, AKG, and glutamate were highly labeled from [U-^{13}C] glutamine. Using [U-^{13}C] glutamine, the observed isotopomer

labeling for intracellular glutamine, AKG and glutamate was over 70%. Figure 3.5 shows the control and high lactate intracellular MID profiles for MDA-MB-231 from [U-^{13}C] glutamine, as an example, for the TCA metabolites. Pyruvate and lactate were minimally enriched from the glutamine isotope across the cell lines and both conditions, where Figure 3.5 shows the MDA-MB-231 data. All the MID profiles for the three cells lines for both conditions are shown in Figure E2 in Appendix E. For MCF 10A and MDA-MB-231, the high-lactate condition resulted in a higher percent isotope labeling of pyruvate and lactate as compared to the control condition. For MCF7, the trend was reversed – the percent isotope labeling of pyruvate and lactate were lower in high-lactate condition compared to the control condition.

The TCA metabolites succinate, fumarate, malate, and citrate were all significantly labeled by the [U-^{13}C] glutamine tracer. The MID profiles for these metabolites were similar for all three cell lines; however, citrate MIDs were significantly different between the control and high-lactate cultures within a cell line, indicating the effect of lactate was significant. More specifically, a significant increase in M5 citrate labeling was observed in the high-lactate conditions for all three cell lines (Figure 3.6A). Increased M5 labeling also corresponded with decreased unlabeled citrate and increased percent isotopomer labeling. Succinate, fumarate, and malate were mostly M2 and M4 labeled from ^{13}C-glutamine labeling, as shown in Figure 3.5 for MDA-MB-23. Figure E2 in Appendix E shows the labeling for the other two cell lines.

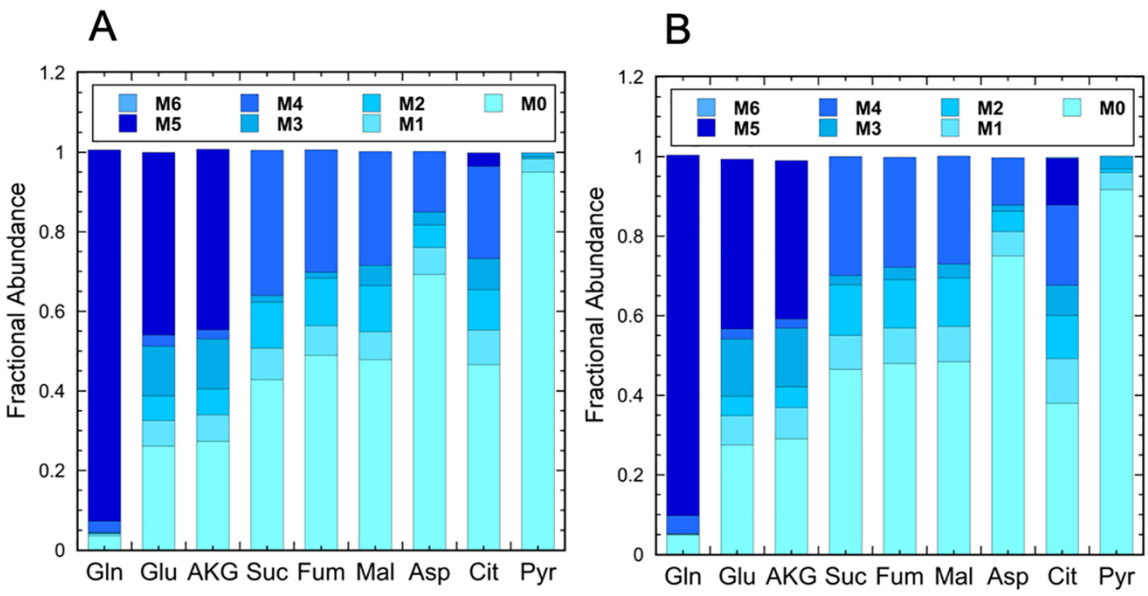

Figure 3.5. Mass isotope distributions (MIDs) for the TCA metabolites from the [U-^{13}C] glutamine labeling of the MDA-MB-231 cells cultured in the control and high-lactate media. A) Control media; B) High-lactate media.

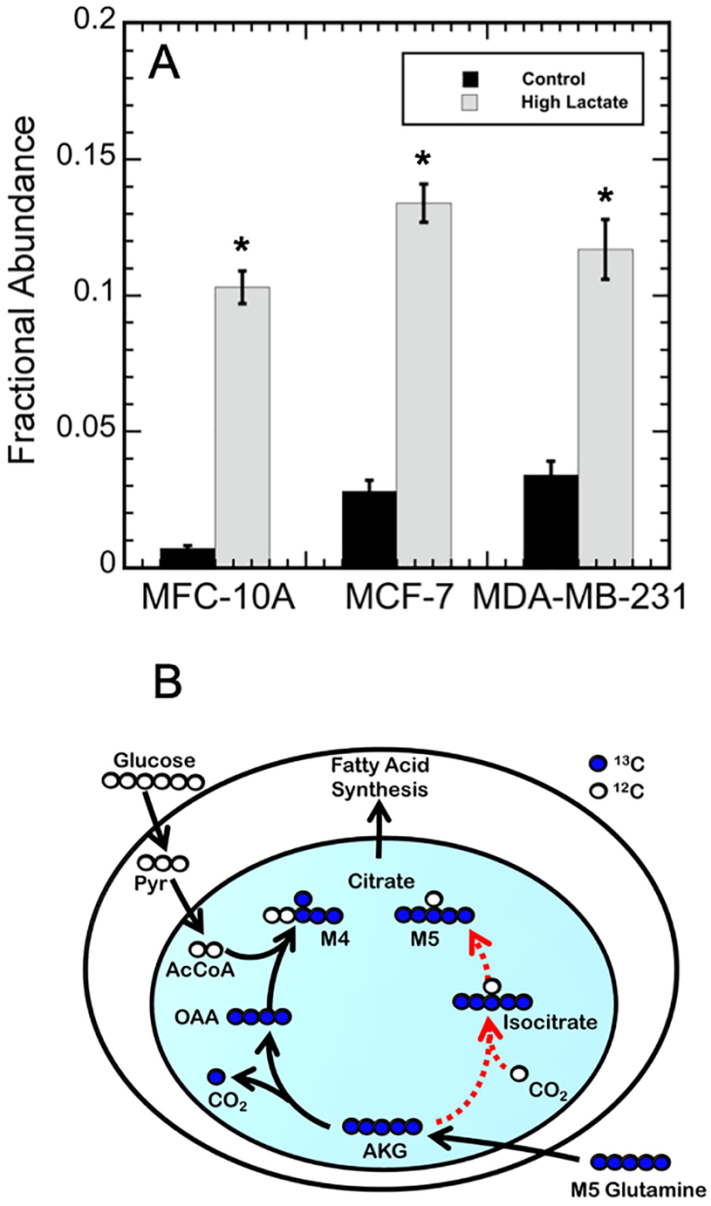

Figure 3.6. Evidence of reductive carboxylation of α-ketoglutarate (AKG) to citrate from [U-^{13}C] glutamine labeling. A) Fractional abundance of M5 labeled citrate for MCF 10A, MCF7, and MDA-MB-231 cells from the control (■) and high-lactate media (■). Error bars represent standard deviations. The asterisk (*) indicates the fractional abundances were significantly different between the control and high-lactate media per cell line ($p \leq 0.01$). B) Carbon atom transition for TCA metabolites from [U-^{13}C] glutamine. The black lines depict oxidative glutamine metabolism that results in M4 citrate. The dashed red lines depict reductive glutamine metabolism that results in M5 citrate. For clarity, some reaction pathways were condensed.

3.4.5. Metabolic flux analysis

To quantify the metabolic activity, Metran was used to predict the intracellular metabolite fluxes for each of the three cell lines under both conditions, six simulations in total. The experimental procedure section describes in detail the intracellular MIDs and extracellular fluxes used for the simulations. Each of the Metran model simulations converged to acceptable SSRes except for the MCF7 control condition, which slightly overfit. This overfitting was traced back to the high standard error for the glutamine MIDs from the biological replicates, where Tables D1 and D3 in Appendix D contain all the raw MID values for the three cell lines. This particular MID had a higher standard error than typically observed. Review of the data could not identify an experimental error, nor did this point meet outlier exclusion test criteria. Thus, this data point could not be discarded. Nevertheless, the effect of excluding this point on the model was examined to determine the effect this one data point had on the simulated flux values. When the Metran model simulation was conducted for the MCF7 control condition with only this metabolite MID standard error value replaced with the 0.6 mol% minimum machine error, the Metran simulation converged to an acceptable SSRes value. More importantly, there was no significant difference obtained for the simulated flux values. As the flux values are the critical outcome, the Metran simulations were conducted using the biological replicate MIDs (with the slight overfit SSRes) for the comparisons. The metabolic flux maps were generated for the three cell lines under each of the culture conditions, six in total using the actual biological replicates, as the flux outcomes were not significantly effected, even though the SSRes was overfit for MCF7. The flux maps are shown with standard deviations

for the cell lines and conditions in Figures F1-F3 in Appendix F. The list of metabolic fluxes for all Metran simulations are provided in Tables G1-G7 in Appendix G, including the MCF7 simulation with the 0.6 mol% standard error for the single biological replicate.

As a part of the validation step, measured MIDs from the parallel glucose and glutamine tracer labeling experiments and extracellular flux measurements were compared to the simulated results from the model to further investigate the effects of lactate on metabolism and to determine cell line specific effects (Ahn and Antoniewicz, 2013; Leighty and Antoniewicz, 2012). The simulated fluxes for major pathway reactions for each cell line and condition are shown in Figure 3.7. As expected, glycolytic reactions exhibited the highest fluxes in both the control and high-lactate cultures. In all three cell lines, the glucose consumption and lactate production rates decreased due to high-lactate exposure. In addition, MFA simulations predicted slightly decreased PPP fluxes for all three cell lines due to high-lactate. As mentioned previously, increased M3 labeling of pyruvate and lactate from glutamine was observed for MCF 10A and MDA-MB-231 under high lactate, while MCF7 under high lactate resulted in a slight decrease in M3 labeling. This was reflected in the MFA simulations as increased malic enzyme fluxes, conversion of malate to pyruvate, for the MCF 10A and MDA-MB-231 cell lines under high lactate and a decreased malic enzyme flux for the MCF7 under high lactate. Furthermore, MDA-MB-231 cells exhibited elevated anaplerotic and TCA cycle fluxes – pyruvate carboxylase (PC), glutamate dehydrogenase (GDH), pyruvate dehydrogenase (PDH), and citrate synthase (CS) – under high lactate, while MCF 10A and MCF7 cells exhibited similar anaplerotic and TCA cycle fluxes between conditions (Figure 3.7).

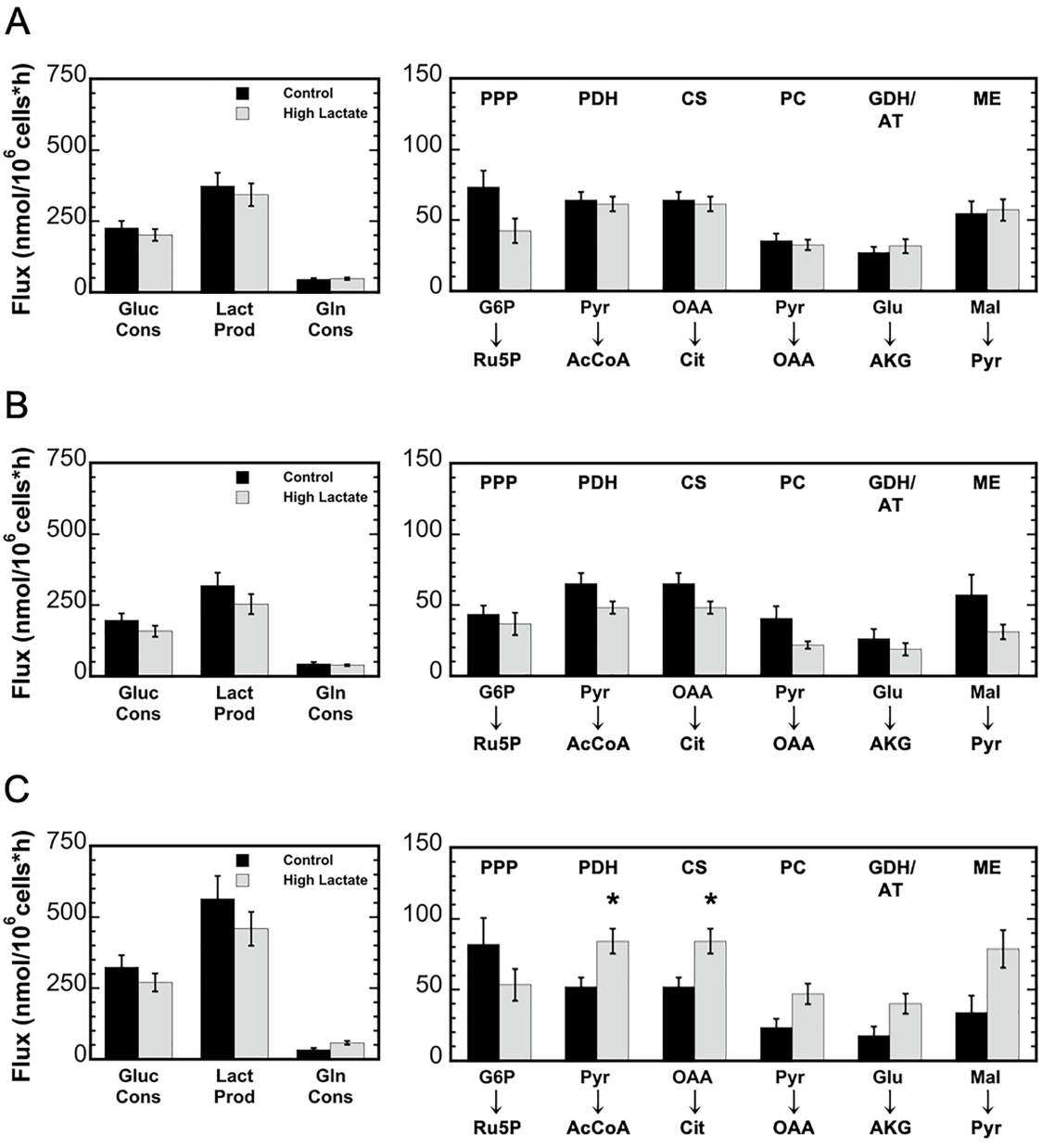

Figure 3.7. Comparison of key metabolic fluxes for MCF 10A (A), MCF7 (B), and MDA-MB-231 (C). Abbreviations: PPP, pentose phosphate pathway; PDH, pyruvate dehydrogenase; CS, citrate synthase; PC, pyruvate carboxylase; GDH/AT, glutamate dehydrogenase/aminotransferase; ME, malic enzyme. Error bars represent standard deviations. The asterisk (*) indicates the simulated fluxes were significantly different between the control and high-lactate conditions ($p \leq 0.05$).

3.5. Discussion

In this study, the metabolic responses of three breast cell lines – MCF 10A, MCF7, and MDA-MB-231 – to high-lactate were examined using ^{13}C-MFA. MCF 10A is a non-tumorous epithelial breast cell line, MCF7 is a tumorigenic, luminal breast cancer cell line, and MDA-MB-231 is a metastatic, basal breast cancer cell line. ^{13}C-glucose, ^{13}C-glutamine, and ^{13}C-lactate tracers were used in parallel experiments to determine the relative contribution of each substrate to intracellular metabolism. [1,2-^{13}C] glucose and [U-^{13}C] glutamine were selected as tracers, since both have previously been shown to be suitable for characterizing fluxes through glycolysis, the PPP, and TCA cycle pathways for mammalian cells (Ahn and Antoniewicz, 2013; Crown et al., 2012; Crown and Antoniewicz, 2012; Metallo et al., 2009). In addition, the [U-^{13}C] lactate tracer was used to determine the metabolic contribution of lactate to breast cancer cell metabolism. For metabolic flux analysis, a detailed metabolic network model was constructed for breast cancer cells based a CHO cell metabolic network model (Ahn and Antoniewicz, 2013). The intracellular MIDs from parallel labeling experiments and extracellular flux measurements were paired with a mammalian metabolic network model to develop intracellular metabolic flux maps for each cell line under the control and high-lactate conditions.

As expected, the high-lactate condition caused a reduction in glucose consumption and lactate production for all cell lines examined (Figure 3.3). This is consistent with previous findings that accumulated lactate acts as a glycolytic signaling molecule and can down-regulate phosphofructokinase activity, a key glycolytic regulatory enzyme, resulting in

decreased rates of glucose consumption (Leite et al., 2007). In addition, lactate consumption was observed in the high-lactate condition, as illustrated by the [U-^{13}C] lactate tracer uptake in each cell line (Figure 3.4). Metabolic flexibility appears to play an important role in enabling cancer to thrive and survive in harsh environments, including inflammation, oxidative stress, and extreme nutrient and oxygen fluctuations (Dayem et al., 2010; Pavlides et al., 2010; Reuter et al., 2010). As a result, the ability to metabolize higher levels of lactate offers potential advantages to cancer cells. The higher fractional abundance of intracellular M3 lactate labeling for MCF7 compared to MCF 10A and MDA-MB-231 in this study (Figure 3.4B) is consistent with previous finding that MCF7 display higher expression of monocarboxylate transporter 1 (MCT1), the lactate transporter associated with increased transport of lactate into the cell (Kennedy et al., 2013; Sonveaux et al., 2008). Furthermore, since TCA metabolites were only observed to be minimally labeled by lactate, this suggests that lactate was not a major source of acetyl-CoA. Also, labeled TCA metabolite pools were diluted by the metabolism of unlabeled pyruvate. Nevertheless, the intracellular MIDs from the high-lactate cultures demonstrated that each cell line consumed and metabolized a significant amount of labeled lactate, most likely to compensate for the decreased carbon flux through glycolysis due to decreased glucose consumption.

Intracellular metabolite labeling from [U-^{13}C] glutamine was similar for the control and high lactate conditions for each cell line, with over 50% isotope labeling of all TCA cycle metabolites. Figure 3.5 shows the labeling for the MDA-MB-231 cells, where Figure E2 in Appendix E shows the labeling for all three cell lines. Conversely, a slight increase in

pyruvate and lactate labeling from glutamine was observed in MCF 10A and MDA-MB-231 due to high-lactate. This suggests that glutamine anaplerosis was enhanced to provide energy via oxidative phosphorylation, and then secreted as alanine and lactate in response to decreased glucose consumption and decreased energy generation via glycolysis. Interestingly, high-lactate also caused an increase in M5 citrate labeling for each cell line (Figure 3.6). The increased M5 citrate labeling in the high-lactate conditions suggests the presence of reductive carboxylation of glutamine via the isocitrate dehydrogenase (IDH) reaction, as shown as a dashed red line in Figure 3.6B. Also, the decrease in M0 citrate indicates an increase in glutamine catabolism through the TCA cycle. Figure 3.5 shows the labeling for the MDA-MB-231 cells, where Figure E2 in Appendix E shows the labeling for all three cell lines. Furthermore, production of citrate from AKG via the IDH reaction – characterized by the exchange flux between AKG and citrate – increased for each cell line due to high-lactate. These results suggest that the IDH reaction is highly reversible for each breast cell line examined. The MFA simulations also suggested cell line specific TCA cycle metabolic responses due to high-lactate, with major anaplerotic and TCA fluxes remaining relatively unchanged for MCF 10A cells and MCF7 cells, while increasing for MDA-MB-231 cells (Figure 3.7). In particular, the MFA model predicted increased fluxes through pyruvate dehydrogenase (PDH) and citrate synthase (CS) for MDA-MB-231 in high lactate; this suggests a more active oxidative mitochondrial metabolism for MDA-MB-231 cells under high lactate, and is consistent with previous work showing that lactate promotes a metastatic phenotype (Bonuccelli et al., 2010; Martinez-Outschoorn et al., 2011).

Increases in fumarate, malate, and aspartate M3 labeling have also previously been observed with increased reductive carboxylation to support lipid synthesis in cancer cells grown under hypoxic conditions (Fan et al., 2013; Fendt et al., 2013; Grassian et al., 2014; Jiang et al., 2016; Metallo et al., 2012; Metallo et al., 2009; Wise et al., 2011). This would result from [U-^{13}C] glutamine serving as the main source of citrate via reductive carboxylation. Yet, M3 labeling of fumarate, malate, and aspartate did not significantly increase in this study. In this study, however, fumarate, malate, and aspartate were primarily M2 and M4 labeled, as shown in Figure 3.5 for the MDA-MB-231 cell line and shown in Figure E2 in Appendix E for all three cell lines. This indicates that the TCA metabolites were mainly derived from the glucose-derived pyruvate via oxidative metabolism rather than reductive glutamine metabolism. This implies that glutamine via reductive carboxylation was not the major carbon source for citrate synthesis in either condition. These observations agree with previous studies in which reductive carboxylation was observed for cancer cells without shifting the net IDH flux from oxidative to reductive glutamine metabolism in the TCA cycle (Fan et al., 2013; Jiang et al., 2016). Jiang et al. 2016 also previously showed that increases in M5 citrate labeling without accompanied changes to M3 fumarate and malate labeling is indicative of reductive carboxylation for citrate and AKG shuttling rather than for lipid synthesis. By shuttling AKG and citrate from the mitochondria to the cytosol and back, cells can shuffle redox equivalents to maintain a net-oxidative TCA metabolism (Jiang et al., 2016). This might suggest that in high-lactate conditions, cancer cells utilize the reversible NADPH-depended IDH reactions (1 and 2) rather than the NAD+-dependent reaction (IDH3) to compensate for the loss in

NAD+ generation as a result of decreased lactate production (Jiang et al., 2016). Recall, the two more aggressive breast cancer cell lines examined in this study maintained equivalent exponential growth rates to the control cultures at 20 mM lactate, while the MCF 10A cell line (a non-tumorigenic epithelial cell line) failed to grow in the 20 mM lactate condition, but could maintain equivalent exponential growth rates with the control cultures at 10 mM lactate.

Mammalian cells, including several cancer cell lines, have been observed to rely on reductive carboxylation of glutamine for lipid synthesis under hypoxia (Metallo et al., 2009; Wise et al., 2011). Reductive carboxylation has also been suggested to be a cellular response to environmental stresses, such as reactive oxygen species (ROS) regulation (Fendt et al., 2013; Jiang et al., 2016). These previous studies differ with the current work in several ways. Mainly, the breast cell lines in this work were cultured in normoxia and in an experimental setup which maintained similar growth rates even under stress. This meant that the high-lactate MCF 10A cultures contained 10 mM lactate initially, whereas the high-lactate MCF7 and MDA-MB-231 contained 20 mM lactate initially. In contrast to our results, Fendt et al. 2013 observed a net consumption of lactate for a lung carcinoma cell line (A549) grown under normoxia in 25 mM supplemented media (Fendt et al., 2013). In addition, Fendt et al. 2013 observed a decreased contribution of reductive glutamine metabolism to citrate synthesis; however, there was no mention if the growth rates were matched between the control and lactate stress conditions (Fendt et al., 2013). Different growth rates could alter the observed metabolic fluxes as there is not a standardized normalization method for fluxes. The non-growth inhibitory lactate concentrations used

in this study may very well have different effects on metabolism than lactate concentrations that have inhibitory growth effects. This work is the first to observe reductive glutamine metabolism due to high extracellular lactate in normoxia, but it may be a common phenomenon, as there are many non-inhibitory levels of waste products within an organism.

While cancer cells have long been known to produce high levels of lactate, especially in hypoxic tumor regions, cancer cells can also consume and metabolize lactate as a substrate (Kennedy et al., 2013; Pavlides et al., 2009; Sonveaux et al., 2008). The findings in this study highlight that high extracellular lactate induces a response mechanism in both non-cancer and cancer cells, which is similar to hypoxia or other mitochondrial stresses, even in the presence of sufficient oxygen. In addition, lactate supplementation resulted in elevated oxidative mitochondrial metabolism activity for MDA-MB-231 cells, as shown from the ^{13}C-MFA simulations, and is consistent with previous work showing that lactate promotes a metastatic phenotype (Bonuccelli et al., 2010; Martinez-Outschoorn et al., 2011). These results suggest that modulation of mitochondrial metabolism and reductive carboxylation are cellular metabolic responses to stress, including high extracellular lactate and hypoxia. The observed response could also contribute to the metabolic flexibility of cancer cells and allow for adaptation to high-lactate exposure. Additionally, the response observed is lactate dependent and cell line independent, under growth conditions where the cells can maintain exponential growth under the lactate stress.

3.6. Acknowledgements

We would like to thank Dr. Brian Booth of Clemson's Bioengineering Department

for kindly provided to us with MDA-MB-231 cells. Additionally, we would like to thank Dr. David Bruce and Dr. Bethany Carter of Clemson's Chemical Engineering Department for assistance with GC-MS analysis.

CHAPTER FOUR

EFFECTS OF LOW GLUCOSE AND HIGH LACTATE CONCENTRATIONS ON INDUCED PLURIPOTENT STEM CELL METABOLISM

4.1. Abstract

Human induced pluripotent stem cells (iPSCs) have the potential to dramatically improve cell-based therapies in the near future. Yet, to meet rising demands and become clinically impactful, sufficient quantities of high quality iPSCs must be generated, a task that exceeds current capabilities. To meet these needs, a comprehensive understanding of the metabolic and phenotypic responses of iPSCs to different environmental conditions is essential. iPSCs rely primarily on aerobic glycolysis to support rapid proliferation *in vitro*. Previous studies have suggested that lactate accumulation is solely a wasteful and inhibitory metabolic process for iPSCs. However, the potential impact of lactate accumulation on intracellular iPSC metabolism has not been determined. Therefore, the goals of this work were to 1) understand the role of lactate as a potential metabolic substrate to support iPSC proliferation, and 2) determine whether lactate production could be modulated by low glucose feeding strategies. The culture media concentrations represent stages of stem cell bioprocessing; the control and low glucose conditions represent a range of initial media concentrations during the batch phase, and the two high lactate conditions represent media concentrations during fed-batch culture prior to and after bolus glucose feed. These concentration ranges are also representative of glucose and lactate conditions that cells would encounter at various locations within 3D cell aggregates when cultured in

suspension. Parallel labeling metabolic flux analysis (^{13}C-MFA) was used to quantify intracellular fluxes for K3 iPSCs under normal glucose, low glucose, and two high extracellular lactate culture conditions. In addition, [U-^{13}C] lactate was used as an isotopic tracer for the high extracellular lactate cultures to provide information regarding lactate catabolism. High extracellular lactate resulted in decreased glucose consumption and lactate production, while glucose concentration alone did not affect rates of aerobic glycolysis. Moreover, for the high lactate cultures, lactate significantly contributed as a metabolic substrate to support oxidative mitochondrial metabolism for iPSCs. These results demonstrate that iPSCs can employ dual consumption of glucose and lactate to support growth. In addition, this is the first study to determine the intracellular contribution of lactate to proliferative iPSC metabolism. These results provide insight into the metabolic flexibility of iPSCs with respect to lactate metabolism and suggest that iPSCs possess the capacity to metabolize lactate to support exponential growth. Also, as iPSC cultures move towards pH-controlled bioreactors, these results suggest that lactate accumulation alone does not adversely impact iPSC proliferation at the concentrations examined in this study.

4.2. Introduction

Human embryonic stem cells (hESCs) and induced pluripotent stem cells (iPSCs) are considered to be dependent on aerobic glycolysis and lactate fermentation for energy production (Gu et al., 2016; Varum et al., 2011; Zhang et al., 2011). In addition, during somatic cell nuclear reprogramming, iPSCs have been shown to shift from oxidative phosphorylation to aerobic glycolysis upon the acquisition of pluripotency (DeBerardinis

et al., 2008; Folmes et al., 2012; Folmes et al., 2011; Ryall et al., 2015). Stimulation of glycolysis also was observed to promote maintenance of stemness for pluripotent stem cells (PSCs) and augmented somatic reprogramming to iPSCs, while inhibition of specific glycolytic reactions in turn inhibited reprogramming (Ezashi et al., 2005; Folmes et al., 2011; Mohyeldin et al., 2010). On the other hand, inhibition of glycolysis was shown to promote spontaneous differentiation, suggesting that metabolism plays a functional role in regulating cell self-renewal and differentiation (Gu et al., 2016; Moussaieff et al., 2015; Zhang et al., 2011). This reliance on glycolysis over oxidative phosphorylation in well-oxygenated systems is a metabolic phenotype called the Warburg effect, and is also a characteristic of cancer cell metabolism (Cairns et al., 2011; DeBerardinis et al., 2008; Vander Heiden et al., 2009; Warburg, 1956). However, unlike cancer cells, which can catabolize lactate for energy, PSCs are hypothesized to be highly sensitive to lactate accumulation (Chen et al., 2010; Kennedy and Dewhirst, 2010; Kennedy et al., 2013; Martinez-Outschoorn et al., 2011; Nath et al., 2017; Ouyang et al., 2007; Pavlides et al., 2010; Sonveaux et al., 2008). Specifically, hESCs exhibited decreased pluripotency after serial passage in 11 mM lactate-containing media (Chen et al., 2010). Moreover, elevated lactate and glucose-depleted media has previously been shown to preferentially induce cardiomyocyte differentiation for iPSCs (Tohyama et al., 2013). Therefore, PSC culture techniques require frequent media exchange to alleviate lactate stresses (Olmer et al., 2012; Wang et al., 2013). Since lactate accumulation appears to be an unavoidable byproduct of iPSC metabolism, deciphering the role of accumulated extracellular lactate on intracellular iPSC metabolism and understanding the regulatory role of glucose concentration to

modulate lactate production are crucial.

Metabolic flux analysis (MFA) is a powerful computational technique used to determine intracellular metabolic pathway fluxes (Bonarius et al., 1997; Stephanopoulos, 1999). In MFA, intracellular fluxes are determined by coupling extracellular metabolite uptake and secretion rates with a discrete stoichiometric metabolic network model (Stephanopoulos et al., 1998). This technique is frequently used to compare metabolism of different cell lines and cell culture conditions to assess the activity of individual pathways under each condition (Niklas and Heinzle, 2011). There are two primary MFA approaches: stoichiometric MFA, which uses mass balance to determine intracellular metabolic fluxes from extracellular consumption and production fluxes, and ^{13}C-MFA, in which stable isotope tracers are used to provide intracellular measurements to resolve fluxes through more complex metabolic pathways (Sa et al., 2015; Sauer, 2006; Stephanopoulos et al., 1998).

The aims of this study were to determine the metabolic contribution of glucose and extracellular lactate to iPSC metabolism, and in particular, to determine 1) whether lactate can serve as a metabolic substrate in support of iPSC proliferation and 2) if glucose concentration can modulate lactate production. K3 iPSCs were grown in both low and normal glucose-containing media and with and without extracellular lactate additions. The low glucose and high lactate concentrations were selected such that exponential growth rates for the cultures were maintained across the four conditions, as would be desired in large-scale cultivation. The pluripotency and differentiation capacity of the iPSCs were assessed from each culture condition to determine if glucose or lactate concentration

impacted these phenotypes. Parallel labeling experiments were conducted with [1,2-^{13}C] glucose, [U-^{13}C] L-glutamine, and [U-^{13}C] sodium L-lactate, while the control and low glucose cultures were labeled with [1,2-^{13}C] glucose and [U-^{13}C] L-glutamine only, since lactate was not added to these cultures. Metabolic flux maps were generated for each condition to compare the resulting flux distributions from culturing iPSCs in low glucose and high lactate culture media. To our knowledge, this is the first ^{13}C-MFA study to investigate the metabolic flexibility of iPSCs respect to lactate catabolism. The implications of these results to iPSC bioprocessing will be discussed.

4.3. Materials and Methods

4.3.1. Cell culture

K3 iPSCs were donated by Dr. Stephen A. Duncan at the Medical University of South Carolina. The K3 iPSCs were generated by transient transfection of human foreskin fibroblast cells (ATCC CRL2097) using plasmids coding for Oct4, Sox2, Nanog, and Lin28 (Si-Tayeb et al., 2010). In this study, K3 iPSCs were grown on non-tissue culture treated 6-well plates and 60 mm cell culture dishes (Corning Inc., Corning, NY) coated with 10 µg/mL StemAdhere™ (Primorigen, Cat. no. S2071-500UG) per manufacturer instructions. StemAdhere™ is a fully defined recombinant surface matrix composed of a fusion protein consisting of E-cadherin and the Fc domain of IgG; this surface matrix has previously been shown to be an effective method for culturing human iPSCs (hiPSCs) (Nagaoka et al., 2010). Cultures were incubated at 37°C and in a humidified 5% CO_2 incubator in Essential 8 Flex™ (E8 Flex) media (Thermo Fisher Scientific, Waltham, MA).

The working volume of media was 3 mL per well in the 6-well plates and 6.5 mL for the 60 mm cell culture dishes. Cells were maintained by passaging every three days at 1:6 and 1:12 depending on confluency. To passage cells, the cells were detached from the surface with Accutase (Sigma-Aldrich, St. Louis, MO) for 2 min at 37°C and washed with phosphate buffered saline (PBS) without calcium or magnesium (Corning Inc., Corning, NY). Cells were centrifuged at 500 x *g* for 5 min and resuspended in fresh E8 Flex supplemented with 10 μM Y-27632 – rho-associated, coiled-coil containing protein kinase inhibitor (ROCKi) (Stem Cell Technologies, Vancouver, Canada). After 24-h, the media was replaced with E8 Flex without ROCKi. For the cell growth and parallel labeling experiments, E8 Flex medium without glucose and glutamine was used. The initial media concentrations are listed in Table 4.1 for the four culture conditions. The control growth media represents standard E8 Flex media concentrations. D-glucose (Fisher Scientific, Hampton, NH), L-glutamine (Corning Inc., Corning, NY), sodium L-lactate (Sigma-Aldrich, St. Louis, MO), and sodium chloride (Fisher Scientific, Hampton, NH) were added to unlabeled experiments at concentrations as indicated in Table 4.1. [1,2-^{13}C] D-glucose (99% enrichment), [U-^{13}C] L-glutamine (99% enrichment), and [U-^{13}C] sodium L-lactate (98% enrichment) isotope tracers were used for the parallel labeling experiments (Cambridge Isotope Laboratories, Tewksbury, MA), and added to the labeled experiments at concentrations matching E8 Flex or as indicated.

Table 4.1. Media formulations for iPSC cultures examined in ^{13}C-MFA studies. The initial glucose, glutamine, sodium L-lactate, and added sodium chloride concentrations are listed for the time corresponding to the isotope labeling (media exchange) addition. Sodium chloride was added to balance osmolarity in cultures without sodium lactate.

	^{13}C-MFA Growth Media			
	Control	**High Lactate**	**Low Glucose**	**Low Glucose + High Lactate**
Component	**Concentrations (mM)**			
Glucose	18.3	18.3	5.6	5.6
L-glutamine	2.75	2.75	2.75	2.75
Sodium L-lactate	-	20.0	-	20.0
Added Sodium chloride	+ 20.0	-	+ 20.0	-

4.3.2. Cell growth and parallel labeling experiments

For the growth and isotope labeling studies, K3 iPSCs were initially seeded at 1.0 x 10^4 cells/cm^2 in E8 Flex with ROCKi to allow for cell attachment and reduce apoptosis associated with single cell detachment and passaging (Watanabe et al., 2007). After 24-h, a media exchange was performed, and the growth media was introduced to the parallel 6-well plates and 60 mm cell culture dishes (indicated as Time 0-h in Figure 4.1). For clarity, a schematic of the full experimental setup is shown in Figure 4.1. In all, six 6-well plates and eighteen 60 mm cell culture dishes were used per high lactate and low glucose + high lactate conditions, and six 6-well plates and twelve 60 mm dishes were used per control and low glucose conditions. The control growth media represented standard E8 Flex media concentrations. Inoculum were used across multiple conditions, such that no condition had only a single inoculum. To limit media carryover, cells were washed with PBS for 5 min at room temperature prior to adding the growth media. Cell numbers and extracellular metabolite concentrations were measured at five time points: 0, 12, 24, 36, and 48-h after the media exchange. Cell numbers, glucose, lactate, pyruvate, ammonia, and amino acid extracellular measurements were obtained from the 6-well plates. The intracellular mass isotope distributions (MIDs) were obtained from 60 mm cell culture dishes at 24-h and 48-h. The control and low glucose cultures had parallel labeling with [1,2-^{13}C] glucose and [U-^{13}C] L-glutamine, whereas the high lactate and low glucose + high lactate cultures had parallel labeling with [1,2-^{13}C] glucose, [U-^{13}C] L-glutamine, and [U-^{13}C] sodium L-lactate.

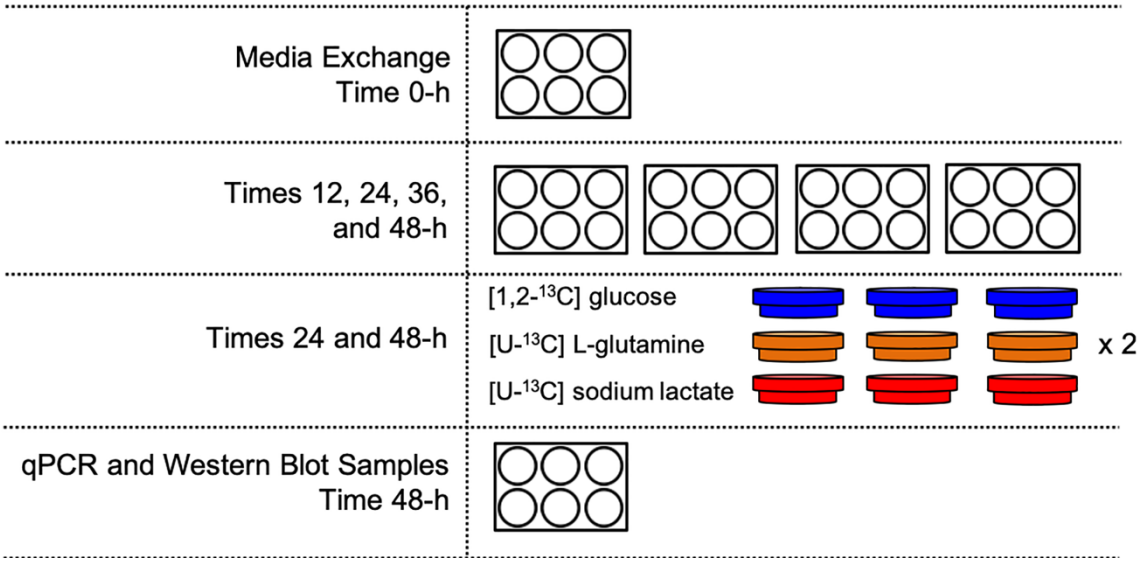

Figure 4.1. Parallel isotope labeling and culture replicate setup for each condition. All 6-well plates and 60 mm cell culture dishes were seeded in parallel 24 hours prior to the media exchange (Time 0-h). The times shown indicate when the plates or dishes were harvested for analysis relative to the isotope media exchange. Isotopic labeling is graphically shown by shading (clear – no isotope, blue – [1,2-^{13}C] glucose, orange – [U-^{13}C] L-glutamine, and red – [U-^{13}C] sodium lactate). The 60 mm cell culture dishes contained isotopically labeled media. Six wells of a 6-well plate were used to measure cell number, glucose, lactate, pyruvate, and amino acid concentrations. The 60 mm cell culture dishes were harvested for intracellular isotope MID values.

4.3.3. Cell numbers and extracellular metabolite concentrations

Cell numbers were obtained using the Vi-Cell XR cell viability analyzer (Beckman Coulter, Brea, CA). Extracellular glucose, lactate, pyruvate, glutamine, glutamate, and ammonia concentrations were measured using a Cedex Bio (Roche Diagnostics, Mannheim, Germany).

4.3.4. Derivatization and GC-FID analysis of extracellular amino acids

Extracellular amino acid concentrations were measured from the cell culture supernatant by derivatization using the EZ:faast^{TM} amino acid analysis kit (Phenomenex, Torrance, CA). Standard solutions were prepared for amino acids – alanine, asparagine, aspartic acid, glycine, histidine, isoleucine, leucine, lysine, phenylalanine, proline, serine, threonine, tryptophan, tyrosine, and valine – to a final concentration of 10 mM in water and pH adjusted to below pH 7.0. Samples were prepared by combining 150 µL of cell culture supernatant and 50 µL of an internal standard (200 µM norvaline). Sample derivatization was performed as per manufacturer instructions (Badawy et al., 2008). Standard curves were generated for each amino acid.

Derivatized samples were analyzed using a gas chromatography-flame ionization detector (GC-FID) instrument (Agilent Technologies, 7890A GC system) equipped with an autosampler (Agilent Technologies, 7683B Series Injector). A Zebron ZB-AAA 10 m x 0.25 mm capillary GC column was used. The initial column temperature was 60°C and increased by 32°C/min to a final temperature of 320°C. The FID detector temperature was held at 320°C and 2 µL of sample was injected at an injection temperature of 250°C and a

split ratio of 1:15 using a 10 µL syringe (Agilent Technologies, Part # 5181-1267). Helium was used as the carrier gas at 1.5 mL/min constant flow.

4.3.5. Extraction of intracellular metabolites

At 24- and 48-h, the culture media was removed from the 60 mm cell culture dishes to remove debris and detached cells. The attached cells were washed with 3 mL of cold PBS (4°C) for 5 min. Then, 1 mL of cold methanol (-20°C, LC/MS grade) was added and incubated on ice for 5 min. Adherent cells were removed from the dishes using a cell scraper. The collected cell suspensions from the dishes were then transferred to 15 mL glass centrifuge tubes (with Teflon-sealed caps) which contained 1 mL of chloroform. The chloroform, methanol, and cell mixtures were vortexed vigorously for 10 s. Next, 1 mL of water was added to each tube, and samples were vortexed vigorously for 1 min. All sample tubes were stored overnight at 4°C. After overnight storage, all tubes were centrifuged at 4000 x *g* at 4°C for 20 min to fully separate the aqueous and organic phases. The upper aqueous phase (methanol and water) contained the polar intracellular metabolites and the lower organic phase (chloroform) contained the non-polar metabolites (fatty acids). Each phase was transferred to separate GC vials for further analysis. The metabolism quenching and separation procedure was adapted from Ahn and Antoniewicz (2013).

4.3.6. Derivatization and GC-MS analysis of intracellular metabolites

The aqueous phases were evaporated to dryness using a CentriVap (Labconco, Kansas, MO). Dried samples were then dissolved in 10 µL of methoxyamine hydrochloride (Sigma-

Aldrich, St. Louis, MO) and incubated with shaking at 30°C and 1000 rpm for 90 min in an EchoTherm™ SC20 Orbital Mixing Dry Bath (Torrey Pines Scientific, Inc., Carlsbad CA). Next, 90 µL of N-methyl-N-(tert-butyldimethylsilyl)-trifluoroacetamide (MTBSTFA) (Sigma-Aldrich, St. Louis, MO) was added to samples to initiate trimethylsilylation. The trimethylsilylation reaction was incubated with shaking at 37°C and 1000 rpm for 60 min. MTBSTFA containing C8–C30 fatty acid methyl esters (FAMEs) was used as a set of internal standards to determine retention times. Derivatized samples were submitted to a Leco Pegasus IV time-of-flight (TOF) MS (Leco Corporation) with electron ionization mode at −70 eV. A Rtx-5Sil MS column (30 m x 0.25 mm, 0.25 µm) was used. The initial temperature was 50°C and held for 1 min, ramped up to 330°C at 20°C/min, then held for 5 min. The flow rate was set to 1.0 mL/min and 0.5 µL of sample was injected. Mass spectrometry detector voltage was 1525 V. Data was acquired at 17 spectra/s with scan range from 85 to 600 Da. Ion source temperature was 250°C and transfer line temperature was 280°C. Standard mixture and blank samples were injected at the beginning of the analysis and every ten samples throughout the analysis for quality control. The GC-MS analysis was conducted at the West Coast Metabolomics Center at the University of California, Davis.

4.3.7. Determination of biomass specific consumption and production rates

Extracellular metabolite fluxes were calculated using the Extracellular Time-Course Analysis (ETA) software package available for Matlab (Murphy and Young, 2013). The ETA software uses a Gaussian error propagation approach to calculate fluxes and standard

errors from averaged time series data (Murphy and Young, 2013). This software was used to assess the goodness-of-fit of measured experimental data to a linear regression model. The glutamine decomposition rate constant (k) was determined for E8-Flex media to be 0.00178 h^{-1} using media without cells held at 37°C for 72-h. First-order glutamine degradation was accounted for to determine glutamine consumption fluxes in ETA (Murphy and Young, 2013).

4.3.8. Dry cell weight measurements

K3 iPSCs were cultured in E8 Flex media representative of the control growth media and harvested from six 100 mm non tissue culture treated dishes at ~ 90% confluence. Cells were washed with 5 mL PBS for 5 min, then detached using Accutase for 2 min at 37°C. Cells from two 100 mm culture dishes were combined for each cell count and corresponding dry cell weight. Cells were pelleted by centrifuging at 5000 x *g* for 5 min. Following centrifugation, the supernatant was removed, and cells were resuspended in 10 mL of water by briefly vortexing. Next, cells were centrifuged again at 5000 x *g* for 5 min. Finally, the water was removed, and the cell pellets were resuspended in 1-2 mL of water, vortexed, and transferred to aluminum drying pans. The tubes were rinsed with water and the contents were added to the aluminum drying pans. Cell pellets were dried in ambient air at 95°C for two days before dry cell weights were obtained. The dry cell weights were determined in triplicate.

4.3.9. Metabolic network model

A generalized mammalian cell model focused on central carbon metabolism was used to model iPSC metabolism. This model was adapted from several previously published metabolic frameworks (Ahn and Antoniewicz, 2013; Jiang et al., 2016; Metallo et al., 2012). The iPSC model contained the major reactions for glucose consumption, the TCA cycle, amino acid metabolism, lactate metabolism, and fatty acid metabolism. Early glycolysis and the pentose phosphate pathway (PPP) reactions were not included in the iPSC model since the intracellular MIDs for these metabolites were poorly resolved experimentally. This approach to simplify glycolysis and PPP is similar to the approach used in Jiang et al. 2016. The carbon flux to the biomass was divided into two compartments – termed the biomass pool and the "lipid biomass" pool (Ahn and Antoniewicz, 2013; Bonarius et al., 1996; Brodsky et al., 2019; Metallo et al., 2012). The biomass fraction contains nucleotides, proteins and carbohydrates, and lipid biomass fractions contains acetyl-CoA. The relative weight fraction of the biomass and lipid biomass pools are 0.9 and 0.1, respectively, based on cell mass composition of hybridoma cells (Sheikh et al., 2005) and the experimentally measured dry cell weight for K3 iPSCs. The measured K3 iPSC dry cell weight was converted to biomass and lipid biomass fluxes using the experimentally determined iPSC growth rates (Bonarius et al., 1996). A full description of the metabolic model development and assumptions can be found in Appendix K. The full list metabolic reactions including the atom carbon transitions is included in Appendix L.

4.3.10. Metabolic flux analysis

^{13}C-Metabolic flux analysis was conducted using the Isotopomer Network Compartmental Analysis (INCA) software package (Young, 2014). INCA utilizes the elementary metabolite unit framework to perform MID simulations, and is capable of performing both isotopic steady-state and isotopic non-stationary MFA (Antoniewicz et al., 2007b; Young et al., 2008). For this work, isotopic steady-state MFA was conducted to estimate intracellular metabolic fluxes, where extracellular uptake and secretion fluxes, coupled with intracellular MIDs from the 24-h samples were used. In this study, INCA software was used to complete the ^{13}C-MFA on the data from the parallel labeling experiments, a process that has been shown to improve flux resolution throughout intracellular metabolism (Leighty and Antoniewicz, 2012; Leighty and Antoniewicz, 2013). Flux estimations were performed for 100 restarts from initial random guesses. This increases the likeliness that a global solution will be obtained (Templeton et al., 2013).

4.3.11. Extended expansion of K3 iPSCs

K3 iPSCs were cultured for five passages in each of the four culture media to assess the effects of glucose and lactate on iPSC proliferation and pluripotency. The cell culture and passage procedures were as described in sections 4.3.2 and 4.3.3. After five passages, cell pellets were obtained and stored at -80°C for gene and protein expression analysis via real-time quantitative reverse transcriptase PCR and western blot, respectively. Additionally, cells from five passages were used for differentiation studies.

4.3.12. iPSC embryoid body formation and spontaneous differentiation

The capacity of K3 iPSCs to spontaneously differentiate towards cell types from each germ layer – ectoderm, endoderm, and mesoderm – was assessed using cells that had been cultured for five passages in the four culture media. For spontaneous differentiation, K3 iPSCs were inoculated into uncoated non-tissue culture treated 60 mm cell culture dishes at $3x10^5$ cells/mL in E8 Flex with ROCKi. The iPSCs had formed cell aggregates (embryoid bodies) in static suspension culture after 24-h. After 24-h, the media was removed and replaced with Essential 6™ (E6) spontaneous differentiation media (Thermo Fisher Scientific, Waltham, MA). Embryoid bodies were cultured in E6 media for seven days, where the media was replaced every other day. After seven days in E6 media, the embryoid bodies were harvested for gene and protein expression analysis to determine loss of pluripotency and onset of differentiation.

4.3.13. RNA extraction and qRT-PCR

Total mRNA was isolated from K3 iPSCs at 48-h and from embryoid bodies at day 7 using a RNeasy® Plus Mini Kit (Qiagen Inc., Valencia, CA) and QIAshredder (Qiagen Inc., Valencia, CA) according to the manufacturer's instructions. Isolated RNA sample quality assessment and quantification was performed using a NanoDrop™ 8000 Spectrophotometer (Thermo Fisher Scientific, Waltham, MA). Real-time quantitative reverse transcriptase polymerase chain reaction (qRT-PCR) was performed using the iTaq™ Univeral SYBR® Green One-Step Kit (Bio-Rad Laboratories, Inc., Hercules, CA). qRT-PCR was carried out using the iQ™5 cycler (Bio-Rad Laboratories, Inc., Hercules, CA) with the following program: reverse transcription for 10 min at 50°C; polymerase

activation and DNA denaturation for 1 min at 95°C; 40 cycles at 95°C for 10 sec, 58.6°C for 15 sec, and 72°C for 15 sec. Relative expression was determined using the $\Delta\Delta C_T$ method with Gapdh used as an internal standard (Livak and Schmittgen, 2001). Primer sequences are listed in Table 4.2. Gapdh, Oct4, Sox2, and Nanog primers were purchased from Integrated DNA Technologies (IDT, Coralville, IA), while Pax6, Sox17, and Gata2 were purchased from Invitrogen (Life Technologies, Carlsbad, CA).

Table 4.2. PCR primer sequences for analysis of K3 iPSCs. Primer sequences used for qPCR analysis of pluripotency and germ-layer differentiation for K3 iPSCs.

Gene	Forward primer sequence (5'→3')	Reverse primer sequence (5'→3')
Gapdh	CTGGGCTACACTGAGCACC	AAGTGGTCGTTGAGGGCAATG
Gata2	CTGTCTGCAACGCCTGTG	GTTCCGAGTCTGGATCCCTT
Oct4	CTTGAATCCCGAATGGAAAGGG	CCTTCCCAAATAGAACCCCCA
Nanog	TTTGTGGGCCTGAAGAAAACT	AGGGCTGTCCTGAATAAGCAG
Pax6	TGTCCAACGGATGTGTGAGT	TTTCCCAAGCAAAGATGGAC
Sox2	GCCGAGTGGAAACTTTTGTCG	GGCAGCGTGTACTTATCCTTCT
Sox17	GTGGACCGCACGGAATTTG	GGAGATTCACACCGGAGTCA

4.3.14. Western blots

Whole cell and embryoid body lysates were prepared using 1X Cell Lysis Buffer (Cell Signaling Technology, Danvers, MA) containing 1X Halt™ Protease and Phosphatase Inhibitor C (Thermo Fisher Scientific, Waltham, MA). The cell lysate protein concentration was quantified using the Pierce™ BCA Protein Assay Kit (Thermo Fisher Scientific, Waltham, MA). Prior to protein separation by electrophoresis, samples were mixed with 4X Laemmli buffer (Bio-Rad Laboratories, Inc., Hercules, CA) to a final concentration of 1X with 5% β-mercaptoethanol and boiled for 5 min at 95°C. Samples were loaded at a concentration of 5 μg of total protein per well. Protein separation was performed on 4-15% Mini-PROTEAN® TGX™ Precast Gels (Bio-Rad Laboratories, Inc., Hercules, CA) and run on a PowerPac™ 1000 (Bio-Rad Laboratories, Inc., Hercules, CA) power supply at 200V for 30 min with running buffer (15 g Tris Base, 72 g glycine, and 5 g SDS per L ultrapure water). Following electrophoresis, the gel was soaked in cold transfer buffer for 30 min. The transfer buffer (20% (v/v) methanol, with 3.03 g Tris Base, and 14.4 g glycine per L) was chilled overnight prior to transfer. Protein transfer was performed using Immun-Blot® PVDF (polyvinylidene difluoride) membranes and extra thick blot paper filter paper (Bio-Rad Laboratories, Inc., Hercules, CA). The PVDF membrane and filter pads were soaked in cold transfer buffer prior to the transfer. The transfer was conducted at 90 V for 1-h. Non-specific protein binding to the PVDF membrane was blocked using 5% non-fat dried milk in Tris buffered saline (TBS) at room temperature on an orbital shaker for 1-h. After blocking, the membrane was washed three times for 5 min each in cold TBS with 0.5% Tween (Bio-Rad Laboratories, Inc., Hercules,

CA) (TBST). Overnight primary antibody incubation was performed at 4°C. Each primary antibody was diluted at 1:1000 in TBST – β-actin (Fisher Scientific, Hampton, NH) and Oct4 (Novus Biologicals, Centennial, CO). Following the overnight primary antibody incubation, the membrane was washed three times for 5 min in TBST to remove unbound primary antibody. The secondary antibody incubations were conducted for 1-h at room temperature at a 1:1000 dilution in TBST using a goat anti-rabbit IgG HRP-linked antibody for β-actin and a goat anti-mouse IgG HRP-linked antibody for Oct4 (Bio-Rad Laboratories, Inc., Hercules, CA). Protein detection was obtained using the Vector® VIP peroxidase substrate kit (Vector Laboratories, Burlingame, CA) and quantified by densitometry using Image Studio Lite (Licor).

Statistical Analysis

Statistical analysis was performed using JMP Pro 14 software (SAS Institute, Cary, NC). The generalized linear model (GLM) procedure ($p \leq 0.05$) and least squares method with Tukey HSD (honest significant difference) were used to determine if cell number, extracellular metabolite concentrations, gene expression, and protein expression were significantly different between conditions ($p \leq 0.05$). An ANCOVA (analysis of covariance) was also used to determine if metabolite consumption and production profile slopes were significantly different between conditions ($p \leq 0.05$). Student's two-tailed t-tests were used to determine if the extracellular fluxes and intracellular MIDs were significantly different between conditions ($p \leq 0.05$). For ^{13}C-MFA model convergence in INCA, an acceptable simulation fit was determined to occur when a global solution was reached that satisfied

the accepted weighted sum of squared residuals (SSR) criteria between the input measurements and simulated measurement outputs. A chi-squared statistical test and sensitivity analysis were performed to determine goodness-of-fit and 95% confidence intervals for each predicted flux, respectively (Antoniewicz et al., 2006; Antoniewicz et al., 2007a).

4.4. Results and Discussion

4.4.1. Cell growth

To determine the effects of low glucose and high extracellular lactate concentrations on iPSC metabolism, K3 iPSCs were grown in media containing either typical glucose concentrations (18.3 mM) or low glucose concentrations (5.6 mM). Also, cultures were either exposed to high extracellular lactate (20 mM) or not exposed to high extracellular lactate. Table 4.1 outlines the media concentrations used, including the glucose, lactate, and glutamine concentrations and the supplemented sodium chloride concentration. The E8 Flex was provided without glucose and glutamine, such that labeled glucose and glutamine could be used for the ^{13}C-MFA studies. An initial screening study was performed to determine the minimum glucose concentration that did not result in glucose depletion prior to 48-h. Not depleting glucose was important to ensure that glucose was not a limiting substrate during exponential growth in order to assume pseudo steady-state. Recently, media acidosis was shown to negatively impact hPSC, with low pH resulting in decreased glucose consumption, cell cycle arrest, and cell death (Liu et al., 2018). Therefore, sodium L-lactate was used as the lactate source to avoid pH shifts due to

the lactate addition and to decouple the effects of pH and lactate on K3 iPSC phenotype. An equal molar concentration of sodium chloride was added to the non-lactate cultures to balance osmolarity. A screening study was performed to determine the maximum sodium lactate concentration that did not inhibit iPSC growth rates and was representative of lactate concentrations reported to occur in cell culture (Chen et al., 2010; Nath et al., 2017; Ouyang et al., 2007). A major objective was to have equivalent growth rates between the cultures across all four conditions; this allowed for any observed metabolic flux differences to be attributed to the media differences and not differences in biomass accumulation.

To characterize cell growth, cell counts were taken every 12-h; growth profiles from each condition are shown in Figure 4.2A. Cells were first grown in the control medium supplemented with 10 μM ROCKi for 24-h to promote cell attachment and reduce apoptosis associated with single cell detachment and passaging (Watanabe et al., 2007). Following this 24-h period of attachment, the culture media was removed and the media to be examined was added and referenced to as a media exchange. The media exchange is indicated by time 0-h in Figure 4.2A. For the parallel labeling experiments, ^{13}C isotopes replaced the unlabeled glucose, glutamine, or lactate in the culture media at the same concentration. To determine the biomass specific flux associated with cell growth, dry cell weight measurements were taken as described in section 4.3.9. The dry cell weight for K3 iPSC was 263 ± 15 pg/cell (mean ± SEM); this measured dry cell weight is similar to those previously reported for two hESC lines cultured in Essential 8 medium – HUES 9 hESC (250 pg/cell) and H9 hESC (200 pg/cell) (Zhang et al., 2016). Exponential growth was observed for all culture conditions for 48-h. Growth rates were calculated from 0 to 36

hours and were similar between conditions ($p > 0.05$). The similar growth rates shown in Figure 4.2B confirm that the glucose and lactate concentrations did not significantly affect the growth rates of K3 iPSCs. Previously, murine PSCs have been shown to proliferate in up to 40 mM lactate, while growth rates for human PSCs decreased in 11 mM lactate containing media (Chaudhry et al., 2009; Chen et al., 2010; Gupta et al., 2017; Nath et al., 2017). However, low glucose and high lactate culture concentrations did not inhibit growth for K3 iPSCs.

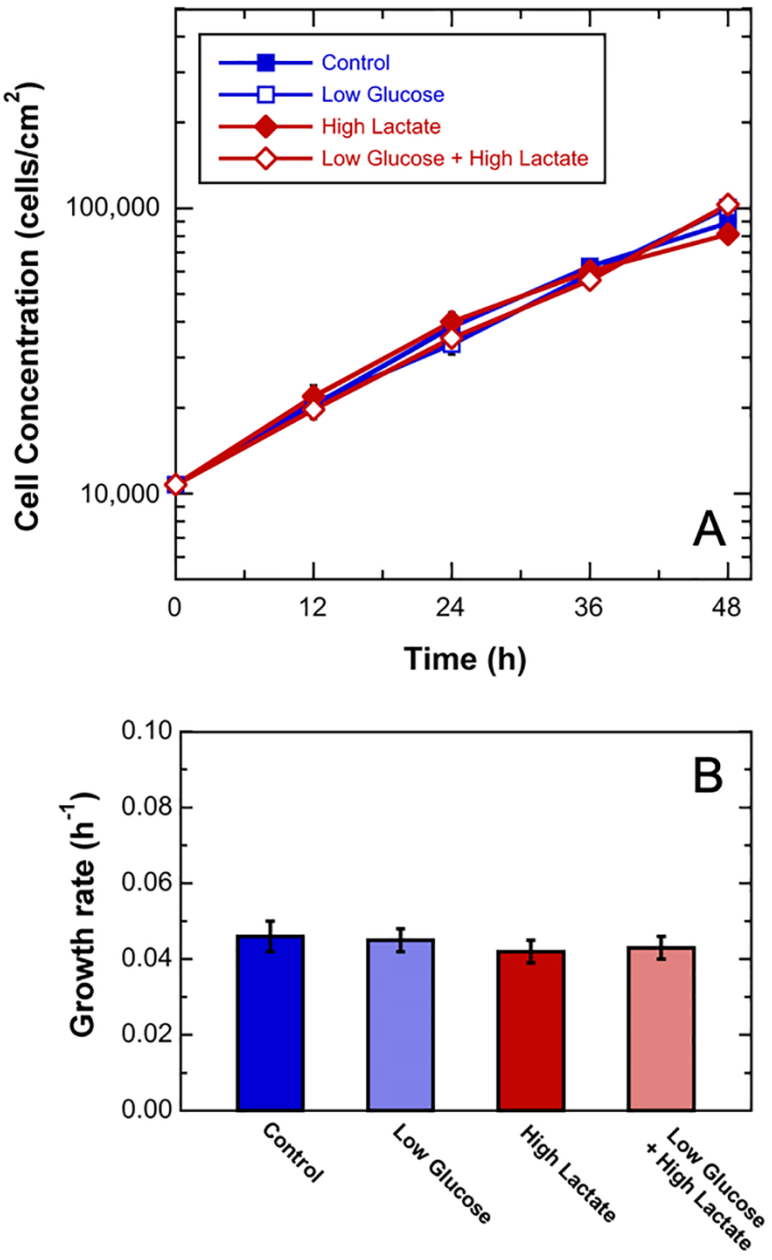

Figure 4.2. Growth characteristics of K3 iPSC cultures in low and high glucose and lactate containing media. A) Growth profiles. The isotope media exchange occurred at 0-h and samples for MID analysis were taken at 24-h and 48-h. Control media – ■; Low Glucose media – □; High Lactate media – ◆; and Low Glucose + High Lactate – ◇. B) Growth rates for the times 0 to 36 hours. Error bars represent standard errors.

4.4.2. Glucose, lactate, and amino acid metabolism

PSCs are dependent on glucose catabolism and lactate production to support cell growth (Gu et al., 2016; Varum et al., 2011; Zhang et al., 2011). To characterize glucose consumption and lactate production for K3 iPSCs, extracellular glucose and lactate concentrations were measured at 0, 12, 24, 36, and 48-h after the media exchange. Figure 4.3 shows the change in glucose and lactate concentrations with time for each culture. The data were normalized to show change in concentration since the initial media concentrations of glucose and lactate had greater differences than the changes observed due to K3 iPSC metabolism in each culture. K3 iPSCs exhibited equal growth rates for each condition (Figure 4.2); however, high extracellular lactate resulted in decreased glucose consumption and reduced lactate accumulation for both high lactate condition ($p \leq 0.05$). Low glucose alone did not significantly impact glucose consumption or lactate production ($p > 0.05$). The average glucose and lactate concentrations for all the 0, 12, 24, 36, and 48-h samples are listed with standard error in Appendix I, Tables I1-I4. Extracellular glucose, lactate, and pyruvate fluxes were calculated using concentrations measured at 12, 24, and 36-h and growth profiles from 0-h through 36-h using the Extracellular Time-Course Analysis (ETA) software (Figure 4.3D) (Murphy and Young, 2013). Additionally, Figure 4.3 shows the pyruvate uptake flux for 0 to 36-h. Both high lactate cultures had decreased pyruvate consumption fluxes ($p \leq 0.05$), whereas the glucose concentration did not have a significant effect on the pyruvate flux ($p > 0.05$). The pyruvate concentration in E8 Flex basal media is only 0.4 mM, and it was observed to be depleted between 36 and 48-h.

Initially, each high lactate culture exhibited a decreased glycolytic efficiency for the first 12-h of culture (Figure 4.3C). Then, from 12 to 48 hours, the glycolytic efficiencies were similar across the four conditions. Glycolytic efficiency is defined as the moles of lactate produced per mole of glucose consumed, with the theoretical maximum glycolytic efficiency being 2.0 moles of lactate produced per mole of glucose consumed. The initial difference in glycolytic efficiencies between the high lactate cultures and the control and low glucose cultures potentially illustrates an initial shift in glucose to lactate metabolism or more likely a lactate shock. This also suggests that iPSCs in the high lactate cultures may not have been at a metabolic steady-state through the first 12-h of growth; therefore, concentration changes during the first 12-h of growth were excluded from flux calculations. Specifically, the low initial glycolytic efficiencies observed immediately following the media exchange (between 0-h and 12-h) for each high lactate culture may be the result of a high initial lactate exchange across the cell membrane (Figure 4.3C), since lactate is transported across the cell membrane through facilitated diffusion by proton-linked monocarboxylate transporters (MCTs) (Halestrap, 2012; Huckabee, 1956). Similarly, pyruvate transport across the plasma membrane is also facilitated by MCTs (Halestrap, 2012). Therefore, the decreased pyruvate consumption in both high lactate culture conditions could be a result of more favorable lactate transport kinetics (Draoui and Feron, 2011). Also, since the glycolytic efficiency observed was always less than 2.0, glucose was not stoichiometrically converted to lactate, as has previously been reported for hESC (Folmes et al., 2011; Turner et al., 2014). However, the similar glycolytic efficiencies between 12-h to 48-h suggest that the same proportion of glucose was catabolized to lactate

in each condition, and only the net glucose consumed decreased for the cells grown in high lactate.

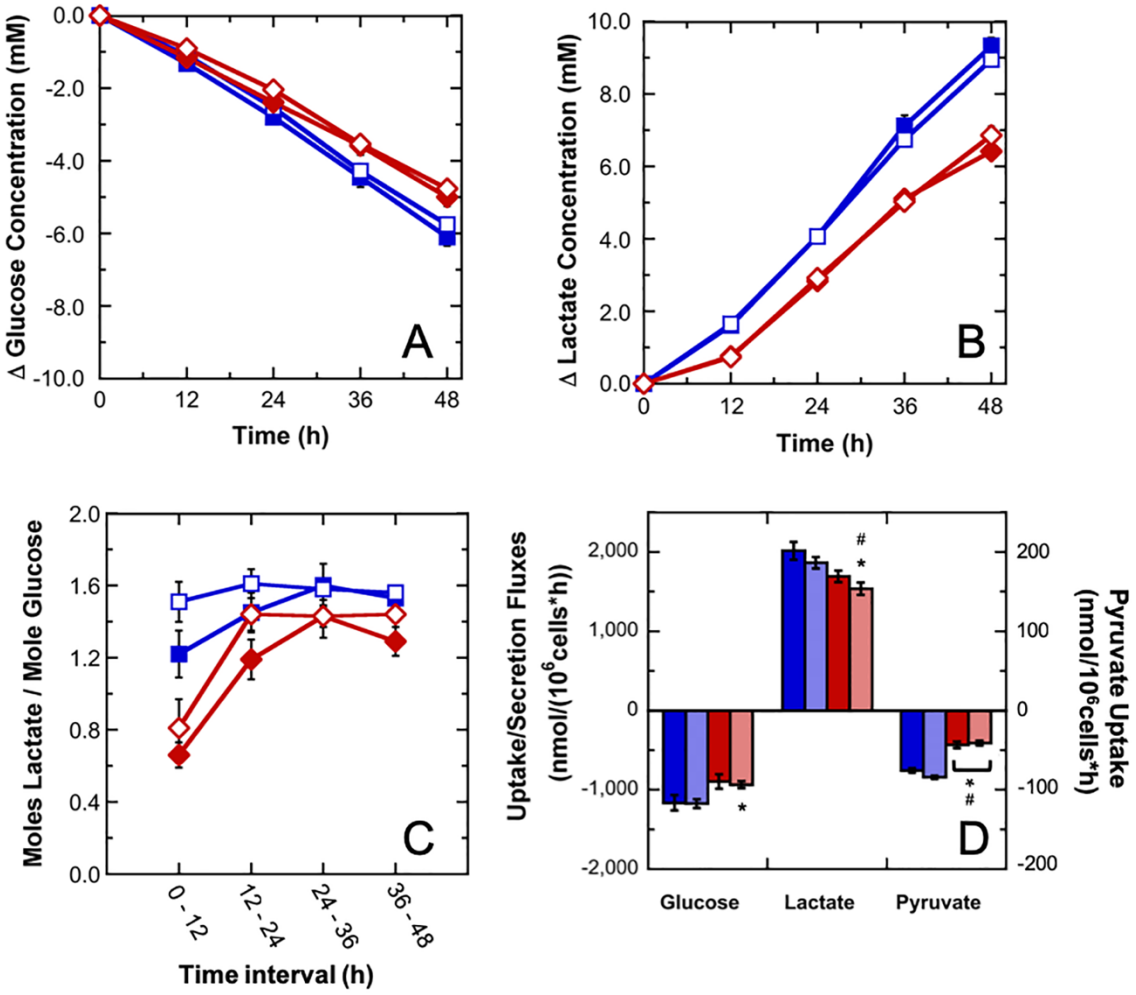

Figure 4.3. Glucose consumption and lactate production profiles for K3 iPSCs. A) Net glucose consumption. B) Net lactate production. C) Glycolytic efficiencies. Control media – ■; Low Glucose media – □; High Lactate media – ◆; and Low Glucose + High Lactate – ◇. Error bars represent standard errors. D) Calculated glucose consumption, pyruvate consumption, and lactate production fluxes for concentration measurements from 12-h to 36-h for Control (■), Low Glucose (■), High Lactate (■), and Low Glucose + High Lactate (■) culture conditions. The asterisk (*) indicates the calculated flux was significantly different from the control condition ($p \leq 0.05$). The pound (#) indicates the calculated flux was significantly different from the low glucose condition ($p \leq 0.05$).

Proliferating cells require significant protein and nucleotide synthesis to maintain rapid growth (Bonarius et al., 1996). As a result, amino acid catabolism plays a critical anaplerotic role in pluripotent stem cell metabolism (Gaspar et al., 2014). Extracellular amino acid concentrations were measured at 0, 12, 24, 36, and 48-h after the media exchange. Statistical analysis was performed to determine if amino acid concentrations were significantly different over time and between the conditions. Asparagine, glycine, lysine, proline, tryptophan, and tyrosine concentrations did not significantly change with respect to time ($p > 0.05$). Therefore, extracellular fluxes were not calculated for these amino acids. All other amino acid concentrations varied significantly with time; thus, fluxes were determined for these amino acids. Serine concentrations did not vary between the culture conditions ($p > 0.05$). However, alanine, aspartate, glutamine, glutamate, histidine, isoleucine, leucine, lysine, methionine, phenylalanine, threonine, and valine concentrations varied between culture conditions ($p \leq 0.05$). Table 4.3 lists the calculated amino acid fluxes with standard error determined using the ETA software, where a Gaussian error propagation approach was implemented (Murphy and Young, 2013). The average amino acid concentrations for all the 0, 12, 24, 36, and 48-h samples are listed with standard error in Appendix I, Tables I1-I4. Amino acid concentration time profiles are included in Appendix J.

High extracellular lactate also caused reduced glutamine consumption, glutamate production, and ammonia accumulation for both high lactate conditions ($p \leq 0.05$). However, the moles of ammonia produced per moles of glutamine consumed remained relatively constant for each of the four culture conditions. Figure 4.4 shows the change in

glutamine, glutamate, and ammonia concentrations with time for each culture. Lactate has previously been suggested to inhibit ammonia secretion in a number of mammalian cell lines (Glacken et al., 1988; Hassell et al., 1991). Two potential mechanisms for this are 1) the metabolic conversion of lactate to pyruvate also promotes alanine production and reduces ammonia accumulation, or 2) lactate inhibits glutaminase activity – the enzyme responsible for converting glutamine to glutamate (Glacken et al., 1988; Hassell et al., 1991). While alanine production did not increase due to high lactate, glutamine consumption decreased for both high lactate cultures. These results suggest that high extracellular lactate inhibits glutamine consumption and ammonia production.

Table 4.3. Experimentally determined biomass specific uptake and production rates for extracellular metabolite (nmol/10^6 cells·h). Fluxes and standard errors were calculated using ETA software using the measured cell growth rates and the metabolite concentrations from 12 to 36 hours (Murphy and Young, 2013). Negative values represent consumption rates and positive values represent production rates.

	Control		Low Glucose		High Lactate		Low Glucose + High Lactate	
Metabolite	**Flux**	**SE**	**Flux**	**SE**	**Flux**	**SE**	**Flux**	**SE**
Glucose	-1164	97.0	-1176	55.1	-897	90.8	-937	43.5
Lactate	2013	113	1861	72.4	1692	73.4	1537	76.2
Pyruvate	-67.6	2.6	-75.3	2.0	-38.6	3.6	-36.5	2.6
Ammonia	135	5.1	125	5.7	105	8.4	107	5.5
Alanine	33.3	2.1	32.2	1.5	28.8	3.5	27.7	3.1
Aspartate	-0.4	0.5	-3.5	0.2	0.3	0.4	-1.8	1.0
Glutamate	36.1	1.7	32.3	1.2	28.3	1.4	29.4	1.6
Glutamine	-141	16.9	-155	9.0	-107	9.6	-119	9.5
Histidine	1.1	3.2	-14.7	1.9	-0.6	2.2	0.0	1.4
Isoleucine	-56.7	10.0	-39.3	5.6	-24.7	6.9	-45.4	8.4
Leucine	-41.8	7.0	-31.3	2.6	-9.8	4.2	-20.9	4.8
Methionine	-7.4	1.6	-4.4	1.1	-0.4	1.5	-0.5	1.9
Phenylalanine	-7.6	4.3	-7.7	2.2	7.8	1.2	8.9	2.4
Serine	-33.5	5.2	-23.8	3.7	-28.0	4.0	-46.3	11.1
Threonine	-9.2	3.8	-2.2	2.0	8.4	2.2	-2.2	2.0
Valine	-15.6	3.6	-15.4	2.2	-4.4	3.2	-6.0	4.4

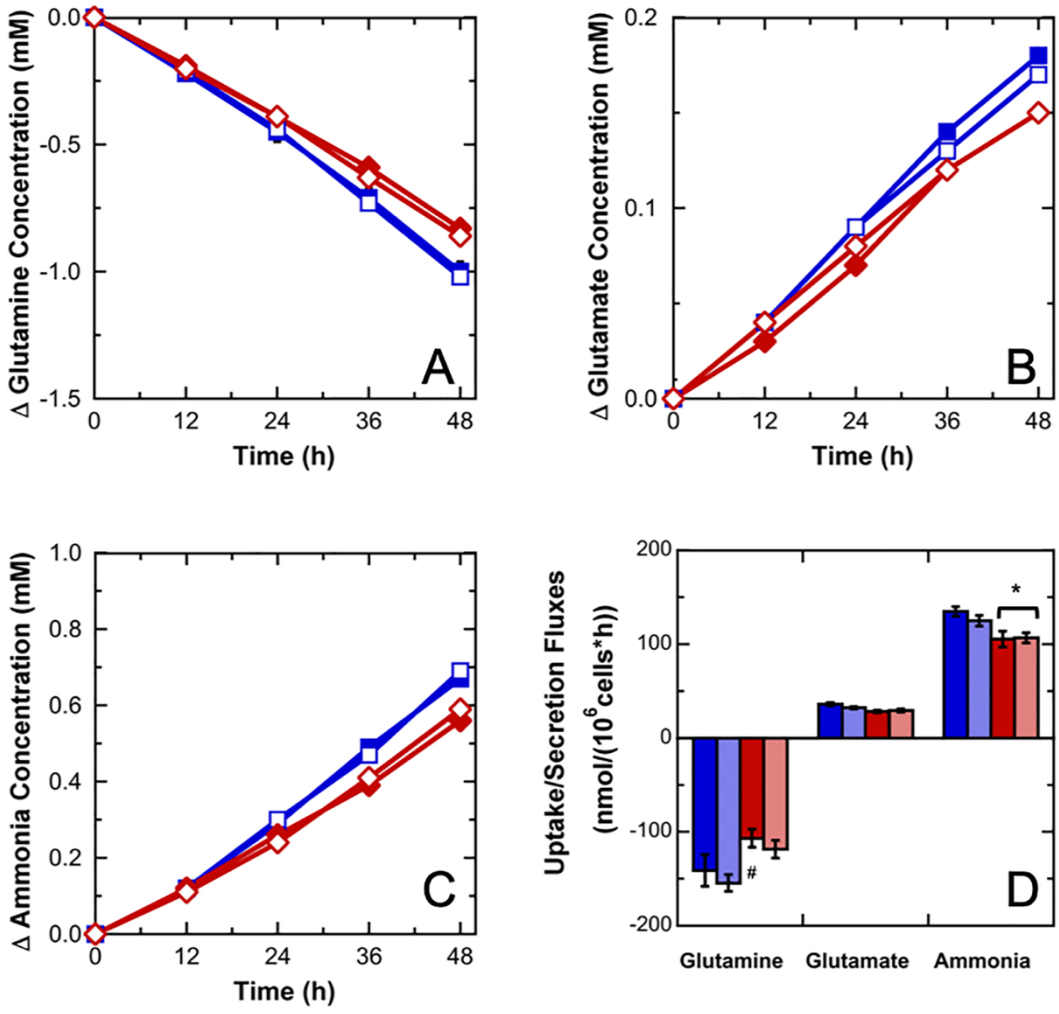

Figure 4.4. Glutamine consumption, glutamate production, and ammonia production profiles for K3 iPSCs. A) Net glutamine consumption. B) Net glutamate production. C) Net ammonia production. Control media – ■; Low Glucose media – □; High Lactate media – ◆; and Low Glucose + High Lactate – ◇. Error bars represent standard errors. D) Calculated glutamine consumption, glutamate production, and ammonia production fluxes for concentration measurements from 12-h to 36-h for Control (■), Low Glucose (■), High Lactate (■), and Low Glucose + High Lactate (■) culture conditions. The asterisk (*) indicates the calculated flux was significantly different from the control condition ($p \leq 0.05$). The pound (#) indicates the calculated flux was significantly different from the low glucose condition ($p \leq 0.05$).

4.4.3. Intracellular metabolite labeling dynamics using [1,2-^{13}C] glucose tracer

To resolve glucose metabolism in the iPSC cultures, [1,2-^{13}C] glucose was used. This tracer has been previously identified as an excellent glucose tracer for resolving metabolic fluxes through glycolysis and the pentose phosphate pathway for mammalian cells (Metallo et al., 2009). Intracellular MIDs were measured for pyruvate, alanine, and lactate from glucose tracer. In this study, poor resolution of the glycolytic metabolites – dihydroxyacetone phosphate, 3-phosphoglycerate, and phosphoenolpyruvate – were obtained; thus, these MIDs were not used in the subsequent model. Steady-state isotope labeling has previously been shown to occur within 24-h for mammalian cells with similar growth rates (Ahn and Antoniewicz, 2013; Metallo et al., 2009). The steady-state fractional labeling for pyruvate, alanine and lactate are shown in Figure 4.5A. The fractional labeling for pyruvate, alanine, and lactate from glucose were lower for the high lactate cultures compared to cultures without added lactate. These results suggest that less glucose-derived carbon was metabolized to pyruvate, lactate, and alanine when lactate levels were high ($p \leq 0.05$). In contrast, the glucose concentration did not significantly affect the fractional labeling for these three species ($p > 0.05$). The fractional labeled species in glycolysis and measured glucose consumption fluxes are consistent with respect to the effects of the lactate concentration and glucose concentration (Figure 4.3D).

In addition to providing overall metabolite enrichment, [1,2-^{13}C] glucose was used to determine the distribution of mass isotopomers for intracellular metabolites. The MIDs for pyruvate, alanine and lactate from [1,2-^{13}C] glucose tracer at 24-h and 48-h for each culture condition are shown in Figure 4.5B-E. Each metabolite was primarily unlabeled

(M+0) and M+2 labeled. The predominant presence of M+2 labeling, compared to M+1 and M+3, suggests that glycolysis was highly active in all four culture conditions. Also, the small fractional abundance of M1 labeling (>2 % in each condition) suggests that the oxidative pentose phosphate pathway was relatively inactive during exponential growth for each culture condition.

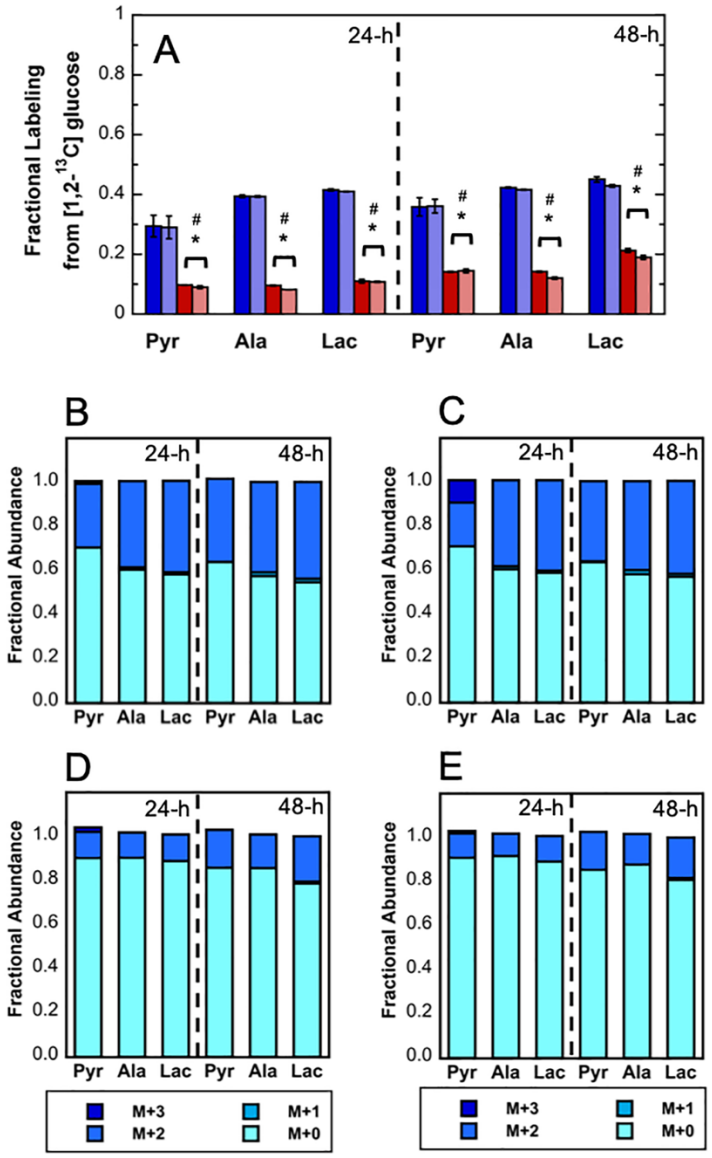

Figure 4.5. Comparison of fractional isotopomer labeling and fractional abundance of MIDs for glycolytic metabolites from [1,2-^{13}C] glucose for K3 iPSCs. A) Percent isotopomer labeling. Control (■), Low Glucose (■), High Lactate (■), and Low Glucose + High Lactate (■) culture conditions. Fractional abundance of MIDs for B) Control media; C) Low glucose media; D) High lactate media; E) Low glucose + high lactate media. Glycolytic metabolites shown are pyruvate (Pyr), alanine (Ala), and lactate (Lac). The mass isotopomer distributions were corrected for natural abundances. The asterisk (*) indicates the calculated flux was significantly different from the control condition ($p \leq 0.05$). The pound (#) indicates the calculated flux was significantly different from the low glucose condition ($p \leq 0.05$).

The fractional labeling of TCA metabolites from [1,2-^{13}C] glucose at 24-h are shown in Figure 4.6. The fractional labeling of citrate was lower for the high lactate cultures, as shown by the higher M+0 fractional abundance. Additionally, the α-ketoglutarate (AKG) labeling from [1,2-^{13}C] glucose was also lower for the high lactate cultures. Together with the overall labeling, fractional abundance of M+2 labeled citrate was lower for the high lactate cultures. These results indicate that glucose-derived carbon entered the TCA cycle either as ^{13}C-labeled acetyl-CoA via the enzyme pyruvate dehydrogenase (PDH) or as ^{13}C-labeled oxaloacetate via the enzyme pyruvate carboxylase (PC). Moreover, the decreased overall labeling, in particular M+2 labeled TCA metabolites, suggests that glucose either served less as a carbon source for mitochondrial metabolism for both of the high lactate cultures, or glucose-derived ^{13}C labeling was diluted by catabolism of another unlabeled carbon substrate.

Lactate accumulation has previously been reported to reduce glycolytic activity by inhibiting hexokinase (HK) and phosphofructokinase (PFK) activity in mammalian cells, where lactate acts as a signaling molecule to down-regulate PFK activity (Ivarsson et al., 2015; Leite et al., 2007; Mulukutla et al., 2012; Mulukutla et al., 2015). In addition, lactate supplementation and conversion to pyruvate impairs NAD^+ generation and promotes pyruvate conversion to acetyl-CoA and entry into the TCA cycle; this also results in repressed glycolytic fluxes due to an increase in NADH/NAD^+ ratio (Fendt et al., 2013; Huckabee, 1956; Mintun et al., 2004). The presence of ^{13}C-labeled TCA metabolites from the [1,2-^{13}C] glucose tracer confirm that some glucose-derived carbon supported oxidative mitochondrial metabolism rather than being used to generate lactate. Furthermore, the

detection of significant intracellular citrate labeling from [1,2-^{13}C] glucose and the low AKG fractional labeling relative to citrate denotes that glucose catabolism supported acetyl-CoA synthesis (Figure 4.6). These results are consistent with recent findings which determined that PSCs relied on a modified Warburg effect, where glucose can be converted to lactate and acetyl-CoA for PSC proliferation (Moussaieff et al., 2015; Zhang et al., 2016).

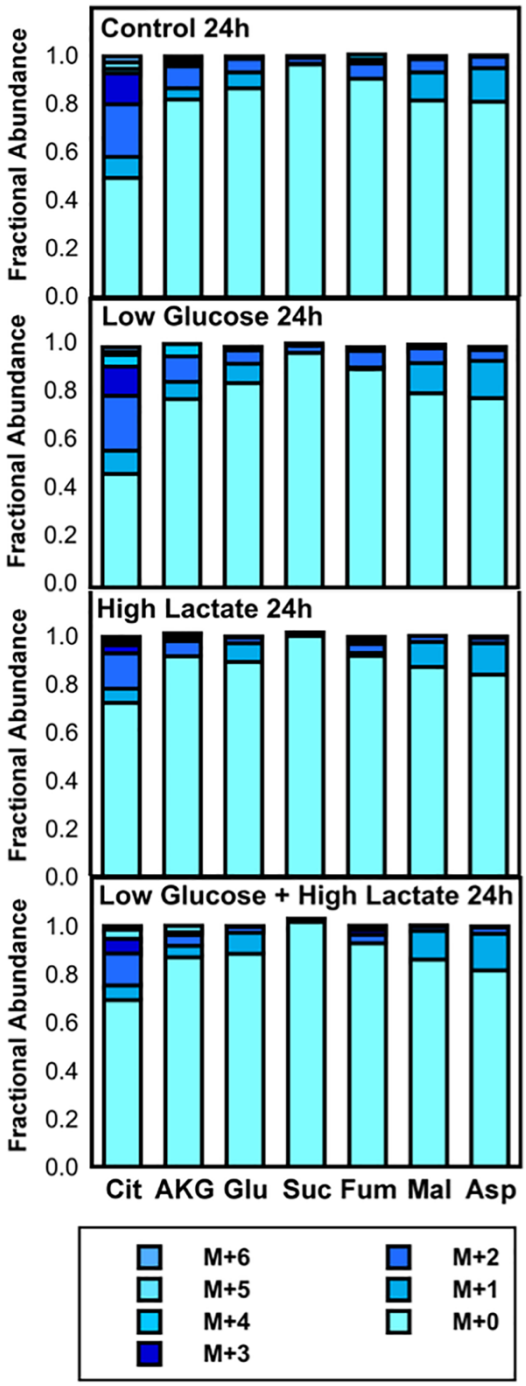

Figure 4.6. Comparison of fractional abundance of MIDs for TCA metabolites from [1,2-^{13}C] glucose for K3 iPSCs at 24-h. TCA metabolites represented are citrate (Cit), α-ketoglutarate (AKG), glutamate (Glu), succinate (Suc), fumarate (Fum), malate (Mal), and aspartate (Asp). The mass isotopomer distributions were corrected for natural abundances.

4.4.4. Intracellular metabolite labeling dynamics from [U-^{13}C] glutamine tracer

To resolve metabolism through the TCA cycle, [U-^{13}C] glutamine was used in parallel with the glucose tracer. The [U-^{13}C] glutamine has previously been shown to be the optimal glutamine tracer for rapidly labeling TCA cycle metabolites and for resolving metabolic fluxes through the TCA cycle for mammalian cells (Metallo et al., 2009). Figure 4.7 shows the fractional labeling of TCA cycle metabolites from [U-^{13}C] glutamine at 24-h. [U-^{13}C] glutamine significantly labeled intracellular TCA cycle intermediate metabolites for all four culture conditions, with over 50% isotope labeling for all measured species (Figure 4.7 and Appendix O, Figure O2). In contrast, pyruvate, alanine, and lactate were minimally labeled from [U-^{13}C] glutamine (data in Appendix N, Table N2). The results suggest that glutamine is not a major carbon source for pyruvate and its byproducts. The overall intracellular metabolite labeling from [U-^{13}C] glutamine was similar for all four conditions; however, there were differences in fractional labeling of TCA metabolites. Overall, these results indicate that for iPSCs, glutamine serves integral anaplerotic role in TCA cycle metabolism, but has little role in pyruvate synthesis, regardless of the extracellular glucose and lactate concentrations investigated in this study (Figure 4.7).

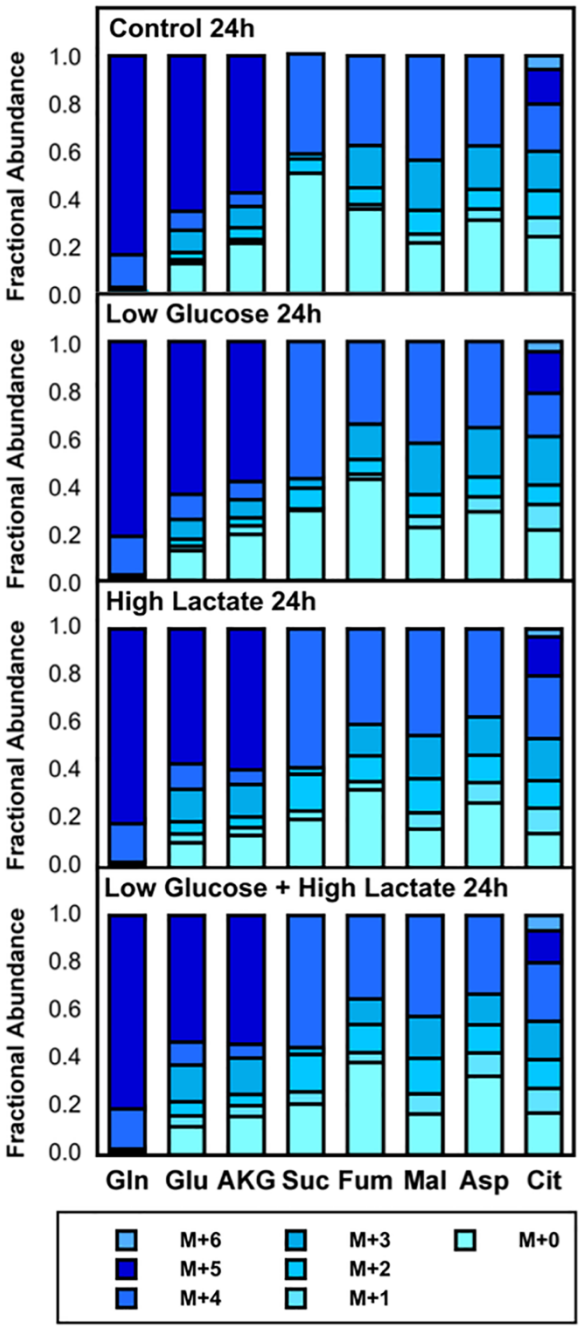

Figure 4.7. Comparison of fractional abundance of MIDs for TCA metabolites from [U-^{13}C] glutamine for K3 iPSCs at 24-h. TCA metabolites represented are glutamine (Gln), glutamate (Glu), α-ketoglutarate (AKG), succinate (Suc), fumarate (Fum), malate (Mal), aspartate (Asp), and citrate (Cit). The metabolites are listed according to the order of oxidative TCA cycle. The mass isotopomer distributions were corrected for natural abundances.

K3 iPSCs utilized reductive glutamine metabolism, irrespective of the glucose or lactate media concentration, as illustrated by the presence of M+5 labeled citrate, along with M+3 malate, fumarate, and aspartate (Figure 4.8A). Figure 4.8B outlines the reaction pathway for reductive carboxylation, including the labeling patterns. These results indicate that the reductive carboxylation appears to be slightly lower for the high lactate cultures; however, this observation is only significant when compared to the low glucose cultures ($p \leq 0.05$). These results demonstrate that glutamine was reductively metabolized through isocitrate dehydrogenase (IDH) and ATP-citrate lyase (ACL) for lipid production in each culture. Reductive carboxylation of glutamine for lipid synthesis has previously been observed in cancer cells grown under hypoxic conditions (≤ 5% O_2) (Fan et al., 2013; Fendt et al., 2013; Grassian et al., 2014; Jiang et al., 2016; Metallo et al., 2012; Metallo et al., 2009; Wise et al., 2011). However, recently it has also been shown that mammalian cells employed reductive carboxylation in response to cell culture stress and due to various media formulations (Brodsky et al., 2019; Jiang et al., 2016). Further, hESCs have been shown to utilize glutamine-mediated reductive carboxylation in chemically defined media – E8 media (Zhang et al., 2016). Similarly, the results from this study indicate that iPSCs used reductive glutamine metabolism to support proliferation in chemically defined media under normoxic (20% O_2) conditions.

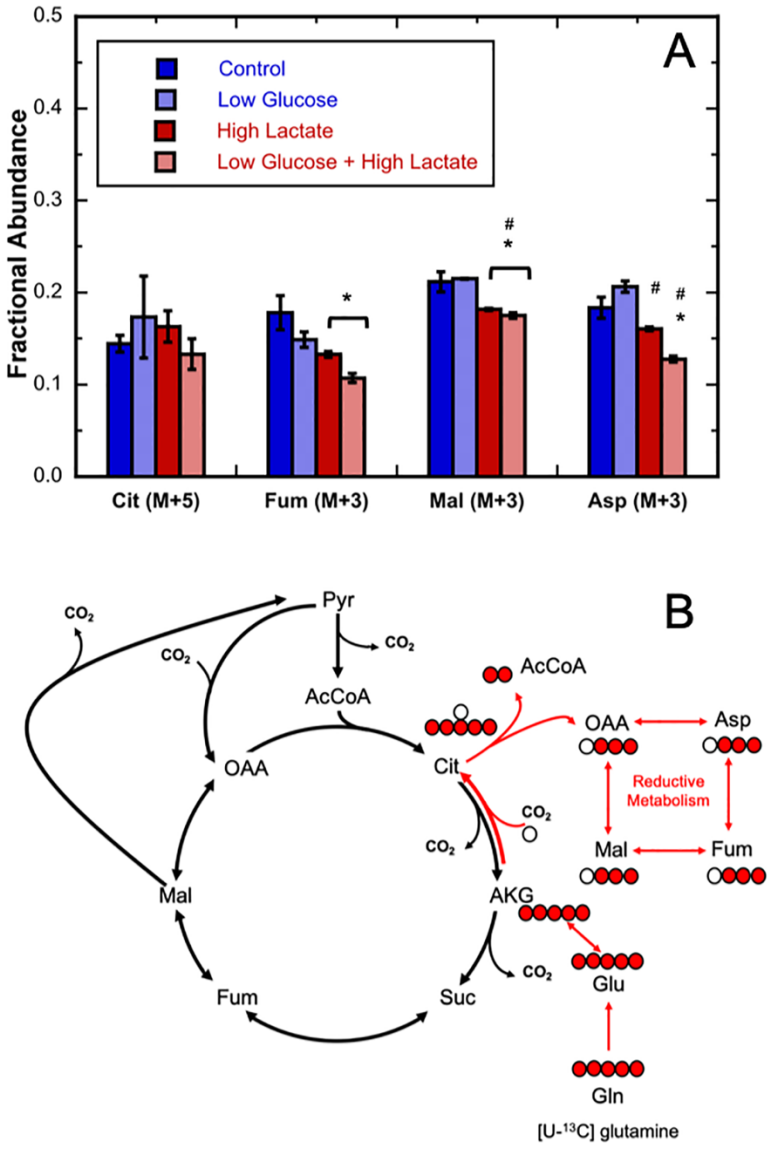

Figure 4.8. Comparison of fractional abundance of reductive carboxylation species from [U-^{13}C] glutamine at 24-h. A) Fractional abundance of M+5 citrate (Cit) and M+3 fumarate (Fum), malate (Mal), and aspartate (Asp) from the Control (■), Low Glucose (■), High Lactate (■), and Low Glucose + High Lactate (■) cultures. MIDs were corrected for natural abundances. The asterisk (*) indicates the fractional labeling was significantly different from the Control cultures ($p \leq 0.05$). The pound (#) indicates the fractional label was significantly different from the Low Glucose cultures ($p \leq 0.05$). B) Carbon atom transition for TCA metabolites from [U-^{13}C] glutamine. Red circles represent ^{13}C and white ^{12}C. The black lines depict oxidative glutamine metabolism. Red lines depict reductive glutamine metabolism that results in M+5 citrate (Cit) and M+3 oxaloacetate (OAA), malate (Mal), fumarate (Fum), and aspartate (Asp).

Interestingly, high lactate in the media also resulted in significantly higher M+4 citrate, M+3 AKG and glutamate, and M+2 succinate, fumarate, malate, and aspartate labeling from [U-^{13}C] glutamine ($p \leq 0.05$) as shown in Figure 4.9A. These changes in intracellular TCA cycle metabolite labeling suggest elevated oxidative glutamine metabolism and retention of glutamine-derived carbon from multiple turns through the TCA cycle for the two high lactate culture conditions (Figure 4.9B). Interestingly, while glutamine consumption diminished for both of the high lactate culture conditions, it appears that the cells compensated for this by retaining more glutamine-derived carbon through multiple rounds of oxidative TCA cycle metabolism. Glutamine oxidation has previously been shown to be indispensable to hPSC metabolism and survival (Tohyama et al., 2016). Also, elevated oxidative glutamine metabolism has previously been shown to occur for PSCs cultured in chemically defined media (Zhang et al., 2016). Similarly, lung carcinoma cells (A549) and osteosarcoma cells (143B) demonstrated increased oxidative glutamine metabolism in response to of 25 mM lactate supplementation, as seen by elevated M+3 AKG and decreased reductive glutamine contribution to citrate (Fendt et al., 2013). Overall, in this study, K3 iPSCs relied primarily on oxidative glutamine metabolism to support proliferation, where the high lactate cultures had higher retention of glutamine-derived carbon through multiple rounds of oxidative TCA cycle metabolism.

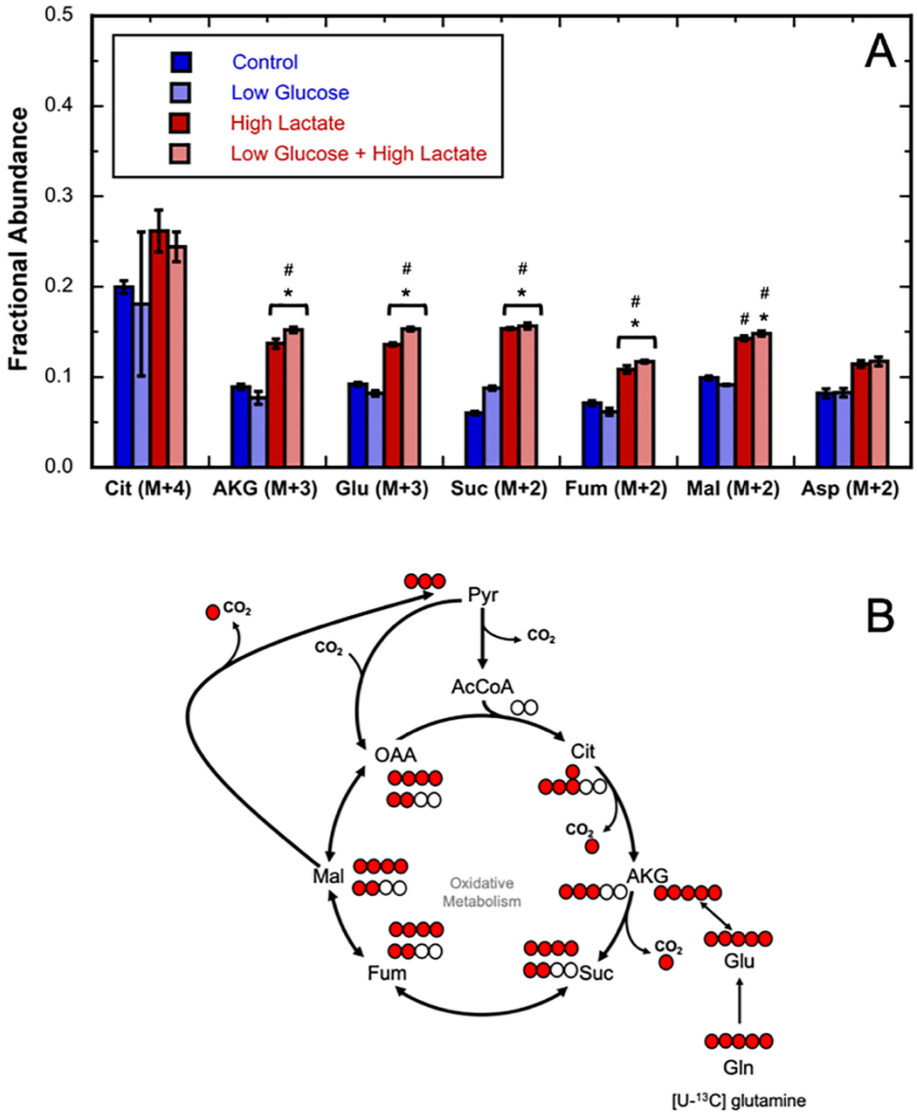

Figure 4.9. Intracellular fractional labeling of oxidative glutamine metabolites from [U-^{13}C] glutamine at 24-h. A) Fractional labeling of TCA cycle metabolites from the Control (■), Low Glucose (■), High Lactate (■), and Low Glucose + High Lactate (■) cultures. B) Potential mechanisms which would result in changes to fractional labeling of TCA cycle metabolites. MIDs were corrected for natural abundances. The asterisk (*) indicates the fractional labeling was significantly different from the control condition ($p \leq 0.05$). The pound (#) indicates the fractional label was significantly different from the low glucose condition ($p \leq 0.05$). Carbon atom transition for TCA metabolites from [U-^{13}C] glutamine. Red circles represent ^{13}C and white ^{12}C. The black lines depict oxidative glutamine metabolism, which results in M+4 citrate (Cit), M+3 α-ketoglutarate (AKG) and glutamate (Glu), and M+2 succinate (Suc), fumarate (Fum), malate (Mal), and aspartate (Asp).

4.4.5. Intracellular metabolite labeling dynamics from [U-^{13}C] lactate tracer

To further understand the role of lactate as a potential metabolic substrate in iPSC metabolism, iPSCs were cultured with high extracellular lactate. [U-^{13}C] lactate was used to allow detection of lactate transport into the cell and metabolic conversion within the cell via MIDs of intracellular species. The amount of time required to reach isotopic steady-state from [U-^{13}C] lactate has not previously been reported for mammalian cells in glucose containing media, so the 24-h and 48-h timepoints were used to evaluate the intracellular lactate labeling dynamics throughout this experiment. Labeled intracellular metabolites [U-^{13}C] lactate included: lactate, pyruvate, alanine, citrate, AKG, succinate, fumarate, malate, and aspartate. For both high lactate culture conditions, the fraction of labeled intracellular pyruvate, alanine and lactate from [U-^{13}C] lactate was observed to be relatively constant between the 24-h and 48-h samples (Figure 4.10A and B). The pyruvate, alanine, and lactate were primarily M+3 labeled. As shown in Figure 4.10C, [U-^{13}C] lactate transport across the cell membrane and direct conversion to pyruvate and alanine results in M+3 labeling. There was also observed M+2 labeling of pyruvate after 24-h, which requires TCA cycle metabolism and conversion to pyruvate via malic enzyme (ME) activity. Figure 4.11A and B illustrate the mechanisms to generate M+2 pyruvate.

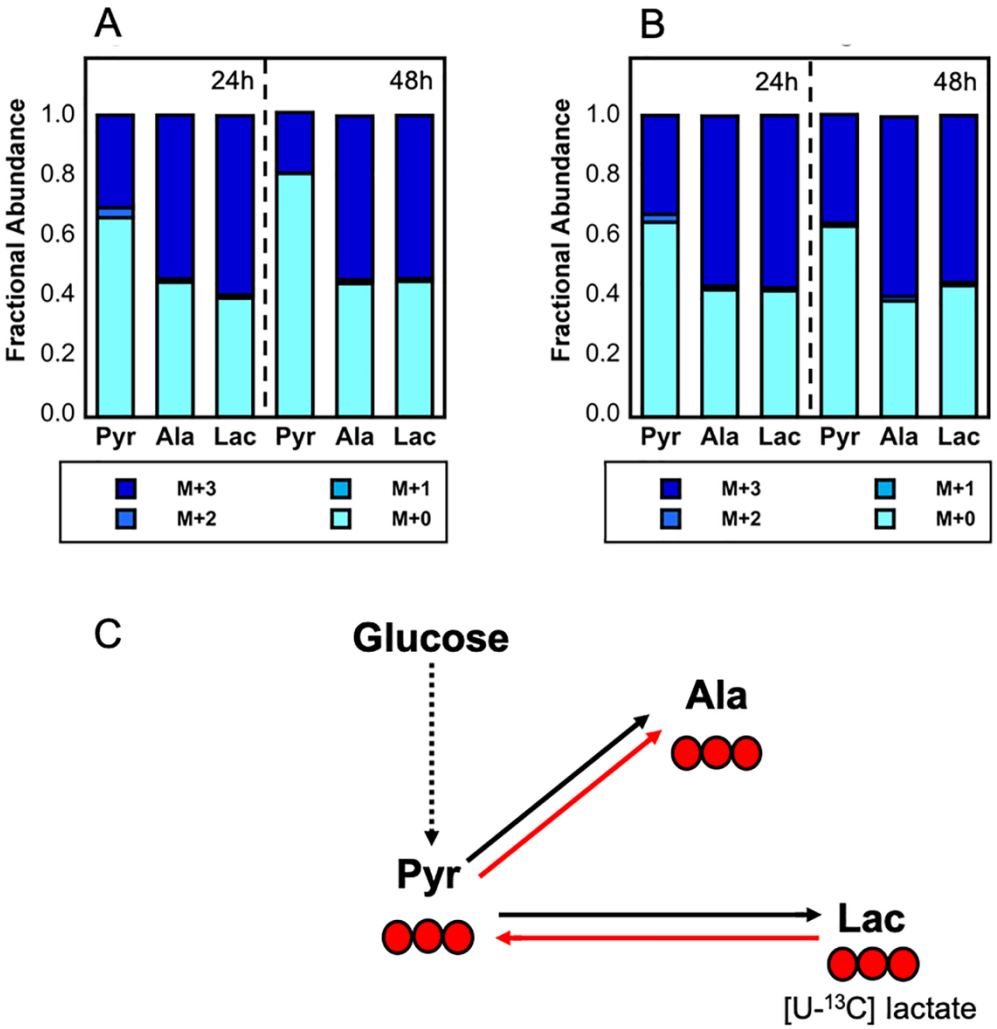

Figure 4.10. Comparison of fractional abundance of MIDs for glycolytic metabolites from [U-^{13}C] lactate labeling for K3 iPSCs. A) High Lactate media; B) Low Glucose + High Lactate media; Pyruvate (Pyr), alanine (Ala), and lactate (Lac) metabolites are shown. MIDs were corrected for natural abundances. C) Carbon atom transition for glycolytic metabolites from [U-^{13}C] lactate. Red circles represent ^{13}C and white ^{12}C. Red lines indicate lactate consumption and metabolism to intracellular pyruvate and alanine. Black lines represent production of alanine and lactate from glucose.

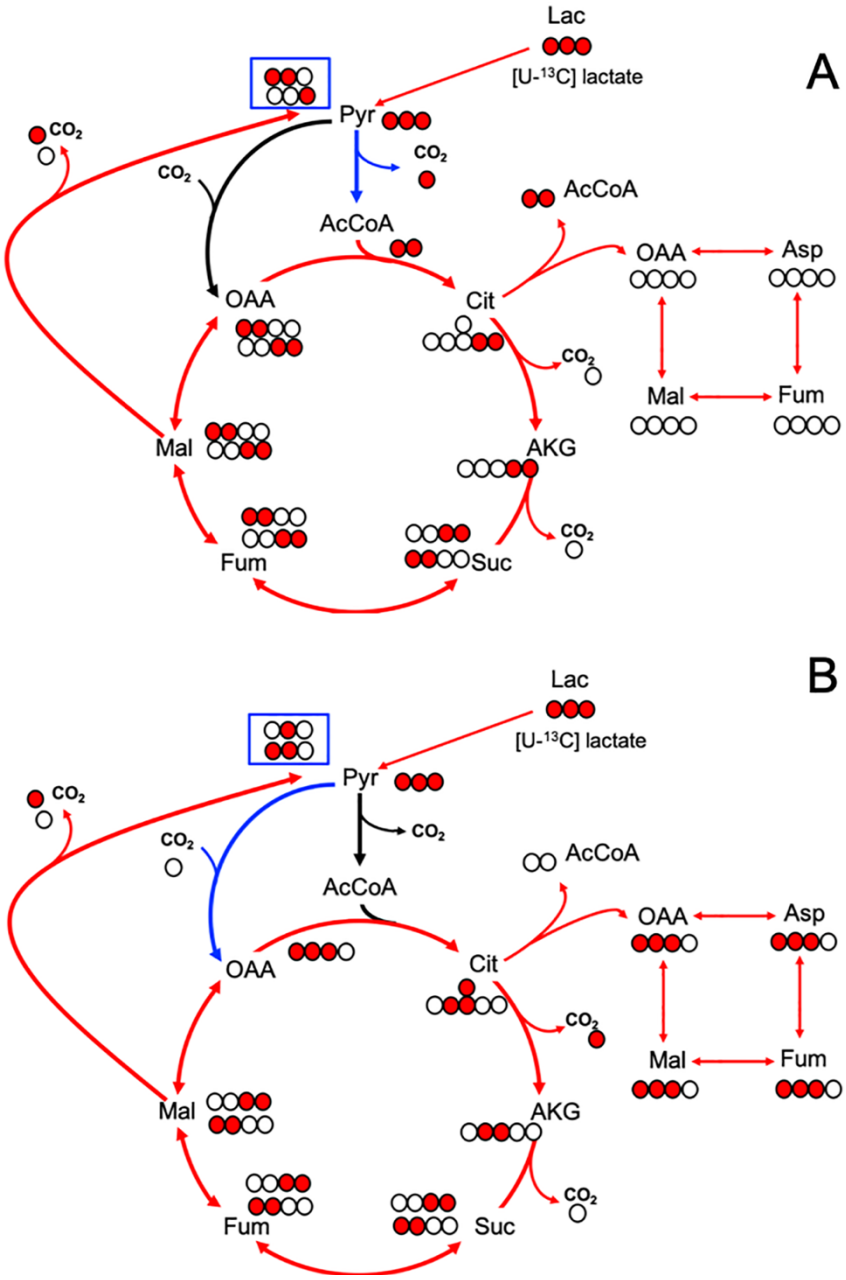

Figure 4.11. Carbon atom transitions outlining potential mechanisms for generating M+2 labeled pyruvate from [U-^{13}C] lactate. Red circles represent ^{13}C and white ^{12}C. The red lines depict reactions involving ^{13}C-labeled metabolites. The black lines indicate reactions involving unlabeled metabolites. The blue lines represent the two reactions responsible for entry of M+3 pyruvate into the TCA cycle. A) Pyruvate conversion to acetyl-CoA via the pyruvate dehydrogenase (PDH) enzyme. B) Pyruvate carboxylation to oxaloacetate via the pyruvate carboxylase (PC) enzyme.

For the TCA cycle metabolites, citrate was highly labeled at 24-h for both high lactate cultures, whereas AKG, malate, and aspartate were all significantly less labeled, as illustrated by the fractional abundance of M+0 in each metabolite (Figure 4.12). Succinate and fumarate were also less labeled than citrate. Succinate and fumarate labeling were lower due to significant dilution from consumption of unlabeled amino acids. As mentioned above, M+2 pyruvate labeling was observed from [U-^{13}C] lactate after 24-h of culture; this would result from metabolism of [U-^{13}C] lactate through one round of the TCA cycle and converted back to pyruvate through ME activity. ^{13}C-lactate can enter into the TCA cycle either through PDH or PC reactions. While metabolism of ^{13}C-lactate through each of these reactions would result in M+2 labeling of pyruvate, as illustrated in Figure 4.11A (PDH) and Figure 4.11B (PC), each pathway would result in differential citrate labeling. The higher fractional abundance of M+2 citrate compared to M+3 would suggest that the PDH reaction was more active in metabolism of ^{13}C-lactate into the mitochondria.

Interestingly, fractional intracellular labeling from ^{13}C-lactate remained relatively constant between 24-h and 48-h for glycolytic byproducts (Figure 4.10A and B), while in contrast, the fractional labeling of the TCA cycle metabolites was significantly higher at 48-h, as shown in Figure 4.12 and in Appendix O, Figure O3. These results suggest that [U-^{13}C] lactate labeling of intracellular alanine, lactate, and pyruvate reached isotopic steady-state by 24-h, while the TCA cycle metabolites had not yet approached isotopic steady-state. Also, along with the decreased contribution of [1,2-^{13}C] glucose to pyruvate and TCA cycle metabolism for the two high lactate cultures, the uptake and metabolism of the [U-^{13}C] lactate tracer implies that lactate can partially replace glucose as a carbon

source for iPSC metabolism. A similar metabolic response was observed for various types of cancer cells cultured in high lactate supplemented media (Fendt et al., 2013). It is widely accepted that cancer cells are capable of consuming and metabolizing lactate as a metabolic substrate (Kennedy et al., 2013; Martinez-Outschoorn et al., 2011; Pavlides et al., 2009; Sonveaux et al., 2008). Similarly, these results indicate that ^{13}C-lactate was continuously in exchange across the cell membrane and served as a metabolic substrate to support K3 iPSC proliferation throughout exponential growth.

The high fractional abundance of labeled citrate relative to other TCA metabolites also suggests that lactate served as a substrate in support of lipid synthesis. Proliferative cells perform *de novo* lipid synthesis rather than scavenging for free fatty acids, which results in truncated TCA cycle metabolism, with high ACL activity to support lipid synthesis; this results in citrate and acetyl-CoA primarily supporting lipid synthesis (DeBerardinis et al., 2008; Zhang et al., 2016). Lactate-derived carbon supported lipid synthesis and histone acetylation in cancer cell metabolism (Chen et al., 2016; Martinez-Outschoorn et al., 2011). Specifically, cells exposed to 10 mM extracellular lactate exhibited increased histone acetylation for a breast cancer cell line and increased malignancy and stemness gene expression (Martinez-Outschoorn et al., 2011). Further, in an *in vivo* human lung tumor model, lactate preferentially supported mitochondrial metabolism over glucose (Faubert et al., 2017). Similarly, acetyl-CoA production has been shown to be critical for the maintenance of PSCs, where decreased glycolytic flux and decreased acetyl-CoA production can result in the onset of spontaneous differentiation; however, acetate media supplementation prevented early spontaneous differentiation

(Moussaieff et al., 2015). Moreover, inhibition of pyruvate dehydrogenase kinase, a pyruvate dehydrogenase inhibitor, redirected glucose-derived carbon to acetyl-CoA rather than lactate and resulted in increased histone acetylation and a higher percentage of Oct4 positive cells (Moussaieff et al., 2015). In a similar manner, lactate appears to play a metabolic role to K3 iPSC metabolism. Therefore, lactate consumption may play an important functional role in iPSC metabolism during proliferation.

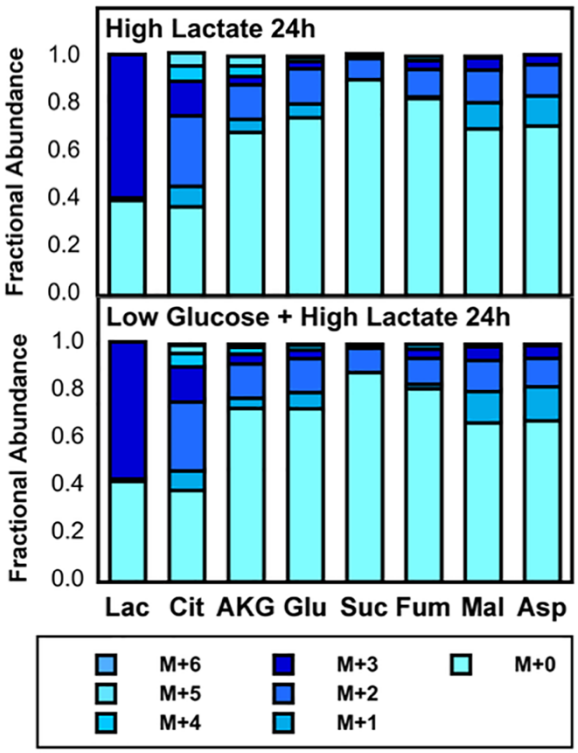

Figure 4.12. Comparison of fractional abundance of MIDs for TCA metabolites from [U-^{13}C] lactate labeling for K3 iPSCs at 24-h. A) Fractional abundance of ^{13}C mass isotopomer distributions for TCA metabolites from High Lactate and Low Glucose + High Lactate cultures. TCA metabolites represented are citrate (Cit), α-ketoglutarate (AKG), glutamate (Glu), succinate (Suc), fumarate (Fum), malate (Mal), and aspartate (Asp). The mass isotopomer distributions were corrected for natural abundances.

4.4.6. Pluripotency and differentiation potential

In order to determine the effects of the glucose and lactate concentrations on iPSC pluripotency, K3 iPSCs were grown for one and five passages under each culture condition. Cells from these cultures were analyzed for pluripotency gene expression using qPCR and protein expression by western blot analysis. Three genes were used to monitor pluripotency – Oct4, Sox2, and Nanog (Boyer et al., 2005). Oct4 expression was selected to assess pluripotency by protein expression via western blots. The gene expression levels for Oct4, Sox2, and Nanog are shown in Figure 4.13A and 4.13C for K3 iPSCs cultured for one or five passages in the four culture media. For the cultures after one passage, none of the genes had significantly different expression ($p > 0.05$). Sox2 and Nanog expression levels were significantly higher for the five passage low glucose + high lactate cultures ($p \leq 0.05$); however, glucose and lactate media concentrations did not affect Oct4 gene expression levels after five passages ($p > 0.05$) (Figure 4.13C). Also, normalized Oct4 protein expression levels were similar for all four cultures after one and five passages in each culture condition ($p > 0.05$) (Figure 4.13B and D).

Tight regulation of Oct4 expression is required to maintain pluripotency for PSCs *in vitro*. Elevated Oct4 expression has been shown to induce differentiation towards the primitive ectoderm and mesoderm, while loss of Oct4 expression caused differentiation towards the trophectoderm (Chambers et al., 2003; Niwa et al., 2000). Sox2 expression must be also tightly regulated to maintain pluripotency. Loss of Sox2 expression induces differentiation towards the trophectoderm (Chew et al., 2005). In addition, a two- to five-fold increase in Sox2 expression resulted in differentiation towards the trophectoderm and

loss of Oct4 and Nanog expression (Adachi et al., 2010). Similarly, Nanog expression represses differentiation towards the primitive ectoderm (Wang et al., 2012). However, overexpression of Nanog also prevented differentiation in ESCs (Chambers et al., 2003). Interestingly, Oct4 serves as a transcriptional regulator for hexokinase (HK) and phosphofructokinase (PFK) – two key glycolytic enzymes – and maintenance of Oct4 expression and elevated glycolytic fluxes are critical factors for maintaining iPSC pluripotency (Kim et al., 2015). In this study, the observed decreased glucose consumption due to high lactate did not affect Oct4 expression. Thus, the reduced glucose catabolism appears to have resulted from high lactate exposure alone, rather than loss of Oct4 expression. In previous work, high lactate concentrations have been shown to have variable effects on PSC pluripotency; murine ESCs and iPSCs proliferated and maintained pluripotency in lactate concentrations up to 40 mM, while hESCs exhibited decreased pluripotency through Tra-1-60 expression after continuous passaging in 22 mM lactate containing media (Chaudhry et al., 2009; Chen et al., 2010; Gupta et al., 2017; Martinez-Outschoorn et al., 2011). The results of this study suggest that glucose and lactate concentrations within ranges that support exponential growth equal to the control media do not negatively affect human K3 iPSC pluripotency.

Passage five K3 iPSCs were spontaneously differentiated through embryoid body (EB) formation to assess the differentiation capacity of iPSCs after prolonged culture in low glucose and high lactate culture conditions. Oct4, Sox2, and Nanog gene expression levels were measured to assess pluripotency. Additionally, expression levels for three germ layer-specific genes were measured in the EBs to assess the germ layer differentiation

potential – Pax6 (ectoderm), Gata2 (mesoderm), and Sox17 (endoderm) (Aasen et al., 2008). After seven days of spontaneous differentiation, EBs from each culture condition had lower Nanog expression; however only cells from the low glucose + high lactate culture exhibited significant loss of Oct4 and Nanog expression ($p \leq 0.05$) (Figure 4.14A). On the other hand, Sox2 expression was higher for the EBs from all four culture conditions. In addition to promoting differentiation towards the trophectoderm, elevated Sox2 expression has previously been shown to play an important role in self-renewal during hESC differentiation towards the endoderm (Kallas et al., 2014). The EBs also showed slightly elevated expression levels of Pax6 and Gata2, which indicates expression towards the ectoderm and mesoderm (Figure 4.14B); however, no change in Sox17 expression was observed. Interestingly, EBs from both low glucose cultures exhibited higher Gata2 expression, suggesting that culturing iPSCs in low glucose concentrations could promote spontaneous differentiation towards the mesoderm. Nonetheless, EBs generated from cells cultured in each of the four different growth media also contained many cells in a pluripotent state after seven days of spontaneous differentiation. Taken together, these results illustrate that spontaneous differentiation of EBs from all four culture conditions showed initial signs of loss of pluripotency and differentiation towards the mesoderm and ectoderm, but longer spontaneous differentiation is required to assess K3 iPSC differentiation capacity.

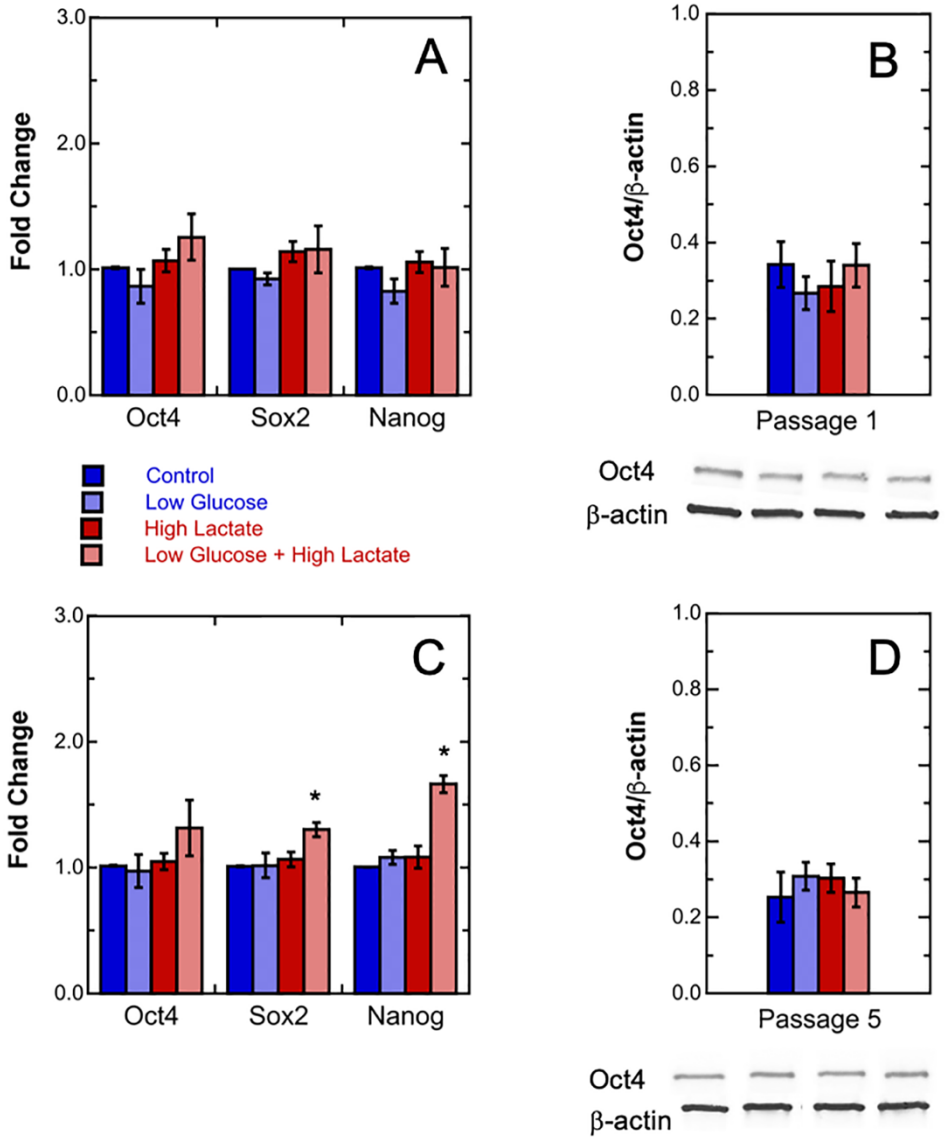

Figure 4.13. Comparison of pluripotency gene and protein expression for K3 iPSCs after one and five passages due to glucose and lactate concentration. A) Normalized gene expression for Oct4, Sox2, and Nanog for undifferentiated iPSCs after one passage in Control (■), Low Glucose (■), High Lactate (■), and Low Glucose + High Lactate (■) culture media. B) Normalized protein expression of Oct4 after one passage. C.) Normalized gene expression of Oct4, Sox2, and Nanog after five passages in culture test conditions. D) Normalized protein expression for Oct4 after five passages in culture test conditions. Error bars represent standard error (N = 6). The asterisk (*) indicates that the normalized gene or protein expressions were significantly different from the control ($p \leq 0.05$)

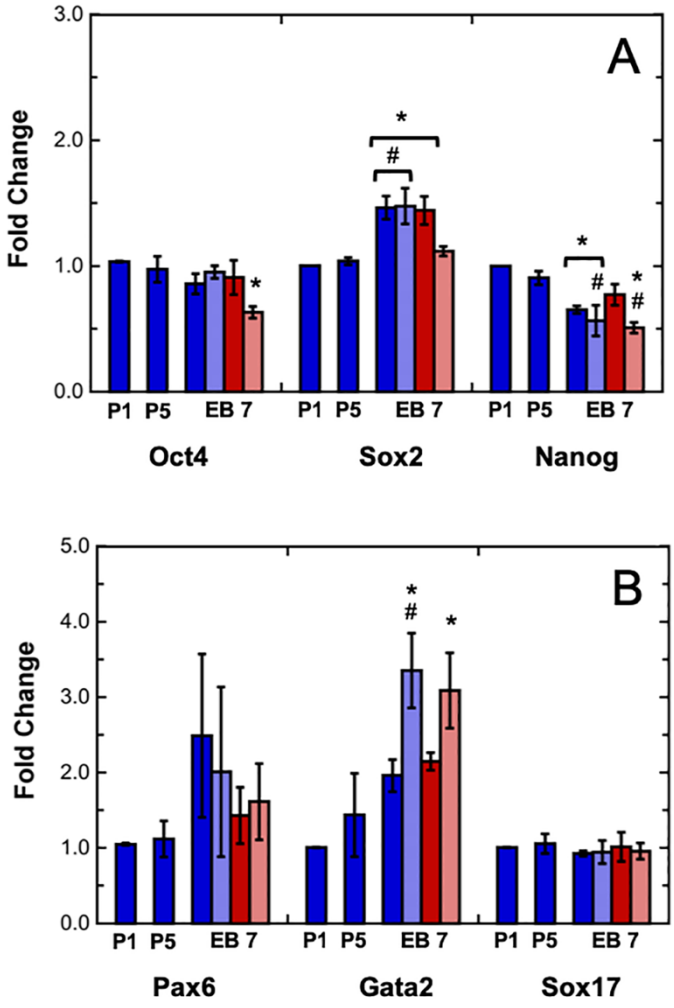

Figure 4.14. Comparison of gene expression for K3 iPSCs after one passage, five passages, and seven days of spontaneous differentiation due to glucose and lactate concentration. A) Normalized gene expression for Oct4, Sox2, and Nanog for iPSCs after one passage (P1), five passages (P5), and seven days of spontaneous differentiation as embryoid bodies (EB 7) in Control (■), Low Glucose (■), High Lactate (■), and Low Glucose + High Lactate (■) culture media. B) Normalized gene expression for Pax6, Gata2, and Sox17 for iPSCs after one passage (P1), five passages (P5), and seven days of spontaneous differentiation as embryoid bodies (EB 7). Error bars represent standard error (N = 3). The asterisk (*) indicates the normalized gene expression was significantly different from P1 ($p \leq 0.05$). The pound (#) indicates normalized gene expression was significantly different from P5 ($p \leq 0.05$).

4.4.7. Metabolic flux analysis

Detailed intracellular metabolic fluxes were generated for the four culture conditions using the parallel ^{13}C-labeling data, the extracellular measured fluxes, and the metabolic network. The parallel labeling data used in the MFA model included the [1,2-^{13}C] glucose and [U-^{13}C] glutamine MIDs for all culture conditions and the [U-^{13}C] lactate MIDs for the high lactate culture conditions. The INCA software was used to obtain the intracellular metabolic fluxes for K3 iPSCs grown in all four growth media.

As previously mentioned, the [U-^{13}C] lactate tracer provided evidence that lactate was consumed and metabolized by K3 iPSCs in both high lactate cultures (Figures 4.10 and 4.12); however, net lactate production was observed for K3 iPSCs in all four culture conditions (Figure 4.3). Thus, lactate was produced and consumed by iPSCs in the high lactate cultures. As no one has previously used ^{13}C-MFA to model the dual consumption and production of a metabolic species with an isotopically labeled tracer, a novel approach was employed to model the reversible metabolism of the lactate tracer. A diagram of the metabolic reactions used to model lactate production and consumption is shown in Figure 4.15A, where reaction v_1 represents the measured net production flux of lactate from the cytosol (Lac.c) to the extracellular media (Lac.x), and reaction v_2 represents the consumption flux of lactate tracer (Lac.t) into the cytosol (Lac.c). The magnitude of the lactate tracer flux was not measured; therefore, the lactate tracer flux could not be constrained to a known measurement. Instead, the lactate tracer reaction into the cell was defined as a reversible reaction and fixed to a net flux of zero. This allowed for the model to simulate an infinite exchange of the lactate tracer into and out of the cell without defining

a net lactate tracer flux. The model predicted net lactate production fluxes for all four culture conditions. Also, lactate tracer exchange fluxes into the cell were also simulated in all four conditions, with the model predicting approximately ten times higher lactate exchange fluxes for both of the high lactate culture conditions (Figure 4.15B). This indicates that the metabolic model was capable of incorporating [U-^{13}C] lactate tracer into the cell even though a net lactate production flux was observed. Previously, Brodsky et al. (2019) used [U-^{13}C] lactate tracer along with ^{13}C-MFA to determine the contribution of lactate to breast cancer metabolism; however, intracellular metabolite labeling from [U-^{13}C] lactate tracer was not incorporated in the ^{13}C-MFA simulations (Brodsky et al., 2019), in part due to much lower intracellular labeling due to lactate. The metabolic network reactions used in this work allowed for [U-^{13}C] lactate MIDs to be incorporated into the ^{13}C-MFA simulations to account for consumption of lactate tracer.

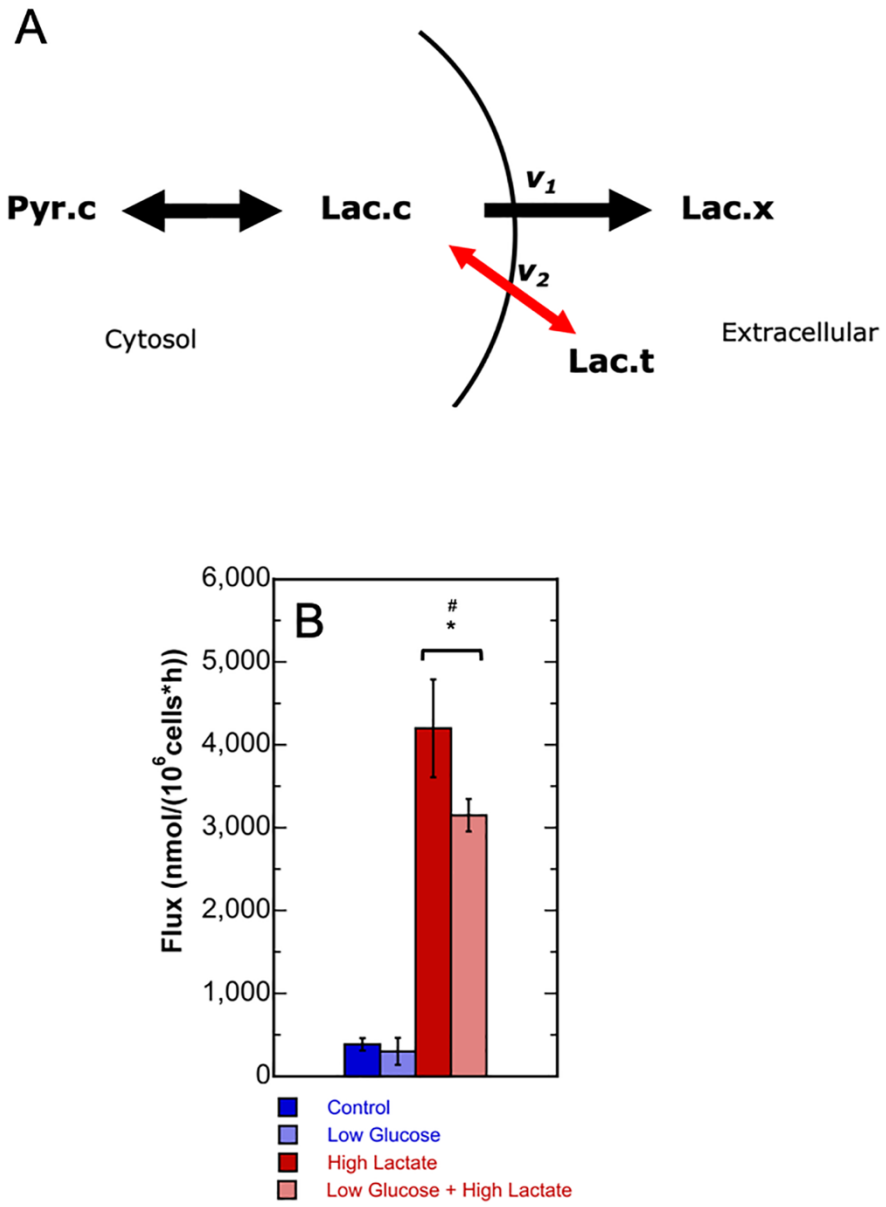

Figure 4.15. Lactate tracer uptake and production for the network model reaction. A) A diagram of the metabolic reactions used to model lactate production and lactate consumption for K3 iPSCs using ^{13}C-MFA. Reaction v_1 represents the net lactate production flux. Reaction v_2 represents the reversible flux of lactate tracer into and out of the cell. B) Simulated lactate tracer exchange flux in Control (■), Low Glucose (■), High Lactate (■), and Low Glucose + High Lactate (■) culture media. Error bars represent standard error. The asterisk (*) indicates the flux was significantly different from the control condition ($p \leq 0.05$). The pound (#) flux was significantly different from the low glucose condition ($p \leq 0.05$).

The intracellular metabolic flux distributions from ^{13}C-MFA simulations for K3 iPSCs from all four culture conditions are shown graphically on the metabolic maps shown in Figures 4.16 and 4.17. As expected, the glucose consumption and lactate production rates had the highest fluxes in each condition. Additionally, the simulations predicted lower glucose consumption and lactate production fluxes for the two high lactate culture conditions compared to the control and low glucose cultures (Figure 4.18A). In order for the model to converge to an acceptable fit for each culture condition, a fatty acid sink (FA.snk) reaction was included in the model. Sink reactions have previously been used to account for loss of carbon through metabolic reactions not included in the metabolic network model (Ahn and Antoniewicz, 2013). Recently, PSCs have been shown to possess some metabolic flexibility in response to media formulations, especially with regards to acetyl-CoA generation and lipid biosynthesis rates (Moussaieff et al., 2015; Zhang et al., 2016). Since lipid content was not measured in this study, the fatty acid sink flux allowed for flexibility with respect to lipid biosynthesis predictions. Interestingly, the model predicted higher fluxes to the fatty acid sink for each of the high lactate cultures (Figures 4.16 and 4.17). Along with the high fractional labeling of citrate from [U-^{13}C] lactate, these metabolic flux simulations indicate that lactate supplementation promoted acetyl-CoA production and lipid biosynthesis in each of the high lactate culture conditions.

Similar to the extracellular concentration measurements, the metabolic flux model simulated lower glutamine consumption fluxes, as well as reduced conversion of glutamine to AKG. As a result, slightly lower fluxes through the TCA cycle were also predicted, as illustrated by consistent citrate synthase (CS), α-ketoglutarate dehydrogenase (AKGD),

succinate dehydrogenase (SDH) and fumarase (FUM) fluxes (Figure 4.17B). The metabolic flux models also predicted high ME activity for the iPSCs in all four culture conditions (Figure 4.18C). However, glutaminolysis was not the major source of pyruvate production, with ME fluxes approximately 10% of the glucose consumption fluxes. Interestingly, the metabolic model predicted lower ME fluxes for the two high lactate conditions (Figure 4.18C); this also corresponded with decreased simulated flux from pyruvate to oxaloacetate through PC. This indicates a lower anaplerotic contribution of glutamine to mitochondrial pyruvate via ME due to high extracellular lactate. Elevated cycling between ME and pyruvate carboxylase (PC) has previously been observed for CHO cells and was suggested to be the cause for low oxidative PPP fluxes during early exponential growth, since the NADP-dependent isoform of ME can provide NADPH to meet cellular demands (Ahn and Antoniewicz, 2011; Templeton et al., 2013). Also, oxidative glutaminolysis to pyruvate through ME served as a significant source of NADPH for glioma cells (DeBerardinis et al., 2007).

As mentioned earlier, the increased M+3 AKG and glutamate labeling, and M+2 succinate, fumarate, malate, and aspartate labeling from [U-^{13}C] glutamine in the high lactate cultures represents increased oxidative glutamine metabolism and higher retention of ^{13}C-labeled metabolites in the TCA. This was also coupled with increased malate dehydrogenase (MDH) activity in the high lactate cultures, as illustrated by increased flux of oxaloacetate to malate in the cytosol and increased flux of malate to oxaloacetate in the mitochondria (Figure 4.16 and 4.17). Along with this, increased malate transport from the cytosol to the mitochondria was predicted. These results suggest increased malate-aspartate

shuttle activity in the high lactate culture conditions. The malate-aspartate shuttle is responsible for transporting reducing cofactors from the cytosol to the mitochondria (Mulukutla et al., 2010). Since lactate was metabolized to pyruvate in the high lactate cultures, this would result in elevated cytosolic NADH production. Therefore, increased malate shuttle activity would support transport of reducing cofactors generated from lactate catabolism into the mitochondria for oxidative phosphorylation. These results illustrate an underlying metabolic flexibility of iPSCs in response to low glucose and high lactate culture conditions.

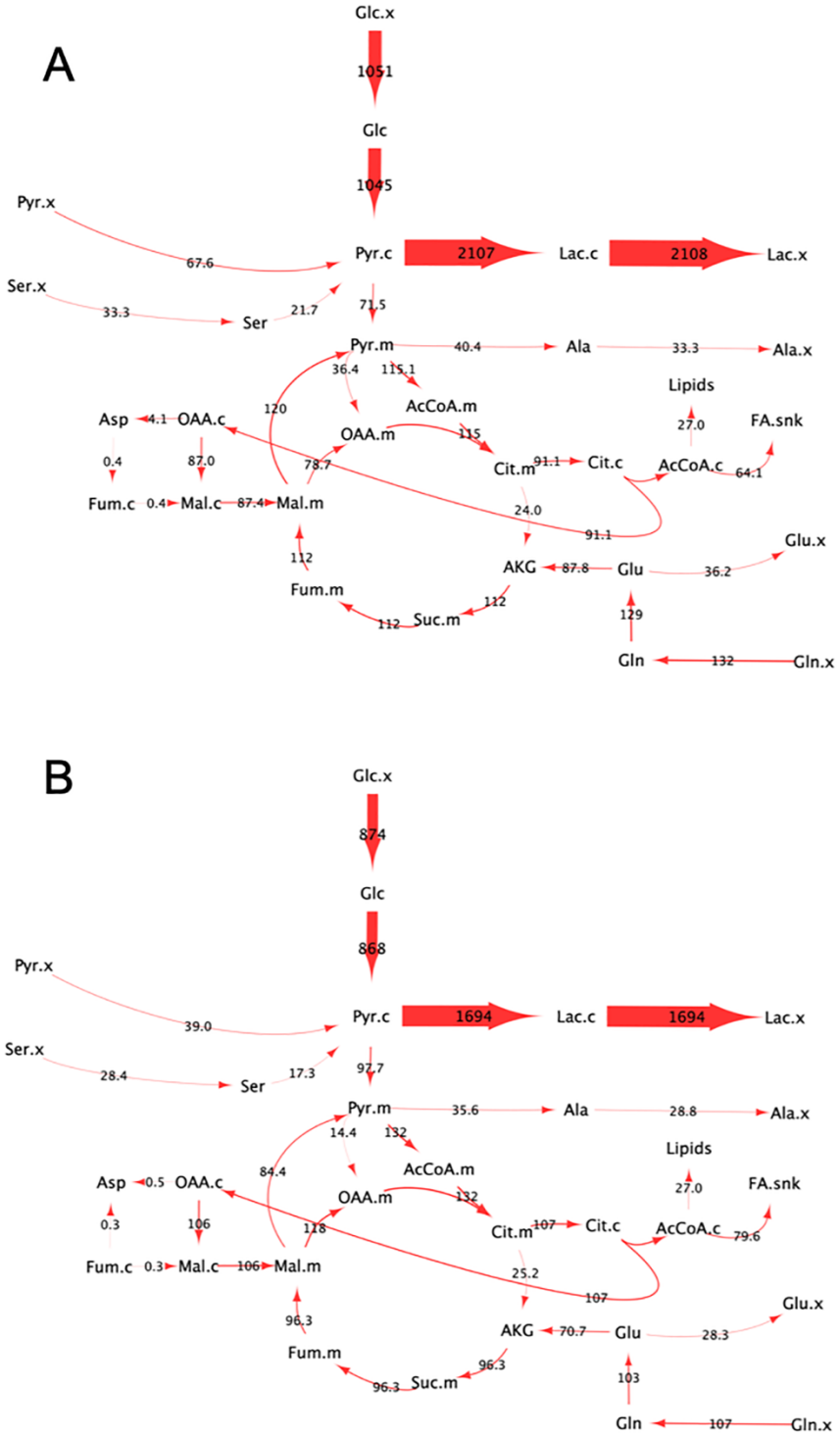

Figure 4.16. Metabolic flux maps for K3 iPSC predicted from the MFA simulations: A) Control and B) High Lactate cultures. The line thicknesses represent the relative fluxes, which are also shown numerically (nmol/10^6 cells·h).

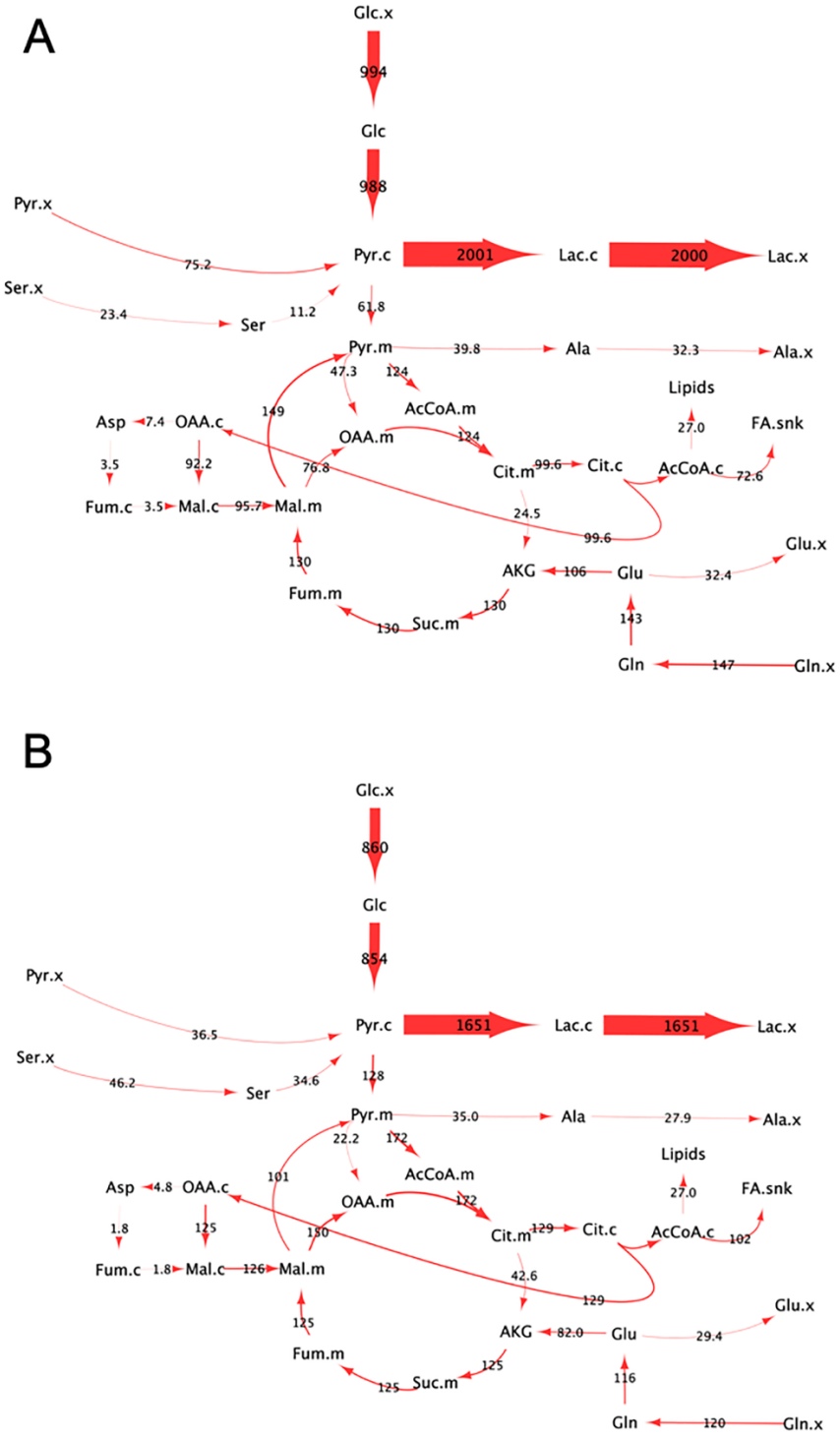

Figure 4.17. Metabolic flux maps for K3 iPSC predicted from the MFA simulations: A) Low Glucose and B) Low Glucose + High Lactate cultures. The line thicknesses represent the relative fluxes, which are also shown numerically (nmol/10^6 cells·h).

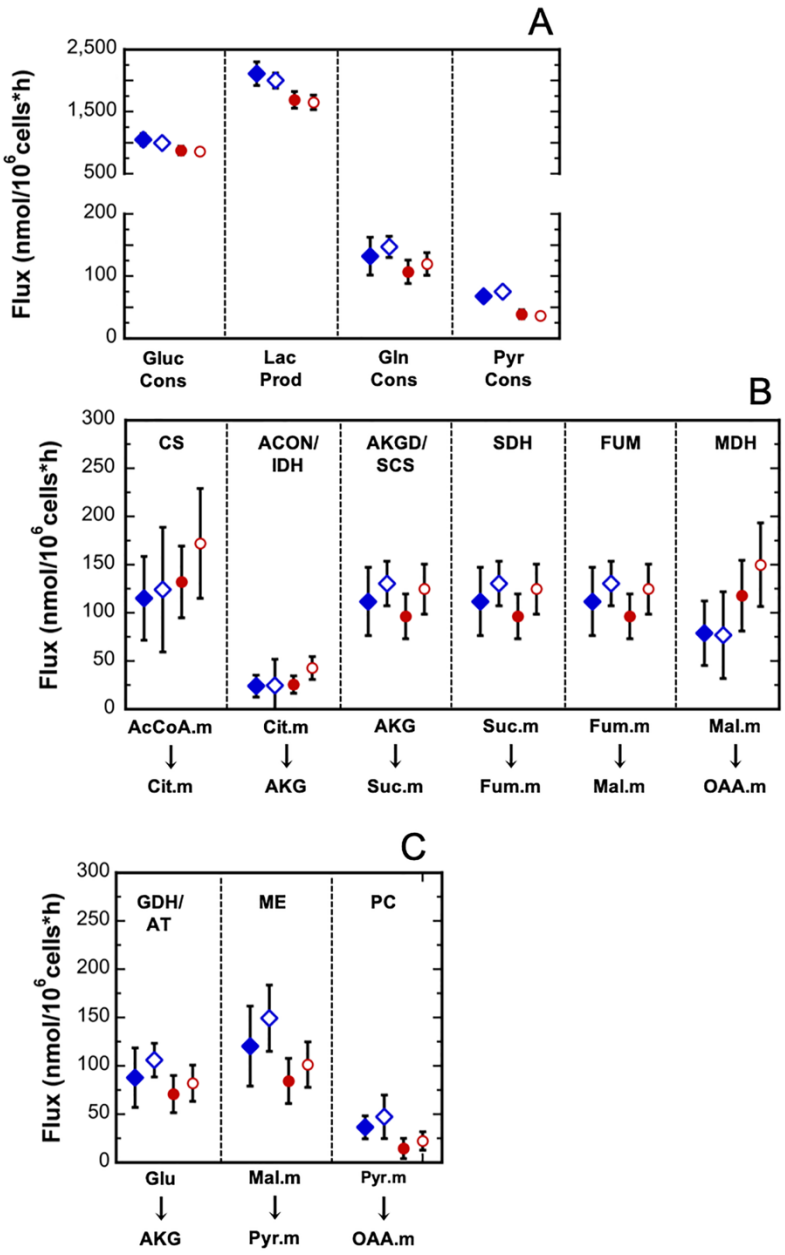

Figure 4.18. Comparison of simulated metabolic fluxes from ^{13}C-MFA for K3 iPSCs. A) Key extracellular uptake and secretion rates. B) TCA cycle metabolic fluxes. C). Anaplerotic fluxes. Control media – ■; Low Glucose media – □; High Lactate media – ◆; and Low Glucose + High Lactate – ◇. Error bars represent 95% confidence intervals. Abbreviations: CS, citrate synthase; ACON/IDH, aconitase/isocitrate dehydrogenase; AKGD/SCS, AKG dehydrogenase/succinyl coenzyme A synthetase; SDH succinate dehydrogenase; FUM, fumarase; MDH, malate dehydrogenase; GDH/AT, glutamate dehydrogenase/aminotransferase; ME, malic enzyme; PC, pyruvate carboxylase.

4.5. Conclusions

In this study, the metabolic responses of K3 iPSCs to different glucose and lactate concentrations that range from normal to low for glucose and zero to high (20 mM) for lactate were examined using ^{13}C-MFA. Parallel labeling experiments were performed using ^{13}C-glucose, ^{13}C-glutamine, and ^{13}C-lactate to determine the contribution of each as metabolites to central carbon metabolism. [1,2-^{13}C] glucose and [U-^{13}C] glutamine were used to resolve intracellular fluxes through glycolysis and the TCA cycle. For the two high lactate culture conditions, the [U-^{13}C] lactate tracer was also used to investigate the metabolic contribution of lactate to iPSC metabolism. The metabolic network model constructed for iPSCs in this study was adapted from metabolic models constructed for Chinese hamster ovary (CHO) cells and for other mammalian cells, including cancer cells. The extracellular flux measurements and measured intracellular MIDS were coupled with a defined metabolic network to predict intracellular fluxes. Pluripotency of the K3 iPSCs were assessed by comparing gene and protein expression levels for cells cultured for one and five passages in each of the media.

While lactate is primarily viewed as a metabolic waste product in *in vitro* iPSC culture, the results from this study suggest that lactate accumulation alone does not adversely impact iPSC growth or pluripotency at the concentrations tested. Also, these results support the idea that media acidification, which results from lactate production, is potentially the root of the problem associated with continuous iPSC culture, rather than lactate alone. Therefore, as more iPSC culture processes move towards pH-controlled bioreactors, lactate accumulation may not be associated with poor quality iPSCs. In

addition, since low glucose and high lactate growth media did not adversely impact iPSC proliferation or pluripotency, this indicates that implementation of fed-batch bioprocessing conditions for iPSCs is feasible in the future.

The findings in this study also illustrate that iPSCs possess metabolic flexibility with regards to lactate metabolism, which has not been previously reported. This flexibility allows for iPSCs to undergo distinct substrate utilization strategies to support self-renewal when cultured in a range of glucose and lactate concentrations. In rapidly proliferating cells, dual consumption of glucose and lactate could support replication and cell division since carbon from glucose and lactate can be compartmentalized to synthesize different biomass precursors. Since iPSCs are frequently cultured in 3D aggregates when grown in suspension, substrate availability depends on aggregate size and the proximity of cells to the aggregate surface. Metabolic flexibility would support proliferation of cells in different regions of a cell aggregate without adversely influencing pluripotency. The results from this study illustrate that K3 iPSCs possess the ability to metabolize lactate as a metabolic substrate to support cell proliferation and pluripotency maintenance, even in the presence of sufficient glucose.

CHAPTER FIVE

CONCLUSIONS AND FUTURE WORK

5.1. Conclusions

The work contained in this dissertation utilized ^{13}C-MFA to investigate the Warburg phenotype in proliferative mammalian cells and determine the role of lactate as a substrate for breast cancer and induced pluripotent stem cell metabolism. In Chapter 3, the intracellular metabolic responses of three breast cell lines – MCF 10A, MCF7, and MDA-MB-231 – to high extracellular lactate were characterized to identify shared and unique metabolic traits associated with cancer progression. Interestingly, it was observed that all three breast cell lines employed reductive glutamine metabolism in each of the high lactate cultures. This suggests a potential response mechanism for breast cancer cells to high lactate stress. In Chapter 4, the metabolic responses of human K3 iPSCs to low glucose and high lactate media culture concentrations were identified using parallel ^{13}C isotope labeling and ^{13}C-MFA. High extracellular lactate resulted in retention of glutamine-derived carbon within TCA cycle and lower glutaminolysis to pyruvate and lactate. Surprisingly, K3 iPSCs also catabolized extracellular lactate to support mitochondrial oxidative metabolism and lipid biosynthesis. Lactate also appears to support lipid synthesis. Moreover, iPSCs utilized lactate as a carbon source while maintaining pluripotency. Overall, this dissertation work provides intracellular metabolic pathway distributions for breast cancer cells and iPSCs in response to high extracellular lactate. This work highlights the flexibility of substrate utilization for cancer and pluripotent stem cells and illustrates that lactate is more than just an inhibitory byproduct of glycolysis. Indeed, wasteful no

more.

5.2. Future Work

The iPSC work in this dissertation was driven by the clinical need to generate sufficient quantities of high quality iPSCs for cell-therapy applications. Therefore, the obvious next step in this project is to determine the effects of glucose and lactate concentration on iPSCs grown in suspension cultures in controlled bioreactors. Using bioreactors will provide a more controlled environment to evaluate the effects of each of these culture parameters. Also, the differentiation capacity of iPSC grown in low glucose and high lactate culture conditions should be assessed further. This will provide valuable information regarding the functional capabilities of iPSCs as a result of culturing in different media formulations. Furthermore, since iPSCs are donor-specific, metabolic responses to cell culture perturbations should be screened on a wider population of iPSCs generated from healthy donors. Ultimately, iPSCs need to be exhaustively characterized to develop efficacious cell-therapies.

APPENDICES

Appendix A

Measured extracellular metabolite concentrations for the three breast cell lines – MCF 10A, MCF7, and MDA-MB-231

Table A1. Measured extracellular metabolite concentrations for the **MCF 10A** breast cell line at 24-h and 48-h after the media exchange. Averages are biological triplicates for the amino acid concentrations and biological 6-replicates for glucose and lactate. Standard deviations are provided for these averages.

	Average Concentration (mM)							
Cell Lines	**MCF 10A**							
Condition	**Control**				**High-Lactate**			
Metabolite	**24-h**	**SD**	**48-h**	**SD**	**24-h**	**SD**	**48-h**	**SD**
Glucose (N=6)	4.3	0.248	3.31	0.345	4.42	0.173	3.63	0.332
Lactate (N=6)	1.12	0.116	2.81	0.139	10.8	0.217	11.9	0.271
Glutamine (N=3)	2.72	0.026	2.39	0.07	2.73	0.034	2.37	0.06
Amino Acids (N=3)								
Alanine	0.03	0.001	0.08	0.002	0.03	0.001	0.08	0.003
Aspartate	0.01	0.001	0.04	0.003	0.01	0.001	0.03	0.002
Glutamate	0.03	0.003	0.09	0.005	0.03	0.003	0.07	0.003
Glycine	0.38	0.006	0.41	0.007	0.38	0.02	0.4	0.013
Isoleucine	0.7	0.012	0.66	0.009	0.69	0.008	0.66	0.006
Leucine	0.7	0.012	0.67	0.007	0.7	0.009	0.67	0.015
Methionine	0.18	0.004	0.17	0.006	0.17	0.004	0.17	0.003
Phenylalanine	0.35	0.009	0.33	0.01	0.35	0.005	0.33	0.008
Proline	0.01	0.001	0.01	0.001	0	0.001	0.01	0.001
Serine	0.31	0.006	0.23	0.008	0.3	0.013	0.21	0.006
Threonine	0.71	0.004	0.71	0.006	0.71	0.004	0.71	0.005
Tyrosine	0.35	0.009	0.33	0.006	0.35	0.006	0.33	0.012
Valine	0.71	0.007	0.68	0.009	0.7	0.005	0.68	0.007

Table A2. Measured extracellular metabolite concentrations for the **MCF7** breast cell line at 24-h and 48-h after the media exchange. Averages are biological triplicates for the amino acid concentrations and biological 6-replicates for glucose and lactate. Standard deviations are provided for these averages.

	Average Concentration (mM)							
Cell Lines	**MCF7**							
Condition	**Control**				**High-Lactate**			
Metabolite	**24-h**	**SD**	**48-h**	**SD**	**24-h**	**SD**	**48-h**	**SD**
Glucose (N=6)	4.32	0.206	3.32	0.231	4.5	0.195	3.78	0.250
Lactate (N=6)	1.03	0.100	2.55	0.131	20.5	0.108	21.1	0.193
Glutamine (N=3)	2.72	0.046	2.35	0.060	2.71	0.034	2.31	0.051
Amino Acids (N=3)								
Alanine	0.04	0.002	0.1	0.004	0.03	0.004	0.09	0.004
Aspartate	0.02	0.002	0.05	0.005	0.01	0.002	0.04	0.003
Glutamate	0.04	0.003	0.09	0.005	0.04	0.003	0.09	0.003
Glycine	0.39	0.016	0.44	0.013	0.39	0.009	0.43	0.017
Isoleucine	0.69	0.010	0.65	0.003	0.69	0.008	0.65	0.008
Leucine	0.7	0.005	0.66	0.018	0.7	0.009	0.66	0.009
Methionine	0.17	0.004	0.16	0.007	0.17	0.003	0.16	0.005
Phenylalanine	0.35	0.006	0.33	0.007	0.35	0.004	0.33	0.009
Proline	0.01	0.001	0.02	0.002	0.01	0.001	0.02	0.001
Serine	0.3	0.015	0.2	0.012	0.29	0.018	0.19	0.013
Threonine	0.72	0.001	0.71	0.004	0.72	0.002	0.71	0.004
Tyrosine	0.35	0.005	0.33	0.007	0.35	0.005	0.33	0.009
Valine	0.69	0.006	0.65	0.009	0.69	0.008	0.64	0.018

Table A3. Measured extracellular metabolite concentrations for the **MDA-MB-231** breast cell line at 24-h and 48-h after the media exchange. Averages are biological triplicates for the amino acid concentrations and biological 6-replicates for glucose and lactate. Standard deviations are provided for these averages.

	Average Concentration (mM)							
Cell Lines	**MDA-MB-231**							
Condition	**Control**				**High-Lactate**			
Metabolite	**24-h**	**SD**	**48-h**	**SD**	**24-h**	**SD**	**48-h**	**SD**
Glucose (N=6)	4.05	0.233	2.38	0.238	4.2	0.124	2.9	0.247
Lactate (N=6)	1.8	0.206	4.8	0.242	21	0.202	22.7	0.323
Glutamine (N=3)	2.75	0.047	2.42	0.079	2.73	0.045	2.34	0.061
Amino Acids (N=3)								
Alanine	0.03	0.002	0.08	0.004	0.03	0.002	0.07	0.003
Aspartate	0.01	0.001	0.03	0.003	0.01	0.001	0.03	0.003
Glutamate	0.03	0.004	0.07	0.003	0.03	0.002	0.08	0.003
Glycine	0.38	0.008	0.42	0.011	0.38	0.010	0.42	0.013
Isoleucine	0.71	0.009	0.68	0.007	0.7	0.007	0.65	0.009
Leucine	0.71	0.009	0.68	0.013	0.69	0.007	0.65	0.007
Methionine	0.18	0.001	0.17	0.003	0.17	0.004	0.16	0.006
Phenylalanine	0.35	0.002	0.34	0.006	0.35	0.002	0.33	0.014
Proline	0	0.000	0.01	0.001	0	0.000	0.01	0.001
Serine	0.32	0.012	0.24	0.011	0.3	0.013	0.2	0.005
Threonine	0.72	0.001	0.71	0.005	0.71	0.002	0.71	0.006
Tyrosine	0.35	0.010	0.33	0.007	0.35	0.004	0.33	0.011
Valine	0.70	0.009	0.67	0.006	0.69	0.002	0.65	0.007

Appendix B

Metabolic reactions used in the ^{13}C-MFA simulations for the three breast cell lines

Table B1. The metabolic reactions used in the ^{13}C-MFA simulations for the three breast cell lines. Suffixes indicate compartmental location of the metabolite: .ext, extracellular; .c, cytosolic; .m, mitochondrial; .tr, tracer; .snk, dilution sink.

v1	Gluc.ext (abcdef) -> G6P.c (abcdef)
v2	G6P.c (abcdef) <=> F6P.c (net) (abcdef) v3F6P.c (abcdef) -> FBP.c (abcdef)
v4	FBP.c (abcdef) <=>DHAP.c (cba) + GAP.c (def)
v5	DHAP.c (abc) <=> GAP.c (abc)
v6	GAP.c (abc) <=> 3PG.c (abc)
v7	3PG.c (abc)<=> Pyr.c (abc)
v8	G6P.c (abcdef) -> CO2 (a) + Ru5P.c (bcdef)
v9	Ru5P.c (abcde) <=> R5P.c (abcde)
v10	Ru5P.c (abcde) <=> X5P.c (net) (abcde)
v11	X5P.c (abcde) + R5P.c (fghij) <=> GAP.c (cde) + S7P.c (abfghij)
v12	S7P.c (abcdefg) + GAP.c (hij) <=> E4P.c (defg) + F6P.c (abchij)
v13	X5P.c (abcde) + E4P.c (fghi) <=> GAP.c (cde) + F6P.c (abfghi)
v14	Pyr.c (abc) <=> Lact.c (abc)
v15	Pyr.c (abc)-> CO2 (a) + AcCoA.m (bc)
v16	AcCoA.m (ab) + OAA.m (cdef) -> Cit.m (fedbac)
v17	Cit.m (abcdef) <=> AKG.m (abcde) + CO2 (f)
v18	AKG.m (abcde) -> CO2 (a) + Suc.m (bcde)
v19	Suc.m (abcd) <=> Fum.m (abcd)

v20 Fum.m (abcd) <=> Mal.m (abcd)

v21 Mal.m (abcd) <=> OAA.m (abcd)

v22 Gln.c (abcde) -> Glu.c (abcde)

v23 Ser.c (abc) <=> Pyr.c (abc)

v24 Gln.ext (abcde) -> Gln.c (abcde)

v25 Asp.c (abcd) -> Asp.ext (abcd)

v26 Ser.ext (abc) -> Ser.c (abc)

v27 Ala.c (abc) -> Ala.ext (abc)

v28 Glu.c (abcde) -> Glu.ext (abcde)

v29 Lact.c (abc) -> Lact.ext (abc)

v30 Glu.c (abcde) <=> AKG.m (abcde)

v31 Mal.m (abcd) -> Pyr.c (abc)+ CO2 (d)

v32 Cit.m (abcdef) -> OAA.m (cdef)+ AcCoA.c (ab)

v33 Pyr.c (abc) + CO2 (d) -> OAA.m (abcd)

v34 0.95 AcCoA.c + 0.05 DHAP.c -> Lipid

v35 Pyr.c (abc) + Glu.c (defgh) <=> Ala.c (abc) + AKG.m (defgh)

v36 OAA.m (abcd) + Glu.c (efghi) <=> Asp.c (abcd) + AKG.m (efghi)

v37 0.23 Ala.c + 0.14 Asp.c + 0.12 Gln.c + 0.15 Glu.c + 0.16 Ser.c + 0.11 G6P.c + 0.09 R5P.c -> Biomass

v38 Lact.c (abc) + Lact.tr (def) -> Lact.c (def) + Lact.snk (abc)

Appendix C

Metabolism of labeled lactate through the TCA cycle

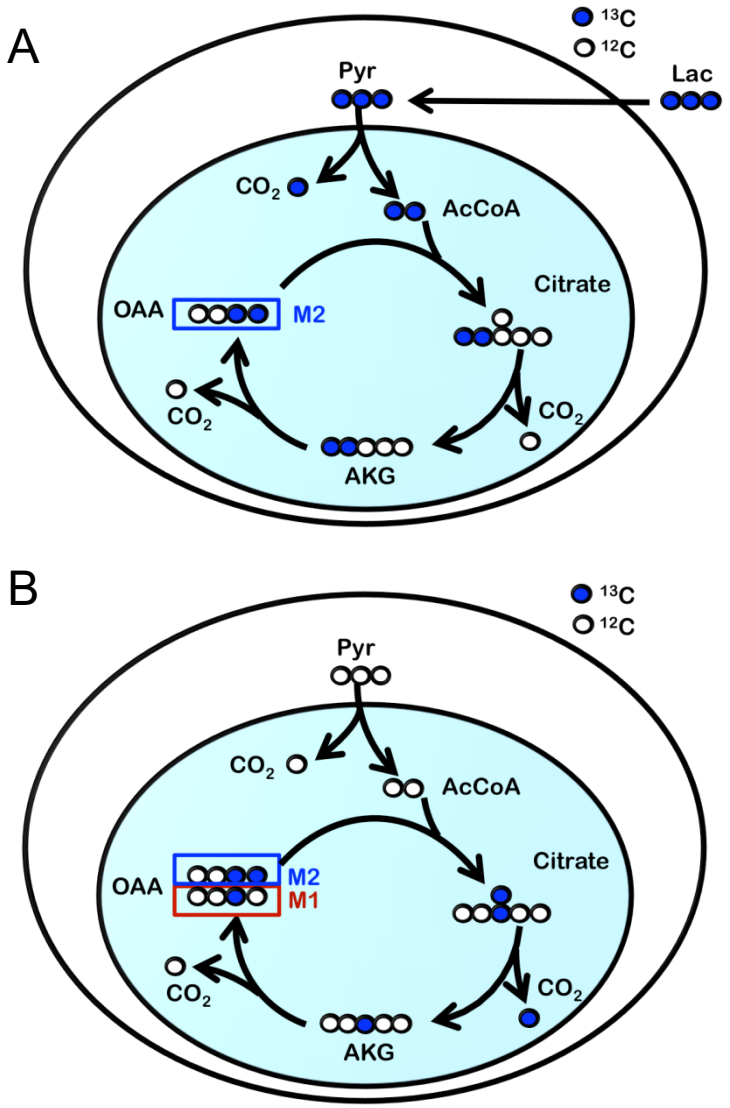

Figure C1. Metabolism of labeled lactate through the TCA cycle. A) M2-labeled TCA intermediates are generated from [U-^{13}C] lactate (Lac). B) M1-labeled a-oxoglutarate (AKG) and oxaloacetate (OAA) are generated from unlabeled pyruvate (Pyr) combining with M2- labeled oxaloacetate (OAA). M1 citrate is generated via citrate synthase through the combination of M1-labeled oxaloacetate (OAA) and M0 acetyl-CoA (AcCoA). For clarity, some reaction pathways were condensed.

Appendix D

Measured intracellular MIDs from [1,2-^{13}C] glucose, [U-^{13}C] glutamine, and [U-^{13}C] lactate for the three breast cell lines

Table D1. Measured intracellular MIDs from the [1,2-^{13}C] glucose tracer for the three breast cell lines for the control and high-lactate conditions with mean and standard errors. MIDs shown below have not been corrected for natural abundance. A standard error of 0.006 represents the lower limit error cutoff reported for most instruments (Ahn and Antoniewicz, 2013; Metallo et al., 2009), which was applied even when the biological replicates had observed lower standard error.

Cell Line	MCF 10A				MCF7				MDA-MB-231			
Condition	Control		High-Lactate		Control		High-Lactate		Control		High-Lactate	
	MID	SE	MID	SE	MID	SE	MID	SE	MID	SE	MID	SE
PEP 453												
M0	0.3701	0.0129	0.3501	0.0078	0.3606	0.0119	0.3666	0.0111	0.3459	0.0147	0.3906	0.0060
M1	0.1654	0.0129	0.1515	0.0078	0.1507	0.0119	0.1527	0.0111	0.1527	0.0147	0.1570	0.0060
M2	0.3159	0.0129	0.3333	0.0078	0.3330	0.0119	0.3248	0.0111	0.3339	0.0147	0.3042	0.0060
M3	0.0994	0.0129	0.1045	0.0078	0.1064	0.0119	0.1008	0.0111	0.1097	0.0147	0.0962	0.0060
M4	0.0394	0.0129	0.0502	0.0078	0.0394	0.0119	0.0448	0.0111	0.0477	0.0147	0.0422	0.0060
M5	0.0098	0.0129	0.0104	0.0078	0.0099	0.0119	0.0101	0.0111	0.0101	0.0147	0.0098	0.0060
3PG 585												
M0	0.3128	0.0083	0.3014	0.0075	0.3119	0.0143	0.3060	0.0142	0.3060	0.0140	0.3018	0.0064
M1	0.1675	0.0083	0.1647	0.0075	0.1650	0.0143	0.1643	0.0142	0.1643	0.0140	0.1653	0.0064
M2	0.3108	0.0083	0.3194	0.0075	0.3119	0.0143	0.3183	0.0142	0.3183	0.0140	0.3202	0.0064
M3	0.1292	0.0083	0.1327	0.0075	0.1308	0.0143	0.1314	0.0142	0.1314	0.0140	0.1322	0.0064
M4	0.0605	0.0083	0.0639	0.0075	0.0603	0.0143	0.0606	0.0142	0.0606	0.0140	0.0610	0.0064
M5	0.0192	0.0083	0.0180	0.0075	0.0201	0.0143	0.0195	0.0142	0.0195	0.0140	0.0196	0.0064
DHAP 484												
M0	0.2323	0.0112	0.3273	0.0100	0.3421	0.0137	0.2781	0.0097	0.2781	0.0139	0.3391	0.0103
M1	0.1413	0.0112	0.1514	0.0100	0.1484	0.0137	0.1379	0.0097	0.1379	0.0139	0.1479	0.0103
M2	0.4147	0.0112	0.3436	0.0100	0.3401	0.0137	0.3893	0.0097	0.3893	0.0139	0.3391	0.0103
M3	0.1404	0.0112	0.1165	0.0100	0.1134	0.0137	0.1290	0.0097	0.1290	0.0139	0.1139	0.0103
M4	0.0617	0.0112	0.0497	0.0100	0.0453	0.0137	0.0556	0.0097	0.0556	0.0139	0.0486	0.0103
M5	0.0096	0.0112	0.0116	0.0100	0.0106	0.0137	0.0101	0.0097	0.0100	0.0139	0.0113	0.0103

Cell Line	MCF 10A				MCF7				MDA-MB-231			
Condition	Control		High-Lactate		Control		High-Lactate		Control		High-Lactate	
	MID	SE	MID	SE	MID	SE	MID	SE	MID	SE	MID	SE
PYR 174												
M0	0.5318	0.0146	0.5581	0.0071	0.5258	0.0188	0.5350	0.0136	0.4816	0.0132	0.5581	0.0114
M1	0.1062	0.0146	0.0948	0.0071	0.0969	0.0188	0.0975	0.0136	0.0976	0.0132	0.0948	0.0114
M2	0.3125	0.0146	0.2983	0.0071	0.3196	0.0188	0.3170	0.0136	0.3579	0.0132	0.2983	0.0114
M3	0.0320	0.0146	0.0335	0.0071	0.0361	0.0188	0.0345	0.0136	0.0412	0.0132	0.0335	0.0114
M4	0.0134	0.0146	0.0125	0.0071	0.0134	0.0188	0.0129	0.0136	0.0130	0.0132	0.0125	0.0114
M5	0.0041	0.0146	0.0029	0.0071	0.0082	0.0188	0.0029	0.0136	0.0087	0.0132	0.0029	0.0114
ALA 260												
M0	0.4656	0.0148	0.4813	0.0111	0.4661	0.0197	0.4654	0.0101	0.4258	0.0131	0.4912	0.0085
M1	0.1453	0.0148	0.1348	0.0111	0.1322	0.0197	0.1347	0.0101	0.1331	0.0131	0.1339	0.0085
M2	0.2993	0.0148	0.2936	0.0111	0.3125	0.0197	0.3069	0.0101	0.3393	0.0131	0.2854	0.0085
M3	0.0616	0.0148	0.0616	0.0111	0.0637	0.0197	0.0634	0.0101	0.0719	0.0131	0.0600	0.0085
M4	0.0234	0.0148	0.0231	0.0111	0.0196	0.0197	0.0237	0.0101	0.0240	0.0131	0.0236	0.0085
M5	0.0048	0.0148	0.0058	0.0111	0.0059	0.0197	0.0059	0.0101	0.0060	0.0131	0.0059	0.0085
LAC 261												
M0	0.4668	0.0124	0.4862	0.0102	0.4611	0.0197	0.4926	0.0112	0.4233	0.0148	0.4971	0.0152
M1	0.1451	0.0124	0.1335	0.0102	0.1332	0.0197	0.1360	0.0112	0.1325	0.0148	0.1345	0.0152
M2	0.2987	0.0124	0.2908	0.0102	0.3176	0.0197	0.2838	0.0112	0.3426	0.0148	0.2807	0.0152
M3	0.0612	0.0124	0.0610	0.0102	0.0615	0.0197	0.0581	0.0112	0.0717	0.0148	0.0585	0.0152
M4	0.0234	0.0124	0.0228	0.0102	0.0205	0.0197	0.0236	0.0112	0.0239	0.0148	0.0233	0.0152
M5	0.0048	0.0124	0.0057	0.0102	0.0061	0.0197	0.0059	0.0112	0.0060	0.0148	0.0058	0.0152
GLP 571												
M0	0.2072	0.0067	0.2895	0.0086	0.2973	0.0166	0.2415	0.0100	0.2394	0.0145	0.2976	0.0121
M1	0.1437	0.0067	0.1619	0.0086	0.1589	0.0166	0.1449	0.0100	0.1455	0.0145	0.1601	0.0121
M2	0.3812	0.0067	0.3278	0.0086	0.3226	0.0166	0.3622	0.0100	0.3606	0.0145	0.3229	0.0121
M3	0.1642	0.0067	0.1369	0.0086	0.1365	0.0166	0.1531	0.0100	0.1559	0.0145	0.1361	0.0121
M4	0.0811	0.0067	0.0648	0.0086	0.0682	0.0166	0.0768	0.0100	0.0770	0.0145	0.0644	0.0121
M5	0.0225	0.0067	0.0191	0.0086	0.0166	0.0166	0.0214	0.0100	0.0216	0.0145	0.0189	0.0121

Table D2. Measured intracellular MIDs from [U-^{13}C] glutamine tracer for the three breast cancer cell lines for the control and high- lactate conditions with mean and standard errors. MIDs shown below have not been corrected for natural abundance. A standard error of 0.006 represents the lower limit error cutoff reported for most instruments (Ahn and Antoniewicz, 2013; Metallo et al., 2009), which was applied even when the biological replicates had observed lower standard error.

Cell Line	MCF 10A				MCF7				MDA-MB-231			
Condition	Control		High-Lactate		Control		High-Lactate		Control		High-Lactate	
	MID	SE	MID	SE	MID	SE	MID	SE	MID	SE	MID	SE
PYR 174												
M0	0.824	0.0088	0.8022	0.006	0.8068	0.0158	0.8301	0.009	0.837	0.0081	0.808	0.0103
M1	0.1061	0.0088	0.1124	0.006	0.1187	0.0158	0.107	0.009	0.105	0.0081	0.111	0.0103
M2	0.0424	0.0088	0.0462	0.006	0.0451	0.0158	0.04	0.009	0.042	0.0081	0.046	0.0103
M3	0.0242	0.0088	0.0358	0.006	0.0261	0.0158	0.0195	0.009	0.013	0.0081	0.033	0.0103
M4	0.0024	0.0088	0.0026	0.006	0.0024	0.0158	0.0025	0.009	0.002	0.0081	0.003	0.0103
M5	0.0009	0.0088	0.0009	0.006	0.0009	0.0158	0.0009	0.009	0.001	0.0081	0.001	0.0103
ALA 260												
M0	0.7278	0.0094	0.7047	0.0097	0.7235	0.018	0.732	0.006	0.737	0.0083	0.713	0.007
M1	0.1654	0.0094	0.1693	0.0097	0.1608	0.018	0.1637	0.006	0.165	0.0083	0.167	0.007
M2	0.0717	0.0094	0.0757	0.0097	0.0769	0.018	0.0713	0.006	0.071	0.0083	0.075	0.007
M3	0.0276	0.0094	0.0415	0.0097	0.031	0.018	0.025	0.006	0.02	0.0083	0.037	0.007
M4	0.0066	0.0094	0.0073	0.0097	0.0069	0.018	0.0066	0.006	0.006	0.0083	0.007	0.007
M5	0.0009	0.0094	0.0014	0.0097	0.0009	0.018	0.0013	0.006	0.001	0.0083	0.001	0.007
LAC 261												
M0	0.7185	0.0072	0.6983	0.006	0.7079	0.0165	0.7275	0.0066	0.731	0.0081	0.708	0.0118
M1	0.1684	0.0072	0.173	0.006	0.1741	0.0165	0.1679	0.0066	0.169	0.0081	0.17	0.0118
M2	0.0752	0.0072	0.0774	0.006	0.0812	0.0165	0.0727	0.0066	0.072	0.0081	0.076	0.0118
M3	0.0303	0.0072	0.0424	0.006	0.029	0.0165	0.0242	0.0066	0.021	0.0081	0.037	0.0118
M4	0.0067	0.0072	0.0075	0.006	0.007	0.0165	0.0064	0.0066	0.006	0.0081	0.007	0.0118
M5	0.0009	0.0072	0.0014	0.006	0.0008	0.0165	0.0012	0.0066	0.001	0.0081	0.001	0.0118
CIT 459												
M0	0.3039	0.0092	0.2524	0.0074	0.3221	0.0126	0.2455	0.0064	0.308	0.0102	0.251	0.0074
M1	0.1583	0.0092	0.1359	0.0074	0.1491	0.0126	0.1417	0.0064	0.154	0.0102	0.153	0.0074

Cell Line	MCF 10A				MCF7				MDA-MB-231			
Condition	Control		High-Lactate		Control		High-Lactate		Control		High-Lactate	
	MID	SE	MID	SE	MID	SE	MID	SE	MID	SE	MID	SE
M2	0.1427	0.0092	0.1306	0.0074	0.1292	0.0126	0.1322	0.0064	0.133	0.0102	0.135	0.0074
M3	0.0874	0.0092	0.09	0.0074	0.0895	0.0126	0.0872	0.0064	0.092	0.0102	0.093	0.0074
M4	0.199	0.0092	0.1845	0.0074	0.1889	0.0126	0.1649	0.0064	0.185	0.0102	0.165	0.0074
M5	0.068	0.0092	0.1359	0.0074	0.0795	0.0126	0.1417	0.0064	0.082	0.0102	0.131	0.0074
M6	0.0291	0.0092	0.0487	0.0074	0.0298	0.0126	0.0614	0.0064	0.034	0.0102	0.05	0.0074
M7	0.0087	0.0092	0.0156	0.0074	0.0089	0.0126	0.0189	0.0064	0.009	0.0102	0.016	0.0074
M8	0.0029	0.0092	0.0066	0.0074	0.003	0.0126	0.0066	0.0064	0.003	0.0102	0.007	0.0074
AKG 346												
M0	0.2076	0.006	0.1916	0.006	0.2326	0.0128	0.2037	0.007	0.207	0.0102	0.221	0.006
M1	0.1023	0.006	0.0993	0.006	0.091	0.0128	0.1034	0.007	0.094	0.0102	0.106	0.006
M2	0.0789	0.006	0.0725	0.006	0.0808	0.0128	0.0755	0.007	0.08	0.0102	0.074	0.006
M3	0.1189	0.006	0.139	0.006	0.1163	0.0128	0.1354	0.007	0.113	0.0102	0.129	0.006
M4	0.0448	0.006	0.0477	0.006	0.0404	0.0128	0.0507	0.007	0.043	0.0102	0.046	0.006
M5	0.3402	0.006	0.3455	0.006	0.3276	0.0128	0.3256	0.007	0.358	0.0102	0.318	0.006
M6	0.078	0.006	0.0745	0.006	0.0811	0.0128	0.0744	0.007	0.075	0.0102	0.076	0.006
M7	0.0292	0.006	0.0301	0.006	0.0303	0.0128	0.0313	0.007	0.028	0.0102	0.031	0.006
GLU 432												
M0	0.1701	0.0082	0.17	0.006	0.1878	0.009	0.1425	0.0074	0.175	0.0097	0.184	0.0065
M1	0.0977	0.0082	0.098	0.006	0.0995	0.009	0.0855	0.0074	0.098	0.0097	0.108	0.0065
M2	0.0791	0.0082	0.076	0.006	0.0832	0.009	0.0617	0.0074	0.082	0.0097	0.076	0.0065
M3	0.1109	0.0082	0.123	0.006	0.1117	0.009	0.1007	0.0074	0.109	0.0097	0.121	0.0065
M4	0.0521	0.0082	0.057	0.006	0.0508	0.009	0.0541	0.0074	0.055	0.0097	0.056	0.0065
M5	0.3353	0.0082	0.3251	0.006	0.3147	0.009	0.3751	0.0074	0.328	0.0097	0.308	0.0065
M6	0.1049	0.0082	0.101	0.006	0.1015	0.009	0.1235	0.0074	0.104	0.0097	0.099	0.0065
M7	0.0501	0.0082	0.05	0.006	0.0508	0.009	0.057	0.0074	0.049	0.0097	0.049	0.0065
GLN 431												
M0	0.027	0.0121	0.0289	0.006	0.0209	0.0184	0.0317	0.006	0.024	0.0086	0.033	0.0073
M1	0.0108	0.0121	0.0108	0.006	0.0105	0.0184	0.0123	0.006	0.012	0.0086	0.012	0.0073
M2	0.0049	0.0121	0.0049	0.006	0.0063	0.0184	0.0058	0.006	0.006	0.0086	0.006	0.0073
M3	0.0023	0.0121	0.0023	0.006	0.0032	0.0184	0.002	0.006	0.003	0.0086	0.002	0.0073
M4	0.028	0.0121	0.0299	0.006	0.0214	0.0184	0.0324	0.006	0.02	0.0086	0.031	0.0073
M5	0.6252	0.0121	0.6232	0.006	0.6216	0.0184	0.6239	0.006	0.638	0.0086	0.622	0.0073

Cell Line	MCF 10A				MCF7				MDA-MB-231			
Condition	Control		High-Lactate		Control		High-Lactate		Control		High-Lactate	
	MID	SE	MID	SE	MID	SE	MID	SE	MID	SE	MID	SE
M6	0.2048	0.0121	0.2033	0.006	0.2107	0.0184	0.2013	0.006	0.198	0.0086	0.203	0.0073
M7	0.097	0.0121	0.0969	0.006	0.1054	0.0184	0.0906	0.006	0.099	0.0086	0.091	0.0073
PRO 258												
M0	0.2022	0.0075	0.2024	0.006	0.2245	0.0126	0.1684	0.0061	0.212	0.0123	0.22	0.0062
M1	0.1085	0.0075	0.1136	0.006	0.102	0.0126	0.0982	0.0061	0.106	0.0123	0.118	0.0062
M2	0.1497	0.0075	0.161	0.006	0.1531	0.0126	0.131	0.0061	0.155	0.0123	0.155	0.0062
M3	0.0493	0.0075	0.0494	0.006	0.051	0.0126	0.0505	0.0061	0.053	0.0123	0.05	0.0062
M4	0.3818	0.0075	0.3703	0.006	0.3571	0.0126	0.4303	0.0061	0.372	0.0123	0.353	0.0062
M5	0.0784	0.0075	0.0731	0.006	0.0816	0.0126	0.0842	0.0061	0.071	0.0123	0.073	0.0062
M6	0.0301	0.0075	0.0302	0.006	0.0306	0.0126	0.0374	0.0061	0.031	0.0123	0.03	0.0061
SUCC 289												
M0	0.3317	0.006	0.3135	0.0074	0.3542	0.015	0.3304	0.0126	0.33	0.0136	0.358	0.0176
M1	0.1275	0.006	0.1302	0.0074	0.1302	0.015	0.1369	0.0126	0.125	0.0136	0.136	0.0176
M2	0.1444	0.006	0.1511	0.0074	0.1354	0.015	0.1479	0.0126	0.131	0.0136	0.143	0.0176
M3	0.0428	0.006	0.0504	0.0074	0.0417	0.015	0.0484	0.0126	0.04	0.0136	0.048	0.0176
M4	0.2739	0.006	0.2803	0.0074	0.2604	0.015	0.2647	0.0126	0.294	0.0136	0.245	0.0176
M5	0.0598	0.006	0.0544	0.0074	0.0573	0.015	0.0523	0.0126	0.057	0.0136	0.051	0.0176
M6	0.0199	0.006	0.0201	0.0074	0.0208	0.015	0.0194	0.0126	0.023	0.0136	0.019	0.0176
FUM 287												
M0	0.3642	0.0093	0.3432	0.0083	0.3769	0.0145	0.3564	0.0082	0.378	0.0124	0.37	0.0122
M1	0.1332	0.0093	0.132	0.0083	0.1296	0.0145	0.1391	0.0082	0.131	0.0124	0.141	0.0122
M2	0.1414	0.0093	0.1452	0.0083	0.1396	0.0145	0.1434	0.0082	0.138	0.0124	0.141	0.0122
M3	0.0407	0.0093	0.0528	0.0083	0.0389	0.0145	0.0489	0.0082	0.039	0.0124	0.053	0.0122
M4	0.2543	0.0093	0.2578	0.0083	0.2443	0.0145	0.2447	0.0082	0.25	0.0124	0.229	0.0122
M5	0.0458	0.0093	0.0504	0.0083	0.0469	0.0145	0.0492	0.0082	0.045	0.0124	0.049	0.0122
M6	0.0203	0.0093	0.0187	0.0083	0.0239	0.0145	0.0182	0.0082	0.02	0.0124	0.018	0.0122
MAL 419												
M0	0.3155	0.0099	0.2949	0.005	0.3287	0.0166	0.31	0.009	0.319	0.0101	0.323	0.0092
M1	0.1555	0.0099	0.1523	0.005	0.1524	0.0166	0.157	0.009	0.147	0.0101	0.16	0.0092
M2	0.143	0.0099	0.1499	0.005	0.1394	0.0166	0.1525	0.009	0.142	0.0101	0.15	0.0092
M3	0.0715	0.0099	0.0688	0.005	0.0797	0.0166	0.062	0.009	0.076	0.0101	0.069	0.0092
M4	0.2145	0.0099	0.2359	0.005	0.2052	0.0166	0.224	0.009	0.218	0.0101	0.205	0.0092
M5	0.0724	0.0099	0.0688	0.005	0.0647	0.0166	0.0647	0.009	0.065	0.0101	0.064	0.0092

Cell Line	MCF 10A				MCF7				MDA-MB-231			
Condition	Control		High-Lactate		Control		High-Lactate		Control		High-Lactate	
	MID	SE	MID	SE	MID	SE	MID	SE	MID	SE	MID	SE
M6	0.0277	0.0099	0.0294	0.005	0.0299	0.0166	0.0299	0.009	0.033	0.0101	0.029	0.0092
ASP 418												
M0	0.4362	0.006	0.4966	0.0111	0.4602	0.011	0.3267	0.009	0.46	0.0142	0.498	0.0121
M1	0.1819	0.006	0.1978	0.0111	0.1902	0.011	0.1584	0.009	0.19	0.0142	0.198	0.0121
M2	0.1309	0.006	0.1233	0.0111	0.1231	0.011	0.1484	0.009	0.123	0.0142	0.124	0.0121
M3	0.0553	0.006	0.0393	0.0111	0.0501	0.011	0.0587	0.009	0.056	0.0142	0.044	0.0121
M4	0.1362	0.006	0.0988	0.0111	0.1202	0.011	0.2082	0.009	0.119	0.0142	0.093	0.0121
M5	0.0426	0.006	0.0302	0.0111	0.0401	0.011	0.0664	0.009	0.037	0.0142	0.03	0.0121
M6	0.017	0.006	0.014	0.0111	0.016	0.011	0.0332	0.009	0.016	0.0142	0.014	0.0121

Table D3. Measured intracellular MIDs from [U-^{13}C] lactate tracer for the three breast cell lines for the control and high-lactate conditions with mean and standard errors. MIDs shown below have not been corrected for natural abundance. A standard error of 0.006 represents the lower limit error cutoff reported for most instruments (Ahn and Antoniewicz, 2013; Metallo et al., 2009), which was applied even when the biological replicates had observed lower standard error.

Cell Line	MCF 10A				MCF7				MDA-MB-231			
Condition	Control		High-Lactate		Control		High-Lactate		Control		High-Lactate	
	MID	SE	MID	SE	MID	SE	MID	SE	MID	SE	MID	SE
PYR 174												
M0	n/a	n/a	0.8219	0.0065	n/a	n/a	0.8166	0.0066	n/a	n/a	0.8172	0.006
M1	n/a	n/a	0.1004	0.0065	n/a	n/a	0.1069	0.0066	n/a	n/a	0.1034	0.006
M2	n/a	n/a	0.0404	0.0065	n/a	n/a	0.0389	0.0066	n/a	n/a	0.0384	0.006
M3	n/a	n/a	0.0331	0.0065	n/a	n/a	0.0339	0.0066	n/a	n/a	0.0374	0.006
M4	n/a	n/a	0.0031	0.0065	n/a	n/a	0.002	0.0066	n/a	n/a	0.0026	0.006
M5	n/a	n/a	0.0008	0.0065	n/a	n/a	0.0014	0.0066	n/a	n/a	0.001	0.006
ALA 260												
M0	n/a	n/a	0.7268	0.0088	n/a	n/a	0.7236	0.006	n/a	n/a	0.7232	0.0072
M1	n/a	n/a	0.1622	0.0088	n/a	n/a	0.1616	0.006	n/a	n/a	0.1599	0.0072
M2	n/a	n/a	0.0706	0.0088	n/a	n/a	0.0663	0.006	n/a	n/a	0.0679	0.0072
M3	n/a	n/a	0.0313	0.0088	n/a	n/a	0.0391	0.006	n/a	n/a	0.0398	0.0072
M4	n/a	n/a	0.0071	0.0088	n/a	n/a	0.0069	0.006	n/a	n/a	0.0068	0.0072
M5	n/a	n/a	0.0019	0.0088	n/a	n/a	0.0024	0.006	n/a	n/a	0.0022	0.0072
LAC 261												
M0	n/a	n/a	0.7201	0.006	n/a	n/a	0.6884	0.0088	n/a	n/a	0.7146	0.0078
M1	n/a	n/a	0.1623	0.006	n/a	n/a	0.158	0.0088	n/a	n/a	0.1623	0.0078
M2	n/a	n/a	0.071	0.006	n/a	n/a	0.0699	0.0088	n/a	n/a	0.0689	0.0078
M3	n/a	n/a	0.0364	0.006	n/a	n/a	0.0703	0.0088	n/a	n/a	0.0435	0.0078
M4	n/a	n/a	0.008	0.006	n/a	n/a	0.0098	0.0088	n/a	n/a	0.008	0.0078
M5	n/a	n/a	0.0021	0.006	n/a	n/a	0.0033	0.0088	n/a	n/a	0.0022	0.0078
CIT 459												
M0	n/a	n/a	0.6202	0.0086	n/a	n/a	0.6157	0.0114	n/a	n/a	0.6182	0.006
M1	n/a	n/a	0.2303	0.0086	n/a	n/a	0.2354	0.0114	n/a	n/a	0.2331	0.006
M2	n/a	n/a	0.1101	0.0086	n/a	n/a	0.1106	0.0114	n/a	n/a	0.1107	0.006
M3	n/a	n/a	0.028	0.0086	n/a	n/a	0.0272	0.0114	n/a	n/a	0.027	0.006
M4	n/a	n/a	0.0073	0.0086	n/a	n/a	0.007	0.0114	n/a	n/a	0.0066	0.006
M5	n/a	n/a	0.0013	0.0086	n/a	n/a	0.0013	0.0114	n/a	n/a	0.0014	0.006

Cell Line	MCF 10A				MCF7				MDA-MB-231			
Condition	Control		High-Lactate		Control		High-Lactate		Control		High-Lactate	
	MID	SE	MID	SE	MID	SE	MID	SE	MID	SE	MID	SE
M6	n/a	n/a	0.0011	0.0086	n/a	n/a	0.0011	0.0114	n/a	n/a	0.0011	0.006
M7	n/a	n/a	0.0008	0.0086	n/a	n/a	0.0009	0.0114	n/a	n/a	0.0009	0.006
M8	n/a	n/a	0.0008	0.0086	n/a	n/a	0.0008	0.0114	n/a	n/a	0.0008	0.006
AKG 346												
M0	n/a	n/a	0.7131	0.009	n/a	n/a	0.7145	0.006	n/a	n/a	0.7147	0.006
M1	n/a	n/a	0.1882	0.009	n/a	n/a	0.1898	0.006	n/a	n/a	0.1884	0.006
M2	n/a	n/a	0.0791	0.009	n/a	n/a	0.0767	0.006	n/a	n/a	0.0774	0.006
M3	n/a	n/a	0.0139	0.009	n/a	n/a	0.0127	0.006	n/a	n/a	0.0138	0.006
M4	n/a	n/a	0.0029	0.009	n/a	n/a	0.0032	0.006	n/a	n/a	0.0029	0.006
M5	n/a	n/a	0.0011	0.009	n/a	n/a	0.0011	0.006	n/a	n/a	0.0011	0.006
M6	n/a	n/a	0.0009	0.009	n/a	n/a	0.001	0.006	n/a	n/a	0.0007	0.006
M7	n/a	n/a	0.0006	0.009	n/a	n/a	0.0008	0.006	n/a	n/a	0.0007	0.006
GLU 432												
M0	n/a	n/a	0.6183	0.0125	n/a	n/a	0.6257	0.006	n/a	n/a	0.6248	0.006
M1	n/a	n/a	0.2354	0.0125	n/a	n/a	0.2304	0.006	n/a	n/a	0.2325	0.006
M2	n/a	n/a	0.1078	0.0125	n/a	n/a	0.108	0.006	n/a	n/a	0.108	0.006
M3	n/a	n/a	0.0293	0.0125	n/a	n/a	0.0269	0.006	n/a	n/a	0.0263	0.006
M4	n/a	n/a	0.0058	0.0125	n/a	n/a	0.0061	0.006	n/a	n/a	0.0056	0.006
M5	n/a	n/a	0.0019	0.0125	n/a	n/a	0.0016	0.006	n/a	n/a	0.0014	0.006
M6	n/a	n/a	0.0009	0.0125	n/a	n/a	0.0009	0.006	n/a	n/a	0.0009	0.006
M7	n/a	n/a	0.0001	0.0125	n/a	n/a	0.0003	0.006	n/a	n/a	0.0001	0.006
GLN 431												
M0	n/a	n/a	0.6261	0.006	n/a	n/a	0.6253	0.0088	n/a	n/a	0.624	0.006
M1	n/a	n/a	0.2323	0.006	n/a	n/a	0.2344	0.0088	n/a	n/a	0.2342	0.006
M2	n/a	n/a	0.108	0.006	n/a	n/a	0.1065	0.0088	n/a	n/a	0.1073	0.006
M3	n/a	n/a	0.0251	0.006	n/a	n/a	0.0259	0.0088	n/a	n/a	0.0262	0.006
M4	n/a	n/a	0.006	0.006	n/a	n/a	0.0057	0.0088	n/a	n/a	0.0059	0.006
M5	n/a	n/a	0.0012	0.006	n/a	n/a	0.0012	0.0088	n/a	n/a	0.0013	0.006
M6	n/a	n/a	0.0008	0.006	n/a	n/a	0.0008	0.0088	n/a	n/a	0.0008	0.006
M7	n/a	n/a	0.0001	0.006	n/a	n/a	0.0001	0.0088	n/a	n/a	0.0001	0.006
PRO 258												
M0	n/a	n/a	0.7343	0.0091	n/a	n/a	0.7378	0.0048	n/a	n/a	0.7373	0.006
M1	n/a	n/a	0.1811	0.0091	n/a	n/a	0.1802	0.0048	n/a	n/a	0.1778	0.006
M2	n/a	n/a	0.0704	0.0091	n/a	n/a	0.0704	0.0048	n/a	n/a	0.0698	0.006
M3	n/a	n/a	0.0101	0.0091	n/a	n/a	0.0082	0.0048	n/a	n/a	0.0113	0.006

Cell Line	MCF 10A				MCF7				MDA-MB-231			
Condition	Control		High-Lactate		Control		High-Lactate		Control		High-Lactate	
	MID	SE	MID	SE	MID	SE	MID	SE	MID	SE	MID	SE
M4	n/a	n/a	0.003	0.0091	n/a	n/a	0.0023	0.0048	n/a	n/a	0.0025	0.006
M5	n/a	n/a	0.0007	0.0091	n/a	n/a	0.0008	0.0048	n/a	n/a	0.0007	0.006
M6	n/a	n/a	0.0003	0.0091	n/a	n/a	0.0003	0.0048	n/a	n/a	0.0004	0.006
SUCC 289												
M0	n/a	n/a	0.7346	0.0097	n/a	n/a	0.7368	0.006	n/a	n/a	0.735	0.006
M1	n/a	n/a	0.1736	0.0097	n/a	n/a	0.1743	0.006	n/a	n/a	0.1754	0.006
M2	n/a	n/a	0.0763	0.0097	n/a	n/a	0.0746	0.006	n/a	n/a	0.0738	0.006
M3	n/a	n/a	0.0108	0.0097	n/a	n/a	0.0109	0.006	n/a	n/a	0.0114	0.006
M4	n/a	n/a	0.0029	0.0097	n/a	n/a	0.0026	0.006	n/a	n/a	0.0029	0.006
M5	n/a	n/a	0.0009	0.0097	n/a	n/a	0.0006	0.006	n/a	n/a	0.0009	0.006
M6	n/a	n/a	0.0005	0.0097	n/a	n/a	0.0002	0.006	n/a	n/a	0.0005	0.006
FUM 287												
M0	n/a	n/a	0.7349	0.006	n/a	n/a	0.7345	0.0061	n/a	n/a	0.7357	0.0101
M1	n/a	n/a	0.1739	0.006	n/a	n/a	0.1756	0.0061	n/a	n/a	0.1751	0.0101
M2	n/a	n/a	0.075	0.006	n/a	n/a	0.0735	0.0061	n/a	n/a	0.0737	0.0101
M3	n/a	n/a	0.012	0.006	n/a	n/a	0.0126	0.0061	n/a	n/a	0.0119	0.0101
M4	n/a	n/a	0.0027	0.006	n/a	n/a	0.0027	0.0061	n/a	n/a	0.0026	0.0101
M5	n/a	n/a	0.0009	0.006	n/a	n/a	0.0005	0.0061	n/a	n/a	0.0006	0.0101
M6	n/a	n/a	0.0005	0.006	n/a	n/a	0.0004	0.0061	n/a	n/a	0.0003	0.0101
MAL 419												
M0	n/a	n/a	0.6328	0.0123	n/a	n/a	0.6325	0.0084	n/a	n/a	0.6338	0.006
M1	n/a	n/a	0.227	0.0123	n/a	n/a	0.2278	0.0084	n/a	n/a	0.2262	0.006
M2	n/a	n/a	0.1075	0.0123	n/a	n/a	0.1074	0.0084	n/a	n/a	0.1075	0.006
M3	n/a	n/a	0.0251	0.0123	n/a	n/a	0.0258	0.0084	n/a	n/a	0.0251	0.006
M4	n/a	n/a	0.0055	0.0123	n/a	n/a	0.0043	0.0084	n/a	n/a	0.005	0.006
M5	n/a	n/a	0.0009	0.0123	n/a	n/a	0.001	0.0084	n/a	n/a	0.0014	0.006
M6	n/a	n/a	0.0008	0.0123	n/a	n/a	0.0009	0.0084	n/a	n/a	0.0009	0.006
ASP 418												
M0	n/a	n/a	0.6289	0.0149	n/a	n/a	0.6312	0.0135	n/a	n/a	0.6319	0.0138
M1	n/a	n/a	0.2295	0.0149	n/a	n/a	0.2295	0.0135	n/a	n/a	0.2286	0.0138
M2	n/a	n/a	0.1096	0.0149	n/a	n/a	0.1067	0.0135	n/a	n/a	0.107	0.0138
M3	n/a	n/a	0.0249	0.0149	n/a	n/a	0.0251	0.0135	n/a	n/a	0.0253	0.0138
M4	n/a	n/a	0.0052	0.0149	n/a	n/a	0.005	0.0135	n/a	n/a	0.005	0.0138
M5	n/a	n/a	0.0011	0.0149	n/a	n/a	0.0016	0.0135	n/a	n/a	0.0013	0.0138
M6	n/a	n/a	0.0007	0.0149	n/a	n/a	0.0008	0.0135	n/a	n/a	0.0007	0.0138

Appendix E

Metabolite isotope labeling distributions from [1,2-^{13}C] glucose and [U-^{13}C] glutamine for three breast cell lines

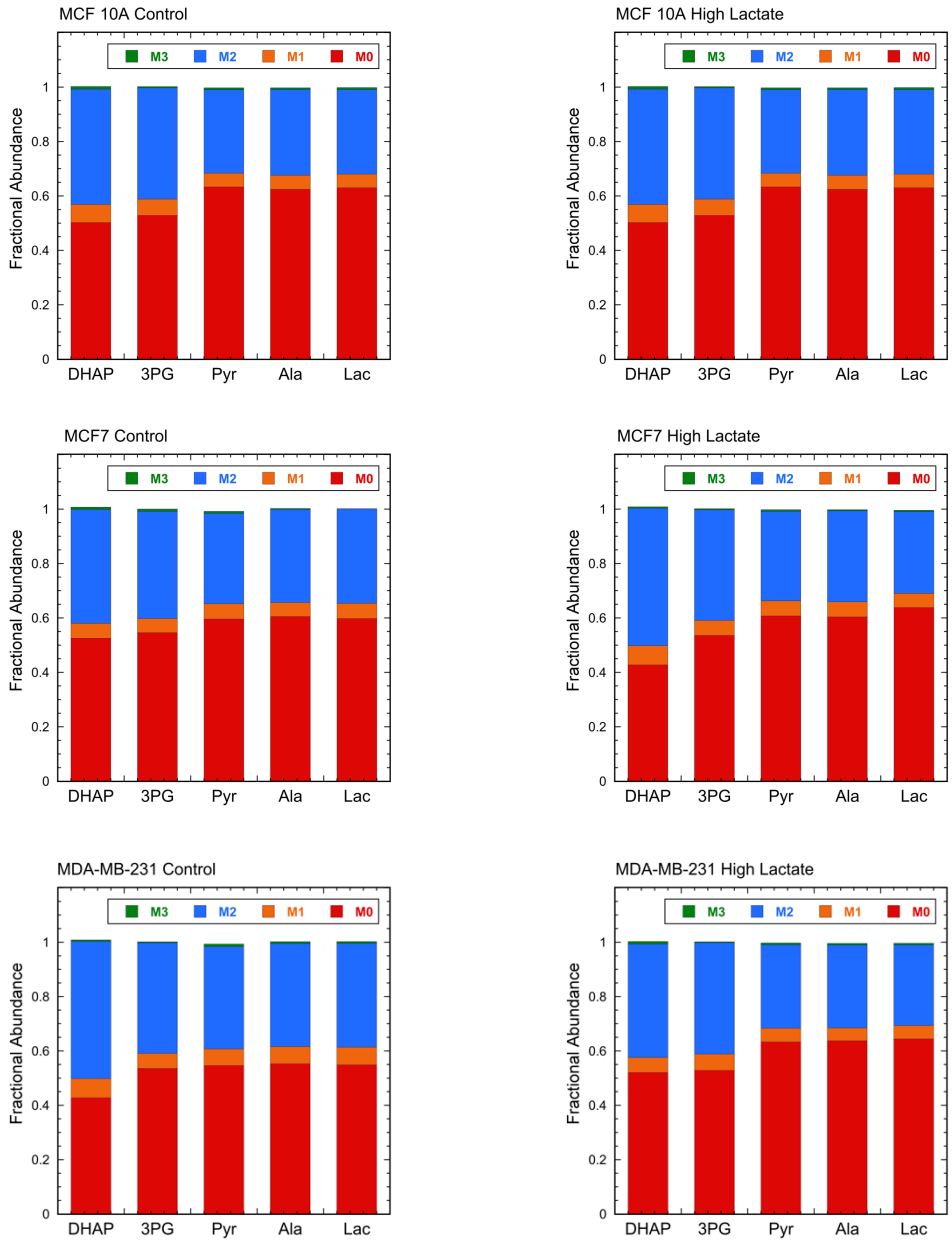

Figure E1. Metabolite isotope labeling distribution from [1,2-^{13}C] glucose for the MCF 10A, MCF7, and MDA-MB-231 cultures for both control and high-lactate conditions. MIDs shown below have been corrected for natural abundance.

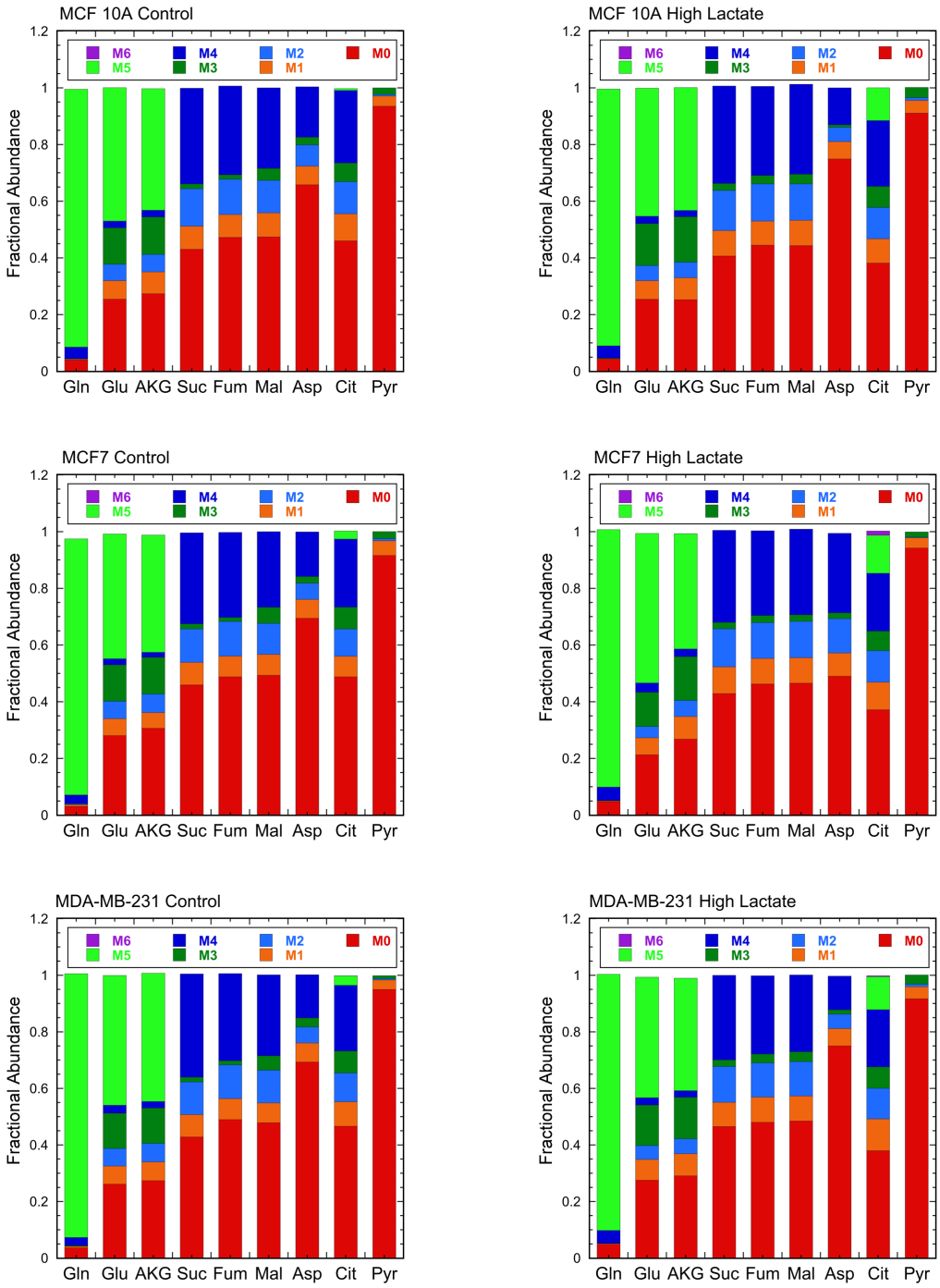

Figure E2. Metabolite isotope labeling distribution from [U-^{13}C] glutamine for the MCF 10A, MCF7, and MDA-MB-231 cultures for both control and high-lactate conditions. MIDs shown below have been corrected for natural abundance.

Appendix F

Metabolic flux maps for three breast cell lines grown in control and high-lactate cultures

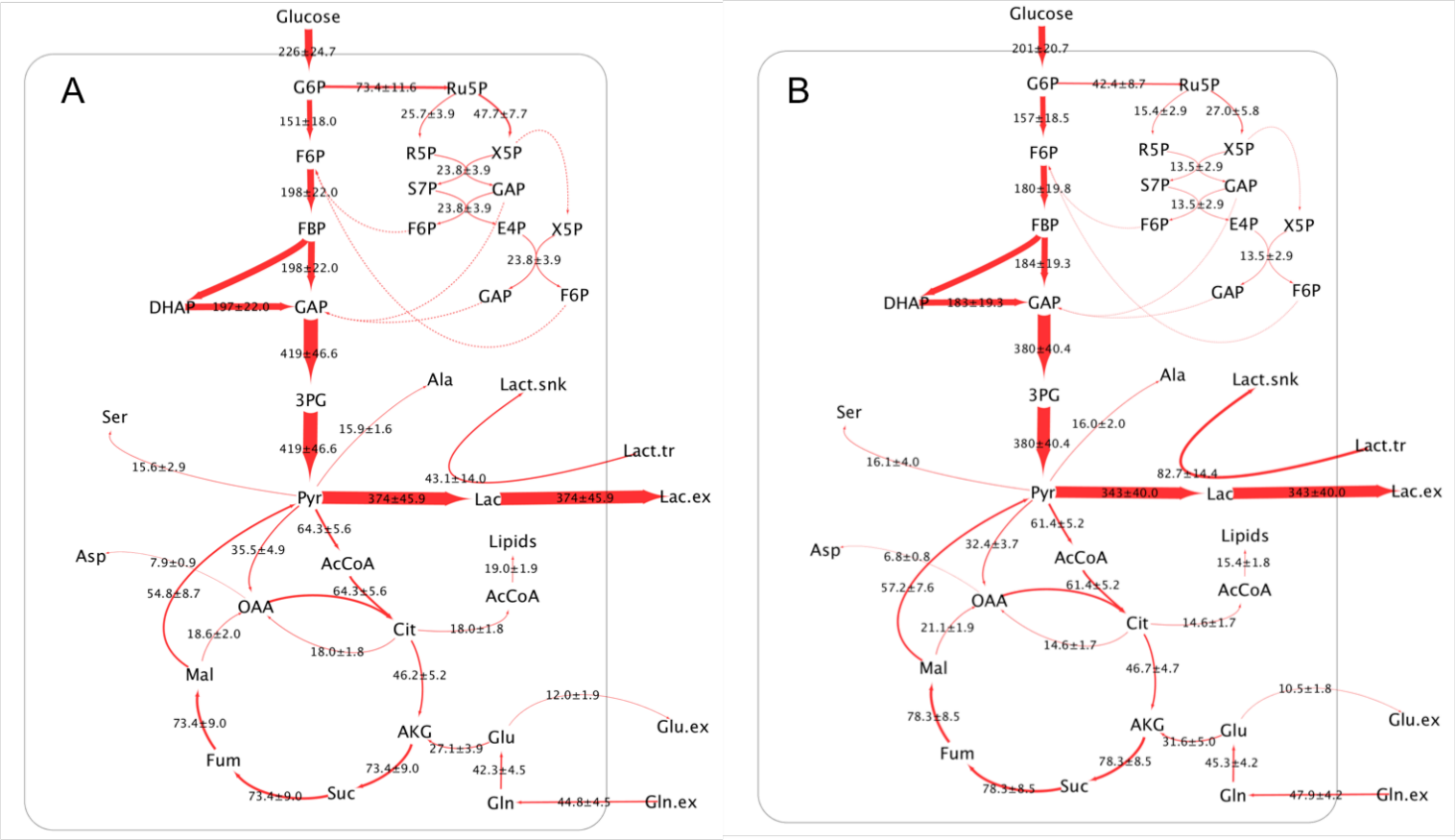

Figure F1. Metabolic flux maps for MCF 10A predicted from the MFA simulations: A) control and B) high-lactate cultures. The line thicknesses represent the relative fluxes, which are also shown numerically (nmol/10^6 cells·h) with standard deviation.

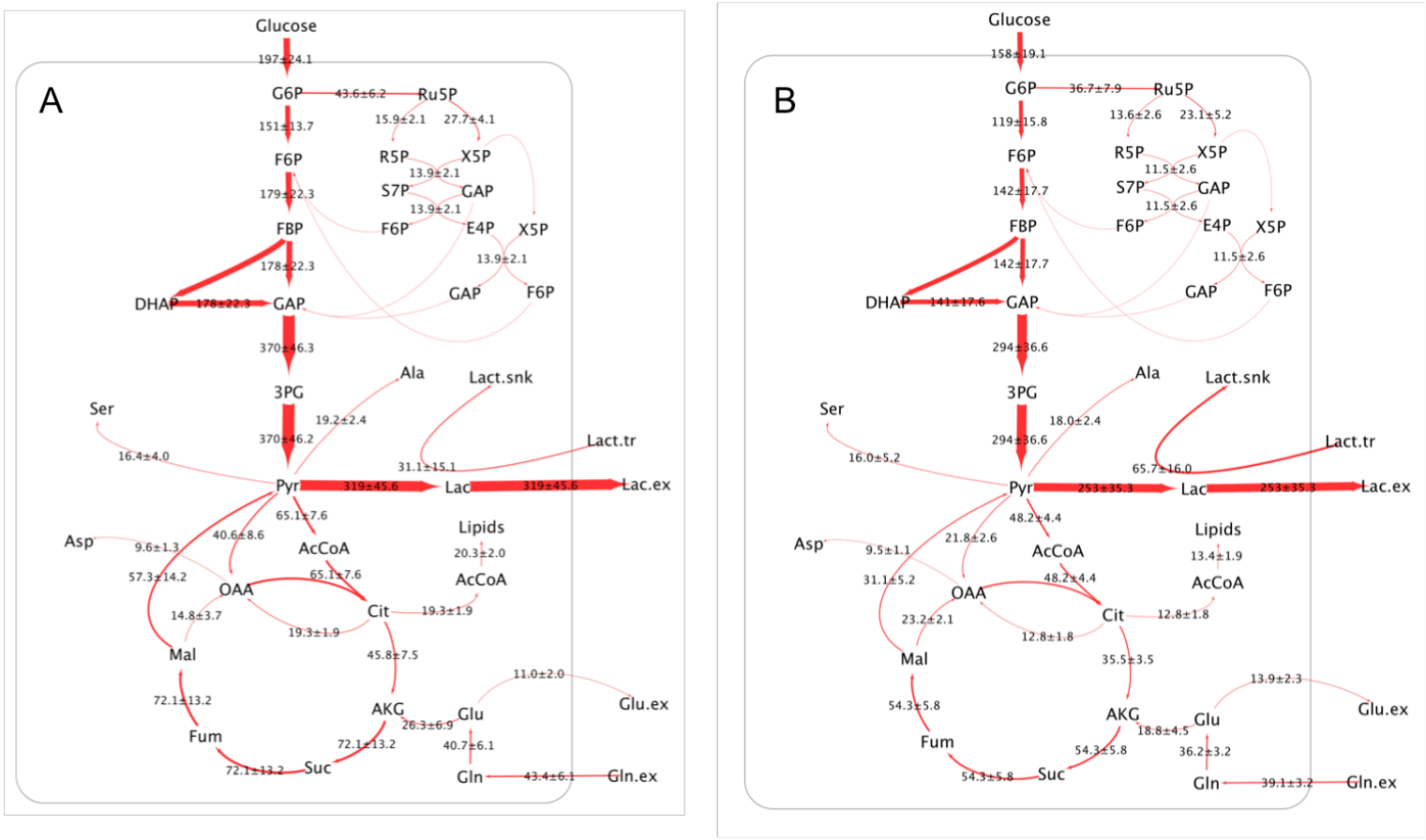

Figure F2. Metabolic flux maps for MCF7 predicted from the MFA simulations: A) control and B) high-lactate cultures. The line thicknesses represent the relative fluxes, which are also shown numerically (nmol/10^6 cells·h) with standard deviations.

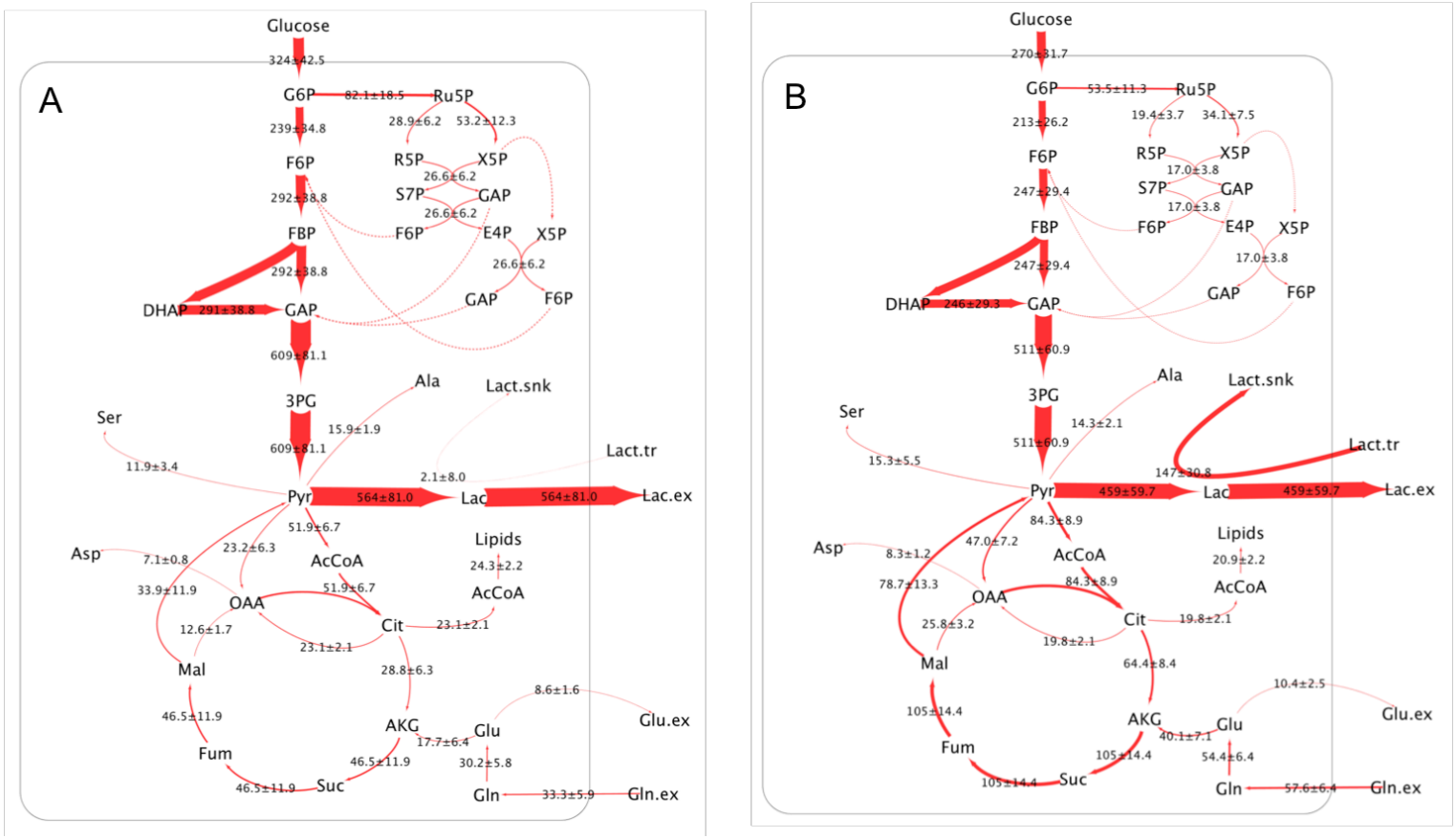

Figure F3. Metabolic flux maps for MDA-MB-231 predicted from the MFA simulations: A) control and B) high-lactate cultures. The line thicknesses represent the relative fluxes, which are also shown numerically (nmol/10^6 cells·h) with standard deviations.

Appendix G

Metabolic flux analysis results for three breast cell lines grown in control and high-lactate cultures

Table G1. Metabolic flux analysis results for MCF 10A control cultures using [1,2-^{13}C] glucose and [U-^{13}C] glutamine. The fluxes are shown with 95% confidence intervals. The sum of squared residuals (SSR) was 60.0 with an expected range of 34.0 to 73.8.

Reaction	**Flux**	**95% Confidence Interval**	
	nmol/10^6 cells/h	Lower Bound	Upper Bound
Gluc.ext -> G6P.c	226.264	179.76	276.13
G6P.c <=> F6P.c (net)	150.514	118.53	188.56
G6P.c <=> F6P.c (exch)	(>1e4, >1e4)	>10000	>10000
F6P.c -> FBP.c	198.197	156.94	242.61
FBP.c <=> DHAP.c + GAP.c (net)	198.197	156.94	242.61
FBP.c <=> DHAP.c + GAP.c (exch)	(0.0, >1e4)	0	>10000
DHAP.c <=> GAP.c (net)	197.247	155.99	241.66
DHAP.c <=> GAP.c (exch)	333.237	249.63	436.75
GAP.c <=> 3PG.c (net)	419.285	331.51	513.41
GAP.c <=> 3PG.c (exch)	(0.0, >1e4)	0	>10000
3PG.c -> Pyr.c	419.285	331.51	513.41
G6P.c -> CO2 + Ru5P.c	73.426	49.97	95.25
Ru5P.c <=> R5P.c (net)	25.743	17.93	33.02
Ru5P.c <=> R5P.c (exch)	(>1e4, >1e4)	0	>10000
Ru5P.c <=> X5P.c (net)	47.683	32.12	62.23
Ru5P.c <=> X5P.c (exch)	(0.0, >1e4)	0	>10000
X5P.c + R5P.c <=> GAP.c + S7P.c (net)	23.841	16.06	31.11
X5P.c + R5P.c <=> GAP.c + S7P.c (exch)	1.685	0	18.81
S7P.c + GAP.c <=> E4P.c + F6P.c (net)	23.841	16.06	31.11
S7P.c + GAP.c <=> E4P.c + F6P.c (exch)	(>1e4, >1e4)	0	>10000
X5P.c + E4P.c <=> GAP.c + F6P (net)	23.841	16.06	31.11
X5P.c + E4P.c <=> GAP.c + F6P (exch)	0	0	19.75
Pyr.c <=> Lact.c (net)	373.984	288.09	467.14
Pyr.c <=> Lact.c (exch)	(>1000, >1e4)	351.11	>10000
Pyr.c -> CO2 + AcCoA.m	64.337	54.81	76.6
AcCoA.m + OAC.m -> Cit.m	64.337	54.81	76.6
Cit.m <=> AKG.m + CO2 (net)	46.289	37.58	58.03
Cit.m <=> AKG.m + CO2 (exch)	1.786	0	3.9
AKG.m -> CO2 + Suc.m	73.402	59.19	94.47
Suc.m <=> Fum.m (net)	73.402	59.19	94.47
Suc.m <=> Fum.m (exch)	268.25	160.72	538.33
Fum.m <=> Mal.m (net)	73.402	59.19	94.47

Reaction	Flux	95% Confidence Interval	
	nmol/10^6 cells/h	Lower Bound	Upper Bound
Fum.m <=> Mal.m (exch)	(609.3, 928.4)	297.52	>10000
Mal.m <=> OAA.m (net)	18.644	14.73	22.67
Mal.m <=> OAA.m (exch)	(642.6, 909.8)	333.54	>10000
Gln.c -> Glu.c	42.29	34.77	52.21
Ser.c <=> Pyr.c (net)	15.633	9.94	21.33
Ser.c <=> Pyr.c (exch)	(>1000, >1e4)	0	>10000
Gln.ext -> Gln.c	44.825	37.15	54.8
Asp.c -> Asp.ext	4.897	3.34	6.46
Ser.ext -> Ser.c	19.013	13.36	24.68
Ala.c -> Ala.ext	10.996	8.07	13.92
Glu.c -> Glu.ext	12.007	8.32	15.7
Lact.c -> Lact.ext	373.984	288.09	467.14
Glu.c <=> AKG.m (net)	3.403	0	13.46
Glu.c <=> AKG.m (exch)	(0.0, 424.8)	0	660.43
Mal.m -> Pyr.c + CO2	54.759	41.87	75.66
Cit.m -> OAA.m + AcCoA.c	18.048	14.53	21.56
Pyr.c + CO2 -> OAA.m	35.5	27.82	47.12
0.95 AcCoA.c + 0.05 DHAP.c -> Lipid	18.998	15.29	22.69
Pyr.c + Glu.c <=> Ala.c + AKG.m (net)	15.856	12.77	18.93
Pyr.c + Glu.c <=> Ala.c + AKG.m (exch)	375.738	0	660.43
OAA.m + Glu.c <=> Asp.c + AKG.m (net)	7.855	6.19	9.51
OAA.m + Glu.c <=> Asp.c + AKG.m (exch)	(0.0, 424.8)	0	660.43
0.23 Ala.c + 0.14 Asp.c + 0.12 Gln.c + 0.15 Glu.c + 0.16 Ser.c + 0.11 G6P.c + 0.09 R5P.c -> Biomass	21.129	17.04	25.21
Lact.c + Lact.tr -> Lact.c + Lact.snk	43.123	20.25	74.95
Glu.c <=> AKG.m (total)	27.114		
Net CO2 production	276.713	226.45	342.45

Table G2. Metabolic flux analysis results for MCF 10A high-lactate cultures using [1,2-^{13}C] glucose and [U-^{13}C] glutamine. The fluxes are shown with 95% confidence intervals. The sum of squared residuals (SSR) was 45.0 with an expected range of 34.8 to 75.0.

Reaction	Flux	95% Confidence Interval	
	nmol/10^6 cells/h	Lower Bound	Upper Bound
Gluc.ext -> G6P.c	201.406	162.31	243.22
G6P.c <=> F6P.c (net)	156.651	123.84	196.17
G6P.c <=> F6P.c (exch)	(>1e4, >1e4)	0	>10000
F6P.c -> FBP.c	183.631	146	221.22
FBP.c <=> DHAP.c + GAP.c (net)	183.631	146	221.22
FBP.c <=> DHAP.c + GAP.c (exch)	(0.0, >1e4)	0	>10000
DHAP.c <=> GAP.c (net)	182.861	145.3	220.68
DHAP.c <=> GAP.c (exch)	(>1000, >1000)	>1000	>10000
GAP.c <=> 3PG.c (net)	379.981	302.12	459.52
GAP.c <=> 3PG.c (exch)	(0.0, >1e4)	0	>10000
3PG.c -> Pyr.c	379.981	302.12	459.52
G6P.c -> CO2 + Ru5P.c	42.398	22.42	56.24
Ru5P.c <=> R5P.c (net)	15.418	8.76	20.05
Ru5P.c <=> R5P.c (exch)	(>1e4, >1e4)	0	>10000
Ru5P.c <=> X5P.c (net)	26.98	13.65	36.2
Ru5P.c <=> X5P.c (exch)	(0.0, >1e4)	0	>10000
X5P.c + R5P.c <=> GAP.c + S7P.c (net)	13.49	6.83	18.1
X5P.c + R5P.c <=> GAP.c + S7P.c (exch)	(>1e4, >1e4)	0	>10000
S7P.c + GAP.c <=> E4P.c + F6P.c (net)	13.49	6.83	18.1
S7P.c + GAP.c <=> E4P.c + F6P.c (exch)	3.214	0	16.9
X5P.c + E4P.c <=> GAP.c + F6P (net)	13.49	6.83	18.1
X5P.c + E4P.c <=> GAP.c + F6P (exch)	0	0	22.54
Pyr.c <=> Lact.c (net)	343.45	266.56	421.74
Pyr.c <=> Lact.c (exch)	(>1e4, >1e4)	>10000	>10000
Pyr.c -> CO2 + AcCoA.m	61.356	51.64	72.08
AcCoA.m + OAC.m -> Cit.m	61.356	51.64	72.08
Cit.m <=> AKG.m + CO2 (net)	46.729	38.24	56.5
Cit.m <=> AKG.m + CO2 (exch)	17.296	13.73	21.52
AKG.m -> CO2 + Suc.m	78.318	62.97	96.02
Suc.m <=> Fum.m (net)	78.318	62.97	96.02
Suc.m <=> Fum.m (exch)	277.593	177.68	476.69
Fum.m <=> Mal.m (net)	78.318	62.97	96.02
Fum.m <=> Mal.m (exch)	(>1e4, >1e4)	>10000	>10000
Mal.m <=> OAA.m (net)	21.112	17.56	25
Mal.m <=> OAA.m (exch)	632.85	362.99	>1000
Gln.c -> Glu.c	45.321	37.65	53.99
Ser.c <=> Pyr.c (net)	16.099	8.29	23.91

Reaction	Flux	95% Confidence Interval	
	nmol/10^6 cells/h	Lower Bound	Upper Bound
Ser.c <=> Pyr.c (exch)	(>1e4, >1e4)	0	>10000
Gln.ext -> Gln.c	47.892	40.16	56.58
Asp.c -> Asp.ext	3.83	2.47	5.19
Ser.ext -> Ser.c	19.527	11.74	27.31
Ala.c -> Ala.ext	11.107	7.4	14.81
Glu.c -> Glu.ext	10.518	7.03	14.01
Lact.c -> Lact.ext	343.45	266.56	421.74
Glu.c <=> AKG.m (net)	8.725	0.35	17.97
Glu.c <=> AKG.m (exch)	(0.0, >1000)	0	>1000
Mal.m -> Pyr.c + CO2	57.207	43.44	73.15
Cit.m -> OAA.m + AcCoA.c	14.627	11.33	18
Pyr.c + CO2 -> OAA.m	32.447	25.88	40.24
0.95 AcCoA.c + 0.05 DHAP.c -> Lipid	15.397	11.92	18.95
Pyr.c + Glu.c <=> Ala.c + AKG.m (net)	16.034	12.22	19.85
Pyr.c + Glu.c <=> Ala.c + AKG.m (exch)	(0.0, >1000)	0	>1000
OAA.m + Glu.c <=> Asp.c + AKG.m (net)	6.83	5.35	8.31
OAA.m + Glu.c <=> Asp.c + AKG.m (exch)	(0.0, >1000)	0	>1000
0.23 Ala.c + 0.14 Asp.c + 0.12 Gln.c + 0.15 Glu.c + 0.16 Ser.c + 0.11 G6P.c + 0.09 R5P.c -> Biomass	21.425	17.34	25.51
Lact.c + Lact.tr -> Lact.c + Lact.snk	82.742	56.54	112.82
Glu.c <=> AKG.m (total)	31.589		
Net CO2 production	253.56	202.62	306.3

Table G3. Metabolic flux analysis results for MCF7 control cultures using [1,2-^{13}C] glucose and [U-^{13}C] glutamine using the biological replicate MIDs for intracellular glutamine, which had a very high standard error. The fluxes are shown with 95% confidence intervals. The sum of squared residuals (SSR) was 30.8 with an expected range of 31.6 to 70.2. **Table G7** has the metabolic flux results for this same culture where the standard error was replaced with 0.6 mol% for one biological replicate. The fluxes are not significantly different between the two simulations.

Reaction	Flux	95% Confidence Interval	
	nmol/10^6 cells/h	Lower Bound	Upper Bound
Gluc.ext -> G6P.c	197.813	150.91	244.41
G6P.c <=> F6P.c (net)	149.733	112.58	190.06
G6P.c <=> F6P.c (exch)	(>1000, >1e4)	0	>10000
F6P.c -> FBP.c	178.799	135.8	221.9
FBP.c <=> DHAP.c + GAP.c (net)	178.799	135.8	221.9
FBP.c <=> DHAP.c + GAP.c (exch)	(0.0, >1e4)	0	>10000
DHAP.c <=> GAP.c (net)	177.784	134.79	220.88
DHAP.c <=> GAP.c (exch)	(>1000, >1e4)	>1000	>10000
GAP.c <=> 3PG.c (net)	371.116	281.09	460.47
GAP.c <=> 3PG.c (exch)	(0.0, >1e4)	0	>10000
3PG.c -> Pyr.c	371.116	281.09	460.47
G6P.c -> CO2 + Ru5P.c	45.615	24.29	67.51
Ru5P.c <=> R5P.c (net)	16.55	9.4	23.86
Ru5P.c <=> R5P.c (exch)	(>1e4, >1e4)	0	>10000
Ru5P.c <=> X5P.c (net)	29.066	14.82	43.66
Ru5P.c <=> X5P.c (exch)	(>1e4, >1e4)	0	>10000
X5P.c + R5P.c <=> GAP.c + S7P.c (net)	14.533	7.41	21.83
X5P.c + R5P.c <=> GAP.c + S7P.c (exch)	(>1e4, >1e4)	0	>10000
S7P.c + GAP.c <=> E4P.c + F6P.c (net)	14.533	7.41	21.83
S7P.c + GAP.c <=> E4P.c + F6P.c (exch)	5.97	0	24.83
X5P.c + E4P.c <=> GAP.c + F6P (net)	14.533	7.41	21.83
X5P.c + E4P.c <=> GAP.c + F6P (exch)	0	0	23.39
Pyr.c <=> Lact.c (net)	319.933	231.31	407.98
Pyr.c <=> Lact.c (exch)	(>1000, >1e4)	233.28	>10000
Pyr.c -> CO2 + AcCoA.m	65.162	51.32	81.11
AcCoA.m + OAC.m -> Cit.m	65.162	51.32	81.11
Cit.m <=> AKG.m + CO2 (net)	45.885	32.23	61.56
Cit.m <=> AKG.m + CO2 (exch)	4.757	1.55	8.22
AKG.m -> CO2 + Suc.m	72.238	48.32	99.57
Suc.m <=> Fum.m (net)	72.238	48.32	99.57
Suc.m <=> Fum.m (exch)	(>1e4, >1e4)	>10000	>10000
Fum.m <=> Mal.m (net)	72.238	48.32	99.57
Fum.m <=> Mal.m (exch)	(198.0, 257.8)	101.87	>10000

Reaction	Flux	95% Confidence Interval	
	nmol/10^6 cells/h	Lower Bound	Upper Bound
Mal.m <=> OAA.m (net)	14.824	7.06	21.41
Mal.m <=> OAA.m (exch)	386.058	171.19	>1000
Gln.c -> Glu.c	40.749	29.66	53.29
Ser.c <=> Pyr.c (net)	16.406	8.58	24.27
Ser.c <=> Pyr.c (exch)	(>1000, >1e4)	0	>10000
Gln.ext -> Gln.c	43.438	32.29	55.94
Asp.c -> Asp.ext	6.485	3.95	9.02
Ser.ext -> Ser.c	19.991	12.2	27.8
Ala.c -> Ala.ext	14.004	9.52	18.49
Glu.c -> Glu.ext	11.035	7.15	14.92
Lact.c -> Lact.ext	319.933	231.31	407.98
Glu.c <=> AKG.m (net)	-2.426	-14.09	10.59
Glu.c <=> AKG.m (exch)	(0.0, 865.7)	0	>1000
Mal.m -> Pyr.c + CO2	57.414	32.1	87.68
Cit.m -> OAA.m + AcCoA.c	19.277	15.59	22.97
Pyr.c + CO2 -> OAA.m	40.683	25.73	59.39
0.95 AcCoA.c + 0.05 DHAP.c -> Lipid	20.291	16.41	24.18
Pyr.c + Glu.c <=> Ala.c + AKG.m (net)	19.157	14.56	23.76
Pyr.c + Glu.c <=> Ala.c + AKG.m (exch)	(0.0, 865.7)	0	>10000
OAA.m + Glu.c <=> Asp.c + AKG.m (net)	9.622	7.01	12.23
OAA.m + Glu.c <=> Asp.c + AKG.m (exch)	(0.0, 865.7)	0	>10000
0.23 Ala.c + 0.14 Asp.c + 0.12 Gln.c + 0.15 Glu.c + 0.16 Ser.c + 0.11 G6P.c + 0.09 R5P.c -> Biomass	22.408	17.93	26.89
Lact.c + Lact.tr -> Lact.c + Lact.snk	32.816	7.77	63.01
Glu.c <=> AKG.m (total)	26.353		
Net CO2 production	245.632	179.25	321.85

Table G4. Metabolic flux analysis results for MCF7 high-lactate cultures using [1,2-^{13}C] glucose and [U-^{13}C] glutamine. The fluxes are shown with 95% confidence intervals. The sum of squared residuals (SSR) was 67.7 with an expected range of 30.8 to 69.0.

Reaction	Flux	95% Confidence Interval	
	nmol/10^6 cells/h	Lower Bound	Upper Bound
Gluc.ext -> G6P.c	157.959	96.22	170.61
G6P.c <=> F6P.c (net)	118.7	70.41	132.1
G6P.c <=> F6P.c (exch)	(>1e4, >1e4)	0	>10000
F6P.c -> FBP.c	141.752	84.68	153.61
FBP.c <=> DHAP.c + GAP.c (net)	141.752	84.68	153.61
FBP.c <=> DHAP.c + GAP.c (exch)	(0.0, >1e4)	0	>10000
DHAP.c <=> GAP.c (net)	141.081	84.19	152.92
DHAP.c <=> GAP.c (exch)	517.276	291.86	613.93
GAP.c <=> 3PG.c (net)	294.359	175.81	318.7
GAP.c <=> 3PG.c (exch)	(0.0, >1e4)	0	>10000
3PG.c -> Pyr.c	294.359	175.81	318.7
G6P.c -> CO2 + Ru5P.c	36.684	13.11	43.82
Ru5P.c <=> R5P.c (net)	13.632	5.75	16.03
Ru5P.c <=> R5P.c (exch)	(0.0, >1e4)	0	>10000
Ru5P.c <=> X5P.c (net)	23.052	7.34	27.81
Ru5P.c <=> X5P.c (exch)	(0.0, 45.4)	0	>10000
X5P.c + R5P.c <=> GAP.c + S7P.c (net)	11.526	3.67	13.9
X5P.c + R5P.c <=> GAP.c + S7P.c (exch)	(415.8, 415.8)	0	>10000
S7P.c + GAP.c <=> E4P.c + F6P.c (net)	11.526	3.67	13.9
S7P.c + GAP.c <=> E4P.c + F6P.c (exch)	(0.0, 0.4)	0	>10000
X5P.c + E4P.c <=> GAP.c + F6P (net)	11.526	3.67	13.9
X5P.c + E4P.c <=> GAP.c + F6P (exch)	0	0	13.76
Pyr.c <=> Lact.c (net)	253.443	139.96	277.5
Pyr.c <=> Lact.c (exch)	405.053	61.34	907.77
Pyr.c -> CO2 + AcCoA.m	48.238	36.79	53.83
AcCoA.m + OAC.m -> Cit.m	48.238	36.79	53.83
Cit.m <=> AKG.m + CO2 (net)	35.486	26.93	40.46
Cit.m <=> AKG.m + CO2 (exch)	19.249	14.16	21.84
AKG.m -> CO2 + Suc.m	54.276	39.6	62.37
Suc.m <=> Fum.m (net)	54.276	39.6	62.37
Suc.m <=> Fum.m (exch)	(155.9, 221.5)	97.48	>10000
Fum.m <=> Mal.m (net)	54.276	39.6	62.37
Fum.m <=> Mal.m (exch)	(>1e4, >1e4)	>10000	>10000
Mal.m <=> OAA.m (net)	23.197	18.3	26.37
Mal.m <=> OAA.m (exch)	(>1e4, >1e4)	438.92	>10000
Gln.c -> Glu.c	36.246	28.23	40.55
Ser.c <=> Pyr.c (net)	16.022	7.21	27.67

Reaction	Flux	95% Confidence Interval	
	nmol/10^6 cells/h	Lower Bound	Upper Bound
Ser.c <=> Pyr.c (exch)	(197.4, >1e4)	0	>10000
Gln.ext -> Gln.c	39.055	30.93	43.37
Asp.c -> Asp.ext	6.199	4.06	8.3
Ser.ext -> Ser.c	19.766	10.95	31.38
Ala.c -> Ala.ext	12.632	7.88	16.85
Glu.c -> Glu.ext	13.946	9.41	18.26
Lact.c -> Lact.ext	253.443	139.96	277.5
Glu.c <=> AKG.m (net)	-8.701	-17.65	-3.55
Glu.c <=> AKG.m (exch)	(0.0, 105.3)	0	126.99
Mal.m -> Pyr.c + CO2	31.078	18.26	38.47
Cit.m -> OAA.m + AcCoA.c	12.751	8.67	15.64
Pyr.c + CO2 -> OAA.m	21.764	15.58	25.74
0.95 AcCoA.c + 0.05 DHAP.c -> Lipid	13.423	9.13	16.46
Pyr.c + Glu.c <=> Ala.c + AKG.m (net)	18.015	13.1	22.29
Pyr.c + Glu.c <=> Ala.c + AKG.m (exch)	92.939	0	126.99
OAA.m + Glu.c <=> Asp.c + AKG.m (net)	9.475	7.22	11.62
OAA.m + Glu.c <=> Asp.c + AKG.m (exch)	(0.0, 105.3)	0	126.99
0.23 Ala.c + 0.14 Asp.c + 0.12 Gln.c + 0.15 Glu.c + 0.16 Ser.c + 0.11 G6P.c + 0.09 R5P.c -> Biomass	23.404	18.9	27.46
Lact.c + Lact.tr -> Lact.c + Lact.snk	65.652	20.76	83.1
Glu.c <=> AKG.m (total)	18.789		
Net CO2 production	183.998	130.52	205.72

Table G5. Metabolic flux analysis results for MDA-MB-231 control cultures using [1,2-^{13}C] glucose and [U-^{13}C] glutamine. The fluxes are shown with 95% confidence intervals. The sum of squared residuals (SSR) was 62.1 with an expected range of 34.8 to 75.0.

Reaction	Flux	95% Confidence Interval	
	nmol/10^6 cells/h	Lower Bound	Upper Bound
Gluc.ext -> G6P.c	323.662	241.31	407.08
G6P.c <=> F6P.c (net)	238.695	177.95	313.69
G6P.c <=> F6P.c (exch)	(>1e4, >1e4)	0	>10000
F6P.c -> FBP.c	291.889	217.43	368.7
FBP.c <=> DHAP.c + GAP.c (net)	291.889	217.43	368.7
FBP.c <=> DHAP.c + GAP.c (exch)	(0.0, >1e4)	0	>10000
DHAP.c <=> GAP.c (net)	290.671	216.23	367.46
DHAP.c <=> GAP.c (exch)	1005.797	691.44	>1000
GAP.c <=> 3PG.c (net)	609.157	452.44	768.83
GAP.c <=> 3PG.c (exch)	(0.0, >1e4)	0	>10000
3PG.c -> Pyr.c	609.157	452.44	768.83
G6P.c -> CO2 + Ru5P.c	82.12	42.77	114.93
Ru5P.c <=> R5P.c (net)	28.926	15.8	39.87
Ru5P.c <=> R5P.c (exch)	(0.0, >1e4)	0	>10000
Ru5P.c <=> X5P.c (net)	53.193	26.96	75.06
Ru5P.c <=> X5P.c (exch)	(0.0, >1e4)	0	>10000
X5P.c + R5P.c <=> GAP.c + S7P.c (net)	26.597	13.48	37.53
X5P.c + R5P.c <=> GAP.c + S7P.c (exch)	(>1e4, >1e4)	0	>10000
S7P.c + GAP.c <=> E4P.c + F6P.c (net)	26.597	13.48	37.53
S7P.c + GAP.c <=> E4P.c + F6P.c (exch)	2.36	0	31.22
X5P.c + E4P.c <=> GAP.c + F6P (net)	26.597	13.48	37.53
X5P.c + E4P.c <=> GAP.c + F6P (exch)	0	0	39.96
Pyr.c <=> Lact.c (net)	563.768	407.51	723.24
Pyr.c <=> Lact.c (exch)	(0.0, >1e4)	0	>10000
Pyr.c -> CO2 + AcCoA.m	51.947	40.32	66.36
AcCoA.m + OAC.m -> Cit.m	51.947	40.32	66.36
Cit.m <=> AKG.m + CO2 (net)	28.816	18.37	43.1
Cit.m <=> AKG.m + CO2 (exch)	6.307	4.27	8.98
AKG.m -> CO2 + Suc.m	46.494	26.68	73.21
Suc.m <=> Fum.m (net)	46.494	26.68	73.21
Suc.m <=> Fum.m (exch)	92.427	43.99	212.9
Fum.m <=> Mal.m (net)	46.494	26.68	73.21
Fum.m <=> Mal.m (exch)	(>1000, >1e4)	266.76	>10000
Mal.m <=> OAA.m (net)	12.57	9.22	16
Mal.m <=> OAA.m (exch)	353.445	161.88	>1000
Gln.c -> Glu.c	30.163	20.23	43

Reaction	Flux	95% Confidence Interval	
	nmol/10^6 cells/h	Lower Bound	Upper Bound
Ser.c <=> Pyr.c (net)	11.898	5.22	18.51
Ser.c <=> Pyr.c (exch)	(>1e4, >1e4)	0	>10000
Gln.ext -> Gln.c	33.269	23.28	46.2
Asp.c -> Asp.ext	3.451	2.09	4.81
Ser.ext -> Ser.c	16.039	9.41	22.62
Ala.c -> Ala.ext	9.989	6.48	13.5
Glu.c -> Glu.ext	8.603	5.49	11.72
Lact.c -> Lact.ext	563.768	407.51	723.24
Glu.c <=> AKG.m (net)	-5.34	-15.81	7.66
Glu.c <=> AKG.m (exch)	(0.0, 628.4)	0	>1000
Mal.m -> Pyr.c + CO2	33.924	14.38	60.72
Cit.m -> OAA.m + AcCoA.c	23.131	19.07	27.23
Pyr.c + CO2 -> OAA.m	23.321	13.27	37.66
0.95 AcCoA.c + 0.05 DHAP.c -> Lipid	24.348	20.08	28.67
Pyr.c + Glu.c <=> Ala.c + AKG.m (net)	15.943	12.25	19.64
Pyr.c + Glu.c <=> Ala.c + AKG.m (exch)	(0.0, 628.4)	0	>1000
OAA.m + Glu.c <=> Asp.c + AKG.m (net)	7.075	5.54	8.61
OAA.m + Glu.c <=> Asp.c + AKG.m (exch)	(0.0, 628.4)	0	>1000
0.23 Ala.c + 0.14 Asp.c + 0.12 Gln.c + 0.15 Glu.c + 0.16 Ser.c + 0.11 G6P.c + 0.09 R5P.c -> Biomass	25.884	20.82	30.95
Lact.c + Lact.tr -> Lact.c + Lact.snk	2.1	0	31.21
Glu.c <=> AKG.m (total)	17.678		
Net CO2 production	219.979	152.69	294.91

Table G6. Metabolic flux analysis results for MDA-MB-231 high-lactate cultures using [1,2- ^{13}C] glucose and [U-^{13}C] glutamine. The fluxes are shown with 95% confidence intervals. The sum of squared residuals (SSR) was 38.3 with an expected range of 34.8 to 75.0.

Reaction	Flux	95% Confidence Interval	
	nmol/10^6 cells/h	Lower Bound	Upper Bound
Gluc.ext -> G6P.c	269.671	209.66	333.36
G6P.c <=> F6P.c (net)	213.317	164.04	266.24
G6P.c <=> F6P.c (exch)	(>1e4, >1e4)	0	>10000
F6P.c -> FBP.c	247.391	191.86	306.37
FBP.c <=> DHAP.c + GAP.c (net)	247.391	191.86	306.37
FBP.c <=> DHAP.c + GAP.c (exch)	(0.0, >1e4)	0	>10000
DHAP.c <=> GAP.c (net)	246.347	190.85	305.29
DHAP.c <=> GAP.c (exch)	(>1e4, >1e4)	>1000	>10000
GAP.c <=> 3PG.c (net)	510.774	395.1	632.72
GAP.c <=> 3PG.c (exch)	(0.0, >1e4)	0	>10000
3PG.c -> Pyr.c	510.774	395.1	632.72
G6P.c -> CO2 + Ru5P.c	53.47	31.02	74.99
Ru5P.c <=> R5P.c (net)	19.397	11.96	26.58
Ru5P.c <=> R5P.c (exch)	(0.0, >1e4)	0	>10000
Ru5P.c <=> X5P.c (net)	34.074	19.09	48.42
Ru5P.c <=> X5P.c (exch)	(0.0, >1e4)	0	>10000
X5P.c + R5P.c <=> GAP.c + S7P.c (net)	17.037	9.54	24.21
X5P.c + R5P.c <=> GAP.c + S7P.c (exch)	(0.0, 4.3)	0	>10000
S7P.c + GAP.c <=> E4P.c + F6P.c (net)	17.037	9.54	24.21
S7P.c + GAP.c <=> E4P.c + F6P.c (exch)	(>1000, >1e4)	0	>10000
X5P.c + E4P.c <=> GAP.c + F6P (net)	17.037	9.54	24.21
X5P.c + E4P.c <=> GAP.c + F6P (exch)	0.791	0	24.62
Pyr.c <=> Lact.c (net)	459.32	346.09	578.84
Pyr.c <=> Lact.c (exch)	(>1000, >1000)	>1000	>10000
Pyr.c -> CO2 + AcCoA.m	84.266	68.37	102.99
AcCoA.m + OAC.m -> Cit.m	84.266	68.37	102.99
Cit.m <=> AKG.m + CO2 (net)	64.437	49.71	82.34
Cit.m <=> AKG.m + CO2 (exch)	31.16	24.15	39.76
AKG.m -> CO2 + Suc.m	104.519	79.32	135.31
Suc.m <=> Fum.m (net)	104.519	79.32	135.31
Suc.m <=> Fum.m (exch)	(652.8, >1000)	263.79	>10000
Fum.m <=> Mal.m (net)	104.519	79.32	135.31
Fum.m <=> Mal.m (exch)	(>1000, >1e4)	668.42	>10000
Mal.m <=> OAA.m (net)	25.781	19.91	32.28
Mal.m <=> OAA.m (exch)	(>1e4, >1e4)	>1000	>10000
Gln.c -> Glu.c	54.444	43.11	68.02
Ser.c <=> Pyr.c (net)	15.336	4.6	26.08

Reaction	Flux	95% Confidence Interval	
	nmol/10^6 cells/h	Lower Bound	Upper Bound
Ser.c <=> Pyr.c (exch)	(169.7, >1e4)	0	>10000
Gln.ext -> Gln.c	57.59	46.16	71.17
Asp.c -> Asp.ext	4.643	2.5	6.78
Ser.ext -> Ser.c	19.531	8.82	30.24
Ala.c -> Ala.ext	8.262	4.36	12.16
Glu.c -> Glu.ext	10.428	5.58	15.27
Lact.c -> Lact.ext	459.32	346.09	578.84
Glu.c <=> AKG.m (net)	17.476	5.55	31.48
Glu.c <=> AKG.m (exch)	366.926	0	>1000
Mal.m -> Pyr.c + CO2	78.738	55.59	107.5
Cit.m -> OAA.m + AcCoA.c	19.83	15.75	23.95
Pyr.c + CO2 -> OAA.m	46.969	34.67	62.74
0.95 AcCoA.c + 0.05 DHAP.c -> Lipid	20.873	16.58	25.21
Pyr.c + Glu.c <=> Ala.c + AKG.m (net)	14.293	10.22	18.36
Pyr.c + Glu.c <=> Ala.c + AKG.m (exch)	357.26	0	>1000
OAA.m + Glu.c <=> Asp.c + AKG.m (net)	8.314	6.06	10.57
OAA.m + Glu.c <=> Asp.c + AKG.m (exch)	(0.0, 964.0)	0	>1000
0.23 Ala.c + 0.14 Asp.c + 0.12 Gln.c + 0.15 Glu.c + 0.16 Ser.c + 0.11 G6P.c + 0.09 R5P.c -> Biomass	26.22	21.15	31.31
Lact.c + Lact.tr -> Lact.c + Lact.snk	147.176	96.59	216.76
Glu.c <=> AKG.m (total)	40.083		
Net CO2 production	338.461	261.22	428.14

Table G7. Metabolic flux analysis results for MCF7 control cultures using [1,2-^{13}C] glucose and [U-^{13}C] glutamine using the 0.6 mol% standard error for the MIDs for intracellular glutamine, where the biological replicates had high standard error. The fluxes are shown with 95% confidence intervals. The sum of squared residuals (SSR) was 56.4 with an expected range of 30.8 to 69.0. **Table G3** has the metabolic flux results for this culture when the standard error for the biological replicates was used. The fluxes are not significantly different between the two simulations.

Reaction	Flux	95% Confidence Interval	
	nmol/10^6 cells/h	Lower Bound	Upper Bound
Gluc.ext -> G6P.c	197.061	149.98	243.88
G6P.c <=> F6P.c (net)	150.994	138.25	191.77
G6P.c <=> F6P.c (exch)	(>1000, >1e4)	0	>10000
F6P.c -> FBP.c	178.712	135.05	222.12
FBP.c <=> DHAP.c + GAP.c (net)	178.712	135.05	222.12
FBP.c <=> DHAP.c + GAP.c (exch)	(0.0, >1e4)	0	>10000
DHAP.c <=> GAP.c (net)	177.697	134.04	221.1
DHAP.c <=> GAP.c (exch)	(>1000, >1000)	>1000	>10000
GAP.c <=> 3PG.c (net)	370.268	279.69	460.17
GAP.c <=> 3PG.c (exch)	(0.0, >1e4)	0	>10000
3PG.c -> Pyr.c	370.268	279.69	460.17
G6P.c -> CO2 + Ru5P.c	43.598	22.77	46.94
Ru5P.c <=> R5P.c (net)	15.88	8.94	17
Ru5P.c <=> R5P.c (exch)	(>1e4, >1e4)	0	>10000
Ru5P.c <=> X5P.c (net)	27.718	13.83	29.95
Ru5P.c <=> X5P.c (exch)	(0.0, 624.4)	0	>10000
X5P.c + R5P.c <=> GAP.c + S7P.c (net)	13.859	6.91	14.97
X5P.c + R5P.c <=> GAP.c + S7P.c (exch)	5.122	0	24.56
S7P.c + GAP.c <=> E4P.c + F6P.c (net)	13.859	6.91	14.97
S7P.c + GAP.c <=> E4P.c + F6P.c (exch)	(>1000, >1e4)	0	>10000
X5P.c + E4P.c <=> GAP.c + F6P (net)	13.859	6.91	14.97
X5P.c + E4P.c <=> GAP.c + F6P (exch)	0	0	61.78
Pyr.c <=> Lact.c (net)	319.073	229.84	407.69
Pyr.c <=> Lact.c (exch)	(>1000, >1e4)	200.13	>10000
Pyr.c -> CO2 + AcCoA.m	65.08	51.25	81
AcCoA.m + OAC.m -> Cit.m	65.08	51.25	81
Cit.m <=> AKG.m + CO2 (net)	45.806	32.18	61.45
Cit.m <=> AKG.m + CO2 (exch)	4.737	1.54	8.2
AKG.m -> CO2 + Suc.m	72.082	48.15	99.54
Suc.m <=> Fum.m (net)	72.082	48.15	99.54
Suc.m <=> Fum.m (exch)	(>1e4, >1e4)	>10000	>10000
Fum.m <=> Mal.m (net)	72.082	48.15	99.54
Fum.m <=> Mal.m (exch)	223.139	101.45	923.97

Reaction	Flux	95% Confidence Interval	
	nmol/10^6 cells/h	Lower Bound	Upper Bound
Mal.m <=> OAA.m (net)	14.806	7.05	21.37
Mal.m <=> OAA.m (exch)	384.54	170.71	>1000
Gln.c -> Glu.c	40.677	29.56	53.19
Ser.c <=> Pyr.c (net)	16.404	8.58	24.22
Ser.c <=> Pyr.c (exch)	(>1000, >1e4)	0	>10000
Gln.ext -> Gln.c	43.371	32.19	55.94
Asp.c -> Asp.ext	6.485	3.95	9.02
Ser.ext -> Ser.c	19.996	12.21	27.79
Ala.c -> Ala.ext	14.002	9.52	18.48
Glu.c -> Glu.ext	11.034	7.14	14.92
Lact.c -> Lact.ext	319.073	229.84	407.69
Glu.c <=> AKG.m (net)	-2.518	-14.21	10.47
Glu.c <=> AKG.m (exch)	(0.0, 865.2)	0	>1000
Mal.m -> Pyr.c + CO2	57.276	32.04	87.48
Cit.m -> OAA.m + AcCoA.c	19.274	15.57	22.97
Pyr.c + CO2 -> OAA.m	40.628	25.72	59.31
0.95 AcCoA.c + 0.05 DHAP.c -> Lipid	20.289	16.39	24.17
Pyr.c + Glu.c <=> Ala.c + AKG.m (net)	19.166	14.55	23.76
Pyr.c + Glu.c <=> Ala.c + AKG.m (exch)	(0.0, 865.2)	0	>10000
OAA.m + Glu.c <=> Asp.c + AKG.m (net)	9.628	7.01	12.24
OAA.m + Glu.c <=> Asp.c + AKG.m (exch)	(0.0, 865.2)	0	>10000
0.23 Ala.c + 0.14 Asp.c + 0.12 Gln.c + 0.15 Glu.c + 0.16 Ser.c + 0.11 G6P.c + 0.09 R5P.c -> Biomass	22.451	17.97	26.93
Lact.c + Lact.tr -> Lact.c + Lact.snk	31.054	5.9	64.89
Glu.c <=> AKG.m (total)	26.276		
Net CO2 production	243.213	176.69	319.8

Appendix H

Measured and simulated MIDs from ^{13}C-MFA simulations for three breast cell lines

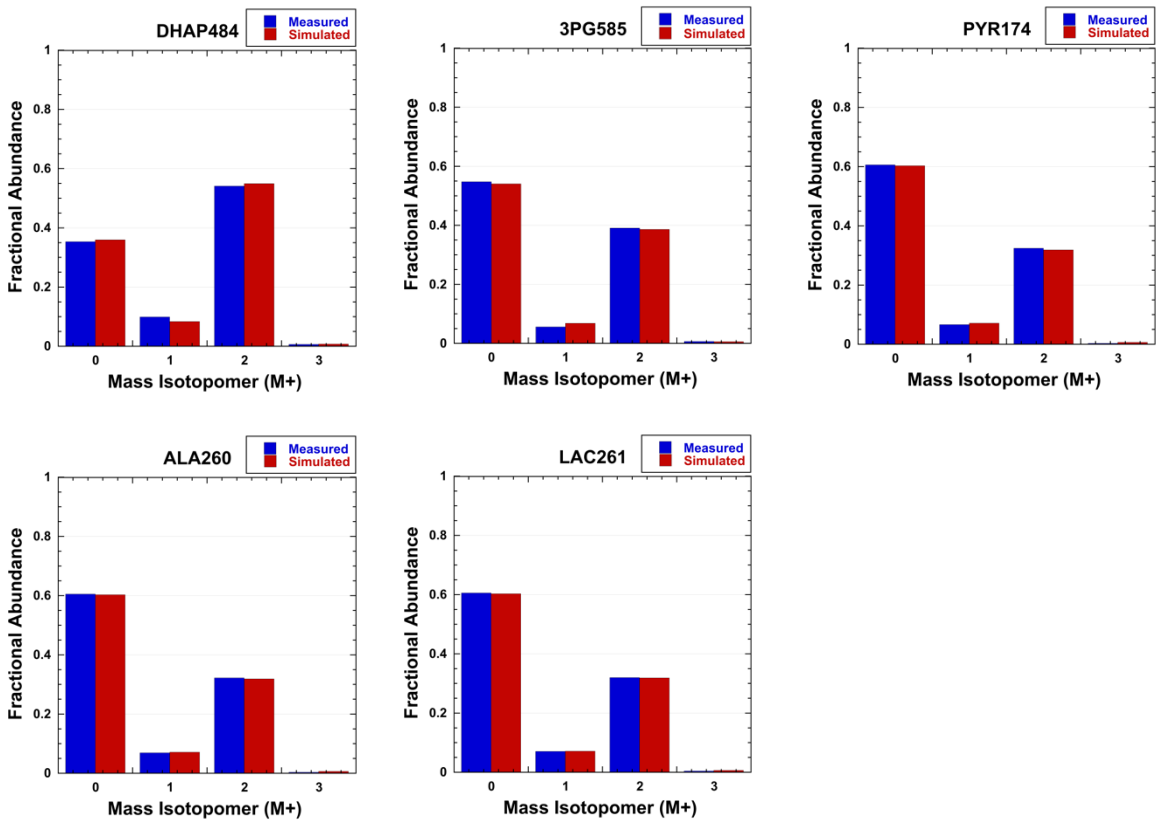

Figure H1. Measured and simulated MIDs for intracellular metabolites from [1,2-^{13}C] glucose labeling for MCF 10A control cultures. MIDs shown below have been corrected for natural abundance.

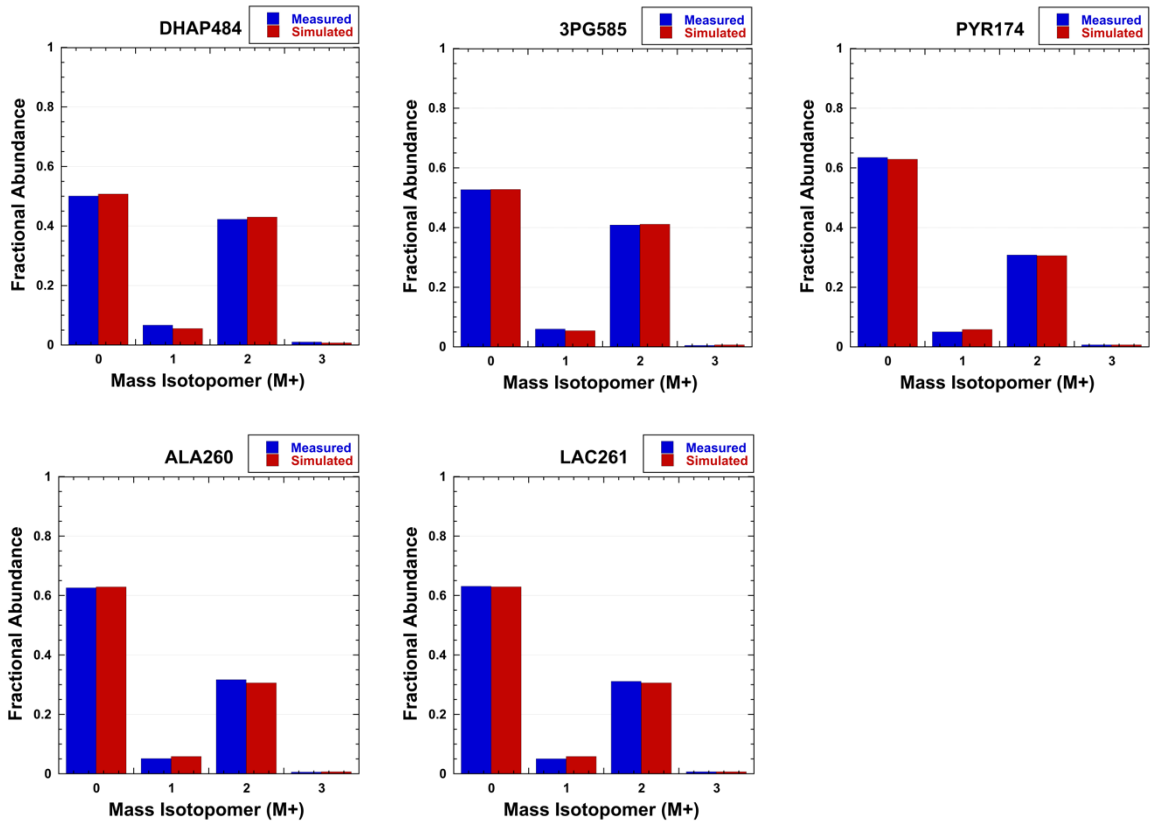

Figure H2. Measured and simulated MIDs for intracellular metabolites from [1,2-^{13}C] glucose labeling for MCF 10A high-lactate cultures. MIDs shown below have been corrected for natural abundance.

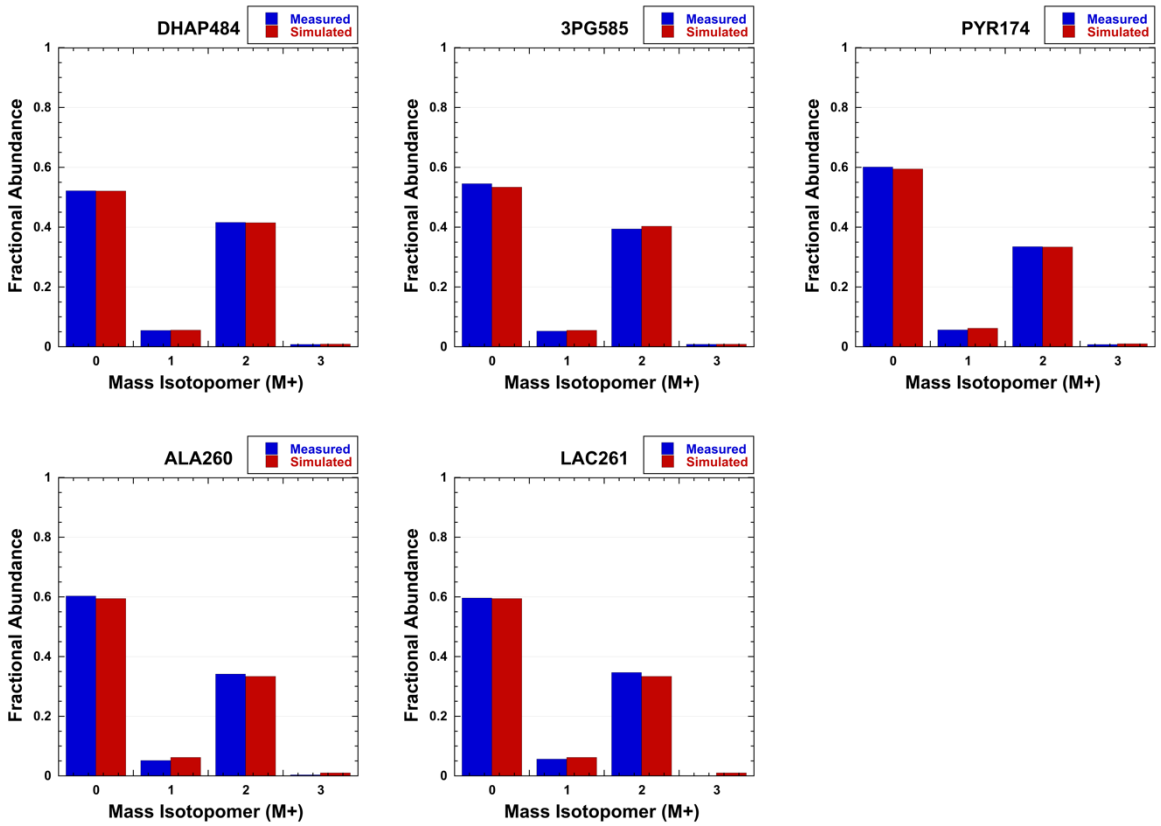

Figure H3. Measured and simulated MIDs for intracellular metabolites from [1,2-^{13}C] glucose labeling for MCF7 control cultures. MIDs shown below have been corrected for natural abundance.

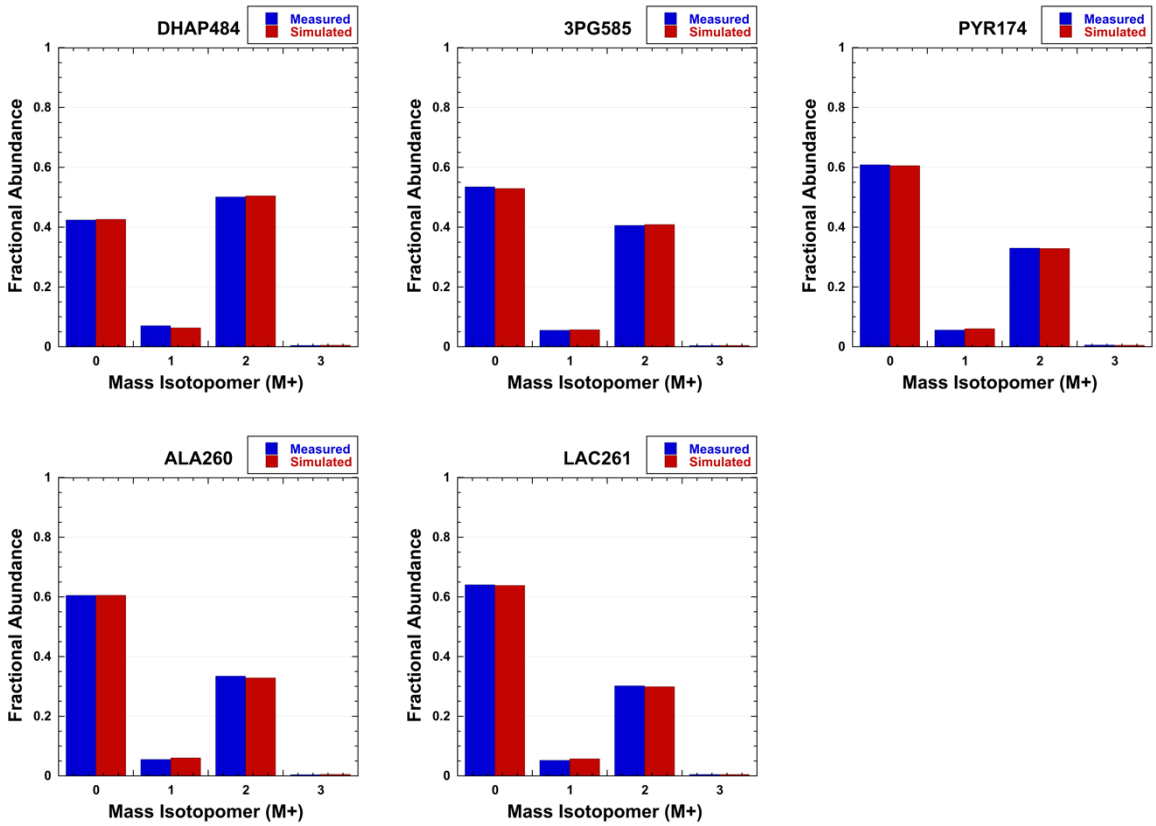

Figure H4. Measured and simulated MIDs for intracellular metabolites from [1,2-^{13}C] glucose labeling for MCF7 high-lactate cultures. MIDs shown below have been corrected for natural abundance.

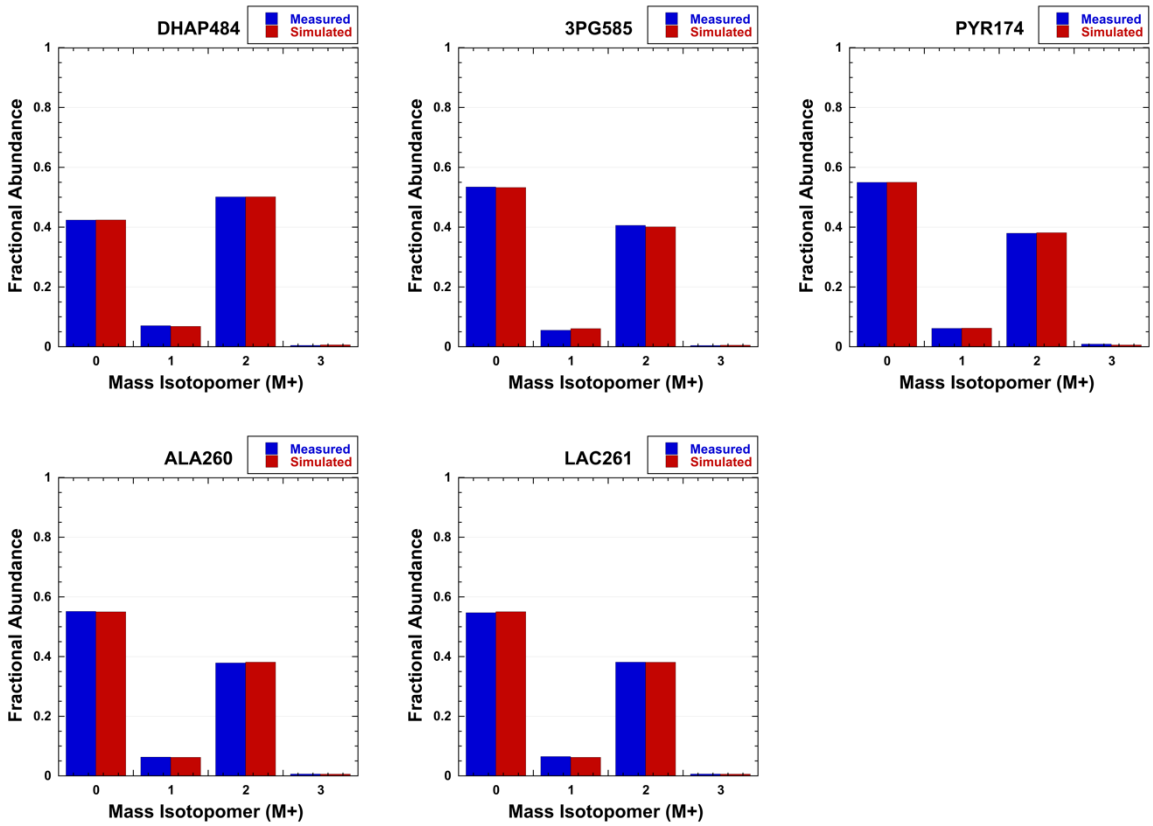

Figure H5. Measured and simulated MIDs for intracellular metabolites from [1,2-^{13}C] glucose labeling for MDA-MB-231 control cultures. MIDs shown below have been corrected for natural abundance.

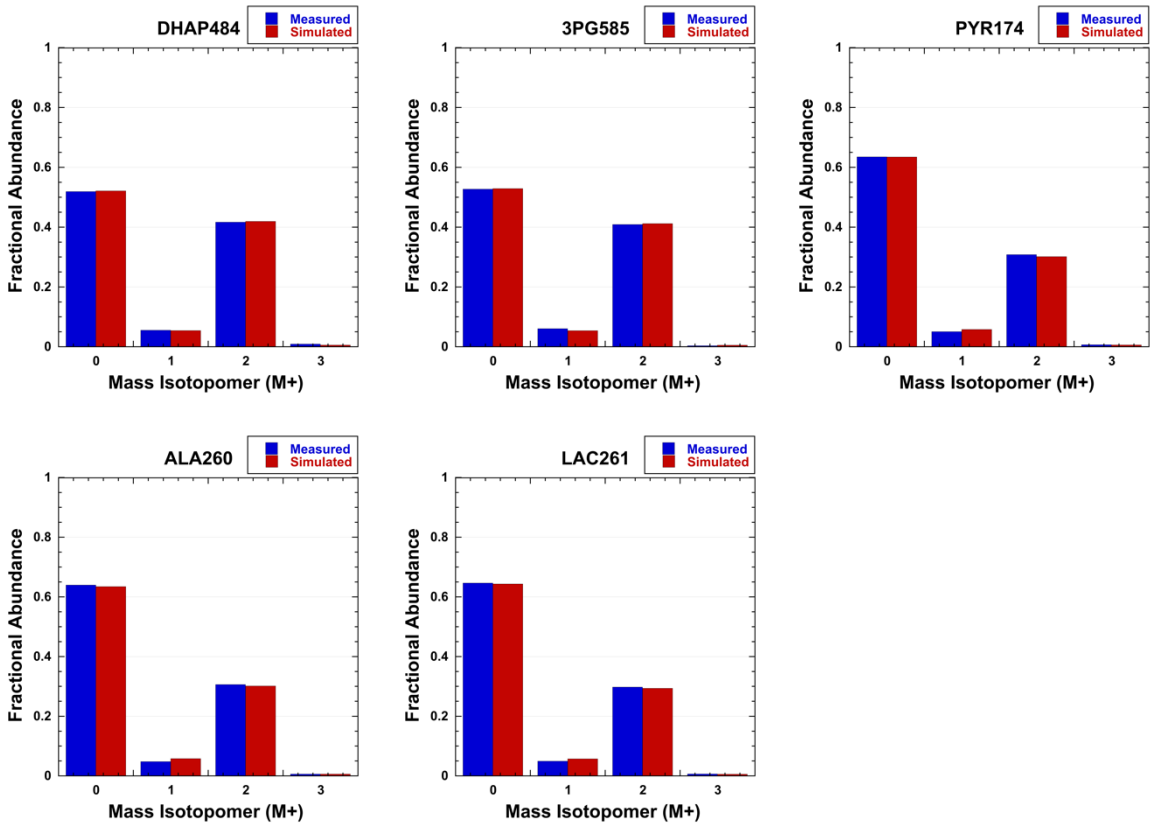

Figure H6. Measured and simulated MIDs for intracellular metabolites from [1,2-^{13}C] glucose labeling for MDA-MB-231 high-lactate cultures. MIDs shown below have been corrected for natural abundance.

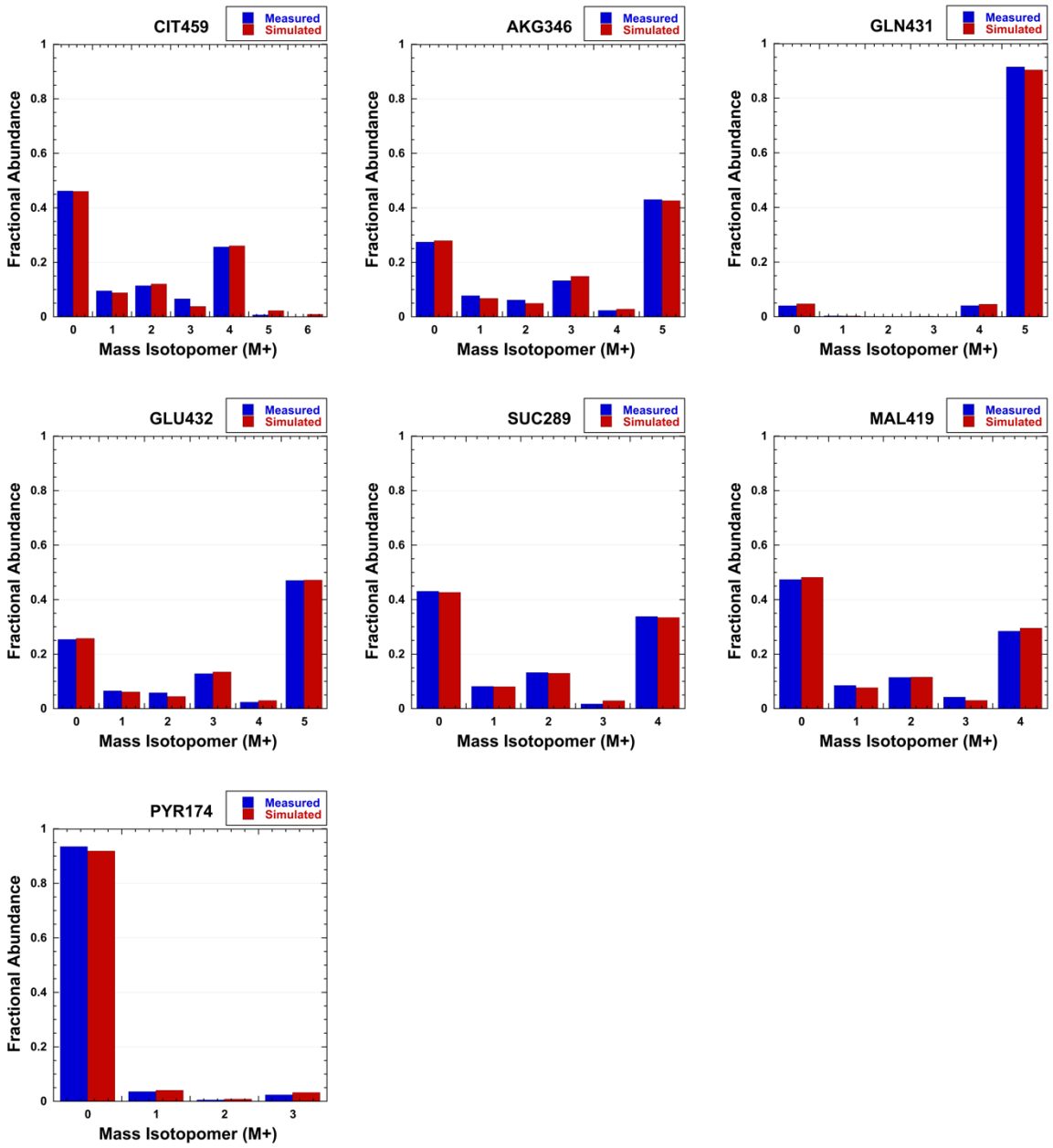

Figure H7. Measured and simulated MIDs for intracellular metabolites from [U-^{13}C] glutamine labeling for MCF 10A control cultures. MIDs shown below have been corrected for natural abundance.

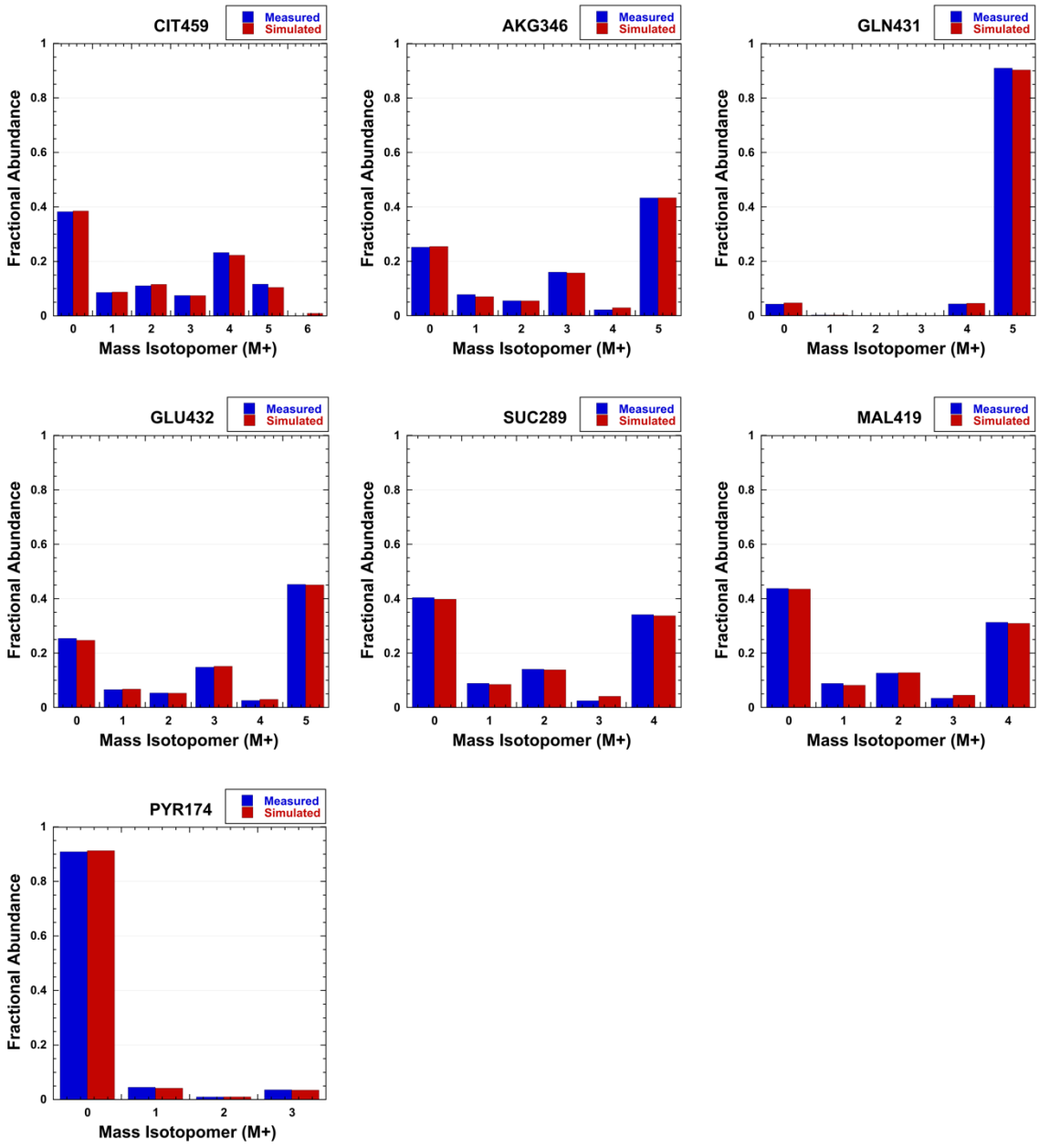

Figure H8. Measured and simulated MIDs for intracellular metabolites from [U-^{13}C] glutamine labeling for MCF 10A high-lactate cultures. MIDs shown below have been corrected for natural abundance.

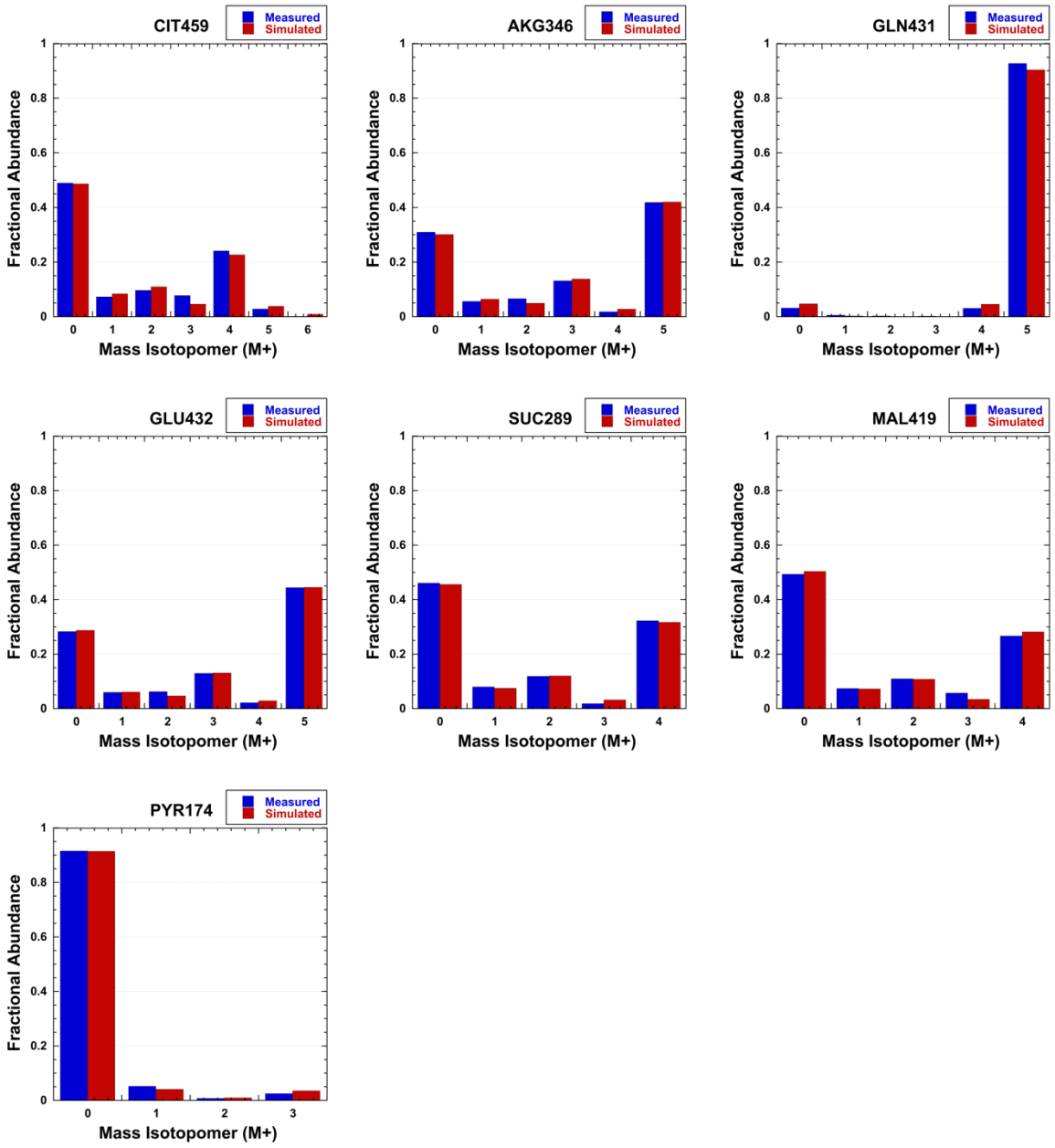

Figure H9. Measured and simulated MIDs for intracellular metabolites from [U-^{13}C] glutamine labeling for MCF7 control cultures. MIDs shown below have been corrected for natural abundance.

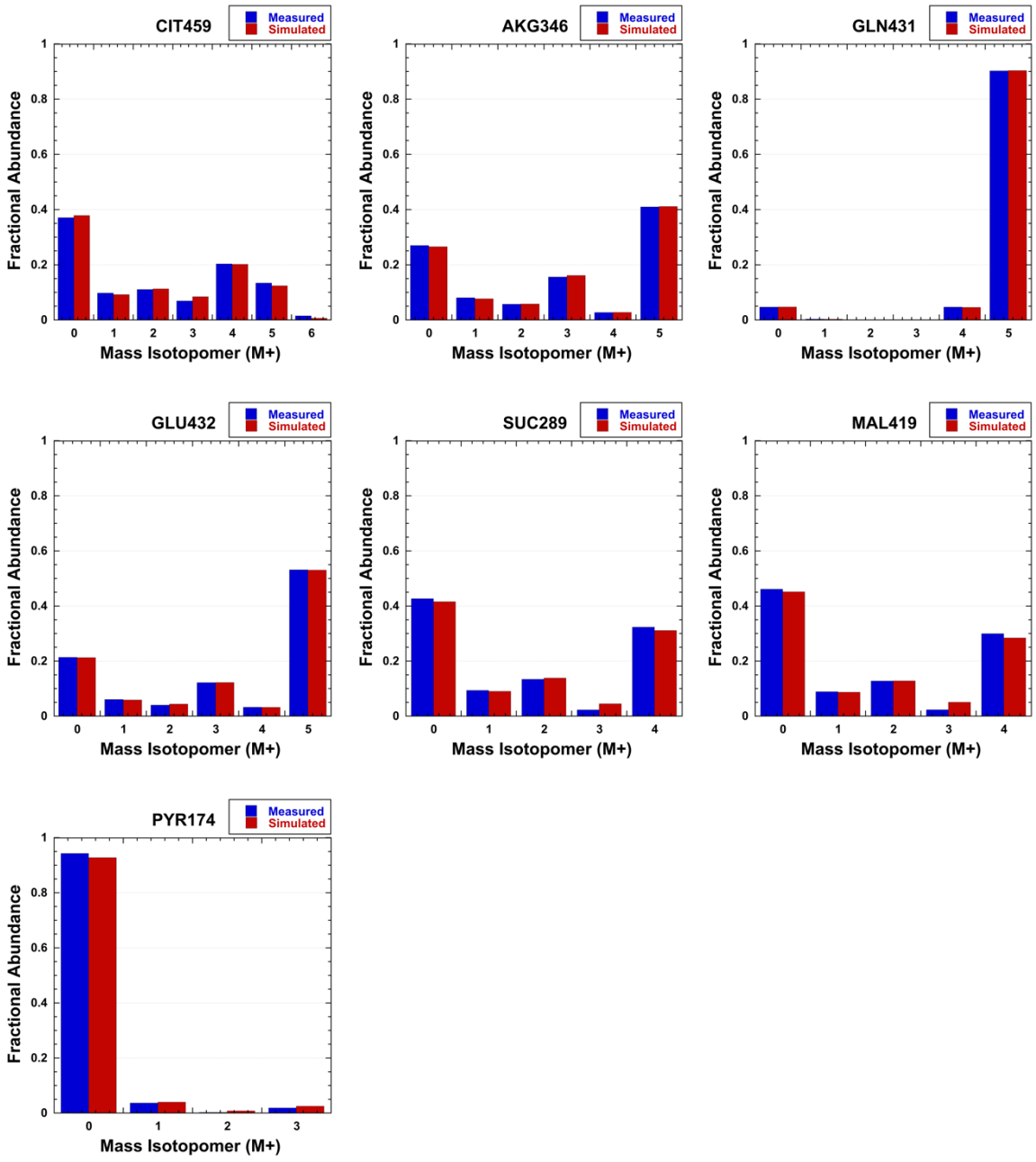

Figure H10. Measured and simulated MIDs for intracellular metabolites from [U-^{13}C] glutamine labeling for MCF7 high-lactate cultures. MIDs shown below have been corrected for natural abundance.

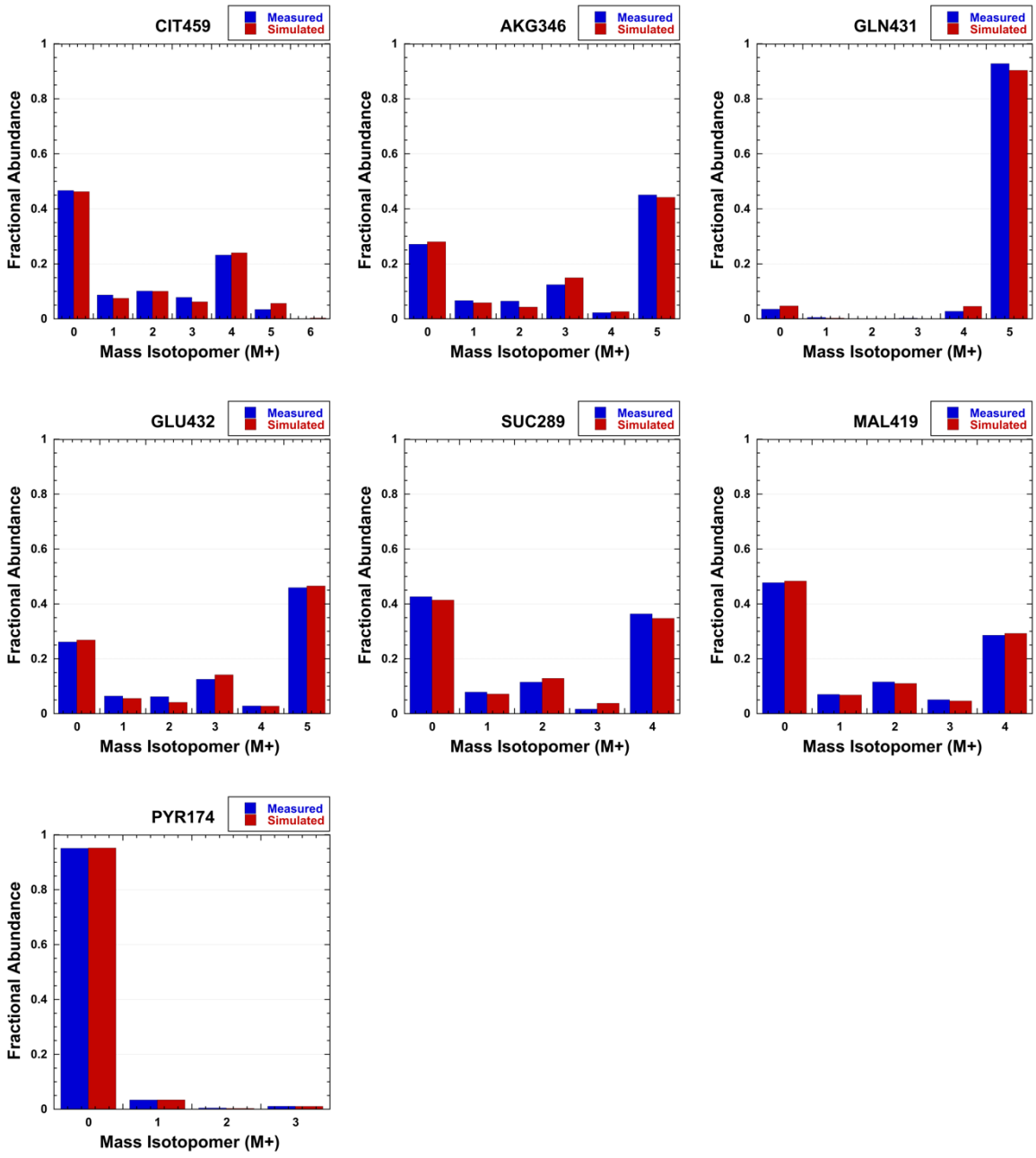

Figure H11. Measured and simulated MIDs for intracellular metabolites from [U-^{13}C] glutamine labeling for MDA-MB-231 control cultures. MIDs shown below have been corrected for natural abundance.

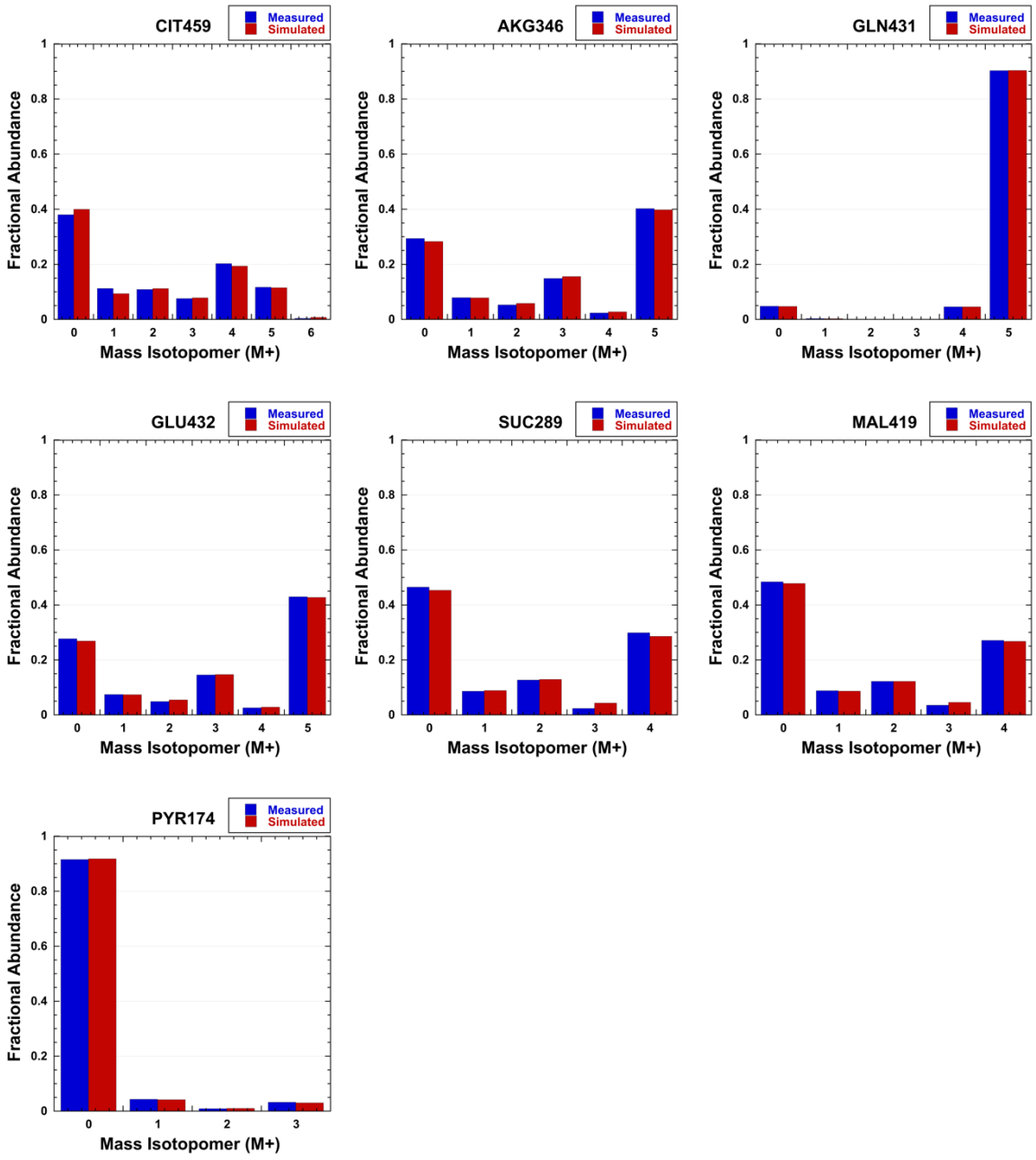

Figure H12. Measured and simulated MIDs for intracellular metabolites from [U-^{13}C] glutamine labeling for MDA-MB-231 high-lactate cultures. MIDs shown below have been corrected for natural abundance.

Appendix I

Measured extracellular metabolite concentrations for K3 iPSCs

Table I1. Measured extracellular metabolite concentrations for the K3 iPSCs grown in control culture at 0, 12, 24, 36, and 48-h after the media exchange. Averages are from biological 6-replicates. Standard errors are provided for these averages.

Control	**Average Concentration (mM)**									
Metabolite	**0-h**	**SE**	**12-h**	**SE**	**24-h**	**SE**	**36-h**	**SE**	**48-h**	**SE**
Glucose	18.72	0.03	17.40	0.09	15.91	0.17	14.27	0.28	12.62	0.24
Lactate	0.00	0.00	1.61	0.13	4.07	0.19	7.12	0.29	9.33	0.22
Pyruvate	0.42	0.01	0.33	0.01	0.22	0.01	0.14	0.01	0.13	0.01
Glutamine	2.54	0.03	2.32	0.02	2.09	0.04	1.84	0.04	1.54	0.04
Ammonia	0.03	0.01	0.15	0.01	0.32	0.01	0.52	0.01	0.71	0.02
Amino Acids										
Alanine	0.03	0.00	0.06	0.00	0.10	0.00	0.15	0.00	0.18	0.01
Asparagine	0.08	0.01	0.06	0.01	0.05	0.00	0.07	0.01	0.06	0.00
Aspartate	0.04	0.00	0.03	0.00	0.03	0.00	0.03	0.00	0.02	0.00
Glutamate	0.03	0.00	0.07	0.00	0.12	0.00	0.17	0.00	0.21	0.00
Glycine	0.24	0.01	0.25	0.01	0.25	0.01	0.25	0.01	0.22	0.01
Histidine	0.11	0.01	0.09	0.01	0.09	0.01	0.09	0.01	0.08	0.01
Isoleucine	0.71	0.02	0.64	0.02	0.55	0.02	0.48	0.02	0.42	0.01
Leucine	0.49	0.01	0.44	0.01	0.39	0.01	0.33	0.02	0.27	0.01
Lysine	0.54	0.05	0.67	0.06	0.66	0.01	0.62	0.03	0.57	0.03
Methionine	0.09	0.01	0.07	0.00	0.06	0.00	0.05	0.00	0.05	0.00
Phenylalanine	0.17	0.01	0.21	0.01	0.19	0.01	0.18	0.01	0.16	0.01
Proline	0.12	0.00	0.12	0.00	0.12	0.00	0.12	0.00	0.11	0.00
Serine	0.39	0.01	0.37	0.01	0.31	0.01	0.27	0.01	0.20	0.01
Threonine	0.24	0.02	0.25	0.01	0.23	0.01	0.22	0.01	0.18	0.01
Tryptophan	0.01	0.00	0.02	0.00	0.01	0.00	0.01	0.00	0.01	0.00
Tyrosine	0.16	0.02	0.20	0.02	0.19	0.01	0.16	0.01	0.15	0.01
Valine	0.30	0.01	0.28	0.01	0.25	0.01	0.23	0.01	0.20	0.01

Table I2. Measured extracellular metabolite concentrations for the K3 iPSCs grown in low glucose culture at 0, 12, 24, 36, and 48-h after the media exchange. Averages are from biological 6-replicates. Standard errors are provided for these averages.

Low glucose	**Average Concentration (mM)**									
Metabolite	**0-h**	**SE**	**12-h**	**SE**	**24-h**	**SE**	**36-h**	**SE**	**48-h**	**SE**
Glucose	5.99	0.02	4.91	0.05	3.47	0.09	1.72	0.14	0.24	0.09
Lactate	0.00	0.00	1.65	0.09	4.07	0.14	6.74	0.16	8.95	0.12
Pyruvate	0.43	0.01	0.35	0.00	0.22	0.01	0.14	0.00	0.13	0.01
Glutamine	2.55	0.02	2.34	0.01	2.11	0.01	1.82	0.02	1.53	0.02
Ammonia	0.03	0.01	0.16	0.01	0.33	0.01	0.50	0.01	0.72	0.02
Amino Acids										
Alanine	0.03	0.00	0.06	0.00	0.10	0.00	0.14	0.00	0.20	0.01
Asparagine	0.06	0.01	0.05	0.00	0.05	0.00	0.07	0.00	0.07	0.00
Aspartate	0.03	0.00	0.03	0.00	0.03	0.00	0.02	0.00	0.02	0.00
Glutamate	0.04	0.01	0.08	0.00	0.13	0.00	0.17	0.00	0.21	0.00
Glycine	0.24	0.01	0.22	0.00	0.23	0.00	0.24	0.00	0.23	0.01
Histidine	0.11	0.01	0.10	0.00	0.08	0.00	0.08	0.01	0.08	0.00
Isoleucine	0.72	0.04	0.62	0.02	0.53	0.01	0.49	0.01	0.45	0.01
Leucine	0.48	0.01	0.42	0.01	0.35	0.01	0.32	0.00	0.30	0.01
Lysine	0.67	0.02	0.64	0.01	0.66	0.01	0.61	0.04	0.61	0.03
Methionine	0.09	0.01	0.07	0.00	0.06	0.00	0.05	0.00	0.05	0.00
Phenylalanine	0.20	0.01	0.20	0.00	0.19	0.00	0.17	0.01	0.17	0.01
Proline	0.12	0.00	0.11	0.00	0.11	0.00	0.11	0.00	0.12	0.00
Serine	0.39	0.03	0.32	0.01	0.28	0.01	0.25	0.01	0.19	0.01
Threonine	0.23	0.01	0.21	0.01	0.20	0.01	0.21	0.00	0.19	0.00
Tryptophan	0.01	0.00	0.01	0.00	0.01	0.00	0.01	0.00	0.01	0.00
Tyrosine	0.18	0.01	0.18	0.01	0.17	0.00	0.15	0.01	0.14	0.01
Valine	0.30	0.01	0.27	0.00	0.24	0.01	0.23	0.01	0.21	0.01

Table I3. Measured extracellular metabolite concentrations for the K3 iPSCs grown in high lactate culture at 0, 12, 24, 36, and 48-h after the media exchange. Averages are from biological 6-replicates. Standard errors are provided for these averages.

High lactate	**Average Concentration (mM)**									
Metabolite	**0-h**	**SE**	**12-h**	**SE**	**24-h**	**SE**	**36-h**	**SE**	**48-h**	**SE**
Glucose	18.69	0.01	17.54	0.09	16.31	0.21	15.12	0.25	13.70	0.26
Lactate	21.35	0.06	22.11	0.06	24.18	0.09	26.46	0.21	27.77	0.21
Pyruvate	0.42	0.01	0.35	0.00	0.30	0.01	0.24	0.01	0.21	0.01
Glutamine	2.51	0.03	2.32	0.02	2.12	0.01	1.93	0.02	1.68	0.02
Ammonia	0.03	0.01	0.15	0.01	0.29	0.01	0.42	0.02	0.59	0.01
Amino Acids										
Alanine	0.02	0.00	0.05	0.01	0.08	0.01	0.13	0.01	0.17	0.00
Asparagine	0.06	0.00	0.06	0.00	0.07	0.00	0.07	0.00	0.07	0.00
Aspartate	0.03	0.00	0.02	0.00	0.02	0.00	0.02	0.00	0.02	0.00
Glutamate	0.03	0.00	0.06	0.00	0.10	0.00	0.15	0.00	0.18	0.00
Glycine	0.20	0.00	0.20	0.00	0.21	0.00	0.21	0.01	0.21	0.01
Histidine	0.08	0.00	0.08	0.00	0.08	0.00	0.08	0.01	0.07	0.00
Isoleucine	0.62	0.01	0.54	0.02	0.54	0.02	0.48	0.01	0.41	0.01
Leucine	0.37	0.01	0.33	0.01	0.34	0.01	0.30	0.01	0.27	0.01
Lysine	0.51	0.01	0.50	0.01	0.57	0.02	0.53	0.01	0.52	0.02
Methionine	0.07	0.01	0.05	0.00	0.06	0.00	0.05	0.00	0.05	0.00
Phenylalanine	0.12	0.00	0.12	0.00	0.14	0.00	0.14	0.00	0.14	0.00
Proline	0.09	0.00	0.09	0.00	0.10	0.00	0.10	0.00	0.10	0.00
Serine	0.36	0.00	0.31	0.01	0.32	0.01	0.24	0.01	0.19	0.01
Threonine	0.18	0.00	0.17	0.00	0.19	0.00	0.18	0.01	0.18	0.00
Tryptophan	0.01	0.00	0.01	0.00	0.01	0.00	0.01	0.00	0.01	0.00
Tyrosine	0.11	0.00	0.11	0.00	0.13	0.00	0.12	0.00	0.12	0.00
Valine	0.24	0.00	0.22	0.01	0.23	0.01	0.21	0.01	0.19	0.00

Table I4. Measured extracellular metabolite concentrations for the K3 iPSCs grown in low glucose + high lactate culture at 0, 12, 24, 36, and 48-h after the media exchange. Averages are from biological 6-replicates. Standard errors are provided for these averages.

Low glucose + high lactate	**Average Concentration (mM)**									
Metabolite	**0-h**	**SE**	**12-h**	**SE**	**24-h**	**SE**	**36-h**	**SE**	**48-h**	**SE**
Glucose	5.98	0.05	5.08	0.06	3.94	0.10	2.45	0.09	1.21	0.15
Lactate	21.39	0.15	22.11	0.13	24.31	0.11	26.42	0.15	28.25	0.24
Pyruvate	0.43	0.01	0.35	0.00	0.30	0.01	0.25	0.01	0.22	0.01
Glutamine	2.55	0.03	2.35	0.01	2.17	0.01	1.92	0.02	1.70	0.02
Ammonia	0.04	0.01	0.15	0.01	0.28	0.01	0.45	0.01	0.63	0.01
Amino Acids										
Alanine	0.02	0.00	0.05	0.00	0.08	0.01	0.12	0.01	0.18	0.01
Asparagine	0.07	0.00	0.06	0.00	0.06	0.01	0.06	0.01	0.06	0.01
Aspartate	0.02	0.00	0.02	0.00	0.02	0.00	0.02	0.00	0.02	0.00
Glutamate	0.03	0.00	0.07	0.00	0.11	0.00	0.15	0.00	0.18	0.00
Glycine	0.21	0.00	0.20	0.00	0.21	0.00	0.21	0.01	0.22	0.01
Histidine	0.10	0.01	0.08	0.00	0.08	0.00	0.08	0.00	0.07	0.00
Isoleucine	0.60	0.01	0.56	0.02	0.48	0.03	0.43	0.02	0.39	0.01
Leucine	0.38	0.00	0.35	0.00	0.30	0.02	0.29	0.01	0.26	0.01
Lysine	0.53	0.01	0.53	0.01	0.49	0.03	0.47	0.05	0.48	0.02
Methionine	0.06	0.00	0.06	0.00	0.06	0.00	0.06	0.00	0.06	0.00
Phenylalanine	0.14	0.00	0.12	0.00	0.13	0.01	0.15	0.01	0.15	0.01
Proline	0.09	0.00	0.09	0.00	0.09	0.00	0.09	0.01	0.11	0.00
Serine	0.33	0.01	0.29	0.01	0.23	0.02	0.18	0.04	0.18	0.02
Threonine	0.19	0.00	0.17	0.00	0.17	0.01	0.16	0.02	0.17	0.01
Tryptophan	0.01	0.00	0.01	0.00	0.01	0.00	0.01	0.00	0.02	0.01
Tyrosine	0.12	0.00	0.12	0.00	0.11	0.01	0.12	0.01	0.12	0.00
Valine	0.24	0.00	0.23	0.00	0.23	0.01	0.21	0.01	0.21	0.01

Appendix J

Measured extracellular amino acid concentration profiles for K3 iPSCs

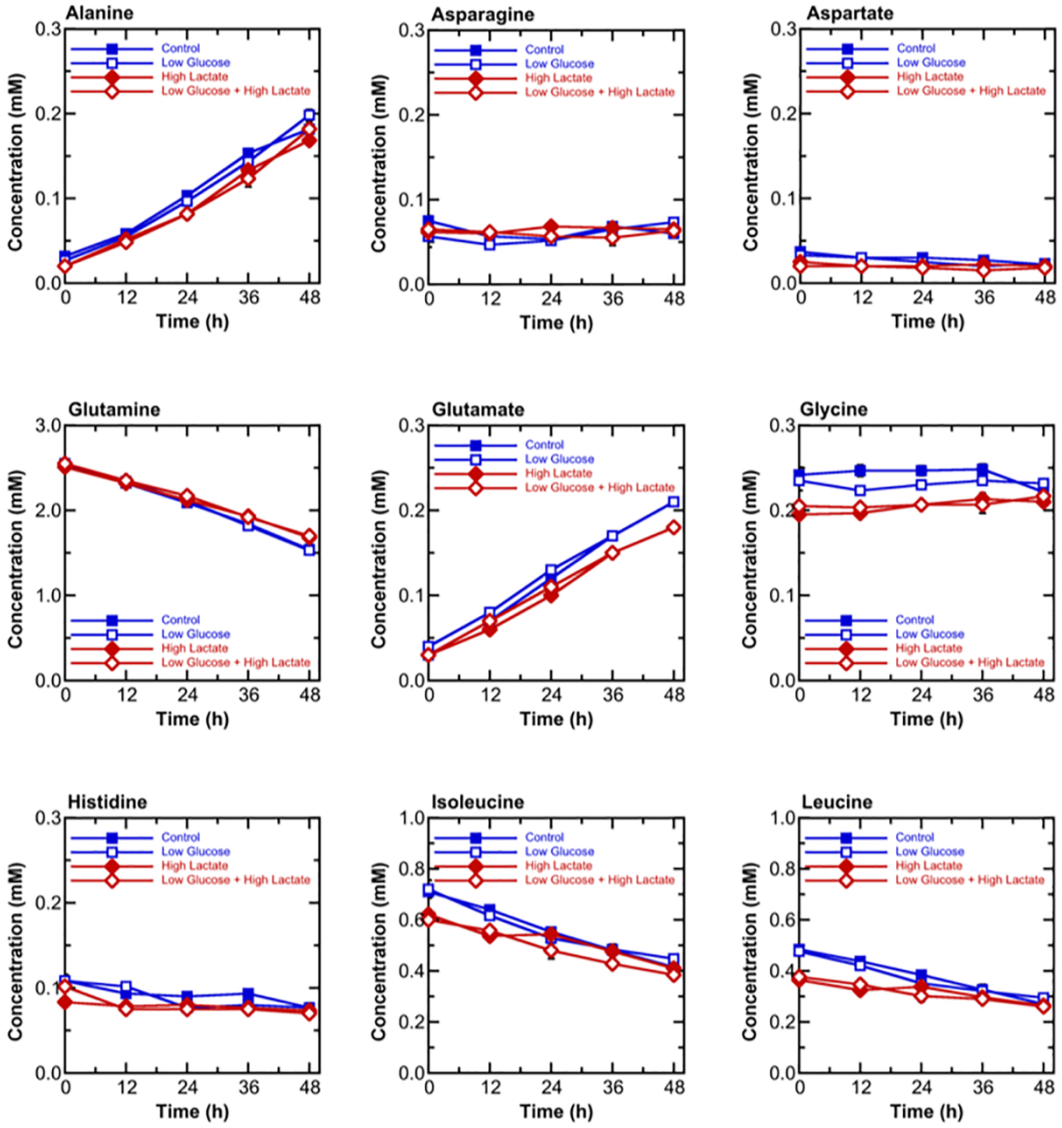

Figure J1. Measured extracellular amino acid concentration profiles for K3 iPSCs. Control media – ■; Low Glucose media – □; High Lactate media – ◆; and Low Glucose + High Lactate – ◇. Error bars represent standard errors.

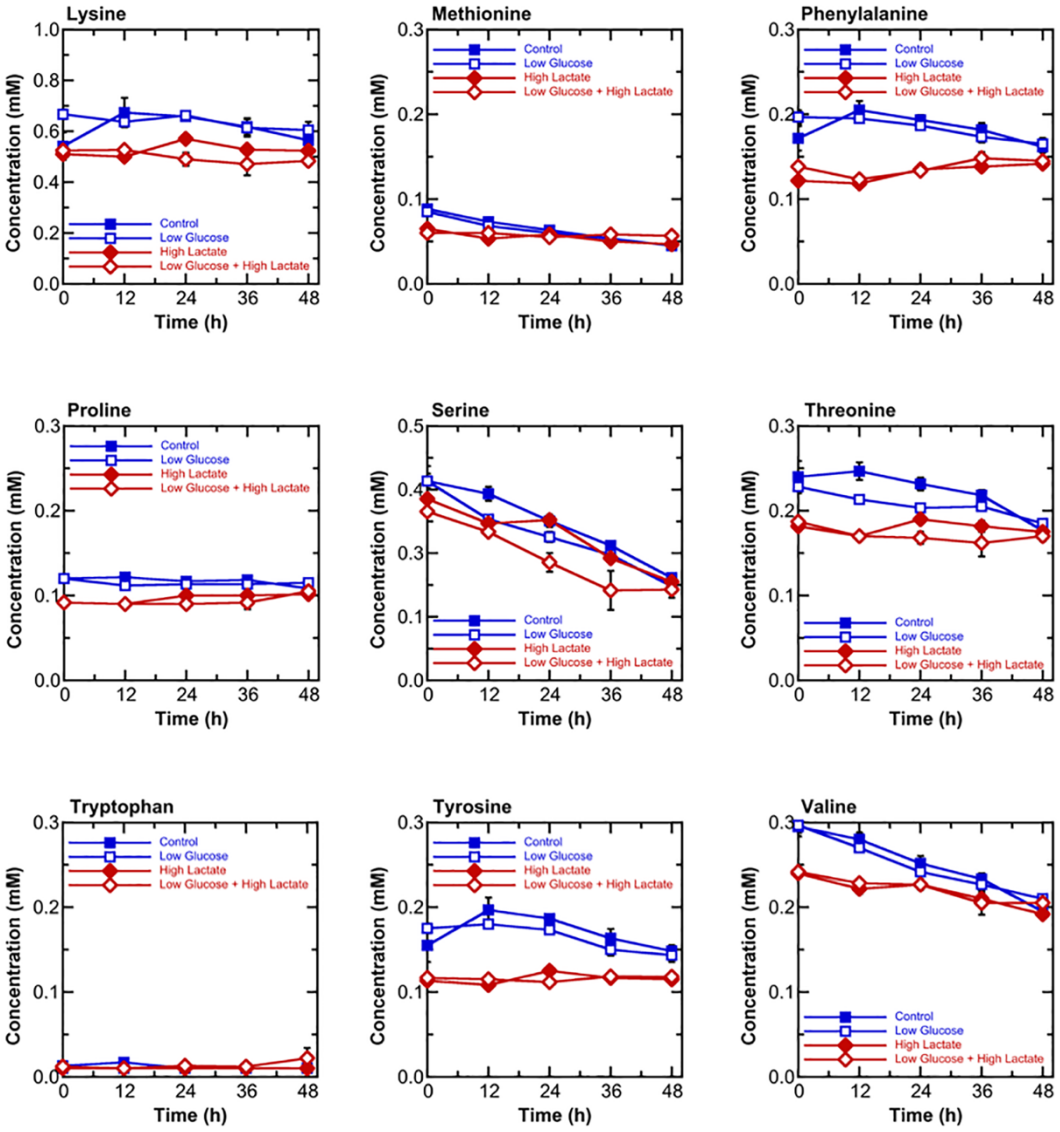

Figure J1 (continued). Measured extracellular amino acid concentration profiles for K3 iPSCs. Control media – ■; Low Glucose media – □; High Lactate media – ◆; and Low Glucose + High Lactate – ◇. Error bars represent standard errors.

Appendix K

Metabolic flux analysis model description and assumptions for iPSC study

1. Cellular metabolism and isotopic labeling are at isotopic steady state. K3 iPSCs were cultured in the presence of [1,2-^{13}C] glucose, [U-^{13}C] glutamine, and [U-^{13}C] lactate in parallel for 48 hours, with intracellular samples taken at 24 and 48 hours.
2. CO_2 is an unbalanced metabolite within the MFA model.
3. Two compartments (cytosolic and mitochondrial) are assumed to exist for pyruvate, citrate, fumarate, malate, and oxaloacetate. The two pyruvate compartments are included to account for differential labeling observed for lactate and alanine. This has previously reported for ^{13}C-MFA to account for lactate being primarily derived from glucose, while alanine contains more labeling from glutamine (Gaglio et al., 2011; Metallo et al., 2012). Since cytosolic and mitochondrial pools could not be distinguished from one another for intracellular metabolites MIDs, mixing reactions are included for citrate, fumarate, and malate to account for a single sampled metabolite pool.
4. Fumarate and succinate are symmetrical metabolites.
5. Dilution pools of unlabeled succinate and fumarate are assumed to exist. These pools do not participate in central carbon metabolism. These dilution fluxes are included to account for dilution of labeled intracellular pools and to account for uptake of amino acids which are not included in the central carbon metabolic model.
6. A lactate dilution flux (Lac.c <-> Lac.t + dummyL) is included in the model to allow for uptake and intracellular labeling from [U-^{13}C] lactate. The net flux of this reaction

is fixed to zero, so it did not participate in carbon balancing. However, this reaction allows the model to simulate infinite exchange between lactate tracer (lac.t) and cytosolic lactate (lac.c) pools to resolve intracellular isotope labeling from [U-^{13}C] lactate tracer.

7. Previously, PSCs have been shown to accumulate different total amounts of lipids depending on the cell culture media used without impacting growth rate (Zhang et al., 2016). A fatty acid sink reaction was included in the model to account for this. This fatty acid sink reaction was also required to reach an acceptable model convergence for each culture condition.

Appendix L

Metabolic reactions used in the ^{13}C-MFA simulations for K3 iPSCs

Table L1. The metabolic reactions used in the ^{13}C-MFA simulations for the K3 iPSC cultures. Suffixes indicate compartmental location of the metabolite: .x, extracellular; .c, cytosolic; .m, mitochondrial; .t, tracer; .p, pooled; .d, diluted; .snk, dilution sink.

v1	Glc.x (abcdef) -> Glc (abcdef)
v2	Glc (abcdef) -> Pyr.c (cba) + Pyr.c (def)
v3	Pyr.c (abc) <-> Lac.c (abc)
v4	Pyr.m (abc) -> CO2 (a) + AcCoA.m (bc)
v5	AcCoA.m (ab) + OAA.m (cdef) -> Cit.m (fedbac)
v6	Cit.m (abcdef) <-> AKG.m (abcde) + CO2 (f)
v7	AKG.m (abcde) -> CO2 (a) + Suc.m (bcde)
v8	Suc.m (abcd) <-> Fum.m (abcd)
v9	Fum.m (abcd) <-> Mal.m (abcd)
v10	Mal.m (abcd) <-> OAA.m (abcd)
v11	Gln (abcde) <-> Glu (abcde)
v12	Glu (abcde) <-> AKG.m (abcde)
v13	Ser (abc) -> Pyr.c (abc)
v14	Ser (abc) -> Gly (ab) + MEETHF (c)
v15	Gln.x (abcde) -> Gln (abcde)
v16	Ser.x (abc) -> Ser (abc)
v17	Ala (abc) -> Ala.x (abc)
v18	Pyr.x (abc) -> Pyr.c (abc)
v19	Glu (abcde) -> Glu.x (abcde)
v20	Lac.c (abc) -> Lac.x (abc)
v21	Asp.x (abcd) -> Asp (abcd)
v25	Pyr.c (abc) <-> Pyr.m (abc)
v22	Pyr.m (abc) + CO2 (d) -> OAA.m (abcd)
v23	Mal.m (abcd) -> Pyr.m (abc) + CO2 (d)
v24	Pyr.m (abc) <-> Ala (abc)
v26	Cit.m (abcdef) -> Cit.c (abcdef)
v27	Cit.c (abcdef) -> OAA.c (fcba) + AcCoA.c (ed)
v28	AcCoA.c -> Lipids
v29	OAA.c (abcd) <-> Asp (abcd)
v30	OAA.c (abcd) <-> Mal.c (abcd)
v31	Mal.c (abcd) <-> Mal.m (abcd)

v32 Mal.c (abcd) <-> Fum.c (abcd)

v33 Asp (abcd) <-> Fum.c (abcd)

v34 0.19*Ala + 0.11*Asp + 0.1*Gln + 0.12*Glu + 0.17*Gly + 0.14*Ser + 0.16*Glc -> Biomass

v35 Lac.c <-> Lac.t + dummyL

v36 AcCoA.c -> sink

v37 0*Cit.c (abcdef) -> Cit.p (abcdef)

v38 0*Cit.m (abcdef) -> Cit.p (abcdef)

v39 Cit.p (abcdef) -> sink

v40 0*Mal.c (abcd) -> Mal.p (abcd)

v41 0*Mal.m (abcd) -> Mal.p (abcd)

v42 Mal.p (abcd) -> sink

v43 0*Fum.c (abcd) -> Fum.p (abcd)

v44 0*Fum.m (abcd) -> Fum.p (abcd)

v45 Fum.p (abcd) -> sink

v46 0*Suc.m (abcd) -> Suc.d (abcd)

v47 0*Suc.u (abcd) -> Suc.d (abcd)

v48 Suc.d -> sink

v49 0*Fum.e (abcd) -> Fum.d (abcd)

v50 0*Fum.u (abcd) -> Fum.d (abcd)

v51 Fum.d -> sink

Appendix M

GC-MS metabolite mass fragments used for intracellular isotope quantification for K3 iPSCs

Table M1. GC-MS metabolite mass fragments used for intracellular isotope quantification.

Metabolite	Mass	Carbon atoms	Fragment formula
Organic acids			
Pyruvate	174	1-2-3	$C_6H_{12}O_3NSi$
Lactate	261	1-2-3	$C_{11}H_{26}O_2NSi_2$
Fumarate	287	1-2-3-4	$C_{12}H_{23}O_4Si_2$
Succinate	289	1-2-3-4	$C_{12}H_{25}O_4Si_2$
AKG	346	1-2-3-4-5	$C_{14}H_{28}O_5NSi_2$
Malate	419	1-2-3-4	$C_{18}H_{39}O_5Si_3$
Citrate	591	1-2-3-4-5-6	$C_{26}H_{55}O_7Si_4$
Amino acids			
Alanine	260	1-2-3	$C_{11}H_{26}O_2NSi_2$
Aspartate	418	1-2-3-4	$C_{18}H_{40}O_4NSi_3$
Glutamine	431	1-2-3-4-5	$C_{19}H_{43}N_2O_3Si_3$
Glutamate	432	1-2-3-4-5	$C_{19}H_{42}O_4NSi_3$

Appendix N

Measured intracellular MIDs from [1,2-^{13}C] glucose, [U-^{13}C] glutamine, and [U-^{13}C] lactate for K3 iPSCs

Table N1. Measured intracellular MIDs from the [1,2-^{13}C] glucose tracer for K3 iPSCs for the Control, Low Glucose, High Lactate, and Low Glucose + High Lactate conditions with mean and standard errors. MIDs shown below have been corrected for natural abundance.

Condition	Control				Low Glucose				High Lactate				Low Glucose + High Lactate			
	24-h		48-h		24-h		48-h		24-h		48-h		24-h		48-h	
	MID	SE	MID	SE	MID	SE	MID	SE	MID	SE	MID	SE	MID	SE	MID	SE
PYR 174																
M+0	0.706	0.037	0.641	0.031	0.710	0.038	0.639	0.023	0.903	0.001	0.859	0.002	0.910	0.005	0.856	0.006
M+1	-0.007	0.006	-0.002	0.005	-0.010	0.035	0.003	0.006	-0.042	0.004	-0.025	0.001	-0.032	0.002	-0.021	0.003
M+2	0.290	0.040	0.376	0.023	0.199	0.011	0.364	0.044	0.119	0.003	0.172	0.001	0.110	0.001	0.172	0.004
M+3	0.011	0.008	-0.016	0.010	0.101	0.007	-0.006	0.028	0.020	0.000	-0.005	0.000	0.012	0.002	-0.007	0.006
ALA 260																
M+0	0.606	0.004	0.577	0.002	0.607	0.002	0.584	0.001	0.904	0.002	0.858	0.002	0.918	0.001	0.880	0.004
M+1	0.011	0.002	0.017	0.001	0.013	0.001	0.018	0.001	-0.016	0.001	-0.009	0.001	-0.016	0.001	-0.015	0.001
M+2	0.390	0.004	0.409	0.001	0.390	0.002	0.404	0.002	0.115	0.002	0.152	0.001	0.101	0.001	0.138	0.003
M+3	-0.007	0.001	-0.003	0.002	-0.009	0.002	-0.006	0.001	-0.004	0.001	-0.001	0.001	-0.003	0.000	-0.002	0.001
LAC 261																
M+0	0.585	0.003	0.549	0.009	0.590	0.002	0.571	0.004	0.585	0.011	0.549	0.011	0.892	0.002	0.810	0.007
M+1	0.009	0.001	0.016	0.003	0.010	0.001	0.014	0.002	0.009	0.011	0.016	0.011	-0.006	0.001	0.008	0.003
M+2	0.415	0.002	0.438	0.008	0.409	0.002	0.421	0.004	0.415	0.011	0.438	0.011	0.116	0.001	0.183	0.004
M+3	-0.009	0.001	-0.003	0.003	-0.009	0.001	-0.006	0.001	-0.009	0.011	-0.003	0.011	-0.003	0.000	-0.002	0.002
FUM 287																

Condition	Control				Low Glucose				High Lactate				Low Glucose + High Lactate			
	24-h		48-h		24-h		48-h		24-h		48-h		24-h		48-h	
	MID	SE	MID	SE	MID	SE	MID	SE	MID	SE	MID	SE	MID	SE	MID	SE
M+0	0.907	0.010	0.836	0.004	0.909	0.013	0.856	0.007	0.920	0.017	0.942	0.005	0.930	0.007	0.916	0.022
M+1	-0.007	0.006	0.026	0.007	0.007	0.004	0.033	0.005	0.012	0.008	-0.004	0.014	-0.003	0.014	0.005	0.010
M+2	0.063	0.005	0.105	0.004	0.068	0.002	0.084	0.003	0.039	0.007	0.054	0.004	0.035	0.004	0.047	0.007
M+3	0.017	0.003	0.020	0.003	0.014	0.006	0.018	0.002	0.014	0.004	0.014	0.002	0.021	0.005	0.013	0.002
M+4	0.021	0.005	0.013	0.004	0.003	0.009	0.008	0.005	0.016	0.012	-0.006	0.006	0.017	0.015	0.019	0.006
SUC 289																
M+0	0.966	0.012	0.925	0.006	0.975	0.028	0.939	0.003	1.003	0.002	0.958	0.014	1.017	0.007	0.997	0.010
M+1	0.003	0.006	0.010	0.004	-0.015	0.008	-0.008	0.003	-0.016	0.002	0.012	0.005	-0.023	0.002	-0.015	0.005
M+2	0.024	0.003	0.060	0.004	0.031	0.013	0.064	0.002	0.007	0.003	0.032	0.007	0.006	0.003	0.027	0.003
M+3	-0.001	0.003	0.005	0.002	0.001	0.008	0.008	0.003	-0.002	0.002	-0.002	0.003	-0.008	0.006	-0.009	0.008
M+4	0.008	0.002	-0.001	0.005	0.007	0.006	-0.002	0.002	0.007	0.003	0.000	0.004	0.008	0.002	0.001	0.003
AKG 346																
M+0	0.821	0.022	0.740	0.023	0.784	0.018	0.687	0.042	0.919	0.015	0.889	0.016	0.869	0.029	0.879	0.026
M+1	0.046	0.010	0.053	0.014	0.071	0.022	0.082	0.015	-0.002	0.008	0.022	0.008	0.050	0.011	0.036	0.016
M+2	0.092	0.014	0.140	0.009	0.106	0.015	0.139	0.008	0.063	0.014	0.080	0.003	0.044	0.012	0.056	0.004
M+3	0.015	0.008	0.031	0.011	-0.003	0.030	0.037	0.015	0.016	0.006	0.005	0.005	0.010	0.004	0.009	0.013
M+4	0.013	0.005	0.015	0.004	0.052	0.010	0.027	0.011	-0.012	0.005	0.001	0.003	-0.001	0.012	0.007	0.005
M+5	0.013	0.021	0.021	0.003	-0.010	0.007	0.027	0.022	0.015	0.008	0.004	0.004	0.028	0.017	0.014	0.006
ASP 418																
M+0	0.812	0.005	0.750	0.010	0.787	0.011	0.726	0.004	0.842	0.021	0.822	0.024	0.815	0.004	0.835	0.023
M+1	0.139	0.004	0.132	0.008	0.156	0.007	0.142	0.002	0.131	0.011	0.134	0.013	0.154	0.006	0.125	0.012
M+2	0.047	0.003	0.089	0.005	0.045	0.008	0.100	0.004	0.021	0.008	0.035	0.005	0.026	0.003	0.042	0.010
M+3	0.005	0.001	0.030	0.003	0.011	0.004	0.027	0.005	0.004	0.008	0.004	0.007	0.004	0.002	0.000	0.005

Condition	Control				Low Glucose				High Lactate				Low Glucose + High Lactate			
	24-h		48-h		24-h		48-h		24-h		48-h		24-h		48-h	
	MID	SE	MID	SE	MID	SE	MID	SE	MID	SE	MID	SE	MID	SE	MID	SE
M+4	-0.003	0.003	-0.001	0.002	0.001	0.004	0.005	0.002	0.002	0.004	0.005	0.007	0.001	0.002	-0.002	0.004
MAL 419																
M+0	0.817	0.002	0.713	0.012	0.808	0.015	0.718	0.003	0.874	0.003	0.829	0.012	0.860	0.005	0.839	0.012
M+1	0.116	0.002	0.136	0.008	0.125	0.008	0.151	0.007	0.104	0.007	0.109	0.008	0.120	0.006	0.117	0.009
M+2	0.054	0.002	0.119	0.004	0.063	0.004	0.107	0.009	0.025	0.005	0.053	0.004	0.019	0.002	0.038	0.004
M+3	0.014	0.001	0.030	0.005	0.014	0.004	0.034	0.004	0.000	0.002	0.010	0.002	0.004	0.001	0.006	0.002
M+4	0.000	0.001	0.002	0.002	-0.009	0.010	-0.010	0.013	-0.003	0.004	0.000	0.001	-0.004	0.004	0.000	0.001
GLU 431																
M+0	0.866	0.002	0.763	0.015	0.850	0.020	0.754	0.004	0.896	0.008	0.861	0.014	0.885	0.003	0.870	0.011
M+1	0.067	0.001	0.064	0.009	0.081	0.009	0.075	0.004	0.077	0.009	0.059	0.011	0.088	0.002	0.068	0.008
M+2	0.055	0.001	0.135	0.003	0.055	0.009	0.133	0.002	0.023	0.004	0.069	0.004	0.024	0.001	0.053	0.003
M+3	0.008	0.001	0.023	0.004	0.009	0.008	0.024	0.002	0.005	0.001	0.009	0.002	0.004	0.001	0.009	0.002
M+4	0.003	0.001	0.013	0.002	0.006	0.005	0.013	0.001	0.000	0.001	0.002	0.001	0.000	0.001	0.001	0.001
M+5	0.000	0.000	0.002	0.001	0.000	0.003	0.002	0.000	-0.001	0.000	0.000	0.001	0.000	0.000	-0.001	0.000
GLN 432																
M+0	0.884	0.007	0.905	0.018	0.880	0.006	0.891	0.005	0.865	0.014	0.922	0.008	0.879	0.004	0.912	0.009
M+1	0.120	0.005	0.097	0.014	0.128	0.006	0.112	0.006	0.145	0.013	0.082	0.007	0.129	0.004	0.089	0.006
M+2	-0.002	0.004	-0.004	0.005	-0.006	0.002	-0.004	0.002	-0.014	0.005	-0.003	0.003	-0.006	0.002	-0.001	0.003
M+3	-0.002	0.001	0.000	0.003	-0.002	0.001	-0.001	0.001	0.003	0.002	0.000	0.002	-0.001	0.001	0.000	0.002
M+4	0.000	0.001	0.001	0.002	-0.001	0.000	0.001	0.000	0.001	0.001	0.000	0.001	-0.002	0.002	0.000	0.001
M+5	0.000	0.001	0.000	0.001	0.000	0.001	0.000	0.000	0.001	0.001	-0.001	0.001	0.001	0.001	-0.001	0.001
CIT 591																
M+0	0.495	0.005	0.510	0.031	0.473	0.022	0.457	0.005	0.724	0.019	0.719	0.028	0.692	0.016	0.717	0.017

Condition	Control				Low Glucose				High Lactate				Low Glucose + High Lactate			
	24-h		48-h		24-h		48-h		24-h		48-h		24-h		48-h	
	MID	SE	MID	SE	MID	SE	MID	SE	MID	SE	MID	SE	MID	SE	MID	SE
M+1	0.087	0.012	0.059	0.021	0.097	0.020	0.096	0.006	0.060	0.020	0.031	0.016	0.061	0.011	0.058	0.012
M+2	0.219	0.021	0.296	0.008	0.227	0.013	0.283	0.010	0.147	0.016	0.189	0.012	0.133	0.013	0.174	0.009
M+3	0.129	0.011	0.045	0.067	0.121	0.038	0.110	0.009	0.034	0.008	0.047	0.008	0.062	0.011	0.046	0.013
M+4	0.018	0.007	0.075	0.036	0.049	0.023	0.036	0.004	0.015	0.005	0.000	0.003	-0.002	0.019	-0.004	0.016
M+5	0.026	0.017	0.004	0.025	0.012	0.024	0.024	0.002	0.017	0.010	0.007	0.007	0.038	0.018	0.016	0.009
M+6	0.026	0.010	0.011	0.015	0.021	0.038	-0.006	0.002	0.003	0.007	0.008	0.017	0.015	0.010	-0.007	0.011

Table N2. Measured intracellular MIDs from the [U-^{13}C] glutamine tracer for K3 iPSCs for the Control, Low Glucose, High Lactate, and Low Glucose + High Lactate conditions with mean and standard errors. MIDs shown below have been corrected for natural abundance.

Condition	Control				Low Glucose				High Lactate				Low Glucose + High Lactate			
	24-h		48-h		24-h		48-h		24-h		48-h		24-h		48-h	
	MID	SE	MID	SE	MID	SE	MID	SE	MID	SE	MID	SE	MID	SE	MID	SE
PYR 174																
M+0	1.005	0.006	1.002	0.020	1.027	0.009	1.028	0.018	1.026	0.005	1.040	0.003	1.037	0.004	1.043	0.005
M+1	-0.023	0.010	-0.029	0.011	-0.033	0.002	-0.040	0.006	-0.036	0.003	-0.039	0.001	-0.035	0.001	-0.041	0.002
M+2	0.003	0.002	0.011	0.003	-0.006	0.008	-0.006	0.010	0.003	0.001	-0.005	0.001	-0.004	0.001	-0.008	0.003
M+3	0.015	0.011	0.017	0.011	0.012	0.004	0.018	0.004	0.007	0.002	0.004	0.003	0.002	0.002	0.006	0.001
ALA 260																
M+0	1.006	0.001	0.989	0.002	1.006	0.001	0.989	0.001	1.026	0.010	1.011	0.002	1.018	0.000	1.011	0.001
M+1	-0.028	0.001	-0.018	0.002	-0.023	0.002	-0.022	0.001	-0.037	0.012	-0.025	0.001	-0.023	0.001	-0.025	0.001
M+2	0.003	0.002	0.005	0.001	0.001	0.002	0.006	0.001	0.002	0.003	0.002	0.001	-0.001	0.001	0.003	0.001
M+3	0.019	0.001	0.025	0.001	0.016	0.001	0.026	0.001	0.009	0.001	0.011	0.000	0.007	0.001	0.010	0.000
LAC 261																
M+0	1.016	0.001	1.010	0.001	1.020	0.002	1.013	0.001	1.014	0.003	0.974	0.004	1.000	0.008	0.977	0.004
M+1	-0.029	0.000	-0.027	0.001	-0.029	0.002	-0.027	0.001	-0.022	0.001	0.006	0.002	-0.008	0.003	0.006	0.003
M+2	0.004	0.000	0.005	0.000	0.002	0.001	0.004	0.001	0.007	0.001	0.018	0.001	0.014	0.002	0.017	0.002
M+3	0.010	0.001	0.012	0.000	0.007	0.000	0.011	0.000	0.001	0.000	0.001	0.001	-0.007	0.006	0.001	0.001
FUM 287																
M+0	0.355	0.012	0.320	0.015	0.423	0.028	0.327	0.008	0.327	0.009	0.269	0.008	0.386	0.012	0.302	0.012
M+1	0.019	0.006	0.059	0.007	0.022	0.011	0.054	0.003	0.034	0.006	0.099	0.002	0.041	0.006	0.098	0.004
M+2	0.071	0.003	0.136	0.002	0.062	0.004	0.145	0.004	0.108	0.004	0.183	0.008	0.117	0.002	0.180	0.003

Condition	Control				Low Glucose				High Lactate				Low Glucose + High Lactate			
	24-h		48-h		24-h		48-h		24-h		48-h		24-h		48-h	
	MID	SE	MID	SE	MID	SE	MID	SE	MID	SE	MID	SE	MID	SE	MID	SE
M+3	0.178	0.007	0.106	0.005	0.149	0.009	0.097	0.004	0.133	0.003	0.091	0.004	0.107	0.005	0.075	0.007
M+4	0.378	0.018	0.379	0.012	0.345	0.026	0.377	0.005	0.399	0.015	0.357	0.001	0.349	0.009	0.346	0.013
SUC 289																
M+0	0.506	0.013	0.550	0.018	0.293	0.012	0.268	0.014	0.203	0.009	0.199	0.005	0.213	0.002	0.223	0.010
M+1	-0.008	0.005	0.031	0.007	0.006	0.006	0.068	0.004	0.035	0.004	0.126	0.004	0.050	0.006	0.110	0.008
M+2	0.060	0.002	0.113	0.006	0.088	0.002	0.172	0.003	0.154	0.001	0.212	0.005	0.156	0.003	0.205	0.004
M+3	0.022	0.002	0.016	0.004	0.039	0.001	0.026	0.005	0.028	0.002	0.016	0.003	0.029	0.004	0.025	0.001
M+4	0.420	0.013	0.290	0.013	0.574	0.017	0.466	0.006	0.581	0.010	0.447	0.006	0.552	0.008	0.437	0.009
AKG 346																
M+0	0.211	0.005	0.187	0.006	0.193	0.005	0.166	0.006	0.135	0.004	0.149	0.002	0.161	0.003	0.166	0.011
M+1	0.016	0.003	0.055	0.002	0.035	0.004	0.064	0.006	0.035	0.002	0.095	0.004	0.046	0.002	0.087	0.004
M+2	0.050	0.003	0.074	0.003	0.034	0.011	0.062	0.006	0.043	0.001	0.079	0.002	0.047	0.005	0.078	0.006
M+3	0.089	0.003	0.159	0.008	0.077	0.007	0.180	0.010	0.137	0.005	0.204	0.004	0.152	0.003	0.185	0.004
M+4	0.058	0.010	0.058	0.004	0.076	0.010	0.048	0.004	0.061	0.003	0.044	0.004	0.057	0.005	0.056	0.003
M+5	0.576	0.023	0.468	0.009	0.586	0.019	0.481	0.007	0.590	0.004	0.430	0.005	0.539	0.005	0.429	0.011
ASP 418																
M+0	0.309	0.005	0.286	0.006	0.287	0.005	0.225	0.002	0.271	0.003	0.290	0.010	0.329	0.005	0.292	0.006
M+1	0.047	0.007	0.105	0.004	0.063	0.004	0.113	0.001	0.086	0.002	0.145	0.005	0.098	0.010	0.150	0.007
M+2	0.082	0.005	0.147	0.003	0.083	0.005	0.164	0.005	0.115	0.004	0.161	0.001	0.117	0.005	0.147	0.006
M+3	0.183	0.004	0.132	0.008	0.206	0.006	0.137	0.002	0.161	0.002	0.114	0.008	0.128	0.003	0.127	0.004
M+4	0.379	0.009	0.329	0.009	0.361	0.007	0.361	0.006	0.369	0.004	0.290	0.013	0.329	0.013	0.283	0.008
MAL 419																
M+0	0.212	0.002	0.182	0.001	0.222	0.004	0.178	0.001	0.163	0.003	0.175	0.000	0.171	0.002	0.177	0.002

Condition	Control				Low Glucose				High Lactate				Low Glucose + High Lactate			
	24-h		48-h		24-h		48-h		24-h		48-h		24-h		48-h	
	MID	SE	MID	SE	MID	SE	MID	SE	MID	SE	MID	SE	MID	SE	MID	SE
M+1	0.039	0.002	0.113	0.006	0.047	0.002	0.115	0.001	0.067	0.002	0.156	0.003	0.085	0.004	0.151	0.002
M+2	0.099	0.002	0.172	0.004	0.092	0.001	0.180	0.002	0.143	0.003	0.200	0.001	0.148	0.003	0.199	0.002
M+3	0.212	0.001	0.142	0.002	0.215	0.001	0.133	0.003	0.182	0.001	0.125	0.008	0.175	0.003	0.126	0.002
M+4	0.439	0.002	0.391	0.009	0.425	0.004	0.394	0.004	0.445	0.006	0.344	0.009	0.421	0.008	0.347	0.006
GLU 431																
M+0	0.126	0.001	0.130	0.001	0.125	0.001	0.128	0.001	0.104	0.001	0.134	0.001	0.118	0.001	0.132	0.000
M+1	0.016	0.001	0.064	0.004	0.019	0.001	0.064	0.001	0.037	0.001	0.100	0.003	0.046	0.001	0.092	0.001
M+2	0.032	0.001	0.070	0.004	0.029	0.002	0.069	0.001	0.051	0.001	0.087	0.003	0.058	0.002	0.085	0.001
M+3	0.092	0.002	0.179	0.003	0.082	0.003	0.177	0.002	0.136	0.002	0.196	0.001	0.153	0.002	0.188	0.002
M+4	0.081	0.001	0.067	0.005	0.106	0.003	0.071	0.001	0.106	0.004	0.064	0.006	0.097	0.003	0.073	0.003
M+5	0.654	0.002	0.491	0.013	0.640	0.008	0.491	0.003	0.565	0.005	0.418	0.010	0.528	0.007	0.430	0.004
GLN 432																
M+0	0.013	0.001	0.015	0.002	0.011	0.001	0.010	0.003	0.008	0.002	0.013	0.001	0.007	0.000	0.014	0.000
M+1	0.003	0.001	0.003	0.001	0.003	0.001	0.003	0.001	0.003	0.001	0.004	0.001	0.003	0.001	0.005	0.000
M+2	0.001	0.001	0.003	0.000	0.001	0.001	0.002	0.000	0.001	0.001	0.005	0.000	0.003	0.002	0.005	0.000
M+3	0.008	0.001	0.012	0.001	0.009	0.001	0.013	0.001	0.011	0.002	0.013	0.005	0.011	0.001	0.017	0.000
M+4	0.138	0.010	0.147	0.010	0.162	0.002	0.166	0.003	0.161	0.001	0.159	0.006	0.169	0.004	0.156	0.002
M+5	0.837	0.011	0.821	0.014	0.815	0.005	0.806	0.007	0.816	0.005	0.806	0.002	0.807	0.005	0.804	0.002
CIT 591																
M+0	0.239	0.007	0.164	0.009	0.211	0.017	0.139	0.016	0.144	0.005	0.166	0.007	0.175	0.011	0.166	0.003
M+1	0.081	0.009	0.13	0.007	0.106	0.019	0.138	0.01	0.106	0.009	0.143	0.013	0.103	0.006	0.158	0.01
M+2	0.113	0.005	0.141	0.004	0.082	0.013	0.152	0.004	0.115	0.006	0.176	0.007	0.12	0.012	0.159	0.008
M+3	0.165	0.008	0.169	0.004	0.204	0.011	0.182	0.005	0.177	0.005	0.189	0.014	0.161	0.017	0.185	0.005

Condition	Control				Low Glucose				High Lactate				Low Glucose + High Lactate			
	24-h		48-h		24-h		48-h		24-h		48-h		24-h		48-h	
	MID	SE	MID	SE	MID	SE	MID	SE	MID	SE	MID	SE	MID	SE	MID	SE
M+4	0.2	0.007	0.241	0.009	0.181	0.08	0.272	0.012	0.262	0.023	0.207	0.012	0.244	0.017	0.218	0.005
M+5	0.144	0.009	0.127	0.005	0.173	0.045	0.111	0.007	0.163	0.017	0.108	0.009	0.133	0.017	0.107	0.008
M+6	0.058	0.007	0.028	0.003	0.043	0.018	0.007	0.004	0.034	0.011	0.011	0.006	0.065	0.008	0.007	0.008

Table N3. Measured intracellular MIDs from the [U-^{13}C] lactate tracer for K3 iPSCs for the High Lactate and Low Glucose + High Lactate conditions with mean and standard errors. MIDs shown below have been corrected for natural abundance.

Condition	Control				Low Glucose				High Lactate				Low Glucose + High Lactate			
	24-h		48-h		24-h		48-h		24-h		48-h		24-h		48-h	
	MID	SE	MID	SE	MID	SE	MID	SE	MID	SE	MID	SE	MID	SE	MID	SE
PYR 174																
M+0	-	-	-	-	-	-	-	-	0.668	0.011	0.815	n/a	0.652	0.013	0.639	0.003
M+1	-	-	-	-	-	-	-	-	-0.010	0.010	-0.019	n/a	-0.009	0.004	-0.012	0.004
M+2	-	-	-	-	-	-	-	-	0.032	0.014	0.001	n/a	0.027	0.027	0.009	0.002
M+3	-	-	-	-	-	-	-	-	0.310	0.028	0.203	n/a	0.331	0.042	0.364	0.008
ALA 260																
M+0	-	-	-	-	-	-	-	-	0.451	0.003	0.448	0.005	0.426	0.000	0.388	0.002
M+1	-	-	-	-	-	-	-	-	-0.010	0.001	-0.007	0.002	-0.007	0.001	-0.004	0.001
M+2	-	-	-	-	-	-	-	-	0.011	0.001	0.012	0.001	0.012	0.001	0.015	0.001
M+3	-	-	-	-	-	-	-	-	0.548	0.003	0.548	0.005	0.570	0.000	0.601	0.002
LAC 261																
M+0	-	-	-	-	-	-	-	-	0.398	0.055	0.454	0.064	0.423	0.004	0.440	0.004
M+1	-	-	-	-	-	-	-	-	-0.008	0.019	-0.010	0.021	-0.010	0.002	-0.009	0.001
M+2	-	-	-	-	-	-	-	-	0.011	0.006	0.010	0.007	0.010	0.001	0.010	0.000
M+3	-	-	-	-	-	-	-	-	0.600	0.070	0.546	0.080	0.577	0.006	0.559	0.004
FUM 287																
M+0	-	-	-	-	-	-	-	-	0.823	0.006	0.726	0.021	0.813	0.009	0.730	0.003
M+1	-	-	-	-	-	-	-	-	0.007	0.008	0.046	0.018	0.018	0.009	0.037	0.004
M+2	-	-	-	-	-	-	-	-	0.115	0.006	0.132	0.007	0.109	0.007	0.133	0.003
M+3	-	-	-	-	-	-	-	-	0.038	0.005	0.075	0.006	0.039	0.005	0.075	0.003

Condition	Control				Low Glucose				High Lactate				Low Glucose + High Lactate			
	24-h		48-h		24-h		48-h		24-h		48-h		24-h		48-h	
	MID	SE	MID	SE	MID	SE	MID	SE	MID	SE	MID	SE	MID	SE	MID	SE
M+4	-	-	-	-	-	-	-	-	0.018	0.004	0.021	0.009	0.021	0.011	0.024	0.006
SUC 289																
M+0	-	-	-	-	-	-	-	-	0.902	0.007	0.884	0.014	0.881	0.028	0.861	0.025
M+1	-	-	-	-	-	-	-	-	-0.010	0.002	0.000	0.008	0.000	0.008	0.007	0.007
M+2	-	-	-	-	-	-	-	-	0.088	0.005	0.070	0.005	0.103	0.015	0.077	0.013
M+3	-	-	-	-	-	-	-	-	0.016	0.004	0.033	0.005	0.014	0.006	0.041	0.008
M+4	-	-	-	-	-	-	-	-	0.004	0.002	0.013	0.003	0.002	0.011	0.014	0.006
AKG 346																
M+0	-	-	-	-	-	-	-	-	0.683	0.014	0.548	0.006	0.730	0.011	0.491	0.015
M+1	-	-	-	-	-	-	-	-	0.054	0.004	0.063	0.003	0.042	0.011	0.075	0.005
M+2	-	-	-	-	-	-	-	-	0.144	0.002	0.224	0.006	0.145	0.012	0.253	0.008
M+3	-	-	-	-	-	-	-	-	0.034	0.007	0.071	0.004	0.041	0.010	0.080	0.005
M+4	-	-	-	-	-	-	-	-	0.044	0.005	0.066	0.006	0.029	0.005	0.079	0.003
M+5	-	-	-	-	-	-	-	-	0.041	0.012	0.028	0.003	0.012	0.003	0.022	0.017
ASP 418																
M+0	-	-	-	-	-	-	-	-	0.709	0.005	0.555	0.015	0.678	0.003	0.555	0.015
M+1	-	-	-	-	-	-	-	-	0.126	0.012	0.172	0.009	0.143	0.004	0.172	0.009
M+2	-	-	-	-	-	-	-	-	0.131	0.006	0.153	0.005	0.119	0.004	0.153	0.005
M+3	-	-	-	-	-	-	-	-	0.041	0.004	0.092	0.006	0.054	0.004	0.092	0.006
M+4	-	-	-	-	-	-	-	-	-0.006	0.014	0.028	0.006	0.005	0.002	0.028	0.006
MAL 419																
M+0	-	-	-	-	-	-	-	-	0.697	0.003	0.494	0.005	0.669	0.005	0.468	0.016
M+1	-	-	-	-	-	-	-	-	0.109	0.007	0.174	0.005	0.132	0.004	0.156	0.012

Condition	Control				Low Glucose				High Lactate				Low Glucose + High Lactate			
	24-h		48-h		24-h		48-h		24-h		48-h		24-h		48-h	
	MID	SE	MID	SE	MID	SE	MID	SE	MID	SE	MID	SE	MID	SE	MID	SE
M+2	-	-	-	-	-	-	-	-	0.135	0.003	0.183	0.003	0.131	0.003	0.202	0.008
M+3	-	-	-	-	-	-	-	-	0.052	0.002	0.118	0.002	0.058	0.003	0.136	0.005
M+4	-	-	-	-	-	-	-	-	0.006	0.001	0.031	0.002	0.010	0.002	0.039	0.003
GLU 431																
M+0	-	-	-	-	-	-	-	-	0.744	0.012	0.553	0.004	0.729	0.005	0.504	0.004
M+1	-	-	-	-	-	-	-	-	0.058	0.012	0.092	0.003	0.068	0.004	0.069	0.003
M+2	-	-	-	-	-	-	-	-	0.147	0.005	0.204	0.002	0.142	0.003	0.234	0.002
M+3	-	-	-	-	-	-	-	-	0.030	0.003	0.080	0.003	0.036	0.002	0.090	0.001
M+4	-	-	-	-	-	-	-	-	0.017	0.002	0.054	0.002	0.020	0.002	0.076	0.001
M+5	-	-	-	-	-	-	-	-	0.004	0.001	0.017	0.000	0.004	0.001	0.026	0.001
CIT 591																
M+0	-	-	-	-	-	-	-	-	0.371	0.017	0.299	0.006	0.384	0.015	0.244	0.007
M+1	-	-	-	-	-	-	-	-	0.086	0.016	0.086	0.009	0.083	0.013	0.072	0.004
M+2	-	-	-	-	-	-	-	-	0.295	0.009	0.257	0.012	0.290	0.008	0.280	0.002
M+3	-	-	-	-	-	-	-	-	0.144	0.012	0.176	0.013	0.148	0.010	0.187	0.006
M+4	-	-	-	-	-	-	-	-	0.064	0.009	0.085	0.007	0.056	0.012	0.123	0.004
M+5	-	-	-	-	-	-	-	-	0.054	0.008	0.073	0.010	0.035	0.010	0.070	0.005
M+6	-	-	-	-	-	-	-	-	-0.014	0.027	0.026	0.005	0.004	0.008	0.025	0.004

Appendix O

Metabolite isotope labeling distributions from [1,2-^{13}C] glucose, [U-^{13}C] glutamine, and [U-^{13}C] lactate for K3 iPSCs

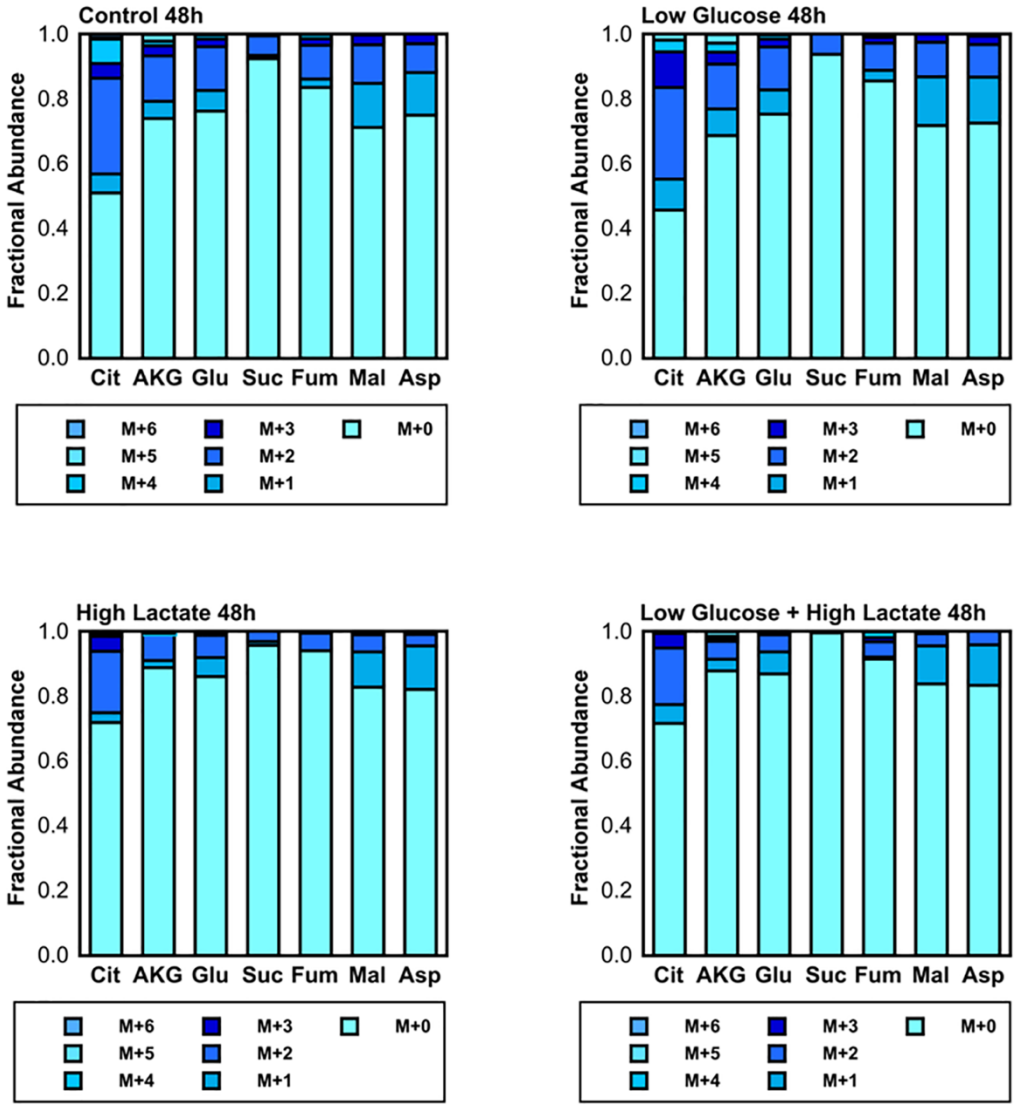

Figure O1. Metabolite isotope labeling distribution from [1,2-^{13}C] glucose for K3 iPSC cultures for Control, Low Glucose, High Lactate, and Low Glucose + High Lactate conditions at 48-h. MIDs shown below have been corrected for natural abundance.

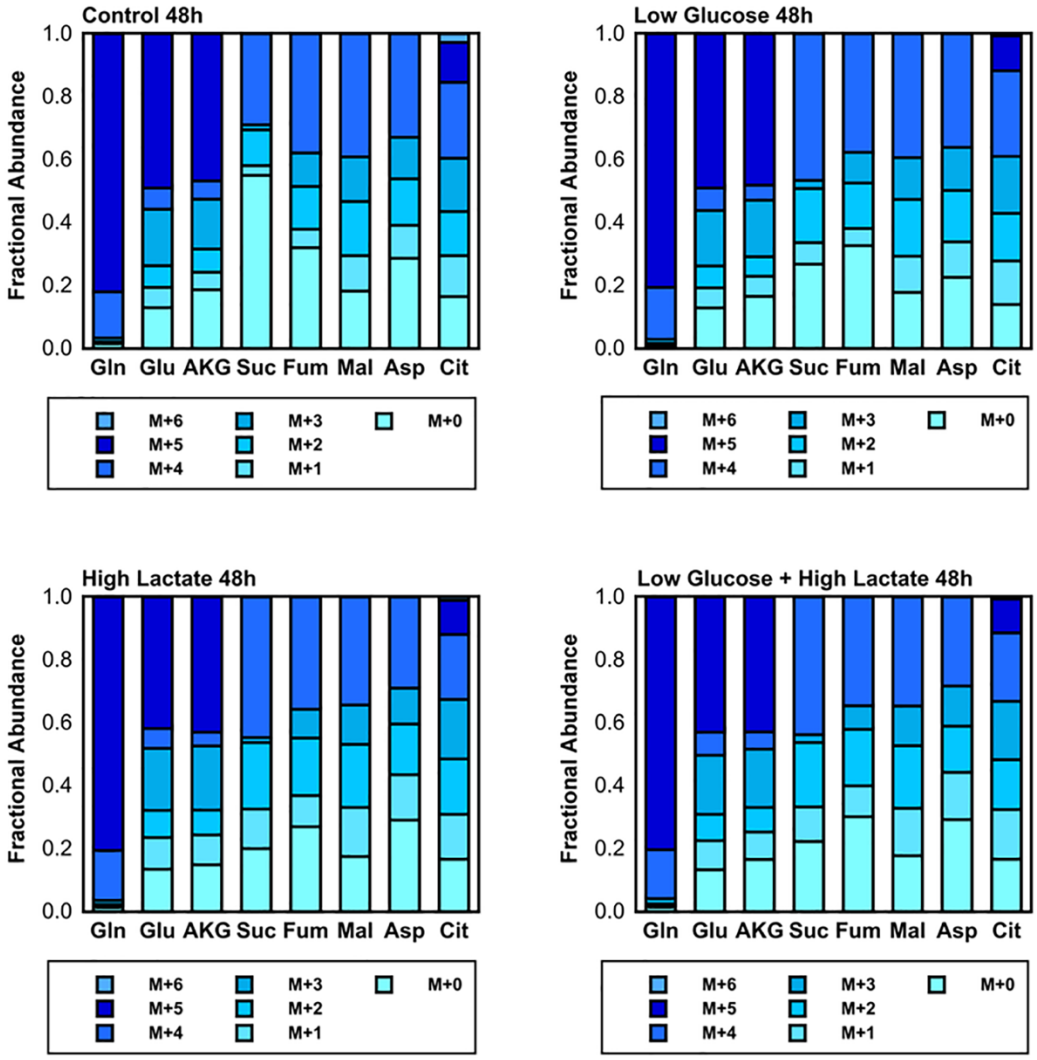

Figure O2. Metabolite isotope labeling distribution from [U-^{13}C] glutamine for K3 iPSC cultures for Control, Low Glucose, High Lactate, and Low Glucose + High Lactate conditions at 48-h. MIDs shown below have been corrected for natural abundance.

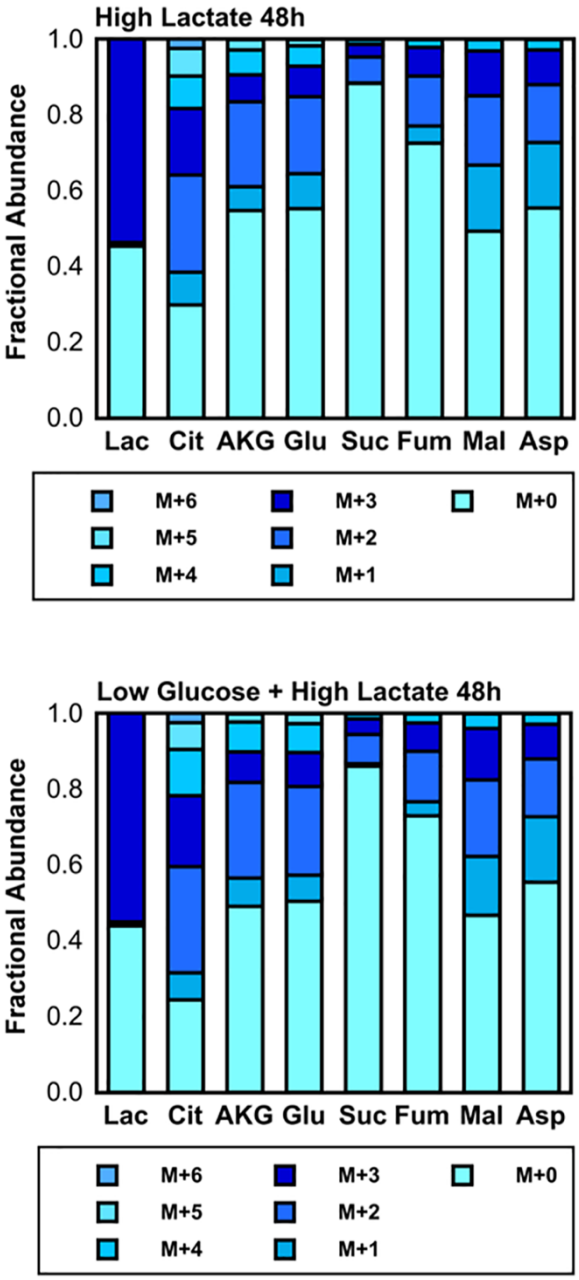

Figure O3. Metabolite isotope labeling distribution from [U-^{13}C] lactate for K3 iPSC cultures for High Lactate and Low-Glucose + High Lactate conditions at 48-h. MIDs shown below have been corrected for natural abundance.

Appendix P

Metabolic flux analysis results for K3 iPSCs grown in Control, Low Glucose, High Lactate, and Low Glucose + High Lactate cultures

Table P1. Metabolic flux analysis results for K3 iPSC Control cultures using [1,2-^{13}C] glucose and [U-^{13}C] glutamine. The fluxes are shown with 95% confidence intervals. The sum of squared residuals (SSR) was 81.4 with an expected range of 45.4 to 90.3.

Reaction	**Flux**	**95% Confidence Interval**	
	nmol/10^6 cells/h	Lower Bound	Upper Bound
Glc.x -> Glc	1.05E+03	9.56E+02	1.15E+03
Glc -> Pyr.c + Pyr.c	1.05E+03	9.50E+02	1.14E+03
Pyr.c <-> Lac.c	2.11E+03	1.92E+03	2.30E+03
Pyr.c <-> Lac.c	1.00E+07	8111.50	Inf
Pyr.m -> CO2 + AcCoA.m	115.07	71.59	171.81
AcCoA.m + OAA.m -> Cit.m	115.07	71.59	171.81
Cit.m <-> AKG.m + CO2	23.96	12.67	57.41
Cit.m <-> AKG.m + CO2	88.34	53.92	149.00
AKG.m -> CO2 + Suc.m	111.73	76.25	158.98
Suc.m <-> Fum.m	111.73	76.25	158.98
Suc.m <-> Fum.m	8.55	0.00	Inf
Fum.m <-> Mal.m	111.73	76.25	158.98
Fum.m <-> Mal.m	1.97E+06	0.00E+00	1.97E+06
Mal.m <-> OAA.m	78.68	45.13	127.83
Mal.m <-> OAA.m	0.00	0.00	21.39
Gln <-> Glu	128.45	98.09	158.74
Gln <-> Glu	0.00	0.00	Inf
Glu <-> AKG.m	87.78	57.18	118.30
Glu <-> AKG.m	804.02	273.35	Inf
Ser -> Pyr.c	21.70	10.43	32.98
Ser -> Gly + MEETHF	6.36	3.70	9.02
Gln.x -> Gln	132.20	101.84	162.48
Ser.x -> Ser	33.30	23.13	43.49
Ala -> Ala.x	33.33	29.22	37.45
Pyr.x -> Pyr.c	67.55	62.45	72.65
Glu -> Glu.x	36.19	32.86	39.52
Lac.c -> Lac.x	2.11E+03	1.92E+03	2.30E+03
Asp.x -> Asp	0.40	0.07	6.00
Pyr.c <-> Pyr.m	71.45	31.61	115.05
Pyr.c <-> Pyr.m	1.00E+07	2.70E+03	Inf
Pyr.m + CO2 -> OAA.m	36.39	24.62	50.40
Mal.m -> Pyr.m + CO2	120.44	79.02	163.43
Pyr.m <-> Ala	40.44	35.36	45.52

Reaction	Flux	95% Confidence Interval	
	nmol/10^6 cells/h	Lower Bound	Upper Bound
Pyr.m <-> Ala	1.09E+03	0.00	1.93E+06
Cit.m -> Cit.c	91.11	24.92	147.86
Cit.c -> OAA.c + AcCoA.c	91.11	24.92	147.86
AcCoA.c -> Lipids	27.00	15.24	38.76
OAA.c <-> Asp	4.11	-1.67	5.97
OAA.c <-> Asp	0.00	0.00	108.98
OAA.c <-> Mal.c	87.00	20.76	143.80
OAA.c <-> Mal.c	5.37E+03	0.00	Inf
Mal.c <-> Mal.m	87.40	21.16	144.18
Mal.c <-> Mal.m	2.46E+03	34.55	Inf
Mal.c <-> Fum.c	-0.39	-1.37	0.58
Mal.c <-> Fum.c	34.95	0.00	Inf
Asp <-> Fum.c	0.39	-0.58	1.37
Asp <-> Fum.c	0.00	0.00	Inf
0.19*Ala + 0.11*Asp + 0.1*Gln + 0.12*Glu + 0.17*Gly + 0.14*Ser + 0.16*Glc -> Biomass	37.40	21.76	53.05
Lac.c <-> Lac.t + dummyL	0.00	0.00	0.00
Lac.c <-> Lac.t + dummyL	386.56	252.94	540.90
AcCoA.c -> sink	64.11	0.00	121.82
Compartmentalization/Mixing Reactions			
0*Cit.c -> Cit.p	31.14	0.00	100.00
0*Cit.m -> Cit.p	68.86	0.00	100.00
Cit.p -> sink	100.00	100.00	100.00
0*Mal.c -> Mal.p	0.00	0.00	100.00
0*Mal.m -> Mal.p	100.00	0.00	100.00
Mal.p -> sink	100.00	100.00	100.00
0*Fum.c -> Fum.p	99.98	0.00	100.00
0*Fum.m -> Fum.p	0.02	0.00	100.00
Fum.p -> sink	100.00	100.00	100.00
Dilution Reactions			
0*Suc.m -> Suc.d	0.63	0.58	0.68
0*Suc.u -> Suc.d	0.37	0.32	0.42
Suc.d -> sink	1.00	1.00	1.00
0*Fum.e -> Fum.d	0.87	0.81	1.00
0*Fum.u -> Fum.d	0.13	0.00	0.19
Fum.d -> sink	1.00	1.00	1.00

Table P2. Metabolic flux analysis results for K3 iPSC Low Glucose cultures using [1,2-^{13}C] glucose and [U-^{13}C] glutamine. The fluxes are shown with 95% confidence intervals. The sum of squared residuals (SSR) was 73.2 with an expected range of 34.0 to 73.8.

Reaction	Flux	95% Confidence Interval	
	nmol/10^6 cells/h	Lower Bound	Upper Bound
Glc.x -> Glc	993.85	931.33	1056.90
Glc -> Pyr.c + Pyr.c	987.51	925.16	1050.40
Pyr.c <-> Lac.c	2.00E+03	1.88E+03	2.12E+03
Pyr.c <-> Lac.c	1.00E+07	3.35E+03	Inf
Pyr.m -> CO2 + AcCoA.m	124.04	59.25	183.61
AcCoA.m + OAA.m -> Cit.m	124.04	59.25	183.61
Cit.m <-> AKG.m + CO2	24.47	-2.81	69.30
Cit.m <-> AKG.m + CO2	128.93	60.22	282.62
AKG.m -> CO2 + Suc.m	130.38	107.19	180.33
Suc.m <-> Fum.m	130.38	107.19	180.33
Suc.m <-> Fum.m	26.63	0.00	2.58E+04
Fum.m <-> Mal.m	130.38	107.19	180.33
Fum.m <-> Mal.m	1.05E+03	0.00	Inf
Mal.m <-> OAA.m	76.75	31.78	134.49
Mal.m <-> OAA.m	0.00	0.00	25.41
Gln <-> Glu	143.09	126.08	160.18
Gln <-> Glu	1.28E+06	0.00	Inf
Glu <-> AKG.m	105.91	88.51	123.37
Glu <-> AKG.m	2.76E+06	0.00	Inf
Ser -> Pyr.c	11.16	2.45	19.87
Ser -> Gly + MEETHF	6.73	4.08	9.39
Gln.x -> Gln	147.05	130.08	164.10
Ser.x -> Ser	23.44	16.19	30.69
Ala -> Ala.x	32.26	29.32	35.20
Pyr.x -> Pyr.c	75.19	71.28	79.11
Glu -> Glu.x	32.43	30.08	34.78
Lac.c -> Lac.x	2.00E+03	1.88E+03	2.12E+03
Asp.x -> Asp	0.44	0.00	7.71
Pyr.c <-> Pyr.m	61.84	-2.39	117.55
Pyr.c <-> Pyr.m	1.00E+07	7.46E+03	Inf
Pyr.m + CO2 -> OAA.m	47.29	24.81	58.90
Mal.m -> Pyr.m + CO2	149.28	115.05	175.57
Pyr.m <-> Ala	39.79	35.61	43.96
Pyr.m <-> Ala	0.06	0.00	Inf
Cit.m -> Cit.c	99.57	21.18	162.92
Cit.c -> OAA.c + AcCoA.c	99.57	21.18	162.92
AcCoA.c -> Lipids	27.00	15.24	38.76

Reaction	Flux	95% Confidence Interval	
	nmol/10^6 cells/h	Lower Bound	Upper Bound
OAA.c <-> Asp	7.42	0.03	9.22
OAA.c <-> Asp	0.00	0.00	Inf
OAA.c <-> Mal.c	92.15	14.49	155.47
OAA.c <-> Mal.c	892.75	0.00	Inf
Mal.c <-> Mal.m	95.65	62.54	158.97
Mal.c <-> Mal.m	8.49E+05	26.41	Inf
Mal.c <-> Fum.c	-3.50	-3.89	-3.11
Mal.c <-> Fum.c	1.02E+04	0.00	Inf
Asp <-> Fum.c	3.50	3.11	3.89
Asp <-> Fum.c	0.00	0.00	Inf
0.19*Ala + 0.11*Asp + 0.1*Gln + 0.12*Glu + 0.17*Gly + 0.14*Ser + 0.16*Glc -> Biomass	39.61	23.99	55.22
Lac.c <-> Lac.t + dummyL	0.00	0.00	0.00
Lac.c <-> Lac.t + dummyL	303.56	180.29	444.07
AcCoA.c -> sink	72.57	0.00	136.62
Compartmentalization/Mixing Reactions			
0*Cit.c -> Cit.p	49.04	0.00	100.00
0*Cit.m -> Cit.p	50.96	0.00	100.00
Cit.p -> sink	100.00	100.00	100.00
0*Mal.c -> Mal.p	0.00	0.00	100.00
0*Mal.m -> Mal.p	100.00	0.00	100.00
Mal.p -> sink	100.00	100.00	100.00
0*Fum.c -> Fum.p	46.55	0.00	100.00
0*Fum.m -> Fum.p	53.45	0.00	100.00
Fum.p -> sink	100.00	100.00	100.00
Dilution Reactions			
0*Suc.m -> Suc.d	0.89	0.83	0.95
0*Suc.u -> Suc.d	0.11	0.05	0.17
Suc.d -> sink	1.00	1.00	1.00
0*Fum.e -> Fum.d	0.77	0.70	0.90
0*Fum.u -> Fum.d	0.23	0.10	0.30
Fum.d -> sink	1.00	1.00	1.00

Table P3. Metabolic flux analysis results for K3 iPSC High Lactate cultures using [1,2-^{13}C] glucose, [U-^{13}C] glutamine, and [U-^{13}C] lactate. The fluxes are shown with 95% confidence intervals. The sum of squared residuals (SSR) was 77.8 with an expected range of 43.8 to 88.0.

Reaction	Flux	95% Confidence Interval	
	nmol/10^6 cells/h	Lower Bound	Upper Bound
Glc.x -> Glc	873.54	803.94	943.81
Glc -> Pyr.c + Pyr.c	867.80	798.41	937.87
Pyr.c <-> Lac.c	1.69E+03	1.56E+03	1.83E+03
Pyr.c <-> Lac.c	1.45E+04	7.78E+03	6.97E+04
Pyr.m -> CO2 + AcCoA.m	132.10	94.74	192.54
AcCoA.m + OAA.m -> Cit.m	132.10	94.74	192.54
Cit.m <-> AKG.m + CO2	25.52	16.43	36.90
Cit.m <-> AKG.m + CO2	52.81	37.80	71.92
AKG.m -> CO2 + Suc.m	96.27	72.98	121.27
Suc.m <-> Fum.m	96.27	72.98	121.27
Suc.m <-> Fum.m	14.67	0.00	72.77
Fum.m <-> Mal.m	96.27	72.98	121.27
Fum.m <-> Mal.m	539.46	0.00	Inf
Mal.m <-> OAA.m	117.70	80.90	174.70
Mal.m <-> OAA.m	0.00	0.00	336.82
Gln <-> Glu	103.35	84.51	122.19
Gln <-> Glu	5.38E+06	0.00	Inf
Glu <-> AKG.m	70.75	51.47	90.03
Glu <-> AKG.m	1.00E+07	0.00	Inf
Ser -> Pyr.c	17.31	8.10	26.53
Ser -> Gly + MEETHF	6.10	3.44	8.76
Gln.x -> Gln	106.94	88.16	125.71
Ser.x -> Ser	28.43	20.60	36.27
Ala -> Ala.x	28.81	21.95	35.66
Pyr.x -> Pyr.c	38.95	31.90	46.00
Glu -> Glu.x	28.30	25.55	31.04
Lac.c -> Lac.x	1.69E+03	1.56E+03	1.83E+03
Asp.x -> Asp	3.19	0.63	15.85
Pyr.c <-> Pyr.m	97.74	62.57	153.99
Pyr.c <-> Pyr.m	3.43E+03	1.12E+03	Inf
Pyr.m + CO2 -> OAA.m	14.40	3.90	22.87
Mal.m -> Pyr.m + CO2	84.39	61.05	108.11
Pyr.m <-> Ala	35.62	28.15	43.10
Pyr.m <-> Ala	0.01	0.00	Inf
Cit.m -> Cit.c	106.58	68.16	168.47
Cit.c -> OAA.c + AcCoA.c	106.58	68.16	168.47

Reaction	Flux	95% Confidence Interval	
	nmol/10^6 cells/h	Lower Bound	Upper Bound
AcCoA.c -> Lipids	27.00	15.24	38.76
OAA.c <-> Asp	0.46	-12.35	4.32
OAA.c <-> Asp	13.58	0.00	212.40
OAA.c <-> Mal.c	106.12	53.78	167.14
OAA.c <-> Mal.c	2.44E+03	0.00	Inf
Mal.c <-> Mal.m	105.82	65.46	166.84
Mal.c <-> Mal.m	1.00E+07	76.76	Inf
Mal.c <-> Fum.c	0.30	-0.48	1.08
Mal.c <-> Fum.c	1.00E+07	0.00	Inf
Asp <-> Fum.c	-0.30	-1.08	0.48
Asp <-> Fum.c	6.67	0.00	164.82
0.19*Ala + 0.11*Asp + 0.1*Gln + 0.12*Glu + 0.17*Gly + 0.14*Ser + 0.16*Glc -> Biomass	35.88	20.21	51.54
Lac.c <-> Lac.t + dummyL	0.00	0.00	0.00
Lac.c <-> Lac.t + dummyL	4.20E+03	3.26E+03	5.63E+03
AcCoA.c -> sink	79.58	39.04	142.31
Compartmentalization/Mixing Reactions			
0*Cit.c -> Cit.p	7.58	0.00	100.00
0*Cit.m -> Cit.p	92.42	0.00	100.00
Cit.p -> sink	100.00	100.00	100.00
0*Mal.c -> Mal.p	0.00	0.00	100.00
0*Mal.m -> Mal.p	100.00	0.00	100.00
Mal.p -> sink	100.00	100.00	100.00
0*Fum.c -> Fum.p	0.00	0.00	100.00
0*Fum.m -> Fum.p	100.00	0.00	100.00
Fum.p -> sink	100.00	100.00	100.00
Dilution Reactions			
0*Suc.m -> Suc.d	0.90	0.86	0.95
0*Suc.u -> Suc.d	0.10	0.05	0.14
Suc.d -> sink	1.00	1.00	1.00
0*Fum.e -> Fum.d	0.81	0.76	0.88
0*Fum.u -> Fum.d	0.19	0.12	0.24
Fum.d -> sink	1.00	1.00	1.00

Table P4. Metabolic flux analysis results for K3 iPSC Low Glucose + High Lactate cultures using [1,2-^{13}C] glucose, [U-^{13}C] glutamine, and [U-^{13}C] lactate. The fluxes are shown with 95% confidence intervals. The sum of squared residuals (SSR) was 88.2 with an expected range of 45.4 to 90.3.

Reaction	Flux	95% Confidence Interval	
	nmol/10^6 cells/h	Lower Bound	Upper Bound
Glc.x -> Glc	859.77	801.34	918.22
Glc -> Pyr.c + Pyr.c	853.80	795.45	912.14
Pyr.c <-> Lac.c	1.65E+03	1.54E+03	1.76E+03
Pyr.c <-> Lac.c	5.32E+04	1.87E+04	Inf
Pyr.m -> CO2 + AcCoA.m	172.07	115.11	250.93
AcCoA.m + OAA.m -> Cit.m	172.07	115.11	250.93
Cit.m <-> AKG.m + CO2	42.64	30.78	63.71
Cit.m <-> AKG.m + CO2	68.43	47.41	94.00
AKG.m -> CO2 + Suc.m	124.63	98.64	156.35
Suc.m <-> Fum.m	124.63	98.64	156.35
Suc.m <-> Fum.m	218.94	0.00	Inf
Fum.m <-> Mal.m	124.63	98.64	156.35
Fum.m <-> Mal.m	26.69	0.00	260.04
Mal.m <-> OAA.m	149.84	106.50	225.93
Mal.m <-> OAA.m	0.00	0.00	149.33
Gln <-> Glu	115.88	97.58	134.59
Gln <-> Glu	2.26E+05	0.00	Inf
Glu <-> AKG.m	81.98	63.18	101.20
Glu <-> AKG.m	2.91E+06	1.08E+03	Inf
Ser -> Pyr.c	34.59	12.49	56.71
Ser -> Gly + MEETHF	6.34	3.68	8.99
Gln.x -> Gln	119.61	101.37	138.25
Ser.x -> Ser	46.15	24.54	67.76
Ala -> Ala.x	27.89	21.81	33.96
Pyr.x -> Pyr.c	36.49	31.40	41.59
Glu -> Glu.x	29.42	26.28	32.55
Lac.c -> Lac.x	1.65E+03	1.54E+03	1.76E+03
Asp.x -> Asp	1.12	0.59	12.00
Pyr.c <-> Pyr.m	128.05	75.86	200.26
Pyr.c <-> Pyr.m	3.63E+06	2.89E+03	Inf
Pyr.m + CO2 -> OAA.m	22.23	12.79	28.77
Mal.m -> Pyr.m + CO2	101.23	77.82	125.30
Pyr.m <-> Ala	34.98	28.21	41.73
Pyr.m <-> Ala	0.32	0.00	Inf
Cit.m -> Cit.c	129.43	61.48	208.48
Cit.c -> OAA.c + AcCoA.c	129.43	61.48	208.48

Reaction	Flux	95% Confidence Interval	
	nmol/10^6 cells/h	Lower Bound	Upper Bound
AcCoA.c -> Lipids	27.00	15.24	38.76
OAA.c <-> Asp	4.77	-6.31	6.93
OAA.c <-> Asp	0.00	0.00	68.82
OAA.c <-> Mal.c	124.66	56.64	203.77
OAA.c <-> Mal.c	1.27E+06	0.00	Inf
Mal.c <-> Mal.m	126.45	58.41	205.55
Mal.c <-> Mal.m	6.88E+05	102.01	Inf
Mal.c <-> Fum.c	-1.78	-3.74	0.16
Mal.c <-> Fum.c	6.42E+03	0.00	Inf
Asp <-> Fum.c	1.78	-0.16	3.74
Asp <-> Fum.c	0.00	0.00	Inf
0.19*Ala + 0.11*Asp + 0.1*Gln + 0.12*Glu + 0.17*Gly + 0.14*Ser + 0.16*Glc -> Biomass	37.31	21.63	52.91
Lac.c <-> Lac.t + dummyL	0.00	0.00	0.00
Lac.c <-> Lac.t + dummyL	3.15E+03	2.79E+03	3.57E+03
AcCoA.c -> sink	102.43	33.42	182.09
Compartmentalization/Mixing Reactions			
0*Cit.c -> Cit.p	10.19	0.00	100.00
0*Cit.m -> Cit.p	89.81	0.00	100.00
Cit.p -> sink	100.00	100.00	100.00
0*Mal.c -> Mal.p	100.00	0.00	100.00
0*Mal.m -> Mal.p	0.00	0.00	100.00
Mal.p -> sink	100.00	100.00	100.00
0*Fum.c -> Fum.p	78.19	28.41	100.00
0*Fum.m -> Fum.p	21.81	0.00	71.59
Fum.p -> sink	100.00	100.00	100.00
Dilution Reactions			
0*Suc.m -> Suc.d	0.92	0.87	0.97
0*Suc.u -> Suc.d	0.08	0.03	0.13
Suc.d -> sink	1.00	1.00	1.00
0*Fum.e -> Fum.d	0.75	0.70	1.00
0*Fum.u -> Fum.d	0.25	0.00	0.30
Fum.d -> sink	1.00	1.00	1.00

Appendix Q

Measured and simulated MIDs from ^{13}C-MFA simulations for K3 iPSC cultures

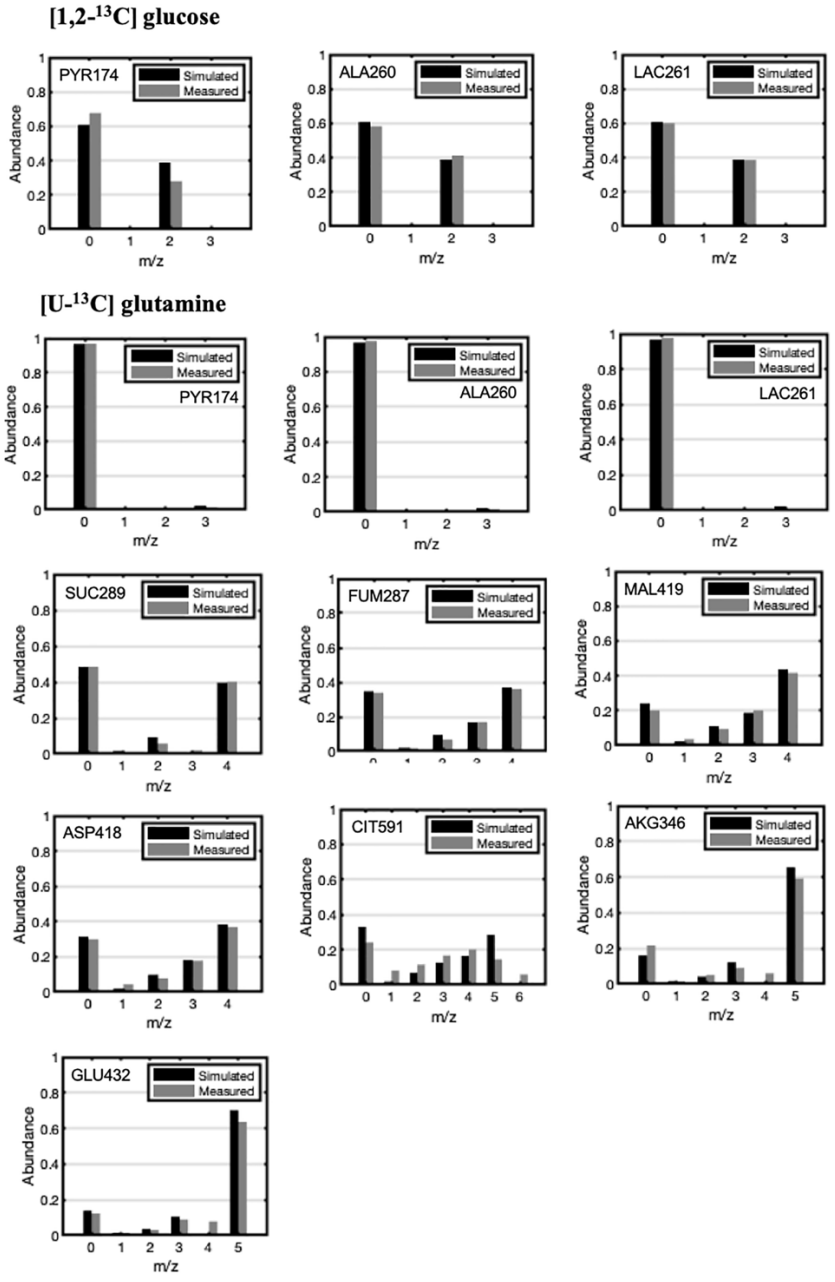

Figure Q1. Measured and simulated MIDs for intracellular metabolites for K3 iPSC Control cultures. MIDs shown below have been corrected for natural abundance.

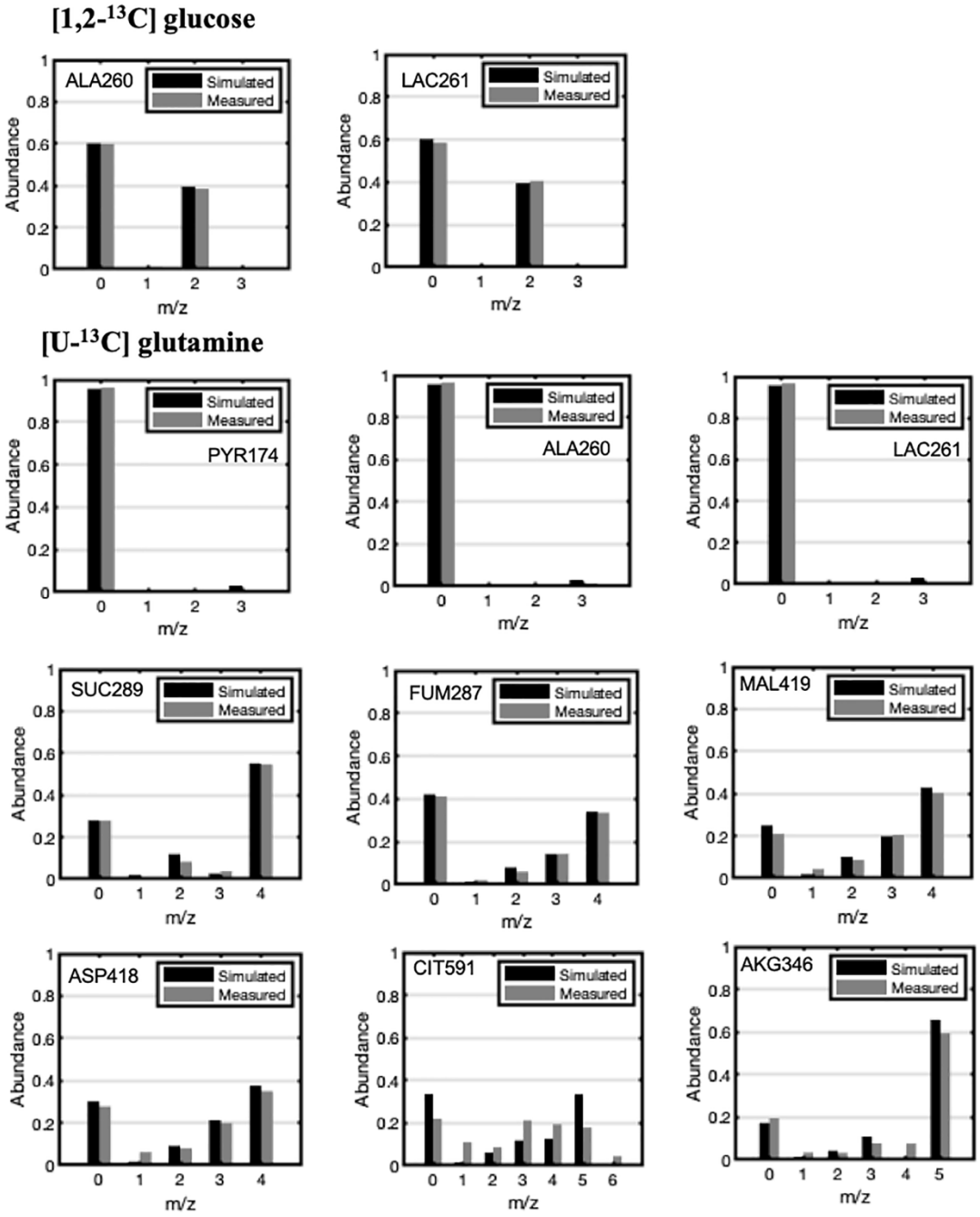

Figure Q2. Measured and simulated MIDs for intracellular metabolites for K3 iPSC Low Glucose cultures. MIDs shown below have been corrected for natural abundance.

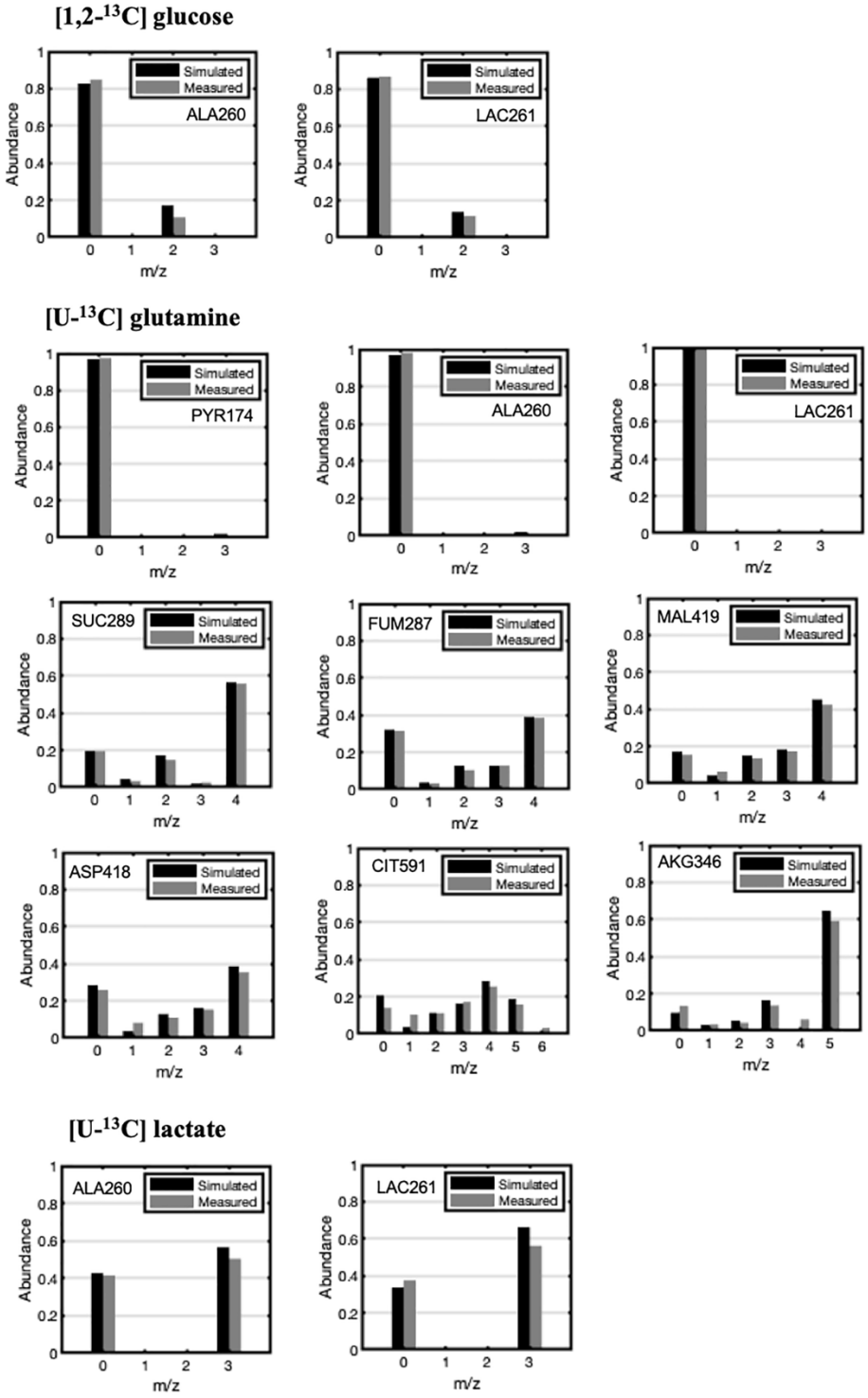

Figure Q3. Measured and simulated MIDs for intracellular metabolites for K3 iPSC High Lactate cultures. MIDs shown below have been corrected for natural abundance.

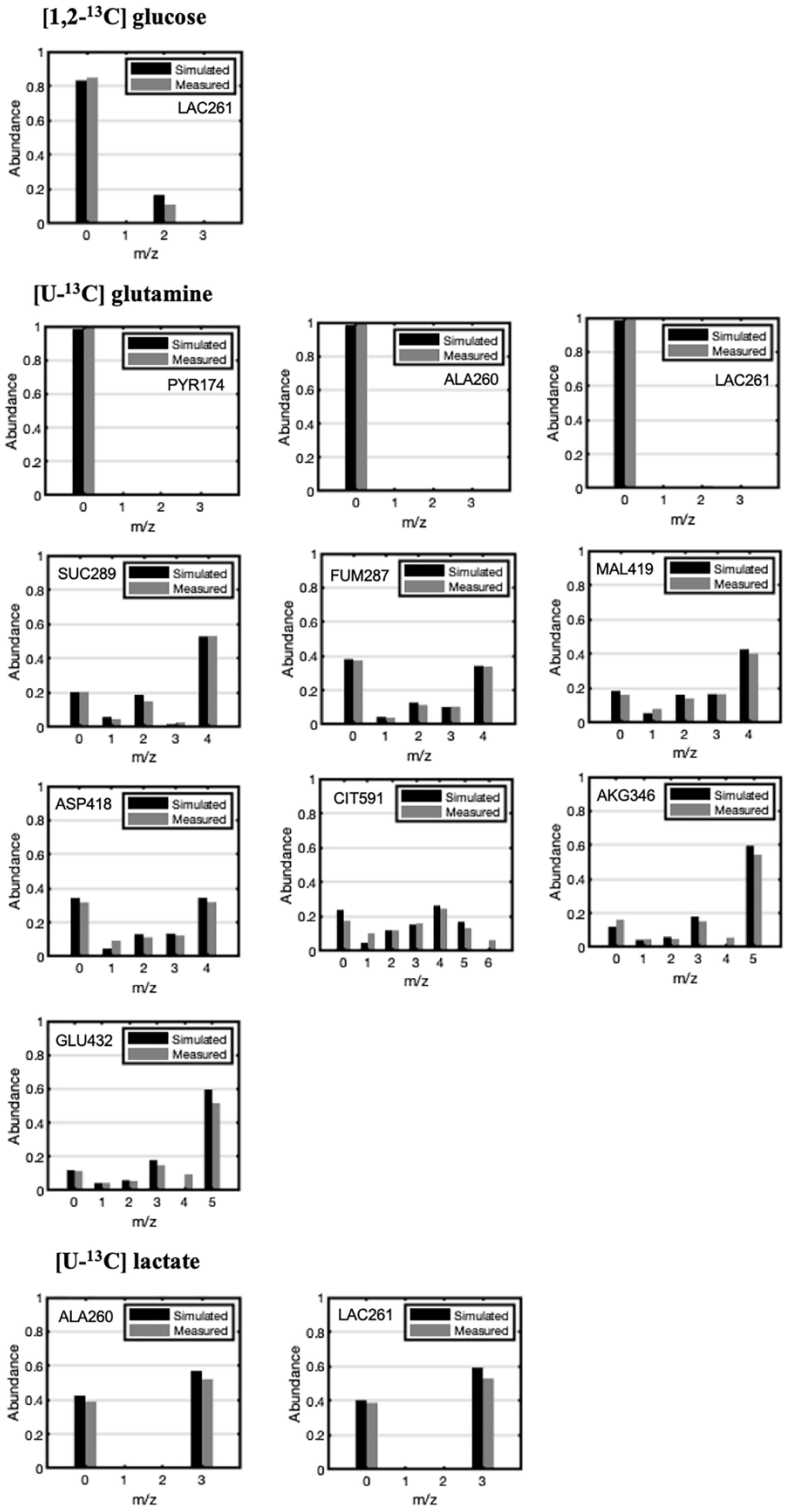

Figure Q4. Measured and simulated MIDs for intracellular metabolites for K3 iPSC Low Glucose + High Lactate cultures. MIDs shown below have been corrected for natural abundance.

REFERENCES

Aasen, T., Raya, A., Barrero, M. J., Garreta, E., Consiglio, A., Gonzalez, F., Vassena, R., Bilić, J., Pekarik, V., Tiscornia, G., 2008. Efficient and rapid generation of induced pluripotent stem cells from human keratinocytes. Nat. Biotechnol. 26**,** 1276.

Abecasis, B., Aguiar, T., Arnault, É., Costa, R., Gomes-Alves, P., Aspegren, A., Serra, M., Alves, P. M., 2017. Expansion of 3D human induced pluripotent stem cell aggregates in bioreactors: Bioprocess intensification and scaling-up approaches. J. Biotechnol. 246**,** 81-93.

Adachi, K., Suemori, H., Yasuda, S. y., Nakatsuji, N., Kawase, E., 2010. Role of SOX2 in maintaining pluripotency of human embryonic stem cells. Genes to cells. 15**,** 455-470.

Ahn, W. S., Antoniewicz, M. R., 2011. Metabolic flux analysis of CHO cells at growth and non-growth phases using isotopic tracers and mass spectrometry. Metab. Eng. 13**,** 598-609.

Ahn, W. S., Antoniewicz, M. R., 2012. Towards dynamic metabolic flux analysis in CHO cell cultures. Biotechnol. J. 7**,** 61-74.

Ahn, W. S., Antoniewicz, M. R., 2013. Parallel labeling experiments with [1, 2-^{13}C] glucose and [U-^{13}C] glutamine provide new insights into CHO cell metabolism. Metab. Eng. 15**,** 34-47.

Altamirano, C., Illanes, A., Becerra, S., Cairó, J. J., Gòdia, F., 2006. Considerations on the lactate consumption by CHO cells in the presence of galactose. J. Biotechnol. 125**,** 547-556.

Antoniewicz, M. R., Kelleher, J. K., Stephanopoulos, G., 2006. Determination of confidence intervals of metabolic fluxes estimated from stable isotope measurements. Metab. Eng. 8**,** 324-337.

Antoniewicz, M. R., Kelleher, J. K., Stephanopoulos, G., 2007a. Accurate assessment of amino acid mass isotopomer distributions for metabolic flux analysis. Analytical Chemistry. 79**,** 7554-7559.

Antoniewicz, M. R., Kelleher, J. K., Stephanopoulos, G., 2007b. Elementary metabolite units (EMU): a novel framework for modeling isotopic distributions. Metab. Eng. 9**,** 68-86.

Avior, Y., Sagi, I., Benvenisty, N., 2016. Pluripotent stem cells in disease modelling and drug discovery. Nat. Rev. Mol. Cell Biol. 17**,** 170.

Badawy, A.-B., Morgan, C., Turner, J., 2008. Application of the Phenomenex EZ: faast™ amino acid analysis kit for rapid gas-chromatographic determination of concentrations of plasma tryptophan and its brain uptake competitors. Amino Acids. 34**,** 587-596.

Badur, M. G., Zhang, H., Metallo, C. M., 2015. Enzymatic passaging of human embryonic stem cells alters central carbon metabolism and glycan abundance. Biotechnol. J. 10**,** 1600-1611.

Bangalore, M. P., Adhikarla, S., Mukherjee, O., Panicker, M. M., 2017. Genotoxic Effects of Culture Media on Human Pluripotent Stem Cells. Sci Rep. 7**,** 12.

Ben-David, U., Benvenisty, N., 2011. The tumorigenicity of human embryonic and induced pluripotent stem cells. Nat. Rev. Cancer. 11**,** 268.

Bergström, J., Fürst, P., Noree, L., Vinnars, E., 1974. Intracellular free amino acid concentration in human muscle tissue. J. Appl. Physiol. 36**,** 693-697.

Berra, E., Roux, D., Richard, D. E., Pouysségur, J., 2001. Hypoxia-inducible factor-1α (HIF-1α) escapes O2-driven proteasomal degradation irrespective of its subcellular localization: nucleus or cytoplasm. EMBO Reoprts. 2**,** 615-620.

Bonarius, H. P., Hatzimanikatis, V., Meesters, K. P., de Gooijer, C. D., Schmid, G., Tramper, J., 1996. Metabolic flux analysis of hybridoma cells in different culture media using mass balances. Biotechnol. Bioeng. 50**,** 299-318.

Bonarius, H. P., Özemre, A., Timmerarends, B., Skrabal, P., Tramper, J., Schmid, G., Heinzle, E., 2001. Metabolic-flux analysis of continuously cultured hybridoma cells using $^{13}CO_2$ mass spectrometry in combination with ^{13}C-lactate nuclear magnetic resonance spectroscopy and metabolite balancing. Biotechnol. Bioeng. 74**,** 528-538.

Bonarius, H. P. J., Schmid, G., Tramper, J., 1997. Flux analysis of underdetermined metabolic networks: The quest for the missing constraints. Trends Biotechnol. 15**,** 308-314.

Bonuccelli, G., Tsirigos, A., Whitaker-Menezes, D., Pavlides, S., Pestell, R. G., Chiavarina, B., Frank, P. G., Flomenberg, N., Howell, A., Martinez-Outschoorn, U. E., Sotgia, F., Lisanti, M. P., 2010. Ketones and lactate "fuel" tumor growth and metastasis. Cell Cycle. 9**,** 3506-3514.

Boumezbeur, F., Petersen, K. F., Cline, G. W., Mason, G. F., Behar, K. L., Shulman, G. I., Rothman, D. L., 2010. The contribution of blood lactate to brain energy metabolism in humans measured by dynamic 13C nuclear magnetic resonance spectroscopy. Journal of Neuroscience. 30**,** 13983-13991.

Boyer, L. A., Lee, T. I., Cole, M. F., Johnstone, S. E., Levine, S. S., Zucker, J. P., Guenther, M. G., Kumar, R. M., Murray, H. L., Jenner, R. G., 2005. Core transcriptional regulatory circuitry in human embryonic stem cells. Cell. 122**,** 947-956.

Brodsky, A. N., Odenwelder, D. C., Harcum, S. W., 2019. High extracellular lactate causes reductive carboxylation in breast tissue cell lines grown under normoxic conditions. PLoS One. 14**,** e0213419.

Brooks, G., 1985. Lactate: glycolytic end product and oxidative substrate during sustained exercise in mammals—the “lactate shuttle”. Circulation, Respiration, and Metabolism. Springer, pp. 208-218.

Cairns, R. A., Harris, I. S., Mak, T. W., 2011. Regulation of cancer cell metabolism. Nat. Rev. Cancer. 11**,** 85-95.

Carey, B. W., Finley, L. W. S., Cross, J. R., Allis, C. D., Thompson, C. B., 2015. Intracellular alpha-ketoglutarate maintains the pluripotency of embryonic stem cells. Nature. 518**,** 413-416.

Cayo, M. A., Cai, J., DeLaForest, A., Noto, F. K., Nagaoka, M., Clark, B. S., Collery, R. F., Si-Tayeb, K., Duncan, S. A., 2012. JD induced pluripotent stem cell–derived hepatocytes faithfully recapitulate the pathophysiology of familial hypercholesterolemia. Hepatology. 56**,** 2163-2171.

Cedar, H., Bergman, Y. J. N. R. G., 2009. Linking DNA methylation and histone modification: patterns and paradigms. 10**,** 295.

Chambers, I., Colby, D., Robertson, M., Nichols, J., Lee, S., Tweedie, S., Smith, A., 2003. Functional expression cloning of Nanog, a pluripotency sustaining factor in embryonic stem cells. Cell. 113**,** 643-655.

Chandel, N. S., Jasper, H., Ho, T. T., Passegue, E., 2016. Metabolic regulation of stem cell function in tissue homeostasis and organismal ageing. Nat. Cell Biol. 18**,** 823-832.

Charaniya, S., Le, H., Rangwala, H., Mills, K., Johnson, K., Karypis, G., Hu, W.-S., 2010. Mining manufacturing data for discovery of high productivity process characteristics. J. Biotechnol. 147**,** 186-197.

Chaudhry, M. A., Bowen, B. D., Piret, J. M., 2009. Culture pH and osmolality influence proliferation and embryoid body yields of murine embryonic stem cells. Biochem. Eng. J. 45**,** 126-135.

Chee Furng Wong, D., Tin Kam Wong, K., Tang Goh, L., Kiat Heng, C., Gek Sim Yap, M. J. B., bioengineering, 2005. Impact of dynamic online fed-batch strategies on metabolism, productivity and N-glycosylation quality in CHO cell cultures. 89**,** 164-177.

Chen, J., Li, Y., Yu, T.-S., McKay, R. M., Burns, D. K., Kernie, S. G., Parada, L. F., 2012. A restricted cell population propagates glioblastoma growth after chemotherapy. Nature. 488**,** 522.

Chen, X. L., Chen, A., Woo, T. L., Choo, A. B. H., Reuveny, S., Oh, S. K. W., 2010. Investigations into the Metabolism of Two-Dimensional Colony and Suspended Microcarrier Cultures of Human Embryonic Stem Cells in Serum-Free Media. Stem Cells Dev. 19**,** 1781-1792.

Chen, Y.-J., Mahieu, N. G., Huang, X., Singh, M., Crawford, P. A., Johnson, S. L., Gross, R. W., Schaefer, J., Patti, G. J., 2016. Lactate metabolism is associated with mammalian mitochondria. Nat. Chem. Biol. 12**,** 937.

Chew, J.-L., Loh, Y.-H., Zhang, W., Chen, X., Tam, W.-L., Yeap, L.-S., Li, P., Ang, Y.-S., Lim, B., Robson, P., 2005. Reciprocal transcriptional regulation of Pou5f1 and Sox2 via the Oct4/Sox2 complex in embryonic stem cells. Molecular and cellular biology. 25**,** 6031-6046.

Cho, Y. M., Kwon, S., Pak, Y. K., Seol, H. W., Choi, Y. M., Park, D. J., Park, K. S., Lee, H. K., 2006. Dynamic changes in mitochondrial biogenesis and antioxidant

enzymes during the spontaneous differentiation of human embryonic stem cells. Biochem. Biophys. Res. Commun. 348**,** 1472-1478.

Cliff, T. S., Wu, T., Boward, B. R., Yin, A., Yin, H., Glushka, J. N., Prestegaard, J. H., Dalton, S. J. C. s. c., 2017. MYC controls human pluripotent stem cell fate decisions through regulation of metabolic flux. 21**,** 502-516. e9.

Corbet, C., Draoui, N., Polet, F., Pinto, A., Drozak, X., Riant, O., Feron, O., 2014. The SIRT1/HIF2 alpha Axis Drives Reductive Glutamine Metabolism under Chronic Acidosis and Alters Tumor Response to Therapy. Cancer Res. 74**,** 5507-5519.

Correia, C., Koshkin, A., Duarte, P., Hu, D., Carido, M., Sebastião, M. J., Gomes-Alves, P., Elliott, D. A., Domian, I. J., Teixeira, A. P., 2018. 3D aggregate culture improves metabolic maturation of human pluripotent stem cell derived cardiomyocytes. Biotechnol. Bioeng. 115**,** 630-644.

Crown, S. B., Ahn, W. S., Antoniewicz, M. R., 2012. Rational design of ^{13}C-labeling experiments for metabolic flux analysis in mammalian cells. BMC Syst. Biol. 6**,** 13.

Crown, S. B., Antoniewicz, M. R., 2012. Selection of tracers for ^{13}C-Metabolic Flux Analysis using Elementary Metabolite Units (EMU) basis vector methodology. Metab. Eng. 14**,** 150-161.

Curi, R., Newsholme, P., Newsholme, E. A., 1988. Metabolism of pyruvate by isolated rat mesenteric lymphocytes, lymphocyte mitochondria and isolated mouse macrophages. Biochem. J. 250**,** 383-388.

Dayem, A. A., Choi, H.-Y., Kim, J.-H., Cho, S.-G., 2010. Role of oxidative stress in stem, cancer, and cancer stem cells. Cancers. 2**,** 859-84.

De Saedeleer, C. J., Copetti, T., Porporato, P. E., Verrax, J., Feron, O., Sonveaux, P., 2012. Lactate Activates HIF-1 in Oxidative but Not in Warburg-Phenotype Human Tumor Cells. PLoS One. 7**,** 12.

DeBerardinis, R. J., Lum, J. J., Hatzivassiliou, G., Thompson, C. B., 2008. The biology of cancer: Metabolic reprogramming fuels cell growth and proliferation. Cell Metab. 7**,** 11-20.

DeBerardinis, R. J., Mancuso, A., Daikhin, E., Nissim, I., Yudkoff, M., Wehrli, S., Thompson, C. B., 2007. Beyond aerobic glycolysis: Transformed cells can engage

in glutamine metabolism that exceeds the requirement for protein and nucleotide synthesis. Proc. Natl. Acad. Sci. U. S. A. 104**,** 19345-19350.

Deng, J., Shoemaker, R., Xie, B., Gore, A., LeProust, E. M., Antosiewicz-Bourget, J., Egli, D., Maherali, N., Park, I.-H., Yu, J. J. N. b., 2009. Targeted bisulfite sequencing reveals changes in DNA methylation associated with nuclear reprogramming. 27**,** 353.

Desai, N., Rambhia, P., Gishto, A., 2015. Human embryonic stem cell cultivation: historical perspective and evolution of xeno-free culture systems. Reprod. Biol. Endocrinol. 13**,** 15.

Doherty, J. R., Cleveland, J. L., 2013. Targeting lactate metabolism for cancer therapeutics. The Journal of clinical investigation. 123**,** 3685-3692.

Draoui, N., Feron, O., 2011. Lactate shuttles at a glance: from physiological paradigms to anti-cancer treatments. Disease models & mechanisms. 4**,** 727-732.

Duarte, T. M., Carinhas, N., Barreiro, L. C., Carrondo, M. J., Alves, P. M., Teixeira, A. P., 2014. Metabolic responses of CHO cells to limitation of key amino acids. Biotechnol. Bioeng. 111**,** 2095-2106.

Dubouchaud, H., Butterfield, G. E., Wolfel, E. E., Bergman, B. C., Brooks, G. A., 2000. Endurance training, expression, and physiology of LDH, MCT1, and MCT4 in human skeletal muscle. American Journal of Physiology-Endocrinology Metabolism. 278**,** E571-E579.

Duckwall, C. S., Murphy, T. A., Young, J. D., 2013. Mapping cancer cell metabolism with13C flux analysis: recent progress and future challenges. Journal of carcinogenesis. 12.

Eagle, H., 1955. The specific amino acid requirements of a mammalian cell (strain L) in tissue culture. J. Biol. Chem. 214**,** 839-852.

Eagle, H., Barban, S., Levy, M., Schulze, H. O., 1958. The utilization of carbohydrates by human cell cultures. J. Biol. Chem. 233**,** 551-558.

Edgar, A., 2002. The human L-threonine 3-dehydrogenase gene is an expressed pseudogene. BMC genetics. 3**,** 18.

Ezashi, T., Das, P., Roberts, R. M., 2005. Low O-2 tensions and the prevention of differentiation of hES cells. Proc. Natl. Acad. Sci. U. S. A. 102**,** 4783-4788.

Fan, J., Kamphorst, J. J., Rabinowitz, J. D., Shlomi, T., 2013. Fatty Acid Labeling from Glutamine in Hypoxia Can Be Explained by Isotope Exchange without Net Reductive Isocitrate Dehydrogenase (IDH) Flux. J. Biol. Chem. 288**,** 31363-31369.

Faubert, B., Li, K. Y., Cai, L., Hensley, C. T., Kim, J., Zacharias, L. G., Yang, C., Do, Q. N., Doucette, S., Burguete, D., 2017. Lactate metabolism in human lung tumors. Cell. 171**,** 358-371. e9.

Fendt, S. M., Bell, E. L., Keibler, M. A., Olenchock, B. A., Mayers, J. R., Wasylenko, T. M., Vokes, N. I., Guarente, L., Vander Heiden, M. G., Stephanopoulos, G., 2013. Reductive glutamine metabolism is a function of the α-ketoglutarate to citrate ratio in cells. Nat. Commun. 4**,** 11.

Ferguson, B. S., Rogatzki, M. J., Goodwin, M. L., Kane, D. A., Rightmire, Z., Gladden, L. B., 2018. Lactate metabolism: historical context, prior misinterpretations, and current understanding. European Journal of Applied Physiology. 118**,** 691-728.

Fernandez, C. A., DesRosiers, C., Previs, S. F., David, F., Brunengraber, H., 1996. Correction of ^{13}C mass isotopomer distributions for natural stable isotope abundance. J. Mass Spectrom. 31**,** 255-262.

Folmes, C. D. L., Arrell, D. K., Zlatkovic-Lindor, J., Martinez-Fernandez, A., Perez-Terzic, C., Nelson, T. J., Terzic, A., 2013. Metabolome and metaboproteome remodeling in nuclear reprogramming. Cell Cycle. 12**,** 2355-2365.

Folmes, C. D. L., Dzeja, P. P., Nelson, T. J., Terzic, A., 2012. Metabolic Plasticity in Stem Cell Homeostasis and Differentiation. Cell Stem Cell. 11**,** 596-606.

Folmes, C. D. L., Nelson, T. J., Martinez-Fernandez, A., Arrell, D. K., Lindor, J. Z., Dzeja, P. P., Ikeda, Y., Perez-Terzic, C., Terzic, A., 2011. Somatic Oxidative Bioenergetics Transitions into Pluripotency-Dependent Glycolysis to Facilitate Nuclear Reprogramming. Cell Metab. 14**,** 264-271.

Folmes, C. D. L., Terzic, A., 2016. Energy metabolism in the acquisition and maintenance of stemness. Semin. Cell Dev. Biol. 52**,** 68-75.

Forbes, N. S., Meadows, A. L., Clark, D. S., Blanch, H. W., 2006. Estradiol stimulates the biosynthetic pathways of breast cancer cells: Detection by metabolic flux analysis. Metab. Eng. 8**,** 639-652.

Gaglio, D., Metallo, C. M., Gameiro, P. A., Hiller, K., Danna, L. S., Balestrieri, C., Alberghina, L., Stephanopoulos, G., Chiaradonna, F., 2011. Oncogenic K-Ras decouples glucose and glutamine metabolism to support cancer cell growth. Mol. Syst. Biol. 7**,** 15.

Gaspar, J. A., Doss, M. X., Hengstler, J. G., Cadenas, C., Hescheler, J., Sachinidis, A., 2014. Unique Metabolic Features of Stem Cells, Cardiomyocytes, and Their Progenitors. Circ.Res. 114**,** 1346-1360.

Gatenby, R. A., Gillies, R. J., 2004. Why do cancers have high aerobic glycolysis? Nat. Rev. Cancer. 4**,** 891.

Gertz, E., Wisneski, J., Stanley, W., Neese, R., 1988. Myocardial substrate utilization during exercise in humans. Dual carbon-labeled carbohydrate isotope experiments. The Journal of clinical investigation. 82**,** 2017-2025.

Glacken, M., Adema, E., Sinskey, A. J. B., bioengineering, 1988. Mathematical descriptions of hybridoma culture kinetics: I. Initial metabolic rates. 32**,** 491-506.

Goll, M. G., Bestor, T. H. J. A. R. B., 2005. Eukaryotic cytosine methyltransferases. 74**,** 481-514.

Grassian, A. R., Parker, S. J., Davidson, S. M., Divakaruni, A. S., Green, C. R., Zhang, X. M., Slocum, K. L., Pu, M. Y., Lin, F., Vickers, C., Joud-Caldwell, C., Chung, F., Yin, H., Handly, E. D., Straub, C., Growney, J. D., Vander Heiden, M. G., Murphy, A. N., Pagliarini, R., Metallo, C. M., 2014. IDH1 Mutations Alter Citric Acid Cycle Metabolism and Increase Dependence on Oxidative Mitochondrial Metabolism. Cancer Res. 74**,** 3317-3331.

Green, R. M., 2007. Can we develop ethically universal embryonic stem-cell lines? Nature Reviews Genetics. 8**,** 480.

Gu, W., Gaeta, X., Sahakyan, A., Chan, A. B., Hong, C. S., Kim, R., Braas, D., Plath, K., Lowry, W. E., Christofk, H. R., 2016. Glycolytic Metabolism Plays a Functional Role in Regulating Human Pluripotent Stem Cell State. Cell Stem Cell. 19**,** 476-490.

Güemes, M., Rahman, S. A., Hussain, K., 2016. What is a normal blood glucose? Archives of disease in childhood. 101**,** 569-574.

Guppy, M., Greiner, E., Brand, K., 1993. The role of the Crabtree effect and an endogenous fuel in the energy metabolism of resting and proliferating thymocytes. European Journal of Biochemistry. 212**,** 95-99.

Gupta, P., Hourigan, K., Jadhav, S., Bellare, J., Verma, P., 2017. Effect of lactate and pH on mouse pluripotent stem cells: Importance of media analysis. Biochem. Eng. J. 118**,** 25-33.

Halestrap, A. P., 2012. The monocarboxylate transporter family—structure and functional characterization. IUBMB life. 64**,** 1-9.

Hassell, T., Gleave, S., Butler, M. J. A. b., biotechnology, 1991. Growth inhibition in animal cell culture. 30**,** 29-41.

Heiden, M. G. V., Cantley, L. C., Thompson, C. B., 2009. Understanding the Warburg Effect: The Metabolic Requirements of Cell Proliferation. Science. 324**,** 1029-1033.

Hensley, C. T., Faubert, B., Yuan, Q., Lev-Cohain, N., Jin, E., Kim, J., Jiang, L., Ko, B., Skelton, R., Loudat, L., Wodzak, M., Klimko, C., McMillan, E., Butt, Y., Ni, M., Oliver, D., Torrealba, J., Malloy, C. R., Kernstine, K., Lenkinski, R. E., DeBerardinis, R. J., 2016. Metabolic Heterogeneity in Human Lung Tumors. Cell. 164**,** 681-694.

Hill, A. V., Long, C., Lupton, H., 1924. Muscular exercise, lactic acid, and the supply and utilisation of oxygen.—Parts l-lll. Proceedings of the Royal Society of London. Series B, Containing Papers of a Biological Character. 96**,** 438-475.

Hiller, K., Metallo, C. M., 2013. Profiling metabolic networks to study cancer metabolism. Curr. Opin. Biotechnol. 24**,** 60-68.

Hope, K. J., Jin, L., Dick, J. E., 2004. Acute myeloid leukemia originates from a hierarchy of leukemic stem cell classes that differ in self-renewal capacity. Nature immunology. 5**,** 738.

Horiguchi, I., Urabe, Y., Kimura, K., Sakai, Y., 2018. Effects of glucose, lactate and basic FGF as limiting factors on the expansion of human induced pluripotent stem cells. J. Biosci. Bioeng. 125**,** 111-115.

Huckabee, W. E., 1956. Control of concentration gradients of pyruvate and lactate across cell membranes in blood. J. Appl. Physiol. 9**,** 163-170.

Hughes, C. S., Postovit, L. M., Lajoie, G. A., 2010. Matrigel: A complex protein mixture required for optimal growth of cell culture. Proteomics. 10**,** 1886-1890.

Hui, S., Ghergurovich, J. M., Morscher, R. J., Jang, C., Teng, X., Lu, W. Y., Esparza, L. A., Reya, T., Zhan, L., Guo, J. Y. X., White, E., Rabinowitz, J. D., 2017. Glucose feeds the TCA cycle via circulating lactate. Nature. 551**,** 115-+.

Hume, D., Weidemann, M. J. J. o. t. N. C. I., 1979. Role and regulation of glucose metabolism in proliferating cells. 62**,** 3-8.

Ivarsson, M., Noh, H., Morbidelli, M., Soos, M., 2015. Insights into pH-Induced Metabolic Switch by Flux Balance Analysis. Biotechnol. Prog. 31**,** 347-357.

Jaakkola, P., Mole, D. R., Tian, Y. M., Wilson, M. I., Gielbert, J., Gaskell, S. J., von Kriegsheim, A., Hebestreit, H. F., Mukherji, M., Schofield, C. J., Maxwell, P. H., Pugh, C. W., Ratcliffe, P. J., 2001. Targeting of HIF-alpha to the von Hippel-Lindau ubiquitylation complex by O-2-regulated prolyl hydroxylation. Science. 292**,** 468-472.

Jazmin, L. J., Young, J. D., 2013. Isotopically nonstationary 13 C metabolic flux analysis. Systems metabolic engineering. Springer, pp. 367-390.

Jiang, L., Boufersaoui, A., Yang, C., Ko, B., Rakheja, D., Guevara, G., Hu, Z., DeBerardinis, R. J. J. M. e., 2017. Quantitative metabolic flux analysis reveals an unconventional pathway of fatty acid synthesis in cancer cells deficient for the mitochondrial citrate transport protein. 43**,** 198-207.

Jiang, L., Shestov, A. A., Swain, P., Yang, C. D., Parker, S. J., Wang, Q. A., Terada, L. S., Adams, N. D., McCabe, M. T., Pietrak, B., Schmidt, S., Metallo, C. M., Dranka, B. P., Schwartz, B., DeBerardinis, R. J., 2016. Reductive carboxylation supports redox homeostasis during anchorage-independent growth. Nature. 532**,** 255-+.

Kallas, A., Pook, M., Trei, A., Maimets, T., 2014. SOX2 is regulated differently from NANOG and OCT4 in human embryonic stem cells during early differentiation initiated with sodium butyrate. Stem cells international. 2014.

Kane, D. A., 2014. Lactate oxidation at the mitochondria: a lactate-malate-aspartate shuttle at work. Front. Neurosci. 8**,** 6.

Kehoe, D. E., Jing, D. H., Lock, L. T., Tzanakakis, E. S., 2010. Scalable Stirred-Suspension Bioreactor Culture of Human Pluripotent Stem Cells. Tissue Eng. Part A. 16**,** 405-421.

Kelleher, J. K., 2001. Flux estimation using isotopic tracers: common ground for metabolic physiology and metabolic engineering. Metab. Eng. 3**,** 100-110.

Kennedy, K. M., Dewhirst, M. W., 2010. Tumor metabolism of lactate: the influence and therapeutic potential for MCT and CD147 regulation. Future Oncol. 6**,** 127-148.

Kennedy, K. M., Scarbrough, P. M., Ribeiro, A., Richardson, R., Yuan, H., Sonveaux, P., Landon, C. D., Chi, J. T., Pizzo, S., Schroeder, T., Dewhirst, M. W., 2013. Catabolism of Exogenous Lactate Reveals It as a Legitimate Metabolic Substrate in Breast Cancer. PLoS One. 8**,** 20.

Kim, C., Amano, T., Park, J., Carter, M. G., Tian, X., Yang, X. J. C., Cells, S., 2009. Improvement of embryonic stem cell line derivation efficiency with novel medium, glucose concentration, and epigenetic modifications. 11**,** 89-100.

Kim, H., Jang, H., Kim, T. W., Kang, B. H., Lee, S. E., Jeon, Y. K., Chung, D. H., Choi, J., Shin, J., Cho, E. J., 2015. Core pluripotency factors directly regulate metabolism in embryonic stem cell to maintain pluripotency. Stem Cells. 33**,** 2699-2711.

Kimbrel, E. A., Lanza, R., 2015. Current status of pluripotent stem cells: moving the first therapies to the clinic. Nat. Rev. Drug Discov. 14**,** 681-692.

Kovacevic, Z., McGivan, J., 1983. Mitochondrial metabolism of glutamine and glutamate and its physiological significance. Physiological Reviews. 63**,** 547-605.

Kropp, C., Kempf, H., Halloin, C., Robles-Diaz, D., Franke, A., Scheper, T., Kinast, K., Knorpp, T., Joos, T. O., Haverich, A., Martin, U., Zweigerdt, R., Olmer, R., 2016. Impact of Feeding Strategies on the Scalable Expansion of Human Pluripotent Stem Cells in Single-Use Stirred Tank Bioreactors. Stem Cells Transl. Med. 5**,** 1289-1301.

Kumar, D., Anand, T., Kues, W. A., 2017. Clinical potential of human-induced pluripotent stem cells. Cell Biol. Toxicol. 33**,** 99-112.

Lee, T. Y., Lin, H. H., Chen, C. L., Hwang, S. M., Tseng, C. P., 2015. Inhibitory Effect of Excessive Glucose on Its Biochemical Pathway and the Growth of Chinese Hamster Ovary (CHO) Cells. J. Carbohydr. Chem. 34**,** 1-11.

Leighty, R. W., Antoniewicz, M. R., 2011. Dynamic metabolic flux analysis (DMFA): a framework for determining fluxes at metabolic non-steady state. Metab. Eng. 13**,** 745-755.

Leighty, R. W., Antoniewicz, M. R., 2012. Parallel labeling experiments with U-^{13}C glucose validate *E. coli* metabolic network model for ^{13}C metabolic flux analysis. Metab. Eng. 14**,** 533-541.

Leighty, R. W., Antoniewicz, M. R., 2013. COMPLETE-MFA: complementary parallel labeling experiments technique for metabolic flux analysis. Metab. Eng. 20**,** 49-55.

Leite, T. C., Da Silva, D., Coelho, R. G., Zancan, P., Sola-Penna, M., 2007. Lactate favours the dissociation of skeletal muscle 6-phosphofructo-1-kinase tetramers down-regulating the enzyme and muscle glycolysis. Biochem. J. 408**,** 123-130.

Li, J., Wong, C. L., Vijayasankaran, N., Hudson, T., Amanullah, A., 2012. Feeding lactate for CHO cell culture processes: impact on culture metabolism and performance. Biotechnol. Bioeng. 109**,** 1173-1186.

Lin, B., Lin, X. M., Stachel, M., Wang, E., Luo, Y. M., Lader, J., Sun, X. F., Delmar, M., Bu, L., 2017. Culture in Glucose-Depleted Medium Supplemented with Fatty Acid and 3,3 ', 5-Triiodo-L-Thyronine Facilitates Purification and Maturation of Human Pluripotent Stem Cell-Derived Cardiomyocytes. Front. Endocrinol. 8**,** 12.

Liu, M., Quek, L.-E., Sultani, G., Turner, N., 2016. Epithelial-mesenchymal transition induction is associated with augmented glucose uptake and lactate production in pancreatic ductal adenocarcinoma. Cancer & metabolism. 4**,** 19.

Liu, W., Ren, Z., Lu, K., Song, C., Cheung, E. C. W., Zhou, Z., Chen, G. J. I. j. o. b. s., 2018. The Suppression of Medium Acidosis Improves the Maintenance and Differentiation of Human Pluripotent Stem Cells at High Density in Defined Cell Culture Medium. 14**,** 485.

Livak, K. J., Schmittgen, T. D., 2001. Analysis of relative gene expression data using real-time quantitative PCR and the 2− ΔΔCT method. methods. 25**,** 402-408.

Lu, H. S., Forbes, R. A., Verma, A., 2002. Hypoxia-inducible factor 1 activation by aerobic glycolysis implicates the Warburg effect in carcinogenesis. J. Biol. Chem. 277**,** 23111-23115.

Lu, S. C., Mato, J. M. J. J. o. g., hepatology, 2008. S-Adenosylmethionine in cell growth, apoptosis and liver cancer. 23**,** S73-S77.

Lunt, S. Y., Vander Heiden, M. G. J. A. r. o. c., biology, d., 2011. Aerobic glycolysis: meeting the metabolic requirements of cell proliferation. 27**,** 441-464.

Luong, E., Gerecht, S., 2008. Stem cells and scaffolds for vascularizing engineered tissue constructs. Engineering of Stem Cells. Springer, pp. 129-172.

Manalo, D. J., Rowan, A., Lavoie, T., Natarajan, L., Kelly, B. D., Ye, S. Q., Garcia, J. G. N., Semenza, G. L., 2005. Transcriptional regulation of vascular endothelial cell responses to hypoxia by HIF-1. Blood. 105**,** 659-669.

Martínez, V. S., Dietmair, S., Quek, L. E., Hodson, M. P., Gray, P., Nielsen, L. K., 2013. Flux balance analysis of CHO cells before and after a metabolic switch from lactate production to consumption. Biotechnol. Bioeng. 110**,** 660-666.

Martinez-Outschoorn, U. E., Prisco, M., Ertel, A., Tsirigos, A., Lin, Z., Pavlides, S., Wang, C. W., Flomenberg, N., Knudsen, E. S., Howell, A., Pestell, R. G., Sotgia, F., Lisanti, M. P., 2011. Ketones and lactate increase cancer cell "stemness", driving recurrence, metastasis and poor clinical outcome in breast cancer. Cell Cycle. 10**,** 1271-1286.

Mathieu, J., Ruohola-Baker, H. J. D., 2017. Metabolic remodeling during the loss and acquisition of pluripotency. 144**,** 541-551.

Mayshar, Y., Ben-David, U., Lavon, N., Biancotti, J. C., Yakir, B., Clark, A. T., Plath, K., Lowry, W. E., Benvenisty, N., 2010. Identification and Classification of Chromosomal Aberrations in Human Induced Pluripotent Stem Cells. Cell Stem Cell. 7**,** 521-531.

Meadows, A. L., Kong, B., Berdichevsky, M., Roy, S., Rosiva, R., Blanch, H. W., Clark, D. S., 2008. Metabolic and morphological differences between rapidly proliferating cancerous and normal breast epithelial cells. Biotechnol. Prog. 24**,** 334-341.

Melton, D., 2014. 'Stemness': definitions, criteria, and standards. Essentials of stem cell biology. Elsevier, pp. 7-17.

Metallo, C. M., Gameiro, P. A., Bell, E. L., Mattaini, K. R., Yang, J. J., Hiller, K., Jewell, C. M., Johnson, Z. R., Irvine, D. J., Guarente, L., Kelleher, J. K., Vander Heiden, M. G., Iliopoulos, O., Stephanopoulos, G., 2012. Reductive glutamine metabolism by IDH1 mediates lipogenesis under hypoxia. Nature. 481**,** 380-U166.

Metallo, C. M., Walther, J. L., Stephanopoulos, G., 2009. Evaluation of ^{13}C isotopic tracers for metabolic flux analysis in mammalian cells. J. Biotechnol. 144**,** 167-174.

Mintun, M. A., Vlassenko, A. G., Rundle, M. M., Raichle, M. E., 2004. Increased lactate/pyruvate ratio augments blood flow in physiologically activated human brain. Proceedings of the National Academy of Sciences. 101**,** 659-664.

Mitalipov, S., Wolf, D., 2009. Totipotency, pluripotency and nuclear reprogramming. Engineering of stem cells. Springer, pp. 185-199.

Miura, K., Okada, Y., Aoi, T., Okada, A., Takahashi, K., Okita, K., Nakagawa, M., Koyanagi, M., Tanabe, K., Ohnuki, M., 2009. Variation in the safety of induced pluripotent stem cell lines. Nat. Biotechnol. 27**,** 743.

Mochizuki, H., Ohnuki, Y., Kurosawa, H., 2011. Effect of glucose concentration during embryoid body (EB) formation from mouse embryonic stem cells on EB growth and cell differentiation. J. Biosci. Bioeng. 111**,** 92-97.

Mohyeldin, A., Garzon-Muvdi, T., Quinones-Hinojosa, A., 2010. Oxygen in Stem Cell Biology: A Critical Component of the Stem Cell Niche. Cell Stem Cell. 7**,** 150-161.

Moussaieff, A., Rouleau, M., Kitsberg, D., Cohen, M., Levy, G., Barasch, D., Nemirovski, A., Shen-Orr, S., Laevsky, I., Amit, M., Bomze, D., Elena-Herrmann, B., Scherf, T., Nissim-Rafinia, M., Kempa, S., Itskovitz-Eldor, J., Meshorer, E., Aberdam, D., Nahmias, Y., 2015. Glycolysis-Mediated Changes in Acetyl-CoA and Histone Acetylation Control the Early Differentiation of Embryonic Stem Cells. Cell Metab. 21**,** 392-402.

Mullen, A. R., Wheaton, W. W., Jin, E. S., Chen, P. H., Sullivan, L. B., Cheng, T., Yang, Y. F., Linehan, W. M., Chandel, N. S., DeBerardinis, R. J., 2012. Reductive

carboxylation supports growth in tumour cells with defective mitochondria. Nature. 481**,** 385-U171.

Mulukutla, B. C., Gramer, M., Hu, W. S., 2012. On metabolic shift to lactate consumption in fed-batch culture of mammalian cells. Metab. Eng. 14**,** 138-149.

Mulukutla, B. C., Khan, S., Lange, A., Hu, W.-S. J. T. i. b., 2010. Glucose metabolism in mammalian cell culture: new insights for tweaking vintage pathways. 28**,** 476-484.

Mulukutla, B. C., Yongky, A., Grimm, S., Daoutidis, P., Hu, W. S., 2015. Multiplicity of Steady States in Glycolysis and Shift of Metabolic State in Cultured Mammalian Cells. PLoS One. 10**,** 20.

Munger, J., Bennett, B. D., Parikh, A., Feng, X. J., McArdle, J., Rabitz, H. A., Shenk, T., Rabinowitz, J. D., 2008. Systems-level metabolic flux profiling identifies fatty acid synthesis as a target for antiviral therapy. Nat. Biotechnol. 26**,** 1179-1186.

Murphy, T. A., Young, J. D., 2013. ETA: robust software for determination of cell specific rates from extracellular time courses. Biotechnol. Bioeng. 110**,** 1748-1758.

Nagaoka, M., Si-Tayeb, K., Akaike, T., Duncan, S. A., 2010. Culture of human pluripotent stem cells using completely defined conditions on a recombinant E-cadherin substratum. BMC Dev. Biol. 10**,** 12.

Nath, S. C., Nagamori, E., Horie, M., Kino-oka, M., 2017. Culture medium refinement by dialysis for the expansion of human induced pluripotent stem cells in suspension culture. Bioprocess. Biosyst. Eng. 40**,** 123-131.

Nelson, D. L., Lehninger, A. L., Cox, M. M., 2008. Lehninger principles of biochemistry. Macmillan.

Nicolae, A., Wahrheit, J., Bahnemann, J., Zeng, A. P., Heinzle, E., 2014. Non-stationary ^{13}C metabolic flux analysis of Chinese hamster ovary cells in batch culture using extracellular labeling highlights metabolic reversibility and compartmentation. BMC Syst. Biol. 8**,** 15.

Niklas, J., Heinzle, E., 2011. Metabolic flux analysis in systems biology of mammalian cells. Genomics and Systems Biology of Mammalian Cell Culture. Springer, pp. 109-132.

Niwa, H., Miyazaki, J., Smith, A. G., 2000. Quantitative expression of Oct-3/4 defines differentiation, dedifferentiation or self-renewal of ES cells. Nature Genet. 24**,** 372-376.

Olmer, R., Lange, A., Selzer, S., Kasper, C., Haverich, A., Martin, U., Zweigerdt, R., 2012. Suspension Culture of Human Pluripotent Stem Cells in Controlled, Stirred Bioreactors. Tissue Eng. Part C-Methods. 18**,** 772-784.

Ouyang, A., Ng, R., Yang, S. T., 2007. Long-term culturing of undifferentiated embryonic stem cells in conditioned media and three-dimensional fibrous matrices without extracellular matrix coating. Stem Cells. 25**,** 447-454.

Paes, B., Moco, P. D., Pereira, C. G., Porto, G. S., Russo, E. M. D., Reis, L. C. J., Covas, D. T., Picanco-Castro, V., 2017. Ten years of iPSC: clinical potential and advances in vitro hematopoietic differentiation. Cell Biol. Toxicol. 33**,** 233-250.

Panopoulos, A. D., Yanes, O., Ruiz, S., Kida, Y. S., Diep, D., Tautenhahn, R., Herrerias, A., Batchelder, E. M., Plongthongkum, N., Lutz, M., Berggren, W. T., Zhang, K., Evans, R. M., Siuzdak, G., Belmonte, J. C. I., 2012. The metabolome of induced pluripotent stem cells reveals metabolic changes occurring in somatic cell reprogramming. Cell Res. 22**,** 168-177.

Papandreou, I., Cairns, R. A., Fontana, L., Lim, A. L., Denko, N. C., 2006. HIF-1 mediates adaptation to hypoxia by actively downregulating mitochondrial oxygen consumption. Cell Metab. 3**,** 187-197.

Parker, S. J., Svensson, R. U., Divakaruni, A. S., Lefebvre, A. E., Murphy, A. N., Shaw, R. J., Metallo, C. M., 2017. LKB1 promotes metabolic flexibility in response to energy stress. Metab. Eng. 43**,** 208-217.

Pavlides, S., Tsirigos, A., Vera, I., Flomenberg, N., Frank, P. G., Casimiro, M. C., Wang, C. G., Fortina, P., Addya, S., Pestell, R. G., Martinez-Outschoorn, U. E., Sotgia, F., Lisanti, M. P., 2010. Loss of stromal caveolin-1 leads to oxidative stress, mimics hypoxia and drives inflammation in the tumor microenvironment, conferring the "reverse Warburg effect" A transcriptional informatics analysis with validation. Cell Cycle. 9**,** 2201-2219.

Pavlides, S., Whitaker-Menezes, D., Castello-Cros, R., Flomenberg, N., Witkiewicz, A. K., Frank, P. G., Casimiro, M. C., Wang, C. G., Fortina, P., Addya, S., Pestell, R. G., Martinez-Outschoorn, U. E., Sotgia, F., Lisanti, M. P., 2009. The reverse

Warburg effect Aerobic glycolysis in cancer associated fibroblasts and the tumor stroma. Cell Cycle. 8**,** 3984-4001.

Perez-Escuredo, J., Dadhich, R. K., Dhup, S., Cacace, A., Van Hee, V. F., De Saedeleer, C. J., Sboarina, M., Rodriguez, F., Fontenille, M. J., Brisson, L., Porporato, P. E., Sonveaux, P., 2016. Lactate promotes glutamine uptake and metabolism in oxidative cancer cells. Cell Cycle. 15**,** 72-83.

Pfeiffer, T., Schuster, S., Bonhoeffer, S., 2001. Cooperation and competition in the evolution of ATP-producing pathways. Science. 292**,** 504-507.

Prigione, A., Fauler, B., Lurz, R., Lehrach, H., Adjaye, J., 2010. The Senescence-Related Mitochondrial/Oxidative Stress Pathway is Repressed in Human Induced Pluripotent Stem Cells. Stem Cells. 28**,** 721-733.

Quek, L. E., Wittmann, C., Nielsen, L. K., Kromer, J. O., 2009. OpenFLUX: efficient modelling software for C-13-based metabolic flux analysis. Microb. Cell. Fact. 8**,** 15.

Rathjen, J., Yeo, C., Yap, C., Tan, B. S. N., Rathjen, P. D., Gardner, D. K., 2014. Culture environment regulates amino acid turnover and glucose utilisation in human ES cells. Reprod. Fertil. Dev. 26**,** 703-716.

Reuter, S., Gupta, S. C., Chaturvedi, M. M., Aggarwal, B. B., 2010. Oxidative stress, inflammation, and cancer How are they linked? Free Radic. Biol. Med. 49**,** 1603-1616.

Rhim, A. D., Mirek, E. T., Aiello, N. M., Maitra, A., Bailey, J. M., McAllister, F., Reichert, M., Beatty, G. L., Rustgi, A. K., Vonderheide, R. H., 2012. EMT and dissemination precede pancreatic tumor formation. Cell. 148**,** 349-361.

Rogatzki, M. J., Ferguson, B. S., Goodwin, M. L., Gladden, L. B., 2015. Lactate is always the end product of glycolysis. Front. Neurosci. 9**,** 7.

Ryall, J. G., Cliff, T., Dalton, S., Sartorelli, V. J. C. s. c., 2015. Metabolic reprogramming of stem cell epigenetics. 17**,** 651-662.

Sa, J. V., Duarte, T. M., Carrondo, M. J. T., Alves, P. M., Teixeira, A. P., 2015. Metabolic Flux Analysis: A Powerful Tool in Animal Cell Culture. In: AlRubeai, M., (Ed.), Animal Cell Culture. vol. 9. Springer International Publishing Ag, Cham, pp. 521-539.

Sa, J. V., Kleiderman, S., Brito, C., Sonnewald, U., Leist, M., Teixeira, A. P., Alves, P. M., 2017. Quantification of Metabolic Rearrangements During Neural Stem Cells Differentiation into Astrocytes by Metabolic Flux Analysis. Neurochem. Res. 42**,** 244-253.

Sauer, U., 2006. Metabolic networks in motion: ^{13}C-based flux analysis. Mol. Syst. Biol. 2**,** 10.

Schurr, A., 2017. Lactate, not pyruvate, is the end product of glucose metabolism via glycolysis. Carbohydrate. IntechOpen.

Semenza, G. L., 2012. Hypoxia-Inducible Factors in Physiology and Medicine. Cell. 148**,** 399-408.

Semenza, G. L., Roth, P. H., Fang, H.-M., Wang, G. L., 1994. Transcriptional regulation of genes encoding glycolytic enzymes by hypoxia-inducible factor 1. J. Biol. Chem. 269**,** 23757-23763.

Sengupta, N., Rose, S. T., Morgan, J. A., 2011. Metabolic Flux Analysis of CHO Cell Metabolism in the Late Non-Growth Phase. Biotechnol. Bioeng. 108**,** 82-92.

Sepúlveda, D. E., Andrews, B. A., Papoutsakis, E. T., Asenjo, J. A., 2010. Metabolic flux analysis of embryonic stem cells using three distinct differentiation protocols and comparison to gene expression patterns. Biotechnol. Prog. 26**,** 1222-1229.

Sheikh, K., Forster, J., Nielsen, L. K., 2005. Modeling hybridoma cell metabolism using a generic genome-scale metabolic model of Mus musculus. Biotechnol. Prog. 21**,** 112-121.

Shi, Y., Inoue, H., Wu, J. C., Yamanaka, S., 2017. Induced pluripotent stem cell technology: a decade of progress. Nat. Rev. Drug Discov. 16**,** 115.

Shiraki, N., Shiraki, Y., Tsuyama, T., Obata, F., Miura, M., Nagae, G., Aburatani, H., Kume, K., Endo, F., Kume, S., 2014. Methionine Metabolism Regulates Maintenance and Differentiation of Human Pluripotent Stem Cells. Cell Metab. 19**,** 780-794.

Shyh-Chang, N., Locasale, J. W., Lyssiotis, C. A., Zheng, Y., Teo, R. Y., Ratanasirintrawoot, S., Zhang, J., Onder, T., Unternaehrer, J. J., Zhu, H. J. S., 2013. Influence of threonine metabolism on S-adenosylmethionine and histone methylation. 339**,** 222-226.

Si-Tayeb, K., Noto, F. K., Sepac, A., Sedlic, F., Bosnjak, Z. J., Lough, J. W., Duncan, S. A., 2010. Generation of human induced pluripotent stem cells by simple transient transfection of plasmid DNA encoding reprogramming factors. BMC Dev. Biol. 10**,** 10.

Silva, M. M., Rodrigues, A. F., Correia, C., Sousa, M. F. Q., Brito, C., Coroadinha, A. S., Serra, M., Alves, P. M., 2015. Robust Expansion of Human Pluripotent Stem Cells: Integration of Bioprocess Design With Transcriptomic and Metabolomic Characterization. Stem Cells Transl. Med. 4**,** 731-742.

Sonveaux, P., Copetti, T., De Saedeleer, C. J., Vegran, F., Verrax, J., Kennedy, K. M., Moon, E. J., Dhup, S., Danhier, P., Frerart, F., Gallez, B., Ribeiro, A., Michiels, C., Dewhirst, M. W., Feron, O., 2012. Targeting the Lactate Transporter MCT1 in Endothelial Cells Inhibits Lactate-Induced HIF-1 Activation and Tumor Angiogenesis. PLoS One. 7**,** 13.

Sonveaux, P., Vegran, F., Schroeder, T., Wergin, M. C., Verrax, J., Rabbani, Z. N., De Saedeleer, C. J., Kennedy, K. M., Diepart, C., Jordan, B. F., Kelley, M. J., Gallez, B., Wahl, M. L., Feron, O., Dewhirst, M. W., 2008. Targeting lactate-fueled respiration selectively kills hypoxic tumor cells in mice. J. Clin. Invest. 118**,** 3930-3942.

Stadtfeld, M., Nagaya, M., Utikal, J., Weir, G., Hochedlinger, K., 2008. Induced pluripotent stem cells generated without viral integration. Science. 322**,** 945-949.

Stephanopoulos, G., 1999. Metabolic Fluxes and Metabolic Engineering. Metab. Eng. 1**,** 1-11.

Stephanopoulos, G., Aristidou, A., Nielsen, J. J. S. D. A. G. S., 1998. Metabolic engineering: principles and methodologies.

Stephanopoulos, G., Stafford, D. E., 2002. Metabolic engineering: a new frontier of chemical reaction engineering. Chem. Eng. Sci. 57**,** 2595-2602.

Takahashi, K., Tanabe, K., Ohnuki, M., Narita, M., Ichisaka, T., Tomoda, K., Yamanaka, S., 2007. Induction of pluripotent stem cells from adult human fibroblasts by defined factors. Cell. 131**,** 861-872.

Takahashi, K., Yamanaka, S., 2006. Induction of pluripotent stem cells from mouse embryonic and adult fibroblast cultures by defined factors. Cell. 126**,** 663-676.

Tang, Y. J., Martin, H. G., Myers, S., Rodriguez, S., Baidoo, E. E. K., Keasling, J. D., 2009. Advances in analysis of microbial metabolic fluxes via ^{13}C isotopic labeling. Mass Spectrom. Rev. 28**,** 362-375.

Templeton, N., Dean, J., Reddy, P., Young, J. D., 2013. Peak antibody production is associated with increased oxidative metabolism in an industrially relevant fed-batch CHO cell culture. Biotechnol. Bioeng. 110**,** 2013-2024.

Templeton, N., Smith, K. D., McAtee-Pereira, A. G., Dorai, H., Betenbaugh, M. J., Lang, S. E., Young, J. D., 2017a. Application of 13C flux analysis to identify high-productivity CHO metabolic phenotypes. Metab. Eng. 43**,** 218-225.

Templeton, N., Xu, S., Roush, D. J., Chen, H., 2017b. C-13 metabolic flux analysis identifies limitations to increasing specific productivity in fed-batch and perfusion. Metab. Eng. 44**,** 126-133.

Teslaa, T., Teitell, M. A. J. T. E. j., 2015. Pluripotent stem cell energy metabolism: an update. 34**,** 138-153.

Thomson, J. A., Itskovitz-Eldor, J., Shapiro, S. S., Waknitz, M. A., Swiergiel, J. J., Marshall, V. S., Jones, J. M., 1998. Embryonic stem cell lines derived from human blastocysts. Science. 282**,** 1145-1147.

Tohyama, S., Fujita, J., Hishiki, T., Matsuura, T., Hattori, F., Ohno, R., Kanazawa, H., Seki, T., Nakajima, K., Kishino, Y., Okada, M., Hirano, A., Kuroda, T., Yasuda, S., Sato, Y., Yuasa, S., Sano, M., Suematsu, M., Fukuda, K., 2016. Glutamine Oxidation Is Indispensable for Survival of Human Pluripotent Stem Cells. Cell Metab. 23**,** 663-674.

Tohyama, S., Hattori, F., Sano, M., Hishiki, T., Nagahata, Y., Matsuura, T., Hashimoto, H., Suzuki, T., Yamashita, H., Satoh, Y., Egashira, T., Seki, T., Muraoka, N., Yamakawa, H., Ohgino, Y., Tanaka, T., Yoichi, M., Yuasa, S., Murata, M., Suematsu, M., Fukuda, K., 2013. Distinct Metabolic Flow Enables Large-Scale Purification of Mouse and Human Pluripotent Stem Cell-Derived Cardiomyocytes. Cell Stem Cell. 12**,** 127-137.

Trounson, A., DeWitt, N. D., 2016. Pluripotent stem cells progressing to the clinic. Nat. Rev. Mol. Cell Biol. 17**,** 194-200.

Turner, J., Quek, L. E., Titmarsh, D., Kromer, J. O., Kao, L. P., Nielsen, L., Wolvetang, E., Cooper-White, J., 2014. Metabolic Profiling and Flux Analysis of MEL-2

Human Embryonic Stem Cells during Exponential Growth at Physiological and Atmospheric Oxygen Concentrations. PLoS One. 9**,** 13.

Vander Heiden, M. G., Cantley, L. C., Thompson, C. B. J. s., 2009. Understanding the Warburg effect: the metabolic requirements of cell proliferation. 324**,** 1029-1033.

Varum, S., Rodrigues, A. S., Moura, M. B., Momcilovic, O., Easley, C. A., Ramalho-Santos, J., Van Houten, B., Schatten, G., 2011. Energy Metabolism in Human Pluripotent Stem Cells and Their Differentiated Counterparts. PLoS One. 6**,** 15.

Volarevic, V., Markovic, B. S., Gazdic, M., Volarevic, A., Jovicic, N., Arsenijevic, N., Armstrong, L., Djonov, V., Lako, M., Stojkovic, M., 2018. Ethical and safety issues of stem cell-based therapy. International journal of medical sciences. 15**,** 36.

Wanet, A., Arnould, T., Najimi, M., Renard, P., 2015. Connecting Mitochondria, Metabolism, and Stem Cell Fate. Stem Cells Dev. 24**,** 1957-1971.

Wang, F., Thirumangalathu, S., Loeken, M. R. J. C., cells, s., 2006. Establishment of new mouse embryonic stem cell lines is improved by physiological glucose and oxygen. 8**,** 108-116.

Wang, G. L., Semenza, G. L., 1995. Purification and characterization of hypoxia inducible factor-1. J. Biol. Chem. 270**,** 1230-1237.

Wang, J., Alexander, P., Wu, L., Hammer, R., Cleaver, O., McKnight, S. L. J. S., 2009. Dependence of mouse embryonic stem cells on threonine catabolism. 325**,** 435-439.

Wang, Y., Chou, B. K., Dowey, S., He, C. X., Gerecht, S., Cheng, L. Z., 2013. Scalable expansion of human induced pluripotent stem cells in the defined xeno-free E8 medium under adherent and suspension culture conditions. Stem Cell Res. 11**,** 1103-1116.

Wang, Z., Oron, E., Nelson, B., Razis, S., Ivanova, N., 2012. Distinct lineage specification roles for NANOG, OCT4, and SOX2 in human embryonic stem cells. Cell Stem Cell. 10**,** 440-454.

Warburg, O., 1956. On the origin of cancer cells. Science. 123**,** 309-314.

Warburg, O., Wind, F., Negelein, E. J. T. J. o. g. p., 1927. The metabolism of tumors in the body. 8**,** 519.

Warren, L., Manos, P. D., Ahfeldt, T., Loh, Y.-H., Li, H., Lau, F., Ebina, W., Mandal, P. K., Smith, Z. D., Meissner, A., 2010. Highly efficient reprogramming to pluripotency and directed differentiation of human cells with synthetic modified mRNA. Cell Stem Cell. 7**,** 618-630.

Watanabe, K., Ueno, M., Kamiya, D., Nishiyama, A., Matsumura, M., Wataya, T., Takahashi, J. B., Nishikawa, S., Nishikawa, S.-i., Muguruma, K., 2007. A ROCK inhibitor permits survival of dissociated human embryonic stem cells. Nat. Biotechnol. 25**,** 681.

Weitzel, M., Noh, K., Dalman, T., Niedenfuhr, S., Stute, B., Wiechert, W., 2013. 13CFLUX2-high-performance software suite for ^{13}C-metabolic flux analysis. Bioinformatics. 29**,** 143-145.

Wellen, K. E., Thompson, C. B., 2012. A two-way street: reciprocal regulation of metabolism and signalling. Nat. Rev. Mol. Cell Biol. 13**,** 270-U1.

Werner, J. C., Sicard, R. E., 1987. Lactate metabolism of isolated, perfused fetal, and newborn pig hearts. Pediatric Research. 22**,** 552.

Wiechert, W., 2001. 13C metabolic flux analysis. Metab. Eng. 3**,** 195-206.

Wilmes, A., Rauch, C., Carta, G., Kern, G., Meier, F., Posch, W., Wilflingseder, D., Armstrong, L., Lako, M., Beilmann, M. J. T. i. V., 2017. Towards optimisation of induced pluripotent cell culture: Extracellular acidification results in growth arrest of iPSC prior to nutrient exhaustion. 45**,** 445-454.

Wise, D. R., Ward, P. S., Shay, J. E. S., Cross, J. R., Gruber, J. J., Sachdeva, U. M., Platt, J. M., DeMatteo, R. G., Simon, M. C., Thompson, C. B., 2011. Hypoxia promotes isocitrate dehydrogenase-dependent carboxylation of α-ketoglutarate to citrate to support cell growth and viability. Proc. Natl. Acad. Sci. U. S. A. 108**,** 19611-19616.

Wu, S. M., Hothedlinger, K., 2011. Harnessing the potential of induced pluripotent stem cells for regenerative medicine. Nat. Cell Biol. 13**,** 497-505.

Wurm, F. M., 2004. Production of recombinant protein therapeutics in cultivated mammalian cells. Nat. Biotechnol. 22**,** 1393.

Yanes, O., Clark, J., Wong, D. M., Patti, G. J., Sanchez-Ruiz, A., Benton, H. P., Trauger, S. A., Desponts, C., Ding, S., Siuzdak, G., 2010. Metabolic oxidation regulates embryonic stem cell differentiation. Nat. Chem. Biol. 6**,** 411-417.

Yoo, H., Antoniewicz, M. R., Stephanopoulos, G., Kelleher, J. K., 2008. Quantifying reductive carboxylation flux of glutamine to lipid in a brown adipocyte cell line. J. Biol. Chem. 283**,** 20621-20627.

Young, J. D., 2014. INCA: a computational platform for isotopically non-stationary metabolic flux analysis. Bioinformatics. 30**,** 1333-1335.

Young, J. D., Walther, J. L., Antoniewicz, M. R., Yoo, H., Stephanopoulos, G., 2008. An elementary metabolite unit (EMU) based method of isotopically nonstationary flux analysis. Biotechnol. Bioeng. 99**,** 686-699.

Yu, J., Thomson, J. A., 2014. Embryonic Stem Cells: Derivation and Properties. Essentials of Stem Cell Biology. Elsevier, pp. 387-398.

Yu, J., Vodyanik, M. A., Smuga-Otto, K., Antosiewicz-Bourget, J., Frane, J. L., Tian, S., Nie, J., Jonsdottir, G. A., Ruotti, V., Stewart, R., 2007. Induced pluripotent stem cell lines derived from human somatic cells. Science. 318**,** 1917-1920.

Yu, M., Bardia, A., Wittner, B. S., Stott, S. L., Smas, M. E., Ting, D. T., Isakoff, S. J., Ciciliano, J. C., Wells, M. N., Shah, A. M., 2013. Circulating breast tumor cells exhibit dynamic changes in epithelial and mesenchymal composition. Science. 339**,** 580-584.

Zamboni, N., 2011. 13C metabolic flux analysis in complex systems. Curr. Opin. Biotechnol. 22**,** 103-108.

Zamboni, N., Fendt, S. M., Ruhl, M., Sauer, U., 2009. ^{13}C-based metabolic flux analysis. Nat. Protoc. 4**,** 878-892.

Zancan, P., Sola-Penna, M., Furtado, C. M., Da Silva, D., 2010. Differential expression of phosphofructokinase-1 isoforms correlates with the glycolytic efficiency of breast cancer cells. Mol. Genet. Metab. 100**,** 372-378.

Zhang, H., Badur, M. G., Divakaruni, A. S., Parker, S. J., Jager, C., Hiller, K., Murphy, A. N., Metallo, C. M., 2016. Distinct Metabolic States Can Support Self-Renewal and Lipogenesis in Human Pluripotent Stem Cells under Different Culture Conditions. Cell Reports. 16**,** 1536-1547.

Zhang, J., Khvorostov, I., Hong, J. S., Oktay, Y., Vergnes, L., Nuebel, E., Wahjudi, P. N., Setoguchi, K., Wang, G., Do, A., Jung, H. J., McCaffery, J. M., Kurland, I. J., Reue, K., Lee, W. N. P., Koehler, C. M., Teitell, M. A., 2011. UCP2 regulates energy metabolism and differentiation potential of human pluripotent stem cells. Embo J. 30**,** 4860-4873.

Zhang, J., Nuebel, E., Daley, G. Q., Koehler, C. M., Teitell, M. A., 2012. Metabolic Regulation in Pluripotent Stem Cells during Reprogramming and Self-Renewal. Cell Stem Cell. 11**,** 589-595.

Zhou, W. C., Rehm, J., Europa, A., Hu, W. S., 1997. Alteration of mammalian cell metabolism by dynamic nutrient feeding. Cytotechnology. 24**,** 99-108.